Outburst Floods in the Greater Himalayas

From Regional Susceptibility to Local Hazard

Melanie Fischer

Cumulative dissertation

for the degree

"doctor rerum naturalium"

(Dr. rer. nat.)

in Natural Hazard Research

submitted to

Institute of Environmental Science and Geography

Faculty of Mathematics and Natural Sciences

University of Potsdam

Submission: 18th of May, 2022

Disputation: 21st of October, 2022

First Supervisor: PD Dr. Ariane Walz
Second Supervisor: Prof. Oliver Korup, PhD

Reviewers: Prof. Fiona Tweed, PhD, Staffordshire University
Prof. em. Monique Fort, Universite Paris Cite

Published online on the
Publication Server of the University of Potsdam:
https://doi.org/10.25932/publishup-56997
https://nbn-resolving.org/urn:nbn:de:kobv:517-opus4-569972

Abstract

High-mountain regions provide valuable ecosystem services, including food, water, and energy production, to more than 900 million people worldwide. Projections hold, that this population number will rapidly increase in the next decades, accompanied by a continued urbanisation of cities located in mountain valleys. One of the manifestations of this ongoing socio-economic change of mountain societies is a rise in settlement areas and transportation infrastructure while an increased power need fuels the construction of hydropower plants along rivers in the high-mountain regions of the world. However, physical processes governing the cryosphere of these regions are highly sensitive to changes in climate and a global warming will likely alter the conditions in the headwaters of high-mountain rivers. One of the potential implications of this change is an increase in frequency and magnitude of outburst floods – highly dynamic flows capable of carrying large amounts of water and sediments. Sudden outbursts from lakes formed behind natural dams are complex geomorphological processes and are often part of a hazard cascade. In contrast to other types of natural hazards in high-alpine areas, for example landslides or avalanches, outburst floods are highly infrequent. Therefore, observations and data describing for example the mode of outburst or the hydraulic properties of the downstream propagating flow are very limited, which is a major challenge in contemporary (glacial) lake outburst flood research. Although glacial lake outburst floods (GLOFs) and landslide-dammed lake outburst floods (LLOFs) are rare, a number of documented events caused high fatality counts and damage. The highest documented losses due to outburst floods since the start of the 20th century were induced by only a few high-discharge events. Thus, outburst floods can be a significant hazard to downvalley communities and infrastructure in high-mountain regions worldwide.

This thesis focuses on the Greater Himalayan region, a vast mountain belt stretching across 0.89 million km^2. Although potentially hundreds of outburst floods have occurred there since the beginning of the 20th century, data on these events is still scarce. Projections of cryospheric change, including glacier-mass wastage and permafrost degradation, will likely result in an overall increase of the water volume stored in meltwater lakes as well as the destabilisation of mountain slopes in the Greater Himalayan region. Thus, the potential for outburst floods to affect the increasingly more densely populated valleys of this mountain belt is also likely to increase in the future. A prime example of one of these valleys is the Pokhara valley in Nepal, which is drained by the Seti Khola, a river crossing one of the steepest topographic gradients in the Himalayas. This valley is also home to Nepal's second largest, rapidly growing city, Pokhara, which currently has a population of more than half a million people – some of which live in informal settlements within the floodplain of the

Seti Khola. Although there is ample evidence for past outburst floods along this river in recent and historic times, these events have hardly been quantified.

The main motivation of my thesis is to address the data scarcity on past and potential future outburst floods in the Greater Himalayan region, both at a regional and at a local scale. For the former, I compiled an inventory of >3,000 moraine-dammed lakes, of which about 1% had a documented sudden failure in the past four decades. I used this data to test whether a number of predictors that have been widely applied in previous GLOF assessments are statistically relevant when estimating past GLOF susceptibility. For this, I set up four Bayesian multi-level logistic regression models, in which I explored the credibility of the predictors lake area, lake-area dynamics, lake elevation, parent-glacier-mass balance, and monsoonality. By using a hierarchical approach consisting of two levels, this probabilistic framework also allowed for spatial variability on GLOF susceptibility across the vast study area, which until now had not been considered in studies of this scale. The model results suggest that in the Nyainqentanglha and Eastern Himalayas – regions with strong negative glacier-mass balances – lakes have been more prone to release GLOFs than in regions with less negative or even stable glacier-mass balances. Similarly, larger lakes in larger catchments had, on average, a higher probability to have had a GLOF in the past four decades. Yet, monsoonality, lake elevation, and lake-area dynamics were more ambiguous. This challenges the credibility of a lake's rapid growth in surface area as an indicator of a pending outburst; a metric that has been applied to regional GLOF assessments worldwide.

At a local scale, my thesis aims to overcome data scarcity concerning the flow characteristics of the catastrophic May 2012 flood along the Seti Khola, which caused 72 fatalities, as well as potentially much larger predecessors, which deposited >1 km^3 of sediment in the Pokhara valley between the 12^{th} and 14^{th} century CE. To reconstruct peak discharges, flow depths, and flow velocities of the 2012 flood, I mapped the extents of flood sediments from RapidEye satellite imagery and used these as a proxy for inundation limits. To constrain the latter for the Mediaeval events, I utilised outcrops of slackwater deposits in the fills of tributary valleys. Using steady-state hydrodynamic modelling for a wide range of plausible scenarios, from meteorological (1,000 $m^3 s^{-1}$) to cataclysmic outburst floods (600,000 $m^3 s^{-1}$), I assessed the likely initial discharges of the recent and the Mediaeval floods based on the lowest mismatch between sedimentary evidence and simulated flood limits. One-dimensional HEC-RAS simulations suggest, that the 2012 flood most likely had a peak discharge of 3,700 $m^3 s^{-1}$ in the upper Seti Khola and attenuated to 500 $m^3 s^{-1}$ when arriving in Pokhara's suburbs some 15 km downstream.

Simulations of flow in two-dimensions with orders of magnitude higher peak discharges in ANUGA show extensive backwater effects in the main tributary valleys. These backwater effects match the

locations of slackwater deposits and, hence, attest for the flood character of Mediaeval sediment pulses. This thesis provides first quantitative proof for the hypothesis, that the latter were linked to earthquake-triggered outbursts of large former lakes in the headwaters of the Seti Khola – producing floods with peak discharges of >50,000 $m^3 s^{-1}$.

Building on this improved understanding of past floods along the Seti Khola, my thesis continues with an analysis of the impacts of potential future outburst floods on land cover, including built-up areas and infrastructure mapped from high-resolution satellite and OpenStreetMap data. HEC-RAS simulations of ten flood scenarios, with peak discharges ranging from 1,000 to 10,000 $m^3 s^{-1}$, show that the relative inundation hazard is highest in Pokhara's north-western suburbs. There, the potential effects of hydraulic ponding upstream of narrow gorges might locally sustain higher flow depths. Yet, along this reach, informal settlements and gravel mining activities are close to the active channel. By tracing the construction dynamics in two of these potentially affected informal settlements on multi-temporal RapidEye, PlanetScope, and Google Earth imagery, I found that exposure increased locally between three- to twentyfold in just over a decade (2008 to 2021).

In conclusion, this thesis provides new quantitative insights into the past controls on the susceptibility of glacial lakes to sudden outburst at a regional scale and the flow dynamics of propagating flood waves released by past events at a local scale, which can aid future hazard assessments on transient scales in the Greater Himalayan region. My subsequent exploration of the impacts of potential future outburst floods to exposed infrastructure and (informal) settlements might provide valuable inputs to anticipatory assessments of multiple risks in the Pokhara valley.

Kurzfassung

Hochgebirgsregionen stellen wertvolle Ökosystemdienstleistungen wie Nahrung, Wasser und Energieerzeugung für weltweit mehr als 900 Millionen Menschen bereit. Prognosen zufolge wird diese Zahl in den nächsten Jahrzehnten weiter rapide ansteigen, begleitet von einer zunehmenden Urbanisierung der in den Bergtälern lebenden Bevölkerung. Dieser anhaltende sozioökonomische Wandel äußert sich unter anderem in der Zunahme von Siedlungsflächen und dem Ausbau der Verkehrsinfrastruktur, während gleichzeitig ein erhöhter Energiebedarf den Bau von Wasserkraftwerken entlang von Hochgebirgsflüssen vorantreibt. Physikalische Prozesse, welche die Hochgebirgs-Kryosphäre beeinflussen, reagieren jedoch sehr empfindlich auf Klimaveränderungen. Die globale Erwärmung wird somit wahrscheinlich auch die Bedingungen in den Einzugsgebieten und Oberläufen dieser Hochgebirgsflüsse verändern. Eine mögliche Folge dieses Wandels ist eine Zunahme der Frequenz und Magnitude von natürlichen Dammbruchfluten (im Englischen *outburst floods*), welche hochdynamisch sind und potenziell große Mengen Wasser und Sedimente mit sich führen können. Plötzliche Ausbrüche von Seen, welche sich zuvor hinter natürlichen Dämmen aufgestaut haben, sind komplexe geomorphologische Prozesse und oft Teil einer mehrteiligen Gefahrenkaskade. Dammbruchfluten sind jedoch, im Gegensatz zu anderen Naturgefahren im Hochgebirge wie beispielsweise Erdrutsche oder Lawinen, sehr selten. Daher sind direkte Beobachtungen und Messdaten, welche z.B. die Art des Ausbruchs oder die hydraulischen Eigenschaften der sich stromabwärts ausbreitenden Strömung festhalten, nur sehr begrenzt vorhanden, was eine der größten Herausforderungen für die gegenwärtige Forschung an natürlichen Dammbruchfluten darstellt. Trotz der Seltenheit von Ausbrüchen von Gletscherseen (*glacial lake outburst floods* oder GLOFs) beziehungsweise von durch Erdrutschmassen aufgestauten Seen (*landslide-dammed lake outburst floods* oder LLOFs), ist dieser Fluttyp für eine hohe Anzahl an dokumentierten Opferzahlen und Schäden weltweit verantwortlich. Ein Großteil dieser Schäden wurde dabei nach Aufzeichnungen seit Beginn des 20. Jahrhunderts durch nur wenige Ereignisse verursacht. Natürliche Dammbruchfluten stellen somit eine ernsthafte Gefahr für weiter talabwärts gelegene Siedlungen und die Infrastruktur in den Hochgebirgsregionen der Welt dar.

Die vorliegende Dissertation fokussiert sich räumlich auf den Himalaya und die angrenzenden Gebirgszüge – die sogenannte Großregion des Himalayas – welche sich über eine Fläche von 0.89 Millionen km^2 erstreckt. Obwohl sich in diesem Gebirgsgürtel seit Beginn des 20. Jahrhunderts möglicherweise Hunderte natürlicher Dammbruchfluten ereignet haben, liegen nur wenige Daten über derartige Ereignisse vor. Aktuelle Prognosen der Veränderungen der Kryosphäre in diesem Gebiet zeigen einen zunehmenden Verlust an Gletschermasse und das Abtauen von

Permafrostböden, was wahrscheinlich wiederum zu einem allgemeinen Anstieg des in den Gletscherseen gespeicherten Wasservolumens sowie zur Destabilisierung der Berghänge in der Großregion des Himalayas führen wird. In Zukunft ist somit auch eine Zunahme des Potenzials für solche Überschwemmungen in den zunehmend dichter besiedelten Tälern dieses Gebirgsgürtels wahrscheinlich.

Ein Paradebeispiel eines solchen gefährdeten Himalaya-Tals ist das Pokhara Tal in Nepal, welches vom Seti Khola („Khola" heißt auf Nepalesisch Fluss) entwässert wird, dem Hochgebirgsfluss mit dem steilsten topographischen Gefälle im zentralen Himalaya. Das Pokhara Tal beherbergt die gleichnamige Stadt Pokhara, welche mit einer Einwohnerzahl von über 500.000 die zweitgrößte und am schnellsten wachsende Stadt Nepals darstellt. Ein Teil der Einwohner Pokharas lebt in informellen Siedlungen, welche sich oftmals direkt im Überschwemmungsgebiet des Seti Khola befinden. Trotz zahlreicher Hinweise auf frühere natürliche Dammbruchfluten entlang dieses Flusses aus jüngerer und historischer Zeit, wurden diese Ereignisse bisher kaum quantifiziert.

Die Hauptmotivation meiner Dissertation besteht darin, den Mangel an Daten über vergangene und potenzielle zukünftige natürliche Dammbruchfluten in der Großregion des Himalayas zu überwinden, sowohl auf regionaler als auch auf lokaler Ebene. Zu diesem Zweck habe ich ein Inventar von mehr als 3.000 hinter Moränen aufgestauten Gletscherseen erstellt, von welchen etwa 1% in den letzten vier Jahrzehnten einen dokumentierten GLOF produziert haben. Auf dieser Datengrundlage testete ich, ob eine Reihe von Prädiktoren, die in bisherigen GLOF-Studien häufig verwendet wurden, statistisch relevant für die Abschätzung der Suszeptibilität von moränengedämmten Gletscherseen für GLOFs in der Vergangenheit sind. Zu diesem Zweck habe ich vier Bayesische hierarchische logistische Regressionsmodelle aufgestellt, mit welchen ich die Glaubwürdigkeit der Prädiktoren Seefläche, Seeflächendynamik, Seehöhe über dem Meeresspiegel, Gletschermassenbilanz und „Monsunalität" (definiert als der Anteil des während der Sommermonate fallenden Niederschlages am Jahresniederschlag) untersuchen konnte. Die Anwendung eines hierarchischen Ansatzes mit zwei Ebenen ermöglichte dabei die Berücksichtigung einer möglichen räumlichen Variabilität der GLOF-Suszeptibilität im Untersuchungsgebiet, was in bisherigen Studien dieser Größenordnung bislang nicht berücksichtigt worden ist. Die Modellergebnisse deuten darauf hin, dass Gletscherseen im Nyainqentanglha und im östlichen Himalaya, also Regionen mit stark negativen Gletschermassenbilanzen, eine höhere Suszeptibilität für GLOFs hatten als Gletscherseen in Regionen mit weniger stark negativen oder stabilen Gletschermassenbilanzen. Größere Gletscherseen in größeren Einzugsgebieten zeigten durchschnittlich ebenfalls eine höhere Wahrscheinlichkeit für einen nachgewiesenen GLOF in den letzten vier Jahrzehnten. Ein Einfluss der

Monsunalität, der Höhe des Sees über dem Meeresspiegel sowie der Dynamik der Seefläche waren jedoch uneindeutig in den Modellen. Dieses Ergebnis stellt die Gültigkeit eines raschen Seewachstums als Indikator eines bevorstehenden GLOFs, ein in regionalen GLOF-Studien häufig angewandter Prädiktor, in Frage.

Auf lokaler Ebene kann meine Dissertation dabei helfen, die Datenknappheit bezüglich der Fließcharakteristika der katastrophalen Flut vom Mai 2012 mit 72 Opfern entlang des Seti Khola sowie deren potenziell viel größeren Vorgängerereignissen des 12. bis 14. Jahrhunderts, welche >1 km^3 an Sedimenten deponierten, zu überwinden. Um Spitzenabflüsse, Fließtiefen und Fließgeschwindigkeiten der 2012 Flut zu rekonstruieren, habe ich die Erstreckung der Flutsedimente aus RapidEye-Satellitenbildern kartiert und diese als Proxy für die Grenzen der Überflutungsflächen verwendet. Um letztere auch für die mittelalterlichen Ereignisse einzuschätzen, nutzte ich die Aufschlüsse von Stauwasserablagerungen (*slackwater deposits*) in den Talverfüllungen der Tributäre des Seti Kholas. Mit Hilfe stationärer hydrodynamischer Modelle simulierte ich eine breite Palette plausibler Fließszenarien, von meteorologischen Fluten (1.000 m^3 s^{-1}) bis hin zu kataklystischen Ausbrüchen (600.000 m^3 s^{-1}). Die Abschätzung der wahrscheinlichen anfänglichen Spitzenabflüsse der rezenten und mittelalterlichen Überschwemmungen geschah dabei auf der Grundlage der geringsten räumlichen Diskrepanz zwischen den sedimentären Beweisen und den simulierten Überflutungsgrenzen. Meine eindimensionalen Flutsimulationen mit der Modellierungssoftware HEC-RAS ergaben, dass die Flut von 2012 höchstwahrscheinlich einen Spitzenabfluss von 3.700 m^3 s^{-1} im oberen Abschnitt des Seti Khola aufwies, sich jedoch beim Erreichen der etwa 15 km flussabwärts gelegenen Randbereiche Pokharas bereits auf 500 m^3 s^{-1} abgeschwächt hatte. Um Größenordnungen höhere zweidimensionale Flutsimulationen mit der Modellierungssoftware ANUGA zeigen extensive Rückstaueffekte in den Haupttributären. Die Grenzen dieser Rückstaueffekte stimmen mit den Vorkommen von Stauwasserablagerungen überein und belegen somit den fluviatilen Charakter der mittelalterlichen Sedimentationsereignisse. Diese Dissertation liefert somit den ersten quantitativen Beweis für die Hypothese, dass die mächtigen mittelalterlichen Sedimentablagerungen des Pokhara Tals durch von starken Erdbeben ausgelösten Ausbrüchen großer ehemaliger Gletscherseen im Oberlauf des Seti Khola zusammenhängen, welche Fluten mit Spitzenabflüssen von >50.000 m^3 s^{-1} produzierten.

Aufbauend auf diesem verbesserten Verständnis vergangener Fluten entlang des Seti Khola analysierte ich die Auswirkungen potenzieller zukünftiger natürlicher Dammbruchfluten auf die Landbedeckung des Pokhara Tals, einschließlich Siedlungsfläche und Infrastruktur, anhand von hochauflösenden Satelliten- und OpenStreetMap-Daten. Meine HEC-RAS-Simulationen von zehn Flutszenarien mit Spitzenabflüssen zwischen 1.000 und 10.000 m^3 s^{-1} ergaben, dass die relative

Überflutungsgefahr in den nordwestlichen Randbereichen Pokharas am höchsten ist. Dort kann eine hydraulische Aufstauung oberhalb von engen Schluchten zu lokal höheren Überflutungstiefen führen, was eine potenzielle Gefahr für die sich in diesen Flussabschnitten befindenden informellen Siedlungen und Kiesabbaulokalitäten darstellt. Meine Analyse der Bebauungsdynamik zweier potenziell betroffener informeller Siedlungen mithilfe von hochauflösenden, multi-temporalen RapidEye-, PlanetScope- und Google Earth-Satellitenbildern ergab, dass sich die Exposition in etwas mehr als einem Jahrzehnt (2008 bis 2021) lokal um das Drei- bis Zwanzigfache erhöhte.

Die vorliegende Dissertation liefert neue quantitative Erkenntnisse einerseits über die Suszeptibilität von moränengedämmten Seen für plötzliche Gletscherseeausbrüche (GLOFs) auf regionaler Ebene und andererseits, auf lokaler Ebene, über die Strömungsdynamik der sich talabwärtsbewegenden Flutwellen vergangener Ereignisse. Meine anschließende Untersuchung der Auswirkungen potenzieller künftiger natürlicher Dammbruchfluten auf exponierte Infrastruktur und (informelle) Siedlungen kann einen wertvollen Beitrag zu zukünftigen Multi-Risikobewertung für das Pokhara Tal leisten.

Acknowledgements

I am deeply grateful for the new experiences, exciting opportunities, and stimulating challenges I have encountered while working on this thesis over the past three and a half years. I wholeheartedly thank everyone who has supported me – both academically and emotionally – during this time.

First and foremost, I want to express my profound gratitude to my supervisors, PD Dr. Ariane Walz und Prof. Oliver Korup, who provided me with valuable guidance and encouragement throughout every stage of my PhD. Thank you very much for your trust and always having an open ear for all of my questions, regardless of them being of scientific or regulatory nature. You greatly helped me when navigating the scientific community and gave me endless opportunities to grow as a young scientist.

I also thank Dr. Sigrid Roessner for all the interesting discussions about my research and my academic carrier path. I am deeply grateful for your strong support and the confidence you gave me – I will always cherish the impressions and experiences made during our joint field visit to the Ahr valley.

A big thank you to Dr. Georg Veh for our stimulating conversations about everything GLOF-related and for providing many invaluable inputs to my manuscripts. I am also very grateful for your and Elisabeth Schönfeldt's support and company in the field, my visit to the Pokhara valley would have not been the same without you two. During this trip, I was very lucky to meet Prof. Monique Fort, who I deeply appreciate for sharing her endless knowledge on Pokhara and her fascinating experiences during decades of field work in Nepal. I am also thankful for Narayan Gurung's generous support in the field. Thank you to Dr. Amelie Stolle for providing me with data on the slackwater outcrop locations.

I am also very grateful for all the valuable opportunities the DFG Research Training Group "Natural Hazards and Risks in a Changing World" gave me and I especially thank Prof. Dr. Annegret Thieken and Prof. Dr. Axel Bronstert as the graduate school's speakers. During my time as a NatRiskChange member, I was not only able to significantly expand my knowledge and methodologic abilities but also spent many hours with amazing colleagues – some of which quickly became my best friends. Thank you for all the precious memories made together with you in these past years!

A big thank you to Matthias Kemter for proofreading this thesis.

I am also deeply thankful for the help provided by my two student assistances, Jana Brettin and Natalie Lützow, and the fruitful cooperation on Himalayan hazard cascades with my co-authors Karin Lehnigk and Prof. Isaac Larsen from the University of Massachusetts Amherst.

Finally, I wholeheartedly thank my parents and my partner for their love and emotional support during these – sometimes also challenging – past years. I would not have made it so far without you!

Declaration of Authorship

I, Melanie Fischer, hereby confirm that I have independently authored this thesis with the title "Outburst Floods in the Greater Himalayas - From Regional Susceptibility to Local Hazard". This thesis was done wholly while in candidature for a doctoral degree at the Institute of Environmental Science and Geography at the University of Potsdam. This thesis or parts of it have not been previously submitted for a degree or any other qualification at this or another university.

I further confirm, that…

… where studies were conducted jointly with co-authors, I state exactly what their and my contributions were in the declaration of authorship

… I clearly referenced where I have consulted the published work of others or additional sources, providing quotations where information was cited both in a literal or figurative sense

… I have acknowledged all main sources of help

_____

Location, Date

_____

Melanie Fischer

Contents

List of Figures

List of Tables

Abbreviations

BCE	before common era
BP	before present
CE	common era
CI	credible interval
DEM	digital elevation model
DRM	disaster risk management
EDW	elevation-dependent warming
EWS	early-warning system
GDP	Gross Domestic Product
GHCC	Greater Himalayan Crystalline
GLOF	glacial lake outburst flood
HDI	highest density interval
HKH	Hindu-Kush Himalayas
HKKHN	Hindu Kush-Karakoram-Himalaya-Nyainqentanglha
HMA	High Mountain Asia
ICIMOD	International Centre for Integrated Mountain Development
IPCC	Intergovernmental Panel on Climate Change
ka	thousand years ago
LHS	Lesser Himalayan Sequence
LIA	Little Ice Age
LLOF	landslide-dammed lake outburst flood
LOO(IC)	leave-one-out cross-validation (information criterion)
LULC	land use and land cover
Ma	million years ago
MCT	Main Central Thrust
NPR	Nepalese Rupee
OSM	OpenStreetMap
RCP	Representative Concentration Pathway
THS	Tethyan Himalayan Sequence
USD	US Dollar

1 Introduction

1.1 Motivation and Thesis Aims

In June of 2013, the sudden outburst of a glacial lake, a process known as a glacial lake outburst flood or GLOF, killed 6,000 inhabitants and pilgrims in the river valley downstream of the Chorabari glacier in the Indian Himalayas (Fig. 1.1; Allen et al., 2016b) – accounting for 95% of all documented fatalities from this rare cryospheric hazard across the whole of High Mountain Asia (Carrivick and Tweed, 2016). More recently, the outburst of a lake impounded behind landslide material, a landslide-dammed lake outburst flood or LLOF, in the headwaters of the Melamchi Khola heavily impacted a 800 million USD water supply project for Nepal's fast growing capital, Kathmandu (Petley, 2021a; Pokhrel, 2021).

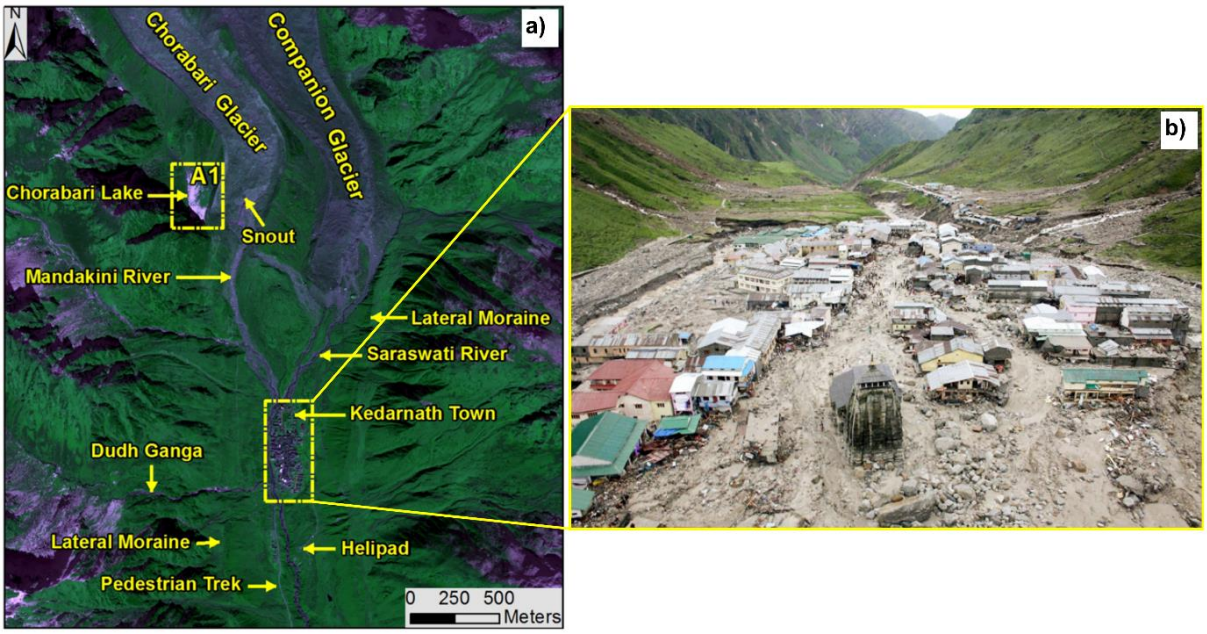

Figure 1.1: Outburst flood from a glacial lake of Chorabari glacier, Uttarakhand, India, also known as the Kedarnath disaster. a) Pre-disaster Worldview satellite imagery and map of the area adapted from Bhambri et al. (2016). b) Post-disaster aerial photo of Kedarnath town (© Reuters 2013; Nautiyal, 2013).

Changes in the global high-mountain cryosphere projected for the 21st century, including overall continued glacier-mass loss and associated growth of meltwater volumes stored in glacial lakes, might increase the occurrence rate of such potentially catastrophic outburst floods (Hock et al., 2019). Mergili et al. (2011a) specify that "Climate change, with its impact on the glacial extent, the hydrological cycle and the condition of ice-bearing dams, may condition the occurrence of GLOFs in manifold ways and on different time scales." Simultaneously, rapidly expanding human activities

and land use in alpine areas might raise the risks from outburst floods (Carrivick and Tweed, 2016). For example, in the Greater Himalayan region, which comprises the world's highest and most-extensively glaciated mountain ranges (>100,000 km^2 glacial cover; Hewitt, 2014), socio-economic projections predict a rapid growth in population numbers from 237 million in 2017 to 304 million in 2030 (Sharma et al., 2019). To meet the energetic needs of these expanding populations, an increasing number of large infrastructure investments in the form of hydropower plants are placed along mountainous rivers – two-third of which are located in the tracks of potential GLOFs (Schwanghart et al., 2016b). Although scientific interest concerning hazard and risks posed by sudden outburst floods in this region has significantly increased in the past decades (Emmer, 2018), fully-data driven approaches at a regional scale are missing. This is potentially caused by a lack of consistent information, owing to the region's size and the remoteness of many of its valleys, on top of its patchwork of political territories with past and ongoing intra- and interstate conflicts. Among these nations, Nepal, a developing country, has had – together with its neighbour Bhutan – the highest documented socio-economic impacts of glacial lake outbursts relative to their Gross Domestic Product (GDP) in the past, not only in the Greater Himalayas but worldwide (Carrivick and Tweed, 2016). Nepal is listed as one of the poorest countries worldwide, where 15% of the population lived below the poverty line (income of 1.90 USD per day) in 2010 (The World Bank, 2022). However, in the past decades, a major source of income emerged from its pre-2020 continuously growing tourism sector (Ministry of Forest and Environment, 2021). Indeed, tourism in Nepal appears to be a main driver of profound changes in both rural, along established trek routes, and urban areas as points of access to mountain treks, cultural sites, and high-mountain communities (Anup et al., 2015).

Pokhara, Nepal's second largest city, is a prime example of the rapid socio-economic changes affecting Himalayan and global high-mountain cities: population growth and rapid urbanisation since the 1970s have been accompanied by a shift from the agricultural to the service sector as the main provider of livelihoods for the local population (Fort et al., 2018). While Pokhara's role as a major tourist destination is likely going to grow following the opening of a new international airport, informal settlements of marginalised communities are expanding in close proximity to the valley's main river (Gurung et al., 2021). On the 5th of May, 2012, a sudden flood along the same river caused 72 fatalities and there is ample evidence for historic outburst floods of varying magnitudes in the valley's past (Gurung et al., 2015; Schwanghart et al., 2016a). Several preconditioning factors for potential future hazard cascades have been identified upstream of the city (Fort, 1987). Hence, Pokhara is a fast-growing city situated in a valley prone to outburst floods.

This thesis aims at a better understanding of all process chain links, following outburst flood generation, propagation, and impacts with both statistical and numerical state-of-the-art models. Using advanced modelling on the sparse available data, including information on the few remotely-sensed GLOF events in the Greater Himalayas during the past four decades as well as sedimentary evidence of a prominent recent example (May 2012 flood in Pokhara), this thesis challenges major constraints in current (glacial) lake outburst flood research. This thesis covers aspects ranging from outburst susceptibility at the lake-site at the regional scale to more detailed, local-scale appraisals of hazards and exposure, using Pokhara as a case example.

1.2 Outburst Floods

The term outburst flood is used to describe a geomorphic process chain, in which a quantity of water, which was naturally retained in a lake, is suddenly released and propagates downstream (Costa and Schuster, 1988). Outburst floods are highly mobile flows which often carry a characteristically high water and sediment load, providing them with remarkable erosion and accumulation dynamics (Kershaw et al., 2005). Thus, outburst floods often leave behind characteristic sediment tails in downstream river channels (Fig. 1.2; Veh et al., 2018). Worni et al. (2014) summarise that "Outburst floods […] are capable of traveling tens of kilometres to more than 100 km at velocities exceeding tens of kilometres per hour" and that "They are a serious threat because of their sudden onset, high-magnitude discharge, long runout distance, and their tendency to flow along existing river channels where humans and property are concentrated."

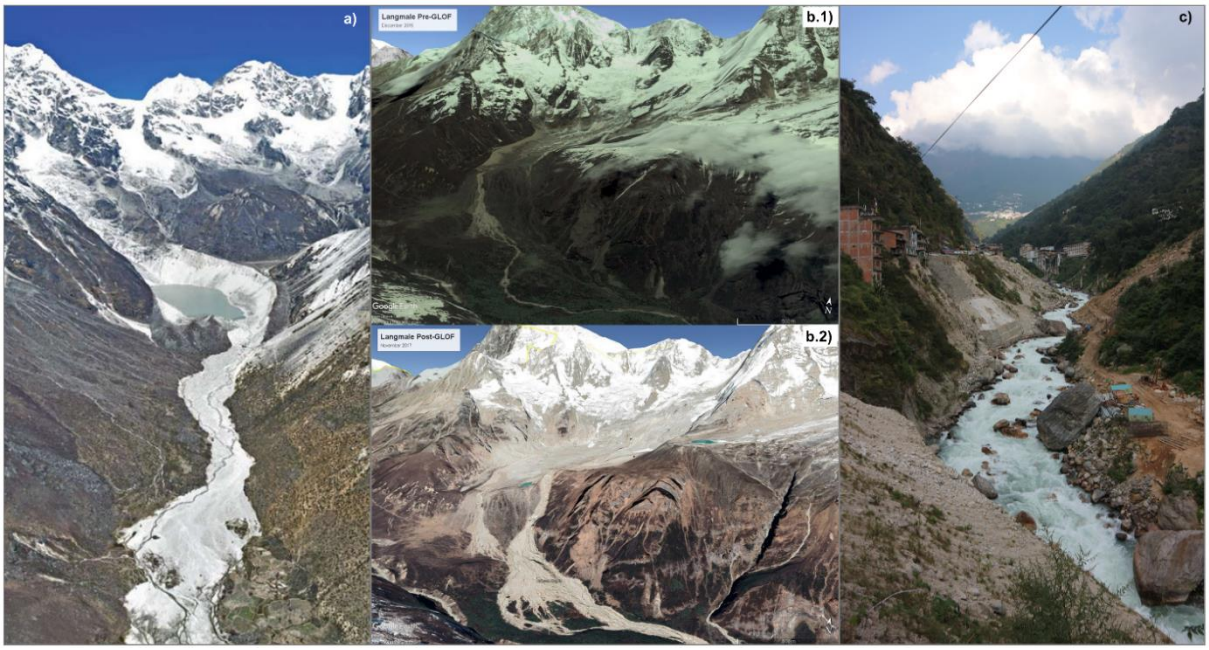

Figure 1.2: Geomorphic impacts of glacial lake outburst floods in the Greater Himalayan region. a) Geomorphic evidence of the 1985 Dig Tsho GLOF, Nepal, as seen in aerial imagery taken in April 2009 (Mool et al., 2011). b) Sediment deposition by the 2017 Langmale GLOF, Nepal, as seen in Google Earth imagery (© Google Earth 2015, 2017) taken before (b.1; December 2015) and after (b.2; November 2017) the outburst. c) Aftermath of the 2016 Bhotekoshi/Sunkoshi GLOF in the Nepalese river reach as seen during a field visit in October 2019.

1.2.1 Types of Outburst Floods

In this thesis, I consider two major types of outburst floods which occur in the high-alpine areas worldwide: glacial lake outburst floods (GLOFs) and landslide-dammed lake outburst floods (LLOFs). Although the Icelandic term jökulhlaup has often been used synonymously with GLOFs originating from lakes dammed by glacier ice (Emmer, 2018), I refrain from using this term to avoid confusion with outburst floods related to volcanic eruptions or geothermal fields (Björnsson and Pálsson, 2008).

GLOFs are described as the most common geomorphological processes affecting areas of high-altitude glacial recession (Iturrizaga, 2011; Richardson and Reynolds, 2000). Quaternary sedimentological records show that Pleistocene and early post-LGM (Last Glacial Maximum) GLOFs had far reaching impacts, which are unparalleled by modern day events (Costa and Schuster, 1988). Some of these reconstructed "megafloods" (with estimated peak discharges $>10^6$ m^3 s^{-1}; Baker, 2002) led to regional-scale landscape changes and temporarily modified ocean currents (O'Connor and Baker, 1992; Teller et al., 2002). Periodic ruptures of an ice-dam impounding Late Pleistocene glacial lake Missoula at around 16 ka BP caused a series of outburst floods along the Columbia River in the north-western USA and peak discharge estimates range between 7.6 and up to 17 x 10^6 m^3 s^{-1} (Lehnigk and Larsen, 2022; O'Connor and Baker, 1992). Along their outburst path, the Lake Missoula

Floods formed a distinct landscape consisting of erosional (i.e. scabland topography) and depositional (i.e. megaripples) geomorphological forms (Lehnigk and Larsen, 2022; Smith, 1993). Another series of megafloods in North America originated in the early Holocene (12.8 to 8.2 ka BP) from Lake Agassiz, a proglacial lake storing meltwater of the Laurentide Ice Shield (Fisher, 2004; Teller et al., 2002). Four reconstructed major outbursts from this lake into the North Atlantic, routed either via the Gulf of Mexico or the Hudson Bay, are linked to onsets of significant phases of climate cooling in the Northern Hemisphere: these substantial inputs of surface freshwater greatly affected the thermohaline circulation of the North Atlantic Deep Water conveyor belt and hence the transport of warm waters in the Gulf stream (Teller et al., 2002). Despite these continental to potentially global scale impacts of past GLOFs, documented recent (20th and 21st century CE) events have had impacts on landscapes and societies at a smaller and mostly local scale (Emmer, 2017). Between 1901 and 2017, 1,997 GLOFs have been observed in the six glaciated mountain ranges of the world (Andes, European Alps, High Mountain Asia, Iceland, Pacific Northwest, Scandinavia), while the average trend in the GLOF occurrence rate "[…] of +0.21 GLOFs yr^{-1} from 1901 to 1973 dropped by a quarter to +0.15 GLOFs yr^{-1} between 1973 and 2017." (Veh et al., 2022).

The formation and successive dynamics of GLOFs are to a first order influenced by the dam type their source-lake is impounded by (Emmer, 2017). These types are broadly distinguished into three major categories based on the dam's material (Emmer, 2017; Emmer and Cuřín, 2021): a) ice-dammed lakes (including supraglacial and englacial lakes as well as those dammed by ice and snow avalanche material), b) bedrock-dammed lakes (formed in ice-scoured depressions after glacial retreat), and c) moraine-dammed lakes (Emmer, 2017; Emmer and Cuřín, 2021; Hewitt and Liu, 2010). The latter can be formed by end-moraines or lateral moraines (Clague and Evans, 2000), and can alternatively be differentiated into moraine-dammed lakes formed by gently inclined valley glaciers or by steep hanging glaciers (Iturrizaga, 2011). Moraine-dammed lakes are currently mostly impounded behind moraines formed by glacier advances during the Little Ice Age (LIA, 16th to 19th century CE), which are commonly few tens of metres but up to >100 m high (Clague and Evans, 2000; Huggel et al., 2002). Clague and Evans (2000) further explain that these moraines are mostly "[…] steep-sided (up to ca. 40°) and have width-to-height ratios of 0.1—0.2 […]" which are "[…] generally smaller than those of landslide dams and comparable to those of constructed dams." Hitherto, the largest documented GLOF from a moraine-dammed lake is the sudden failure of the Laguna del Cerro Lago in Chile in 1989, which released an estimated outburst volume of 229 x 10^{6} m^{3} (Clague and Evans, 2000).

Landslides are a common natural hazard in high mountains as these geologically active areas provide ample source material as well as potential triggers, i.e. intense precipitation, snowmelt, and

seismic activity (Costa and Schuster, 1988). These landslides, most commonly in the form of rock avalanches or slides, and debris flows, can block river valleys and impound the river's water upstream of the landslide dam. The volume of impounded water is directly related to the geometry and volume of the dam, the blocked river's watershed characteristics including river discharge, and the valley morphology (Evans, 2006). Although landslide dams are more common in narrow, steep walled valleys, which can be blocked by a smaller amount of debris, Costa and Schuster (1988) identified five additional landslide-dam types based on their relation with the valley floor. The timing of sudden outburst of these landslide-dammed lakes or the longevity of the landslide dam is highly variable and ranges from few minutes to hundreds of years (Shrestha and Nakagawa, 2016). However, Costa and Schuster (1988) note that about a quarter of studied landslide dams failed within one day after their formation while half of the LLOFs occurred within 10 days after dam formation. Evans (2006), who studied the worldwide frequency of landslide-dam formation by large rock avalanches (>20 x 10^6 m^3 volume) in the 20^{th} century found that catastrophic LLOFs occurred at a frequency of one every 11.3 years and that landslide dams impounding large landslide-dammed lakes (>10^9 m^3 volume) formed every 50 years. Repeated formation of landslide-dammed lakes and subsequent outburst floods also have long-lasting effects on the geomorphology and sedimentology of mountain rivers, which is evident in the valley fill sequences of some intramontane basins (Hewitt, 1998; Korup and Tweed, 2007).

1.2.2 Outburst Flood Mechanisms

Geomorphic and societal impacts of outburst floods are the product of an entire process chain, which can be distinguished into three major stages: a) the trigger(s), b) overtopping and/or breach, and c) downstream flood propagation (Westoby et al., 2014).

Each outburst flood begins with (at least) one triggering mechanism as "Even unstable […] dams require a trigger event to initiate partial or complete dam failure and lake drainage." (Worni et al., 2014). Based on observations made at the time of or in the immediate aftermath of past events, a number of triggering mechanisms have been identified (Table 1.1 and Fig. 1.3; Costa and Schuster, 1988). One can distinguish between climatically driven triggers linked to patterns of precipitation, temperature, and insolation, and non-climatically driven triggers, which include mechanical failures of the dam as well as surrounding hill slopes (Clague and Evans, 2000; Westoby et al., 2014). Each of these triggers is potentially capable of causing a sudden lake outburst on their own or in combination with or even facilitating one another (i.e. cascading triggering mechanisms). For example, heavy precipitation might rapidly increase overland inflow into a lake and, hence, lead to a sudden increase in hydrostatic pressure acting onto the dam (Allen et al., 2019). Such rising lake

levels due to heavy rainfall and the subsequent failure of a natural dam were observed in the Ventisquero Negro GLOF (Patagonian Andes, Argentina) in 2009, which produced a peak discharge of 4,100 $m^3 s^{-1}$ (Worni et al., 2012). However, heavy precipitation can also trigger landslides, including rockfalls, rock slides, or rock avalanches, from the surrounding hillslopes, which might also enter the lake – potentially causing a displacement wave (GAPHAZ, 2017; Worni et al., 2014). A well-studied example of this common trigger (Haeberli et al., 2017) is the GLOF from the Laguna Safuna Alta, Cordillera Blanca, Peru, in 2002, which was caused by a seiche wave following the impact of a rock avalanche with a volume of 8–20 $\times$ 10^6 m^3 (Hubbard et al., 2005). Surprisingly, empirical evidence for earthquake-triggered outburst floods is rare (GAPHAZ, 2017; Kargel et al., 2015) and most documented cases are linked to the settlement and piping of at least two moraine dams in the Peruvian Andes following an earthquake in 1970 (Lliboutry et al., 1977). Eventually, an outburst flood in the upper parts of a drainage network can also trigger the sudden failures of other naturally impounded lakes situated downstream (Emmer, 2017). This cascading process was termed "multi-lake outburst flood" by Mergili et al. (2018) describing the 2012 flood in the Santa Cruz Valley, Cordillera Blanca, Peru, which involved the drainage of four lakes. Another prominent example for this type of trigger is the GLOF from moraine-dammed Lake Palcacocha, Peru, in 1941, in which an unknown trigger initiated the release of >10 $\times$ 10^6 m^3 of water (Somos-Valenzuela et al., 2016). The propagating flood wave caused a secondary outburst from the landslide-dammed Lake Jiracocha, some 8 km downstream, which added another 3-4.8 $\times$ 10^6 m^3 of flood water (Mergili et al., 2020). Some 15 km further downstream, this multi-lake outburst flood eventually reached the city of Huaraz, where it deposited 4-6 $\times$ 10^6 m^3 of material and caused between 1,800 and 5,000 fatalities (Carey, 2005; Mergili et al., 2020).

Table 1.1: Mechanisms reported or assumed to trigger sudden outbursts of naturally impounded lakes in high altitudes, compiled from Costa and Schuster (1988), Emmer (2017), Richardson and Reynolds (2000), and Westoby et al. (2014). (MDL = moraine-dammed lake; IDL = ice-dammed lake; BDL = bedrock-dammed lake; LDL = landslide-dammed lake)

Triggering mechanism	Trigger type	Lake type
Glacier calving and rapid mass movement from slope failure into lake causing displacement wave	climatic and non-climatic	MDL, IDL, BDL, LDL
Rapid mass movement from slope failure hitting dam	climatic and non-climatic	MDL, LDL
Heavy rainfall/snowmelt	climatic	MDL, IDL, BDL, LDL
Cascading processes (flood from lake situated upstream)	climatic and non-climatic	MDL, IDL, BDL, LDL
Earthquake	non-climatic	MDL, IDL, LDL
Ice core melting incorporated in dam/forming dam	climatic	MDL, IDL
Blocking of subsurface outflow tunnels	climatic and non-climatic	IDL, MDL, LDL
Long-term dam degradation (permafrost degradation, seepage, piping)	climatic and non-climatic	MDL, LDL

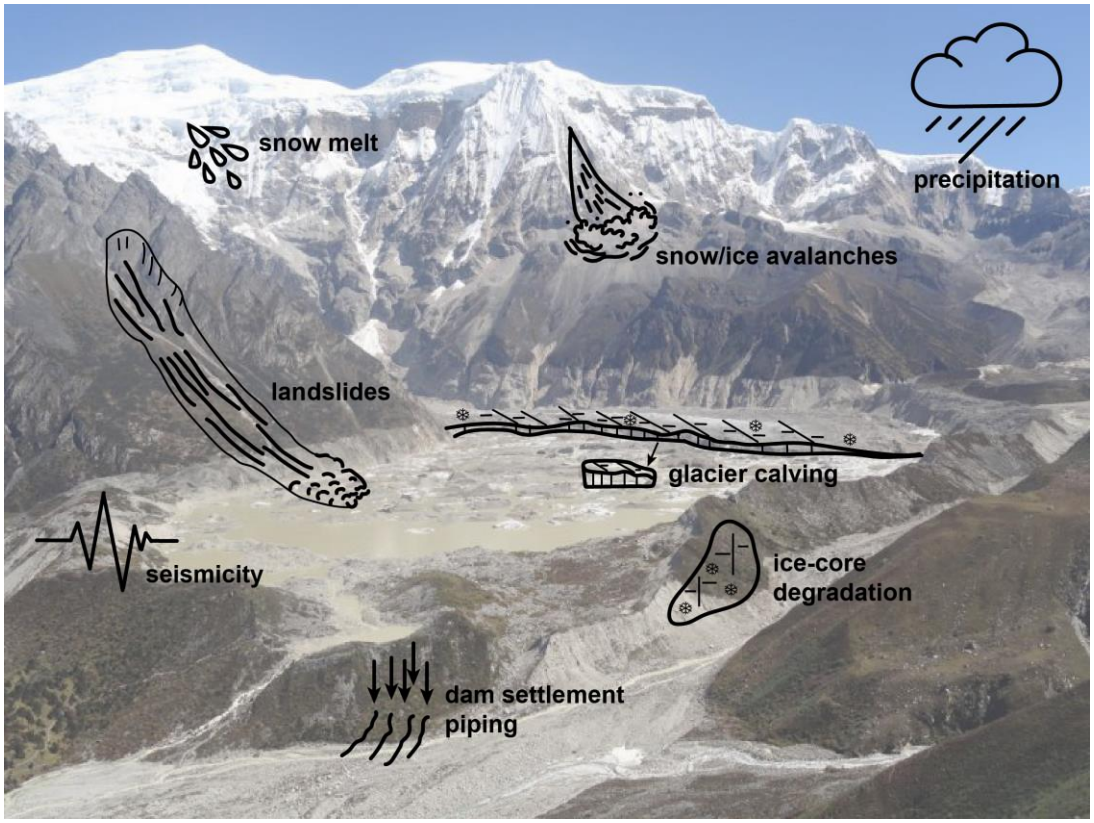

Figure 1.3: Selection of potential trigger mechanisms of outburst floods (not to scale). Background image shows Lake Thorthormi, Bhutan, sourced from Cole and Guiltenane (2020).

The two major outburst mechanisms, a) the overtopping of the dam caused by a displacement wave and b) the failure of the dam, largely depend on the dam type (Emmer and Cuřín, 2021). Whereas outburst from bedrock-dammed glacial lakes can be only facilitated by an overflow of water masses across the dam crest, both dam overtopping and breaching have been reported for outbursts from moraine-, ice-, and landslide-dammed lakes (Emmer, 2017). Emmer and Cuřín (2021) further state that "[…] GLOFs originating from dam failures have comparably larger volume of released water and might also have higher peak discharge comparing to GLOFs resulting from dam overtopping.". Sudden dam failures are caused by either internal processes, i.e. the gradual reduction of mechanical properties of the dam material, for example by thermokarst degradation, or external forces like the mechanical destruction by seismic activity or erosion by overflow (Westoby et al., 2014). Thus, shear stresses exerted on the dam during the latter mechanism can also lead to complete failure, given that they exceed the material strength of the dam (Korup and Tweed, 2007; Worni et al., 2013), which is directly linked to its material properties including lithological composition, cohesivity, and sorting (Costa and Schuster, 1988; McKillop and Clague, 2007b). Overtopping may involve channelised or unconfined sheet flow; and subsequent dam failure can result from either a gradually deepening incision into the dam, which starts at the steepest part of the dam where the outflow velocities are the highest (Worni et al., 2013), or a more lateral crest erosion. Regarding the former, Worni et al. (2013) further explain that "As the dam is incised, the breach sidewalls become steeper and fail when critical angles, related to the properties and pore water pressure of the dam material, are exceeded. Thus, the breach widens as it deepens, resulting in a progressive increase in the breach cross-section and increasing outflow." However, instances of channel armouring with coarse material and, hence, stabilisation of the outflow channels have been described for GLOFs from moraine-dammed lakes in British Columbia, Canada (Clague and Evans, 2000). These differences in outburst mechanisms are, besides the relation between lake and dam geometry (Walder and O'Connor, 1997), a major control on the shape of the outburst hydrograph (Westoby et al., 2014). This hydrograph shows the evolution of discharge (Q) out of the lake over time (T) and is an upper boundary condition for advanced unsteady-state hydraulic flood modelling (Fig. 1.4; Westoby et al., 2014; Zhang and Liu, 2015).

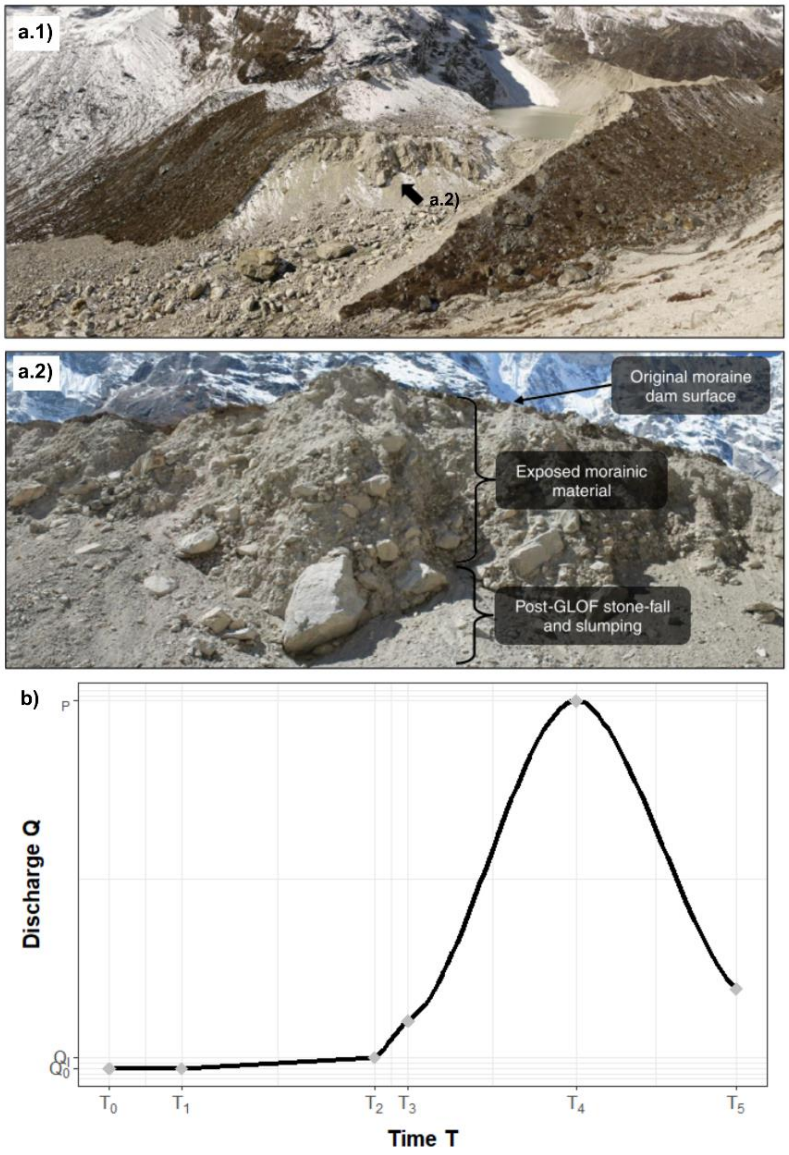

Figure 1.4: Moraine-dam breaches. a) Breach in the moraine dam of Dig Tsho, Nepal, (a.1) and detail of exposed moraine-dam sediments (a.2). b) Generic dam breach outflow hydrograph. Modified after Westoby et al. (2014).

The final outburst flood stage involves the downvalley motion of a flood wave, which is characterised by non-uniform, unsteady flow dynamics (Westoby et al., 2014). Worni et al. (2014) describe these outburst flood waves as "[…] highly dynamic processes - their volume and peak discharge can increase by a factor of three or more relative to initial values owing to erosion and entrainment of sediment.". However, when Cenderelli and Wohl (2001) compared the downstream flow behaviour of GLOFs with that of meteorological floods, they found that GLOF discharges attenuate downstream while the discharges of meteorological floods increase because of the inflow of tributaries and, hence, enlargement of the contributing drainage area. Although direct measurements are rare, Cook et al. (2018) were able to use seismic station data to analyse the flood wave propagation of the 2016 GLOF in the Bhotekoshi/Sunkoshi river, Nepal, which was caused by

the sudden release of 1.1×10^5 m^3 of water from Gongbatongshacuo Lake, China. They found that the initial water front (estimated peak discharge of 1,500 to 2,100 m^3 s^{-1}) travelled at a velocity of 8.7 m s^{-1} and was followed by a package of coarse sediments, transported as bedload at a velocity of 5 m s^{-1} (Cook et al., 2018). Flow hydraulics of outburst floods near the lake are mainly controlled by the outburst mechanism and discharge rate, but the availability of dam material for erosion and entrainment also plays an important role (Richardson and Reynolds, 2000; Westoby et al., 2014). Further downstream, characteristics of the channel and valley floor, including channel morphology, surface roughness, vegetation density, and sediment availability, become the dominant controls of flow dynamics (Kershaw et al., 2005; Westoby et al., 2014). Entrainment of sediment can lead to a transition from turbulent and low-viscose clear-water floods to hyperconcentrated flows (sediment makes up c. 20% of flood volume) and eventually laminar and high-viscose debris flows (Westoby et al., 2014; Worni et al., 2014). The average channel slope may also have an effect on the flow behaviour as outburst-generated debris flows rarely propagated in valleys with average inclinations below 11°, as shown in the Alps by Huggel et al. (2002). For outburst floods with higher water contents, this peak-discharge-dependent critical slope is lower and they have greater runout distances (Huggel et al., 2002). Thus, the viscosity of outburst floods has implications when assessing the hazards they pose to downstream infrastructure and settlements (Huggel et al., 2004).

1.2.3 Hazards and Risks from Outburst Floods

Judging from existing reports, outburst floods occur less frequently than other natural hazards in the mountain cryosphere, including ice or snow avalanches, landslides, and rock falls. Coupled with generally high distances between source and impact areas, exceeding 100 km in some reported events (Richardson and Reynolds, 2000; Turzewski et al., 2019), the populations living in the paths of past outburst floods were often not aware or prepared for this hazard (Mergili et al., 2011). The swiftly moving flood waves of outburst floods often hit populated areas along downstream river reaches unexpectedly or with little warning time (Kargel et al., 2013).

Outburst floods have affected mountain societies worldwide and they are reported to have caused numerous fatalities, loss of property, and extensive damage to infrastructure, in particular bridges and hydropower schemes (Clague and Evans, 2000; McKillop and Clague, 2007b). Particularly large prehistoric events even might have had major cultural consequences (i.e. Yellow River Flood of 1920 BCE facilitating cultural transition from Neolithic to Bronze Age in the Yellow River valley; Wu et al., 2016). The highest historically documented death toll caused by an outburst flood occurred during the Dadu River flood of 1786, in which the failure of an earthquake-triggered landslide dam in south-western China caused approximately 100,000 fatalities (Dai et al., 2005). Considering GLOFs since

1900, Carrivick and Tweed (2016) propose that 36% of them had societal impacts, including >12,000 deaths worldwide. In contrast, Richardson and Reynolds (2000) report on 32,000 GLOF-related fatalities in Peru in the 20th century alone. In the past two centuries, outburst floods had the highest societal impacts in the mountains of South America (especially the Cordillera Blanca, Peru) and Asia (especially the Greater Himalayas). The two most devastating events, the Palcacocha GLOF of 1941 (Huaráz, Peru) and the Chorabari GLOF of 2013 ("Kedarnath disaster", India) caused nearly 90% of all reported losses in human lives (Carrivick and Tweed, 2016). Glacier retreat in high-mountain areas due to atmospheric warming coupled with rapid population growth and resulting land-use pressures led to an increased exposure and vulnerability to outburst floods in the past few decades (Hock et al., 2019; Richardson and Reynolds, 2000): Glacier forefields and the valleys downstream become increasingly denser populated and economically exploited, including the extraction of water for irrigation and hydropower generation and the development of tourism infrastructure (McKillop and Clague, 2007a). The associated rapid expansion of, often haphazardly constructed, mountain road networks contributes to global outburst flood exposure but also directly facilitates landslides, which could potentially form unstable landslide dams (Sidle and Ziegler, 2012).

Although pioneered in the Cordillera Blanca in the 1940s, global administrative awareness of the outburst flood hazard has increased since the 1990s and a growing number of disaster risk management (DRM; UNISDR, 2009) frameworks have been developed for the Andes (Carey et al., 2012; Emmer et al., 2018), the Alps (Haeberli et al., 2001; Schaub et al., 2013), and the Greater Himalayan region (Ives et al., 2010; Reynolds, 1998). Risk prevention and preparedness constitute the ex-ante phase of the DRM cycle (UNISDR, 2009), and numerous examples for structural and non-structural mitigation strategies of outburst flood hazard have been implemented accordingly (Emmer et al., 2018; Wang et al., 2022). Common engineering solutions include dam remediation, lake-level lowering through artificial outlets (tunnels, concrete outflows, open cuts) as well as flood protection measures (flood walls); while non-structural efforts include early-warning systems, land-use planning, and public awareness campaigns (Emmer et al., 2018).

1.3 The Greater Himalayan Region

This thesis focuses on outburst floods in the Greater Himalayan region, which is defined here as the mountainous region spanning from 16° to 39°N and 61° to 105° E. This definition includes seven Asian mountain ranges, which comprise from east to west the Hindu-Kush, the Karakoram, the Western Himalaya, the Central Himalaya, the Eastern Himalaya, the Nyainqentanglha, and the Hengduan Shan, i.e. the Hindu Kush-Karakoram-Himalayas-Nyainqentanglha region or HKKHN (Fig. 1.5). This subdivision follows the distinctions made by Veh et al. (2020) and is based on

categorisations of High Mountain Asia applied by Brun et al. (2017) and in the Randolph Glacier Inventory (RGI Consortium, 2017).

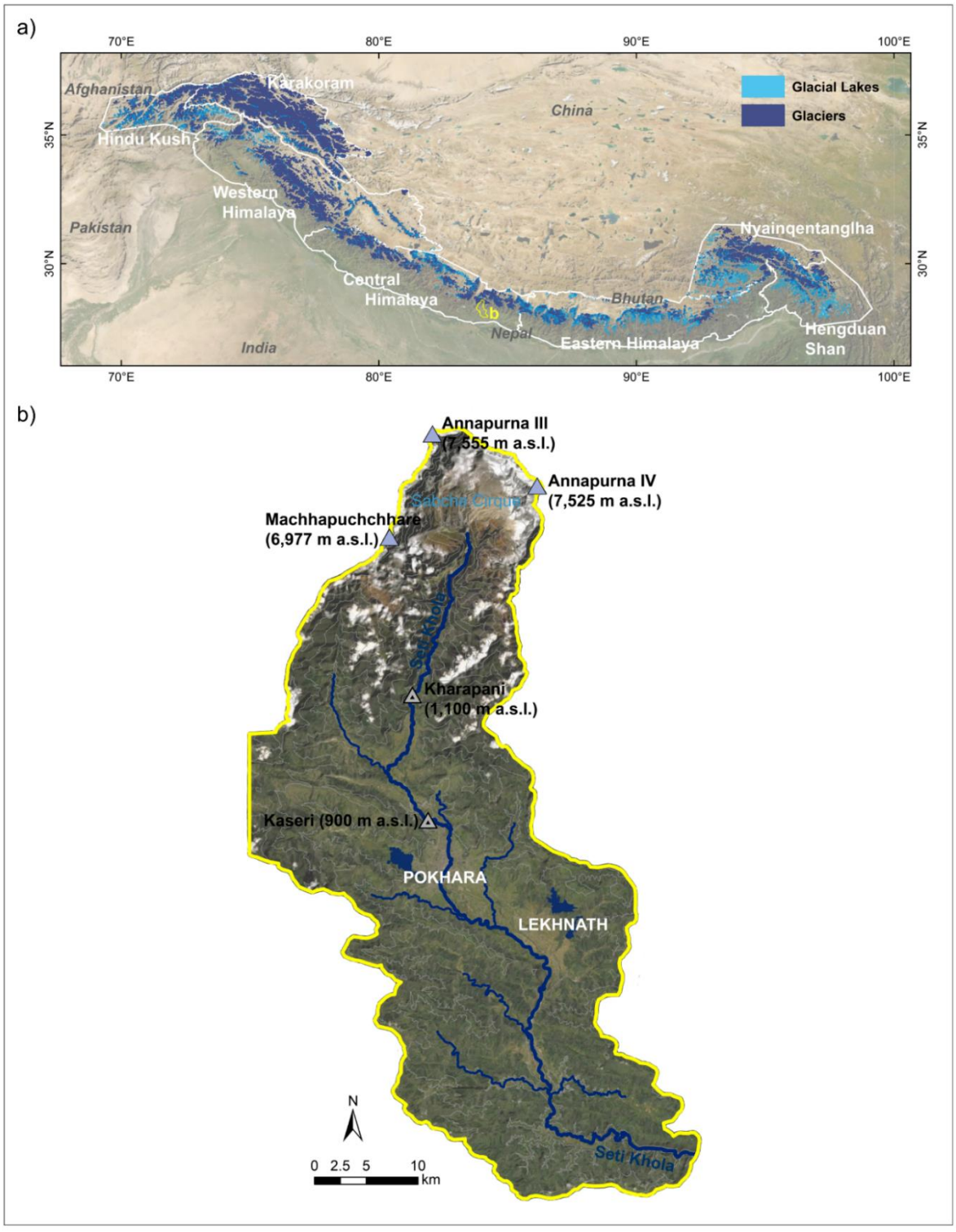

Figure 1.5: Greater Himalayan region and Pokhara valley. a) Distribution of glaciers (RGI Consortium, 2017) and glacial lakes (Maharjan et al., 2018) across the Hindu Kush-Karakoram-Himalayas-Nyainqentanglha, displayed on ESRI basemap Maxar satellite imagery (ESRI and Maxar Technologies, 2022). Yellow outline labelled "b" marks the location of the Pokhara valley within the Greater Himalayan region. b) Pokhara valley and course of its main river, the Seti Khola, which originates on some >5,000 m a.s.l. in the Sabche Cirque. Displayed on ESRI basemap Maxar satellite imagery (ESRI and Maxar Technologies, 2022).

1.3.1 Geology of the Greater Himalayan Region

The distinct mountain arc of the Greater Himalayan region is formed by a thrust-and-fold belt which is the result of the world's youngest and archetypical continent-continent collision, i.e. the ongoing northward subduction of the Indian beneath the Eurasian crustal plate, which began in Paleocene to Eocene times (65 to 55 Ma BP) (Dhital, 2015; Yin, 2006). The subsequent tectonic activity along a >2,500-km long front caused crustal shortening and >70 km of crustal thickening (Hewitt, 2014). The geologic architecture of the region is most variable along strike and reflective of a sequential deformation caused by an oblique collision style, in which first the north-western and, after an anticlockwise rotation, the north-eastern parts of the Indian Plate were subducted (Dhital, 2015). Initial collision occurred along the Indus-Tsangpo Suture Zone, which consists of the heavily diagenetically altered remnants of the Tethys ocean floor and forms the tectonic boundary between the Tibetan Plateau with the Lhasa terrane, which is a microcontinent of the Eurasian plate, to the north and the Himalayas on the northern edge of the Indian plate to the south (Dhital, 2015; Yin and Harrison, 2000).

Although alternating terminologies have evolved during the years, most authors agree that the Himalayan orogen itself comprises four major lithostratigraphic units, each bound by a major tectonic structure (Yin, 2006). The core of the orogen includes the highest mountain peaks and is formed by the high-grade metamorphic Paleoproterozoic to Ordovician rocks of the Greater Himalayan Crystalline Complex (GHCC), also often referred to as the Higher Himalayas. The Higher Himalayas are bound towards the sedimentary rocks of the Tethyan Himalayan Sequence (THS, Late Precambrian to Eocene, also Tethyan Himalaya) in the north by the South Tibet Detachment and delimited in the south by the Main Central Thrust (MCT) (Yin and Harrison, 2000). The Main Central Thrust's footwall comprises the Lesser Himalayan Sequence (LHS, also Lesser Himalaya), which predominantly consists of metasediments and metavolcanites of Proterozoic to Cambrian age (Yin, 2006). The Lesser Himalaya is, in turn, bound in the south by the Main Boundary Thrust towards the Cenozoic continental strata of the Sub-Himalayan Sequence or the Siwaliks (Group) (Decelles et al., 2001; Dhital, 2015). The Main Frontal Thrust structurally delineates the orogen's southern toe towards the foreland basin of the Ganges Plains in the south (Decelles et al., 2001; Yin and Harrison, 2000). Exhumation rates along these major fault zones have greatly varied since the onset of the collisional regime. Ongoing post-collisional deformation by reactivation of the MCT and other faults produces seismic activity and recent uplift rates of c. 3 mm and locally even up to 10 mm per year (Hewitt, 2014; Yin, 2006).

Intramontane basins in the Greater Himalayan region also reflect the along-strike variations in deformation as they become progressively more elongated and narrower towards the eastern parts

of the mountain belt (Yin, 2006). The sediment fills of these valleys record the postglacial developments of river systems still present today and many of them document major aggradation episodes due to temporary blockages behind natural dams and subsequent outbursts (Hewitt, 2014).

1.3.2 Geography of the Greater Himalayan Region

The >2,500 km long and mostly 200 km to 400 km wide mountain belt of the HKKHN describes a prominent southward-convex arc with a radius of c. 1,500 km in its central parts, while its north-western and south-eastern continuations both form sharp syntaxial bends towards the south (Dhital, 2015). The rugged topography of the study area covers 0.89 million km^2 and comprises all of the world's 14 mountain peaks with an elevation >8,000 m a.s.l., most of which are located in the central and eastern Himalayas. Although elevations >6.000 m a.s.l. occur throughout the mountain belt, elevation increases eastward on average (Yin, 2006). A variation in topography can also be seen across the mountain belt: while the footwalls of the Lesser and Higher Himalayas form a distinct two-step topography in the central Himalayas, this break is absent in the eastern and north-western parts where high relief is closer to the range front (Bookhagen and Burbank, 2006).

The Greater Himalayan region has an area of >100,000 km^2 covered by the highest concentrations of glaciers and perennial snow found outside of the polar regions and is, hence, often referred to as "The Third Pole" (Hewitt, 2014). Meltwaters of these high-altitude ice masses feed into major Asian river systems, which provide water to 1.3 billion people living in the downstream lowlands (Molden et al., 2014). The HKKHN is the "water tower" of five of these major rivers as it comprises the alpine catchments of the Amu Darya, the Irrawaddy, the Indus, the Ganges, and the Yarlung Zangbo or Brahmaputra (Immerzeel et al., 2010; Scott et al., 2019). The latter three comprise large antecedent Cretaceous river systems of the Greater Himalayan region, whose drainage pattern has seen dramatic changes during the course of the orogeny (Dhital, 2015; Yin, 2006).

The discharge of these rivers is greatly influenced by the regional climate and synoptic weather patterns modulated by the rugged mountain topography (Krishnan et al., 2019; Palazzi et al., 2013): while alpine climate conditions prevail, tropical to subtropical climates characterise the southern lowlands and the low-elevation intramontane valley floors. Apart from topographic effects, climate and weather patterns along the HKKHN are also strongly affected by large external drivers like the North Atlantic Oscillation, the El Niño–Southern Oscillation, and the Indian Ocean Dipole (Krishnan et al., 2019). The main source of precipitation from humid air masses along the mountain belt is the Bay of Bengal towards the south-east, which causes a distinct east to west gradient in rainfall (Krishnan et al., 2019). A second major precipitation gradient runs south-north, with humid

conditions towards the Ganges Plain and arid conditions toward the Tibetan Plateau (Bookhagen and Burbank, 2006). This gradient is influenced by the topographic relief along the HKKHN, which forms a mountain barrier for moist air rolling in from the Indian Ocean and, hence, causes a strong orographic effect along its southern flanks (Bookhagen and Burbank, 2006). Precipitation along the HKKHN is also distinctly seasonal with the Indian Summer Monsoon bringing high amounts of snow and rainfall from June to September. This synoptic regime, which is part of the Intertropical Convergence Zone and caused by a strong air pressure gradient between the Indian Ocean and the Tibetan Plateau, produces the bulk of annual precipitation that falls in the Greater Himalayas' central and eastern parts (Krishnan et al., 2019). Although monsoonal precipitation is also affecting western regions, most precipitation there falls during winter (Hewitt, 2014; Palazzi et al., 2013). Moist air masses are brought by extra-tropical western disturbances, a synoptic-scale regime which is also often referred to as (winter) westerlies (Krishnan et al., 2019). Heavy precipitation of these westerlies predominantly falls as snow and many glaciers of the Karakoram receive >1,000 mm of water equivalent (w.e.) each year on average (Hewitt, 2014).

The HKKHN is home to an estimated 250 million people who live in the territories of the eight riparian states Afghanistan, Bangladesh, Bhutan, China, India, Myanmar, Nepal, and Pakistan (Schild, 2008). While the HKKHN's high-mountain areas are sparsely populated, a number of metropolitan areas are located in the mountain arc's intramontane valleys. Kabul, the capital of Afghanistan, with 3.5 million inhabitants in 2013, is the most populous of these high-mountain cities, followed by Nepal's capital, Kathmandu, with a population of c. 2.5 million in 2012 (Scott et al., 2019). However, a majority of the HKKHN's population lives in rural areas while population density is highest along the southern border of the Higher Himalayan arc (Wang et al., 2019).

1.3.3 Changes in the Greater Himalayan Cryosphere and Anthroposphere

Brun et al. (2017) estimated, that glaciers across High Mountain Asia (HMA, i.e. the HKKHN region plus the Tibetan Plateau, Pamir, and Tien-Shan) lost 0.18 ± 0.04 m w.e. yr^{-1} of their mass between 2000 and 2017, a continuation of the net negative trends in ice-mass budget documented for the five decades prior (Bolch et al., 2012). Focusing on the Himalayas, Maurer et al. (2019) propose a doubling of the average ice-loss rate between the 1975 to 2000 interval (–0.22 ± 0.13 m w.e. yr^{-1}) and the 2000 to 2016 interval (–0.43 ± 0.14 m w.e. yr^{-1}). The overall negative glacier-mass balance trend is accompanied by an observed decrease in glacier length (i.e. increase in glacial retreat) and increased glacier-ice thinning (Bolch et al., 2019).

However, these trends in glacier dynamics are heterogeneous across the study area's regions: while eastern parts of the HKKHN, particularly the Nyainqentanglha, have seen strong continuous

negative glacier-mass balance trends in the past decades (Brun et al., 2017), high-altitude glaciers of the Western Himalayas and the Karakoram showed constant or even increased ice masses since the 1990s, a phenomenon known as "Karakoram Anomaly" (Bolch et al., 2012, 2019; Hewitt, 2005). Although differences in debris cover have been discussed as a potential cause of this divergent glacial response to rising air temperature (Hewitt, 2005), recent work has found synoptical-scale meteorological forcings to be more plausible (Kapnick et al., 2014). In detail, the difference in seasonal weather patterns across the HKKHN leads to monsoon-driven snowfall maxima during summer across the eastern HKKHN while glaciers in the western HKKHN are predominantly fed by heavy precipitation falling as snow provided by the winter westerlies (Kapnick et al., 2014; Krishnan et al., 2019).

Apart from these regional-scale differences in glacier-mass balances across the Greater Himalayan region, King et al. (2019) propose that at a local scale, ice-mass loss rates were nearly doubled in glaciers which had a terminus in direct contact with glacial lakes compared to those terminating on land. These glacial lakes have been growing in number but also in area and depth (King et al., 2019), as the total glacial lake area expanded by 14% between 1990 and 2015 in the Himalayas (Nie et al., 2017) and by 15% between 1990 and 2018 across whole High Mountain Asia (Wang et al., 2020). Additional recently published regional inventories of glacial lakes in the Greater Himalayan region and neighbouring mountain ranges include the studies by Maharjan et al. (2018; HKH, static, lakes mapped from scenes aquired between 2004 and 2007), Chen et al. (2021; HMA, annual, lakes mapped from scenes aquired between 2008 and 2017), Zheng et al. (2021; HMA, lakes mapped from scenes aquired between 2014 and 2018) – all mapped from optical Landsat satellite imagery.

These and other changes to the HKKHN's cryosphere, including an observed reduction in snowfall and changing permafrost distributions (Bolch et al., 2019), can be at least partially traced back to an increase in air temperatures across the region of 0.1 °C per decade in the 20th and beginning 21st century (Krishnan et al., 2019). This observed warming might be related to the concept of elevation-dependent warming (EDW), which poses that increases in the temperature of the global air masses are most pronounced in high-mountain areas and that it "has important implications for the mass balance of the high-altitude cryosphere and associated runoff; [and] for ecosystems and farming communities in high-mountain environments […]" (Pepin et al., 2015). High-mountain processes that are thought to contribute to EDW include the snow albedo feedback, aerosol pollutants, and changes in water vapour and radiative fluxes (Pepin et al., 2015). Although the applicability of this concept is still discussed for some of the world's mountain ranges, for example in the European Alps (Tudoroiu et al., 2016), it has been described as highly relevant in the Greater Himalayan region (Krishnan et al., 2019; Palazzi et al., 2017).

Current projections for the cryosphere in the HKKHN generally assume a continuation of these trends observed in the past (Bolch et al., 2019; Hock et al., 2019). By the end of the 21st century, decreased snow precipitation at lower elevations and extended thawing seasons might cause an overall loss of glacier mass by 36 ± 7% (Representative Concentration Pathway RCP2.6) or even up to 64 ± 5% (RCP8.5) (Kraaijenbrink et al., 2017).

The past cryospheric changes have been accompanied by rapid developments in human activities in past decades: first and foremost, the overall socio-economic status of the HKKHN's population has improved, judging from a steep decline in fertility rates coupled with an increase in life expectancy (Wang et al., 2019). Urbanisation has been rapid since the 1990s and its major drivers are increased industrialisation and rural-to-urban migration, and the inflow of refugees from conflicts and natural disasters (Schild, 2008; Wang et al., 2019). These refugees predominantly move into informal settlements, which emerge along the peripheries of cities and larger towns (Wang et al., 2019). The United Nations define informal settlements as "[…] 1. areas where groups of housing units have been constructed on land that the occupants have no legal claim to, or occupy illegally; 2. unplanned settlements and areas where housing is not in compliance with current planning and building regulations (unauthorized housing)." (United Nations Department of Economic and Social Affairs, 1997).

Although all of the study area's riparian states have been undergoing a transformation from subsistence to market-driven economies in the second half of the 20th century, rates of economic growth have been highly diverse and partially hampered by inner conflicts and difficulties in transborder trade of goods (Wang et al., 2019). The tourism sector, including leisure activities but also religious pilgrimages, has rapidly expanded since the 1970 and plays a major role in low-GDP countries like Nepal, where it is considered as "[…] a vehicle for socio-economic development and prosperity because of its significant potential for earning foreign exchange, creating employment, reducing income and employment disparities, strengthening linkages among economic sectors, and helping alleviate poverty." (Ministry of Forest and Environment, 2021). Simultaneously, hard infrastructure in the form of (predominantly unpaved) roads has been rapidly expanding, especially in Bhutan and Nepal, where these major engineering projects have also been built with international support (Wang et al., 2019). Improved socio-economic status also resulted in a growing energy need, which led to a rise in the number of hydropower facilities harvesting some 20% of the Himalaya's >500-GW hydropower potential (Schwanghart et al., 2016b). For economies like Nepal and Bhutan, hydropower projects are large, but potentially sustainable, economic investments (Carrivick and Tweed, 2016; Richardson and Reynolds, 2000), which are often exposed to natural hazards – including outburst floods (Schwanghart et al., 2016b) but also other high-mountain hazards like

earthquakes (e.g. the 2015 Ghorka earthquake; Schwanghart et al., 2018) and landslides (e.g. the 2021 Chamoli disaster; Shugar et al., 2021). Nevertheless, the Greater Himalayan region is considered to be one of the hotspots of hydropower development worldwide in the near future (Schwanghart et al., 2018).

1.3.4 Past Outbursts in the Greater Himalayan Region

During phases of pronounced deglaciation in the course of the Quaternary, especially after the Last Glacial Period (c. 20 ka BP), outburst flood events have been a prominent geomorphologic process to shape the valley floors of intramontane basins in the Greater Himalayan region (Hewitt, 2014; Richardson and Reynolds, 2000). Peak discharge reconstructions of some of these outbursts are greater than 10^6 m^3 s^{-1} and, hence, warrant their definition as "megafloods" (Montgomery et al., 2004). The deposits of these cataclysmic events of the Pleistocene interglacial periods and the Holocene are evident in the geological record of many valley fill sequences across the HKKHN range (Iturrizaga, 2011). There, sedimentary evidence of GLOFs was used to reconstruct glacial fluctuations and regional palaeoclimate for at least 12.6 ka BP (Iturrizaga, 2011; Richardson and Reynolds, 2000). A prominent example is a GLOF originating from palaeo-lake Batal that happened between 26.9 and 43.4 ka BP in the Lahul Himalayas of northern India (Coxon et al., 1996). There, discontinuous, but laterally extensive beds of bouldery diamicts in the Chandra valley's sediment fill allow some estimates of the outburst flood, which may have had a flood volume of 1.5 km^3 and a peak discharge of 21,000 to 27,000 m^3/s (Coxon et al., 1996). Yet, higher discharges have been inferred for outbursts from large former lakes on the Tibetan Plateau, which drained along the Tsangpo River some 9.9 ka BP ago (Montgomery et al., 2004). Estimates based on reconstructed lake volumes reveal a potential peak discharge Q_p of 1-5 x 10^6 m^3 s^{-1}, while unit stream power estimates indicate high erosive potential (Korup and Montgomery, 2008; Montgomery et al., 2004).

A number of authors have worked towards an as complete as possible compilation of GLOFs since the beginning of the 20th century by reviewing and compiling literature and eye-witness reports (Carrivick and Tweed, 2016; Mool et al., 2011; Richardson and Reynolds, 2000) as well as mapping from remote-sensing data (Nie et al., 2017; Veh et al., 2019; Zheng et al., 2021b). Harrison et al. (2018) used these GLOF inventories of the HKKHN to propose their lag-time concept, which relates the observed worldwide increase in GLOF frequency in the 1930 to a lagged response of the glacial system to climate forcing by the post-LIA atmospheric warming. Based on their updated GLOF inventory, Veh et al. (2019) propose that the average frequency of 1.3 GLOFs per year in the HKKHN remained constant over the past four decades. This finding is at odds with that of Richardson and Reynolds (2000), who argued that GLOF frequency was increasing throughout the 20th century. This

mismatch might be the effect of reporting biases, which are inherent to literature and eye-witnessed-based GLOF compilations. In detail, factors like low outburst flood volumes or low population densities in the affected valleys potentially decrease the chance of a GLOF to be reported or even witnessed (Veh et al., 2018, 2019).

The most frequently documented processes (56%) to trigger GLOFs in the Greater Himalayan region were ice avalanches and glacier calving that led to displacement waves and subsequent dam overtopping (Gurung et al., 2017; Richardson and Reynolds, 2000; Rounce et al., 2016). Although the HKKHN is a seismically active region, as last seen in the 2015 Gorkha earthquake (M7.8), none of the known recent GLOFs in this region was triggered by earthquakes (Kargel et al., 2015). Worldwide, reported outburst flood discharges are generally an order of magnitude greater than peak discharges reached in seasonal floods triggered by high precipitation (Iturrizaga, 2011). For the south and south-eastern HKKHN, these climatic seasonal high flow floods of the late spring to early autumn are caused by the combined effects of melting of snow and glaciers at higher elevations as well as increased precipitation by the Indian Summer Monsoon. Discharges generated by documented GLOFs in the Nepal Himalayas of the 1970s and 1980s were up to 60 times greater than those of seasonal meteorological floods in the same period (Cenderelli and Wohl, 2003). However, the few HKKHN GLOFs with known outburst date also show some seasonality: they mainly happened between June and October, which might be linked to increased lake levels and pronounced glacier calving due to high monsoonal precipitation and summer ablation (Richardson and Reynolds, 2000).

Past outburst floods in the Greater Himalayan region have caused intense societal impacts in its riparian states, including high infrastructural damage and fatality counts (Carrivick and Tweed, 2016). Based on the countries' GDP, Bhutan and Nepal are potentially facing the greatest relative economic consequences when impacted by outburst floods, especially concerning the possible destruction of mature hydropower schemes (Carrivick and Tweed, 2016; Schwanghart et al., 2016b). Although not an outburst flood *sensu strictu*, the highly mobile rock and ice avalanche of the 2021 Chamoli disaster is a prominent example of the destructive impact of hazard cascades on major infrastructure projects in the Greater Himalayas (Shugar et al., 2021). This issue was first recognised in the aftermath of the Dig Tsho GLOF event of August 1985 (flood volume 6-10 x 10^6 m^3, peak discharge 2,000 m^3 s^{-1}), which caused five fatalities and destroyed – besides numerous communal buildings and infrastructure – also a run-of-the-river hydropower scheme in the Nepal Himalayas (Mool et al., 2011; Richardson and Reynolds, 2000). A prominent example for a LLOF in the Greater Himalayas is the 2000 Yigong outburst of a temporary, rockslide-dammed lake, which had an estimated flood volume of >2 Gm^3 and a >500 km runout distance – affecting major transportation

infrastructure and killing >90 persons in China and northern India (Delaney and Evans, 2015). More recently, an outburst of a presumably landslide-dammed lake along the Melamchi Khola caused several fatalities and damage to numerous bridges but also heavily impacted the drinking water supply for the Nepalese capital Kathmandu (Maharjan et al., 2021; Petley, 2021a).

The hitherto most destructive GLOF in the HKKHN originated from a small seasonal periglacial lake of Chorabari glacier (Rafiq et al., 2019). The flood had a peak discharge of 1,700 $m^3 s^{-1}$ and principally contributed to the death of c. 6,000 persons in the upper part of the Mandakini river valley, Uttarakhand, northern India in June 2013 (Allen et al., 2016b; Carrivick and Tweed, 2016). Heavy rainfall due to an early onset of the monsoon as well as rapid snowmelt led to increased surface runoff into the lake, causing a hydrostatic dam failure (Allen et al., 2016b; Bhambri et al., 2016). Thus, the Chorabari GLOF remains the only documented case of a hydro-meteorologically-triggered GLOF in the HKKHN region (Allen et al., 2016b). The Chorabari GLOF as well as multiple associated smaller, rainfall-triggered landslides also caused severe damage to settlements and infrastructure, including the complete or partial destruction of 30 hydropower schemes (Allen et al., 2016b).

1.4 The Pokhara Valley, Nepal

A large part of my studies of outburst floods is focused on the Pokhara valley, which is situated in the Central Himalayas of Nepal (Fig. 1.5). On an administrative level, the valley belongs to the Gandaki province of central Nepal and its major population centre, the city of Pokhara, is the capital of the Kaski province. The valley's main drainage system is the Seti Khola (Khola = river), which is the lifeline of more than half a million people living in the Pokhara valley, but also has a history of sudden sediment pulses (Central Bureau of Statistics, 2022; Stolle et al., 2017).

1.4.1 Geology of the Pokhara Valley

The Pokhara valley is part of a series of elongated intramontane basins in the Midland or Pahar Zone between the Higher and Lesser Himalayas and it is crossed in its northernmost parts by the MCT in approx. west-north-west to east-south-east strike. Thus, the valley is bordered towards the north by rocks of the Higher Himalayas, mostly high-grade metamorphic quartzites and gneisses of the GHCC, and marine metasediments and limestones of the THS. Most bedrock in the valley consists of Proterozoic and Paleozoic metasandstones, phyllites, amphibolites, and schists of the LHS (Dhital, 2015; Schwanghart et al., 2016a).

The Quaternary valley fill, described as "[…] a product of natural catastrophe" (Fort, 2010), constitutes of a large alluvial fan with an area of c. 125 km^2 and an estimated volume of >4 x 10^9 m^3 (Blöthe and Korup, 2013; Fort, 2010). Similar to the fluviatile lacustrine origin of the Kathmandu valley infill (Dangol, 1985), the several hundred metre thick stratigraphic record of the Pokhara valley was assigned to lacustrine sedimentation by early researches (Hagen, 1969) but soon after interpreted as having a LGM glacio-fluvial origin (Hormann, 1974). Today, the valley fill, which mostly consists of Higher Himalayan material originating from the Annapurna massif, is distinguished into three major depositional units: the basal Tallakot Formation, which is stratigraphically overlain by the Ghachok Formation, whose undulated palaeo-topography is capped by the younger Pokhara Formation. Whereas the former two remain undated but are believed to be of Pleistocene to post-LGM age, Fort (1987) was the first to suggest a historic age for the Pokhara Formation, confirmed by detailed radiocarbon dating by Schwanghart et al. (2016a). Outcrops of the Tallakot Formation, comprising poorly sorted clasts in a cemented, silty matrix, are restricted to few locations in the northernmost parts of the valley (Fig. 1.6; Stolle et al., 2017). In contrast, material of the Ghachok Formation (previously also described as Gaunda Conglomerates), can be found throughout the valley where it – although stratigraphically older – steps above the Pokhara Formation in the north and is overlain by these younger gravels in the central parts of the valley (Fort, 2010). In these northern outcrops, the brecciated conglomerates of the Ghachok Formation have a distinctive beige-yellow colour of their silt- to clay-sized matrix, in which angular to subangular, poorly sorted and polymictic clasts of pebble to boulder size are embedded. Outcrops of the Ghachok Formation have a massive appearance and are, in contrast to the Pokhara Formation, devoid of distinct beds. The material of the Ghachok Formation is cemented and forms pillar-like karst features (Fig. 1.6). The valley fill is dominated by the thick (60 to >100 m) sequence of metre to decimetre thick gravel beds of the Pokhara Formation, which have attracted the most scientific attention in the past (Fort, 1987; Hormann, 1974; Yamanaka, 1982) and have been recently described in detail by Stolle et al. (2017). They distinguish the characteristic massive conglomerates and associated thick layers of sands and muds in this formation into four lithofacies describing different depositional environments within the alluvial fan, including the fan's central and marginal parts or the tributary mouths. In most of the valley's tributaries, fine-grained slackwater deposits are found several kilometres upstream of their confluences with the Seti Khola.

Similar to other intramontane valleys in the HKKHN (Hewitt, 2014), large aggradation events originating from the High Himalayan Front and routed along the Seti Khola are thought responsible for laying down the three depositional units (Fort, 2010). Although the triggering mechanisms of the sedimentation pulses depositing the two older formations are still unknown, Schwanghart et al. (2016) found that radiocarbon dating of depositional sub-units within the Pokhara Formation

correlates with at least three known M>8 seismic events in 1100 CE, 1255 CE, and 1344 CE, respectively. However, no historical records of these presumably cataclysmic post-seismic sediment pulses exist and the nature of the underlying geomorphic processes is still unknown (Hanisch et al., 2013; Schwanghart et al., 2016a; Stolle et al., 2017).

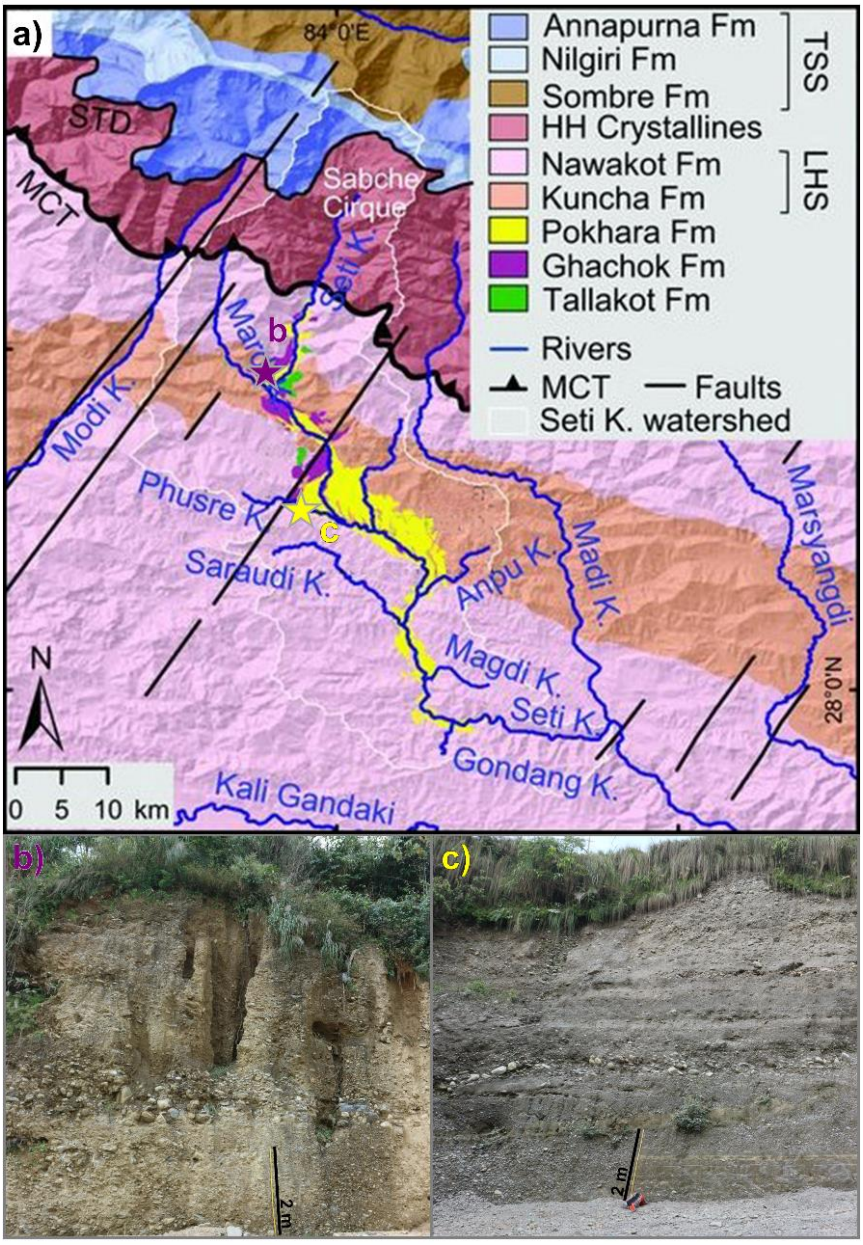

Figure 1.6: Sediment infill of the Pokhara valley. a) Geologic map modified after Schwanghart et al. (2016a), stars mark the locations of the outcrops b and c (TSS = Tethyan Sedimentary Series, LHS = Lesser Himalayan Series). b) Pillar-like karst features in an outcrop of the Ghachok Formation. c) Distinct gravel beds of the Pokhara Formation.

1.4.2 Geography of the Pokhara Valley

Today, the landscape of the Pokhara valley is still dominated by the Quaternary valley fill and its differences in resistance to erosion: extensive reaches of broad, unpaired, and up to 100-m high fluvial terraces consisting of Pokhara Formation material characterise the northern and southern part of the valley while the more competent calcareous Ghachok Formation in the valley centre is associated with short (<1 km), narrow (mostly <10 m), and deep (>50 m) gorges and karst features such as sinkholes and caves (Fig. 1.7; Fort, 2010). This characteristic landscape was formed by the post-aggradation incision of the Seti Khola, which is fed by meltwaters of the Sabche glacier in the >7,500 m a.s.l. Annapurna massif and transverses the High Himalayan Front to reach the valley floor at about 800 m a.s.l. (Stolle et al., 2019). The discharge in the Seti Khola is characterised by the exceptionally heavy >3,200 mm of seasonal orographic rainfall which occurs during the summer monsoon (Gabet et al., 2004).

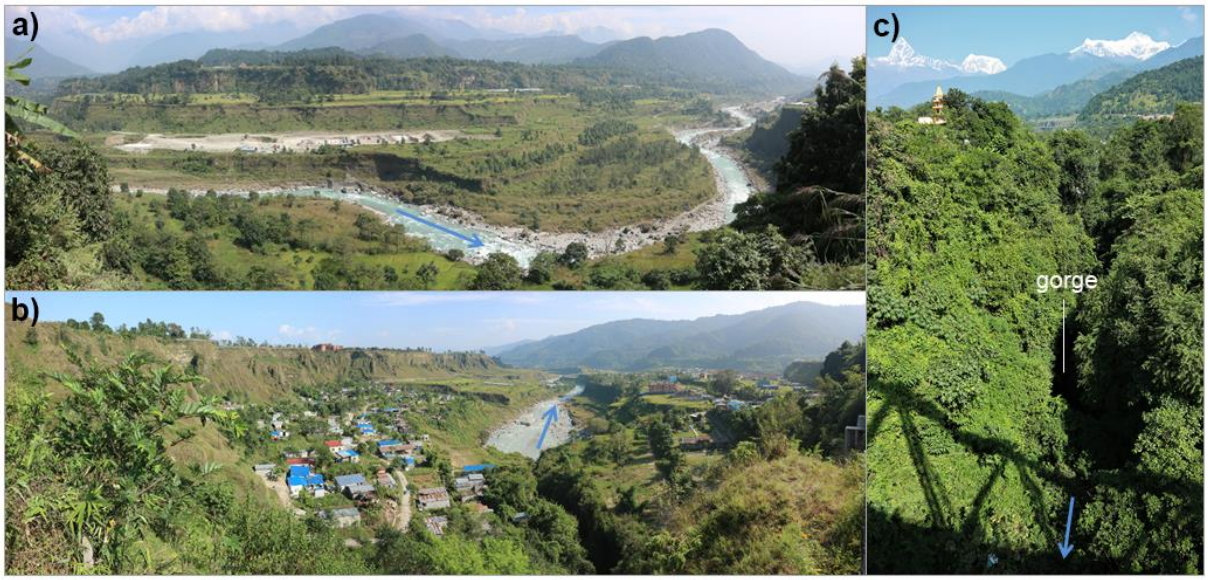

Figure 1.7: Landscape of the Pokhara valley. a) Broad, unpaired fluvial terraces at Hemja, north of Pokhara city. b) Seti Khola exits its southernmost gorge at Dhunge Sangu, south of Pokhara city. c) Overgrown edges of one of the narrow and deep gorges in central Pokhara, peaks of the Annapurna massif in the background. Blue arrows mark flow direction of the Seti Khola.

In 2021, some 518,500 persons lived in Pokhara (Central Bureau of Statistics, 2022), making it the second largest city in Nepal and one of the most rapidly growing Himalayan cities (United Nations Department of Economic and Social Affairs, 2019). Together with the neighbouring municipality of Lekhnath, Pokhara has seen rapid changes in its socio-economics since the 1960s and the beginning 1970s, which lastingly transformed this former local market town on the trading routes between China and India (Upreti et al., 2013). These dynamics have been fuelled by the completion of major

transportation infrastructure projects: beginning with the construction of bridges across the Seti Khola gorges and subsequently major highways connecting the valley with Kathmandu towards the east and the Indian boarder towards the south and eventually resulting in the ongoing construction of an international airport since 2016 (Fort et al., 2018). While Pokhara's population tripled since the 1990s (Rimal et al., 2015), urban areas rapidly spread across the fan surface, primarily along major roads (Fig. 1.8). Simultaneously, cultivated land in the Pokhara valley is dwindling as a result of ongoing rural-to-urban migration and a shift from agriculture to service sector as the main source of income for more and more people (Rimal et al., 2015).

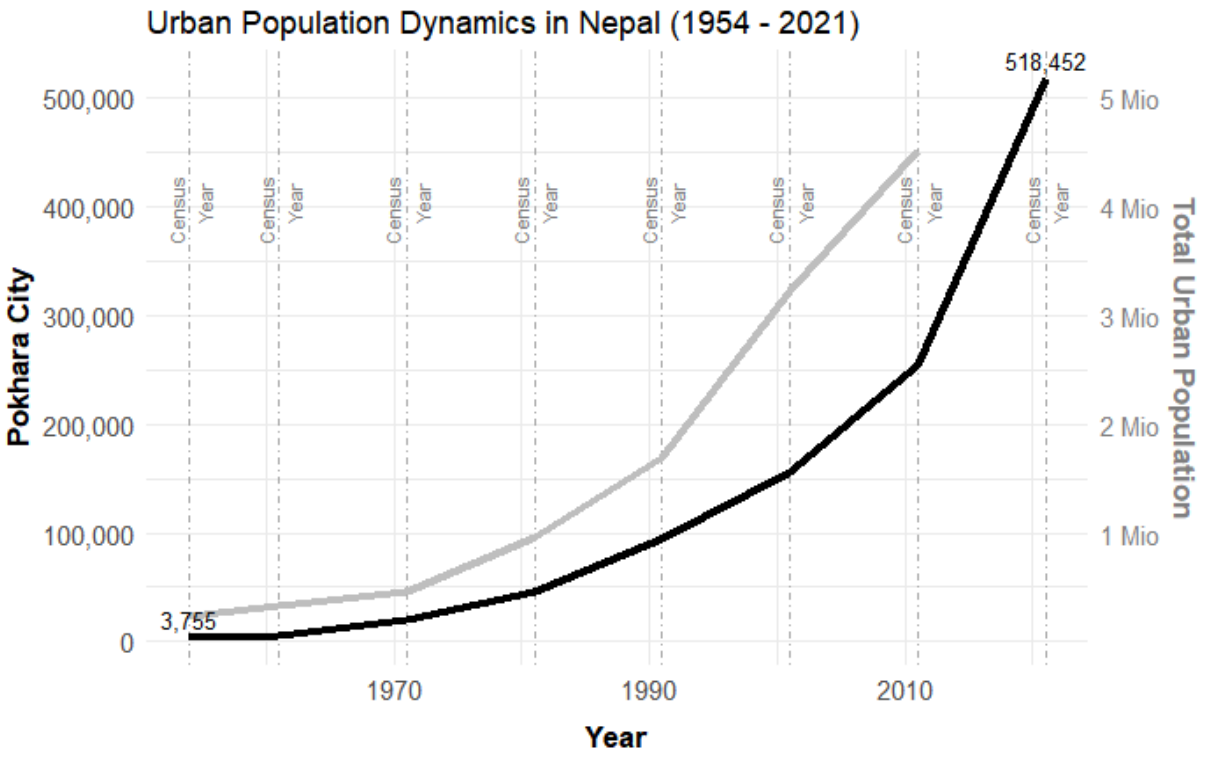

Figure 1.8: Dynamics of urban population numbers in Pokhara (black) and Nepal (grey) since the 1950s. Data derived from the Central Bureau of Statistics (2022) and Rimal (2012).

Many of these new job opportunities emerged in Pokhara's tourism sector, which has been growing rapidly following the opening of Nepal to foreign tourists in the 1950s: While in the 1960s to 1980s Pokhara mainly served as an entry point for mountaineering expeditions to the surrounding peaks of the Annapurna massif, the sector diversified in the past decades and successively more domestic and foreign tourists visit Pokhara for outdoor and wellness activities, and for religious and cultural reasons (Upreti et al., 2013). It is estimated that more than half a million people visit Pokhara every year, although official statistics are not resolved at this level (MCTCA, 2020; Upreti et al., 2013).

Urbanisation pressure and the inflow of migrants from other Nepalese districts led to a rise in informal settlements in the periphery of Pokhara's urban areas in the past decades (Fort et al., 2018; Thapa et al., 2022). The oldest of these informal settlements started to form in the 1980s at Kaseri (Bazaar) in the north-west of Pokhara, perched on top of one of the lower terraces between the Baglung Rajmarg highway and the Seti Khola's main channel (Gurung et al., 2021). The majority of the residents in these settlements have a low income (<10 USD per day) or live in poverty (<2 USD per day) and manual labour is the main way of income for most households (Thapa et al., 2022). Unregulated sites of sand and gravel extraction within the Seti Khola's bed are often associated with these informal settlements and their residents are the main work force to excavate these increasingly sought after construction materials (Fort et al., 2018).

1.4.3 The May 2012 Seti Khola Flood

On the morning of the 5th of May, 2012, a sudden hyperconcentrated flood along the Seti Khola heavily impacted the Pokhara valley's northern and central parts (Fig. 1.9). Claiming 72 lives, the outburst flood also caused an economic loss of 50 million NPR (390,000€) as it destroyed several buildings and vital rural infrastructure like suspended bridges and a potable water pipeline. A full account of losses and damages was first reported by Gurung et al. (2015) and later substantiated by Gurung et al. (2021).

As the Seti Khola was ungauged during the event, descriptions and estimates of the flood wave's propagation are based on available video footage of the event, which was taken at two sites: Kharapani village (1,100 m a.s.l.), c. 23 km downstream of the flood source, and at the Seti dam (900 m a.s.l.) in the north-east of Pokhara's urban area. Between these two locations, previously published peak discharge estimates range between 1,000 and 8,400 $m^3 s^{-1}$ (Kargel et al., 2013; Oi et al., 2012).

In the past, the main scientific focus was on the reconstruction of the triggering mechanism that led to the downstream flood wave (e.g. Gurung, 2013; Hanisch et al., 2013; Kargel et al., 2013; Petley, 2012). All authors agree, that a rock-slope failure originating from the south-western ridgeline of Annapurna IV (7,525 m a.s.l.) played a central part within this hazard cascade (Hanisch et al., 2013; Kargel et al., 2013). The volume of this slide, consisting of THS material and fragments of the snow and ice cap, is estimated at 10-15 x 10^6 m^3 (Bhandary et al., 2012), 22 x 10^6 m^3 (Petley and Stark, 2012), or 33 x 10^6 m^3 (Oi et al., 2014). The high-energetic impact of this mass after a vertical fall of 1,000 to 2,000 m on the Sabche Cirque's floor is documented by the seismic signal it generated at 09:10 am local time (Petley, 2012b). Fragmentation and pulverisation of the landslide material and loose glacio-lacrustine sediments in the impact area led to a transformation of the flow into an avalanche, which eventually developed into a slurry flow when exiting the narrow Seti Khola gorge – the

bottleneck-like drainage of the bowl-shaped Sabche Cirque (Hanisch et al., 2013; Kargel et al., 2013; Petley and Stark, 2012). However, interpretations of the event chain diverge at this point as the process behind the transformation into this water-bearing, less viscous flow remains debated: Kargel et al. (2013) and Kargel (2014) argue, that an earlier, undated rockfall partially blocked the Seti Khola gorge and impounded a large amount of water whose outburst was then triggered by the May 5th rock-slope failure (Fig. 1.9). In contrast, both Hanisch et al. (2013) and Petley and Stark (2012) exclude the existence of such a landslide-dammed lake within the gorge prior to the event and Petley and Stark (2012) propose that snow- and ice-melt by friction could have provided the necessary amounts of water to facilitate flow transformation. Regardless of these disagreements, eyewitness accounts and video footage testify that the front of the flood reached Kharapani village at 09:38 am and the Seti dam in Pokhara's urban outskirts at 10:35 am (Hanisch et al., 2013).

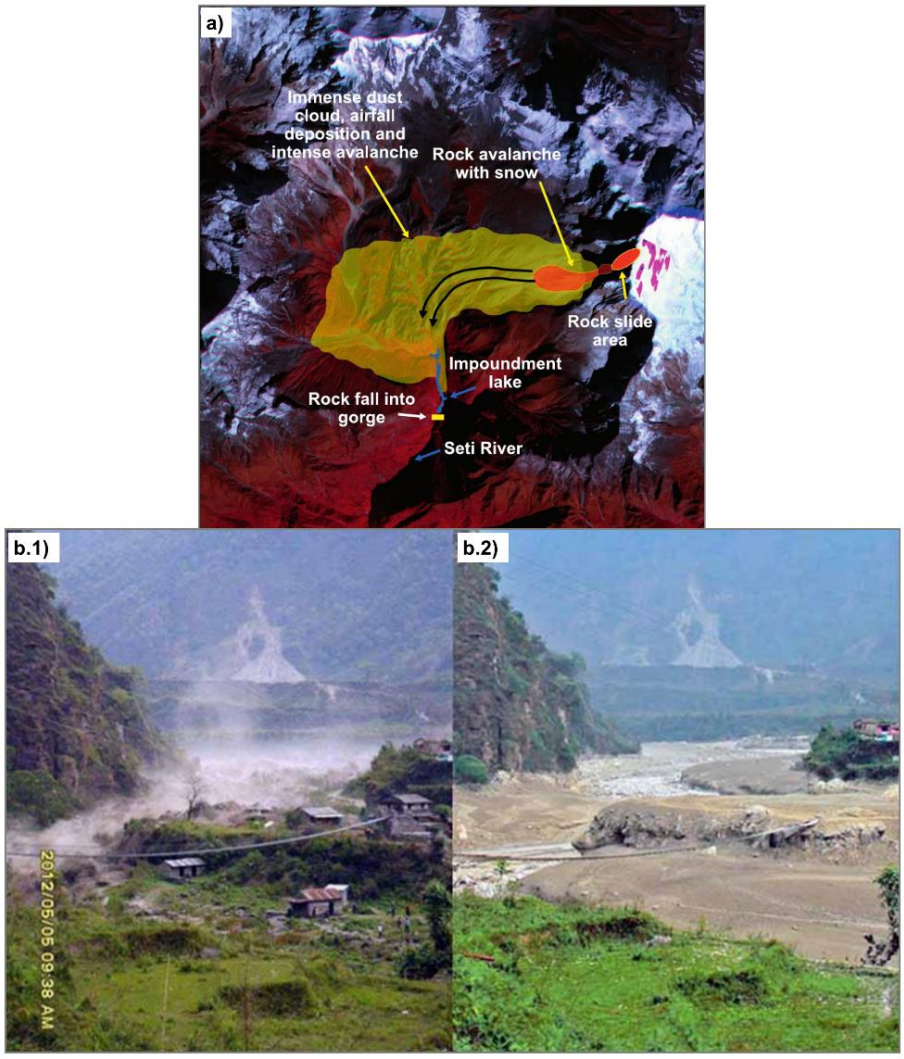

Figure 1.9: The May 2012 Seti Khola flood. a) Schematics of the triggering processes in the Sabche Cirque, following Kargel et al.'s (2013) interpretation (modified after Byers et al., 2022). b) Photo stills taken from video footage documenting the arrival of the flood wave (b.1) and the immediate aftermath at Kharapani village (b.2; modified after Oi et al., 2014).

1.5 Previous Methodologies of Outburst Flood Assessments in the Greater Himalayas

Motivated largely by the impacts of the Dig Tsho event of 1985, studies on outburst floods in the Greater Himalayan region in the past have concentrated on GLOFs, especially when performing hazard and risk assessments. While the number of studies on GLOFs in the HKKHN has rapidly increased in the past two decades (Emmer, 2018), hazards and risks posed by LLOFs appear to be less well studied and scientific work is often restricted to the reconstruction of past events (Dunning et al., 2006; Hewitt, 1998; Shrestha and Nakagawa, 2016).

1.5.1 Regional GLOF Archive Compilations and Hazardous Lake Classification Schemes

Many recent GLOF studies in the Greater Himalayan region focused on the identification of "potentially hazardous lakes" using a two-step approach: (1) the compilation of a regional glacial lake inventory derived from literature or by implementing remote-sensing techniques, i.e. the normalised difference water index (NDWI; Huggel et al., 2002) and (2) an ordinal classification of glacial lakes using a decision scheme based on multiple criteria describing the glacial lake and its surroundings (Bolch et al., 2011; Khadka et al., 2021; Mergili et al., 2011; Mohanty and Maiti, 2021; Worni et al., 2013). The core of each of these studies builds a set of descriptive parameters which Rounce et al. (2016) summarised as covering a) the stability of the dam (moraine slope steepness, width-to-height ratio, lake freeboard, dam type, existence of a buried ice core, etc.), b) the potential triggering mechanisms (seismic activity, distance to and steepness of parent glacier snout, mass movements, etc.), and c) the potential downstream impacts (lake volume, etc.). Many of these predictors have been adapted from dam-stability assessments in various mountain regions. In some cases, expert-knowledge-based thresholds of these parameters were transferred from other regions despite known regional differences between the Greater Himalayan and other high-mountain cryospheres worldwide, including generally smaller lake sizes in the Alps (Huggel et al., 2004), the importance of earthquakes as triggers of past GLOFs in the Peruvian Andes (Emmer and Vilímek, 2013), or the surging behaviour of some glaciers in the Karakoram (Hewitt and Liu, 2010). Previous assessments were partly subjective by introducing various selections of predictors and their associated thresholds, by relying heavily on expert knowledge and, thus, raising the possibility of conflicting assessments (Rounce et al., 2016). For example, most authors considered the slope of the moraine dam's distal flank to be a criterion for its stability, assuming that steepening would increase the susceptibility to sudden failure. Yet, the thresholds for a "critical" steepness were variably set to 14°(Wang et al., 2011) or 20° (Worni et al., 2013). Further bias can also be introduced by the subjective ranking or weighting of predictors, commonly used in semi-quantitative scoring systems (Bolch et al., 2011). This issue is often addressed by applying an analytical hierarchical process, a

multi-criteria decision making technique in which weights are assigned by using a pairwise predictor comparison matrix (Khadka et al., 2021; Mohanty and Maiti, 2021; Prakash and Nagarajan, 2017). However, fully statistical approaches to reduce the inherent subjective bias of the applicator remain rare. For example, Wang et al. (2011), who classified 78 moraine-dammed lakes on the south-eastern Tibetan Plateau, used a fuzzy consistent matrix to determine the weights of their five selected stability parameters (mother glacier area, distance lake and glacier terminus, slope between lake and glacier, mean slope moraine dam, mother glacier snout steepness). They further derived cut-off thresholds from the distribution of each parameter to classify four hazard intervals (Wang et al., 2011). Outside of this thesis' study area, McKillop and Clague (2007b, 2007a) used frequentist logistic regression to assess GLOF hazard from glacial lakes in British Columbia, Canada, drawing on more than a dozen morphometric parameters of 175 moraine-dammed lakes. They found that outburst probabilities are larger for lakes with larger surface areas, dammed by ice-free moraines with higher height-to-width ratios and lower for dams consisting of metamorphic material (McKillop and Clague, 2007b).

1.5.2 Local Outburst Event Reconstructions and Hazard/Risk Assessments

Although some ice-dammed lakes show repeated drainage cycles, for example Catalina Lake in Greenland (Grinsted et al., 2017), outburst floods from other types of glacial and land-slide dammed lakes are mostly reported as single events due to complete drainage and lasting dam incision (Huggel et al., 2004). Thus, the applicability of magnitude-frequency relationships, which allow for an estimation of the future occurrence probability of a given hazard magnitude based on time series of recorded events and are often used in assessments of other natural hazards (e.g. riverine floods), is compromised (Huggel et al., 2004). Although few studies have applied the return period concept at a regional scale, i.e. defining the peak discharge of the 100-year GLOF in the greater Himalayan region as $15{,}600^{+2{,}000}_{-1{,}800}$ $m^3 \cdot s^{-1}$(Veh et al., 2020), scenario-based modelling is imperative when assessing local outburst flood hazard and related risks (Worni et al., 2014). Augmenting this scenario-based approach in terms of future events, a number of studies have aimed at a retrospective modelling of past outbursts in the Greater Himalayan region (Cenderelli and Wohl, 2001; Shrestha and Nakagawa, 2016). Despite the popularity of both empirical modelling of peak discharge released by a dam breach (Vuichard and Zimmermann, 1987) and GIS-based downstream flow models (Allen et al., 2016a), an increasing number of studies now provide numerical simulations of dam stability and breach as well as flood wave propagation (Worni et al., 2014; Zhang and Liu, 2015). Applied hydrodynamic models include: BASEMENT (Faeh et al., 2011; Lala et al., 2018; Worni et al., 2013, 2014), Flo-2D (Mergili et al., 2011; O'Brien et al., 1993; Somos-Valenzuela et al., 2014), DAMBRK

(Fread, 1988; Meon and Schwarz, 1993; Shrestha et al., 2010), FLDWAV (Bajracharya et al., 2007), and HEC-RAS (Table 1.2; Cenderelli and Wohl, 2001; Wang et al., 2018).

Table 1.2: Examples for the application of HEC-RAS in GLOF studies worldwide.

Reference	Study area		Hydrodynamic and model characteristics	Application
	Glacial lake(s)	Country		
Alho and Aaltonen, 2008	Lakes upstream of Möðrudalur floodplain	Iceland	One-dimensional unsteady flow	Comparison of one-dimensional HEC-RAS modelling capabilities with a two-dimensional model (TELEMAC-2D)
Bajracharya et al., 2007	Imja Tsho, Dig Tsho	Nepal	One-dimensional steady mixed flow	Inundation and flood depth maps compilation of numeric data derived from NWS-FLWAV modelling
Byers et al., 2013	Chamlang North Pokhari	Nepal	One-dimensional unsteady flow	Simulation (breach and downstream flood propagation) of a potential GLOF from Chamlang North Pokhari lake
Cenderelli and Wohl, 2001	Lakes of the Nare Glacier and Langmoche Glacier draining into Imja Khola, Dudh Kosi and Bhoti Kosi river network	Nepal	One-dimensional steady subcritical flow	Quantification of three historic GLOFs (1977, 1985, and unknown date) based on geomorphic palaeostage indicators, comparison of GLOF peak discharges with those reached during SHFFs (seasonal high flow floods)
Cenderelli and Wohl, 2003	Lakes of the Nare Glacier and Langmoche Glacier	Nepal	One-dimensional steady subcritical flow	Quantification of two historic GLOFs (1977, 1985)
Jha and Khare, 2016	Lake L2 in Dhauliganga River basin	India (Uttarakhand)	One-dimensional unsteady flow	Simulation (breach and downstream flood propagation) of potential GLOF from Lake L2, comparison with dam breach hydrographs derived from empirical relations
Klimeš et al., 2014	Lake 513 in Chucchun River basin	Peru	One-dimensional steady mixed flow	Reconstruction and quantification (esp. inundation depth mapping) of the April 2010 event based on geomorphic palaeostage indicators
Osti and Egashira, 2009	Tam Pokhari	Nepal	One-dimensional unsteady flow	Reconstruction and quantification of 1998 event
Somos-Valenzuela and McKinney, 2011	Lake Palcacocha	Peru	One-dimensional unsteady flow	Simulation of potential GLOF from Lake Palcacocha

Reference	Study area		Hydrodynamic and model characteristics	Application
	Glacial lake(s)	Country		
Wang et al., 2012	Longli Co	China (Tibetan Autonomous Region)	One-dimensional unsteady flow	Simulation of potential GLOF from Longli Co, comparison of ASTER GDEM and SRTM as geometric input DEMs for hydraulic modelling
Wang et al., 2018	Lake Cirenmaco	China (Tibetan Autonomous Region)	Two-dimensional unsteady flow	Reconstruction of 1981 GLOF and simulation of a potential future event (complete drainage scenario)
Zhang et al., 2021	Seven lakes in the Poiqu River basin (incl. Lake Cirenmaco)	China (Tibetan Autonomous Region)	Two-dimensional unsteady flow	Inundation simulations and potential socio-economic impact mapping based on modelling of different drainage-percentage scenarios

1.6 Research Questions and Thesis Structure

This thesis explores, what new insights we can gain about outburst floods in the data-scarce Greater Himalayan region using data-driven and numerical modelling approaches, drawing on remote-sensing and field data. Chapter 1.5 introduced that on a regional scale, GLOF assessments comprising thousands of lakes are rare and that rigorous statistical analysis of past GLOFs in the Greater Himalayas is missing. Chapter 1.4 demonstrated that the city of Pokhara and its surrounding valley are a prime locality for the study of both past and future outburst floods as well as the diverse socio-economic changes affecting high-mountain cities worldwide. However, quantitative assessments of past and potential future outburst flood characteristics, including flow limits, depths, and velocities, are missing.

Beginning with a regional assessment of susceptibility of HKKHN glacial lakes and ending with the local appraisal of informal settlement dynamics in one of the most rapidly growing Himalayan cities, this thesis addresses research gaps and highlights various aspects of outburst floods which are often studied separately.

The three core chapters, Chapters 3 to 5, comprehensively deal with the **susceptibility** to, the **flow characteristics** of, and the **hazards** posed by outburst floods (Fig. 1.10). While Chapter 3 consist of a comprehensive, purely data-driven approach across the Greater Himalayan region, Chapter 4 and Chapter 5 progressively zoom-in on a single, outburst-flood-prone watershed and eventually narrow down to the scale of individual, potentially exposed, informal settlements and roads along the Seti Khola in the Pokhara valley. This structure is aligned with the three overarching research questions that I aim to answer in this thesis:

I *What can the few data on past glacial lake outburst floods in the Greater Himalayan region tell us about a glacial lake's* ***susceptibility*** *to this hazard?*

In Chapter 3, two inventories of moraine-dammed glacial lakes, listing all lakes with and without a known outburst flood in the past four decades, as well as regional morphologic, glaciologic, and climatic datasets are used to test whether commonly-applied GLOF predictors like lake area and its dynamics, lake elevation, parent-glacier-mass balance and monsoonality have been significant controls of past susceptibility to outburst floods.

II *What can we learn from sedimentary evidence and numerical modelling about* ***flow characteristics*** *of moderate modern to cataclysmic historic floods in the Pokhara valley?*

In Chapter 4, missing hydraulic information is substituted with the sedimentary evidence to reconstruct the flow velocities and depths of a recent flood (2012) and historic (12^{th} to 14^{th} century CE) outburst floods along the Seti Khola, which transverses one of the steepest topographic gradients in the Greater Himalayan region.

III *What* ***hazards*** *could potential future outburst flood scenarios pose to a rapidly growing high-mountain city like Pokhara?*

In Chapter 5, an anticipatory hazard assessment is performed by exploring the physically plausible range of potential peak discharge scenarios along the Seti Khola in lieu of documented outburst flood frequencies. We overlay our spatially-resolved hazard scenarios with data on current land cover in Pokhara valley and analyse the dynamics of Pokhara's informal settlements identified as being at risk.

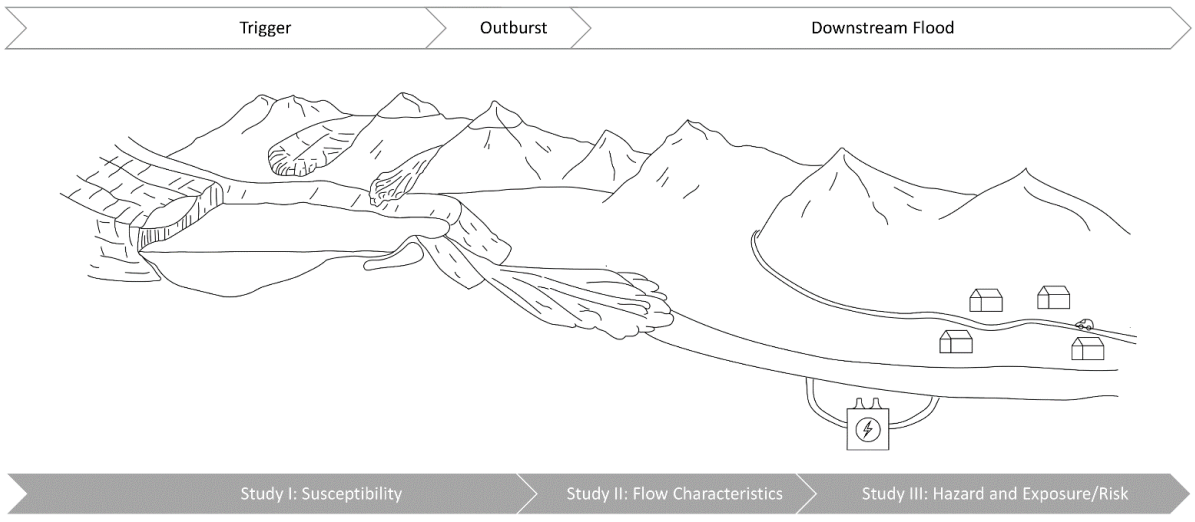

Figure 1.10: The structure of this thesis loosely follows the outburst flood process chain. Schematics adapted from Westoby et al. (2014) (not to scale).

The key findings of these three studies are summarised in Chapter 6, in which I jointly discuss their implications not only for theoretical research but also for practical hazard and risk management in the Greater Himalayan region and the Pokhara valley. After providing further potential starting points of future research in this specific Nepalese valley, I close this thesis with a brief summary of my main study results in Chapter 7.

2 Author Contributions

The Chapters 3, 4, and 5 of this PhD thesis comprise original studies, which have been published or accepted for consideration to be published in international peer-reviewed journals. I (Me.F.) wrote these manuscripts in cooperation with a number of co-authors, whom I am very grateful for their following contributions:

Chapter 3: This study was conceptualised by all authors. While formal analysis and methodology were conducted by Me.F. and O.K., data curation was mainly carried out by G.V. Visualisations of data and results, including maps, were prepared by G.V., O.K., and Me.F. Me.F. prepared the original manuscript; O.K., G.V., and A.W. reviewed and edited the writing.

Chapter 4: This study was conceptualised by Me.F., G.V., I.J.L., O.K., and A.W. Me.F., G.V., and O.K. carried out the field work. Me.F., N.L., J.B., and G.V. curated the data while Me.F. and K.L. performed the formal analysis and methodology. Me.F. and G.V. visualised the data and results. Me.F. prepared the manuscript, K.L., G.V., I.J.L., O.K., and A.W. reviewed and edited the writing.

Chapter 5: Me.F., A.W., O.K., and S.R. conceptualised the study. The field data were collected by Me.F. and O.K. while Me.F. and J.B. curated field and additional data. All data were processed and visualised by Me.F. Me.F. prepared the original manuscript, which was reviewed and edited by A.W., S.R., Mo.F. and O.K.

A.W. – Ariane Walz
G.V. – Georg Veh
I.J.L. – Isaac J. Larsen
J.B. – Jana Brettin
K.L. – Karin Lehnigk
Mo.F. – Monique Fort
N.L. – Natalie Lützow
O.K. – Oliver Korup

To distinguish between these co-authored, (to be) published studies and their greater scientific background as established in Chapters 1, 6, and 7, the first-person plural is used in the former while the first-person singular is applied in the latter.

3 Controls of Outbursts of Moraine-dammed Lakes in the Greater Himalayan Region

Published as:

Fischer, M., Korup, O., Veh, G., and Walz, A. (2021): Controls of outbursts of moraine-dammed lakes in the greater Himalayan region, The Cryosphere, 15, 4145–4163, https://doi.org/10.5194/tc-15-4145-2021.

Abstract

Glacial lakes in the Hindu Kush-Karakoram-Himalaya-Nyainqentanglha (HKKHN) region have grown rapidly in number and area in past decades, and some dozens have drained in catastrophic glacial lake outburst floods (GLOFs). Estimating regional susceptibility of glacial lakes has largely relied on qualitative assessments by experts, thus motivating a more systematic and quantitative appraisal. Before the backdrop of current climate-change projections and the potential of elevation-dependent warming, an objective and regionally consistent assessment is urgently needed. We use an inventory of 3,390 moraine-dammed lakes and their documented outburst history in the past four decades to test whether elevation, lake area and its rate of change, glacier-mass balance, and monsoonality are useful inputs to a probabilistic classification model. We implement these candidate predictors in four Bayesian multi-level logistic regression models to estimate the posterior susceptibility to GLOFs. We find that mostly larger lakes have been more prone to GLOFs in the past four decades regardless of the elevation band in which they occurred. We also find that including the regional average glacier-mass balance improves the model classification. In contrast, changes in lake area and monsoonality play ambiguous roles. Our study provides first quantitative evidence that GLOF susceptibility in the HKKHN scales with lake area, though less so with its dynamics. Our probabilistic prognoses offer improvement compared to a random classification based on average GLOF frequency. Yet they also reveal some major uncertainties that have remained largely unquantified previously and that challenge the applicability of single models. Ensembles of multiple models could be a viable alternative for more accurately classifying the susceptibility of moraine-dammed lakes to GLOFs.

3.1 Introduction

Glacial lake outburst floods (GLOFs) involve the sudden release and downstream propagation of water and sediment from naturally impounded meltwater lakes (Costa and Schuster, 1988; Emmer, 2017). About one third of the 25,000 glacial lakes in the Hindu Kush-Karakoram-Himalaya-Nyainqentanglha (HKKHN) region are dammed by moraines, and some of these are potentially unstable (Maharjan et al., 2018). Such impounded meltwater can overtop or incise dams rapidly with catastrophic consequences downstream (Costa and Schuster, 1988; Evans and Clague, 1994). High Mountain Asian countries are among the most affected by these abrupt floods if considering both damage and fatalities (Carrivick and Tweed, 2016). For example, in June 2013, a GLOF from Chorabari Lake in the Indian state of Uttarakhand caused >6,000 deaths in what is known as the "Kedarnath disaster" (Allen et al., 2016b). The peak discharges of GLOFs can be orders of magnitude higher than those of seasonal floods. GLOFs can move large amounts of sediment, widen mountain channels, undermine hillslopes, and thus increase the hazard to local communities (Cenderelli and Wohl, 2003; Cook et al., 2018). Still, GLOFs in the HKKHN are rare and have occurred at an unchanged rate of about 1.3 per year in the past four decades (Veh et al., 2019). Ice avalanches and glacier calving are the most frequently reported triggers of GLOFs in the HKKHN (Richardson and Reynolds, 2000; Rounce et al., 2016). Most dated outbursts have occurred between June and October and might be linked to high lake levels fed by monsoonal precipitation and summer ablation of glaciers (Richardson and Reynolds, 2000). The Kedarnath GLOF is the only case attributed to a rain-on-snow event early in the monsoon season (Allen et al., 2016b). This particularly destructive GLOF underlines the need for understanding better how and why meltwater lakes can be susceptible to sudden outburst triggered by rainstorms, especially given projected impacts of atmospheric warming on the high-mountain cryosphere.

Current scenarios entail that atmospheric warming may change the susceptibility of HKKHN glacial lakes to sudden outburst floods: the IPCC's (Intergovenmental Panel on Climate Change) most recent projections attribute the decay of low-lying glaciers and permafrost to increases in lake number and area because of rising air temperatures, more frequent rain-on-snow events at higher elevations, and changes in precipitation seasonality (Hock et al., 2019). Air surface temperature in the HKKHN rose by about 0.1 °C per decade from 1901 to 2014 (Krishnan et al., 2019), likely having reduced snowfall, altered permafrost distribution, and accelerated glacier melt at lower elevations (Hock et al., 2019). Ice loss in the Himalayas has significantly increased in the past four decades, from -0.22 ± 0.13 m w.e. y^{-1} (metres of water equivalent per year) between 1975 and 2000 to -0.43 ± 0.14 m w.e. y^{-1} between 2000 and 2016 (Maurer et al., 2019). Parts of this meltwater have been trapped in glacial lakes that have expanded by approximately 14% between 1990 and 2015 (Nie et al., 2017).

King et al. (2019) found that Himalayan glaciers terminating in lakes had higher rates of mass loss since the 1970s than those not in direct contact with a glacial lake. The notion of elevation-dependent warming (EDW) posits that increases in air temperature are most pronounced at higher elevations (Hock et al., 2019; Pepin et al., 2015). EDW has affected cold temperature metrics, including the number of frost days and minima of near-surface air temperature in the HKKHN in the past decades (Krishnan et al., 2019; Palazzi et al., 2017). Essentially, all scenarios of atmospheric warming concern aspects of elevation, glacial lake size and dynamics, and local climatic variability. Yet whether and how these aspects affect GLOF hazards still awaits more quantitative support.

Previous work on GLOF susceptibility and hazard in the region focused on identifying or classifying potentially unstable glacial lakes, including local case studies largely informed by fieldwork, dam-breach models (Koike and Takenaka, 2012; Somos-Valenzuela et al., 2012, 2014), and basin-wide assessments (Bolch et al., 2011; Mool et al., 2011; Rounce et al., 2016; Wang et al., 2011). GLOF hazard appraisals for the entire HKKHN, however, remain rare (Veh et al., 2020). Most basin-wide studies proposed qualitative to semi-quantitative decision schemes using selective lists of presumed GLOF predictors (Table 3.1; Rounce et al., 2016). Yet researchers have used subjective rules to choose these variables and associated thresholds, leading to diverging hazard estimates (Rounce et al., 2016). Expert knowledge has thus been essential in GLOF hazard appraisals despite an increasing amount of freely available climatic, topographic, and glaciological data. Statistical models can help to estimate the occurrence probability of GLOFs and thus reduce the inherent subjective bias (Emmer and Vilímek, 2013). For example, Wang et al. (2011) classified the outburst potential of moraine-dammed lakes on the southeastern Tibetan Plateau by applying a fuzzy consistent matrix method. They used as inputs the size of the parent glacier, the distance and slope between lake and glacier snout, and the mean steepness of the moraine dam and the glacier snout to come up with different nominal hazard categories. This and many similar qualitative ranking schemes are accessible to a broader audience and policy makers but are difficult to compare, and they potentially oversimplify uncertainties.

One way to deal with these uncertainties in a more objective way involves a Bayesian approach. Here we used this probabilistic reasoning with data-driven models. Specifically, we tested how well some of the more widely adopted predictors of GLOF susceptibility and hazard fare in a multi-level logistic regression that is informed more by data rather than by expert opinion. We checked how well this approach identifies glacial lakes in the HKKHN that had released GLOFs in the past four decades. Our method estimates the probability of correctly detecting historic GLOFs from a set of predictors which act as proxies subsuming various physical processes described as being relevant to GLOFs. Triggering mechanisms of these GLOFs are rarely reported, however. Thus, we discuss

what more we can learn about how these historic GLOFs were linked to readily available measures of topography, monsoonality, and glaciological changes. Our model results provide a posterior probability of outburst conditioned on detection, and this may be used as a relative metric of GLOF release from a given lake. Therefore, our approach is an alternative to a formal assessment of moraine-dam stability, which is (geo-)technically feasible only at selected sites and at scales much finer than our regional and decadal focus.

Table 3.1: Frequently used predictors of GLOF susceptibility and hazard in the HKKHN.

Predictor groups	GLOF susceptibility and hazard predictors	Tested in this study	Reference
Lake characteristics and dynamics	Glacial lake elevation	✓	Mergili and Schneider, 2011
	Catchment area	✓	Allen et al., 2019; GAPHAZ, 2017
	Glacial lake area	✓	Aggarwal et al., 2016; Allen et al., 2019; Bolch et al., 2011; GAPHAZ, 2017; Ives et al., 2010; Khadka et al., 2021; Mergili and Schneider, 2011; Prakash and Nagarajan, 2017; Wang et al., 2012; Worni et al., 2013
	Lake-area change (growth and shrinkage, absolute change)	✓	Aggarwal et al., 2016; Bolch et al., 2011; Ives et al., 2010; Khadka et al., 2021; Mergili and Schneider, 2011; Prakash and Nagarajan, 2017; Rounce et al., 2016; Wang et al., 2012
Potential downstream impact	Lake volume	-	Aggarwal et al., 2016; Bolch et al., 2011; GAPHAZ, 2017; Kougkoulos et al., 2018; Mergili and Schneider, 2011
Dam stability	Moraine-wall steepness	-	Allen et al., 2019; Bolch et al., 2011; Dubey and Goyal, 2020; GAPHAZ, 2017; Ives et al., 2010; Khadka et al., 2021; Prakash and Nagarajan, 2017; Rounce et al., 2016; Wang et al., 2011; Worni et al., 2013
	Width-to-height ratio	-	Aggarwal et al., 2016; Bolch et al., 2011; GAPHAZ, 2017; Ives et al., 2010; Prakash and Nagarajan, 2017; Worni et al., 2013
	Lake freeboard	-	Bolch et al., 2011; GAPHAZ, 2017; Kougkoulos et al., 2018; Mergili and Schneider, 2011; Prakash and Nagarajan, 2017; Worni et al., 2013
	Existence of a buried ice core	-	Bolch et al., 2011; Dubey and Goyal, 2020; GAPHAZ, 2017; Ives et al., 2010; Rounce et al., 2016
	Dam type	✓	GAPHAZ, 2017; Kougkoulos et al., 2018; Mergili and Schneider, 2011; Wang et al., 2011; Worni et al., 2013
	Moraine lithology	-	GAPHAZ, 2017
Potential triggering mechanisms (geomorphic)	Seismic activity	-	GAPHAZ, 2017; Ives et al., 2010; Kougkoulos et al., 2018; Mergili and Schneider, 2011; Prakash and Nagarajan, 2017
	Distance from parent glacier snout	-	Aggarwal et al., 2016; Ives et al., 2010; Khadka et al., 2021; Kougkoulos et al., 2018; Prakash and Nagarajan, 2017; Wang et al., 2011, 2012; Worni et al., 2013
	Steepness parent glacier snout	-	Bolch et al., 2011; Ives et al., 2010; Kougkoulos et al., 2018; Prakash and Nagarajan, 2017; Wang et al., 2011

Predictor groups	GLOF susceptibility and hazard predictors	Tested in this study	Reference
Potential triggering mechanisms (geomorphic) (*continued*)	Parent glacier calving potential (width, crevasse density)	-	GAPHAZ, 2017; Ives et al., 2010; Mergili and Schneider, 2011
	Regional or parent glacier-mass balance	✓	Bolch et al., 2011; Ives et al., 2010
	Mass movements (traces, trajectories, probabilities)	-	Allen et al., 2019; Bolch et al., 2011; Dubey and Goyal, 2020; GAPHAZ, 2017; Ives et al., 2010; Khadka et al., 2021; Mergili and Schneider, 2011; Prakash and Nagarajan, 2017; Rounce et al., 2016; Worni et al., 2013
	Permafrost conditions	-	GAPHAZ, 2017
	Upstream lake (with GLOF potential)	-	Dubey and Goyal, 2020; GAPHAZ, 2017; Khadka et al., 2021
Potential triggering events (climatic)	Annual mean temperature	-	GAPHAZ, 2017; Liu et al., 2014; Wang et al., 2008
	Temperature seasonality	-	Ives et al., 2010; Kougkoulos et al., 2018
	Temperature extremes (intensity, frequency)	-	GAPHAZ, 2017
	Annual precipitation	-	Wang et al., 2008, 2012
	Precipitation seasonality	-	Ives et al., 2010; Kougkoulos et al., 2018
	Precipitation extremes (intensity, frequency)	-	GAPHAZ, 2017; Prakash and Nagarajan, 2017
	Summer precipitation or proxy of monsoonality	✓	Wang et al., 2008, 2012

3.2 Study Area, Data, and Methods

3.2.1 Study Area and Data

We studied glacial lakes of the Hindu Kush-Karakoram-Himalaya-Nyainqentanglha (HKKHN) region that we defined here as the Asian mountain ranges between 16° to 39°N and 61° to 105°E, i.e. from Afghanistan to Myanmar (Fig. 3.1; Bajracharya and Shrestha, 2011). Following the outlines of glacier regions in High Mountain Asia used in the Randolph Glacier Inventory version 6.0 (RGI Consortium, 2017) and those defined by Brun et al. (2017), Veh et al. (2020) subdivided our study area into seven mountain ranges: the Hindu Kush, the Karakoram, the Western Himalaya, the Central Himalaya, the Eastern Himalaya, the Nyainqentanglha, and the Hengduan Shan. Meltwater from the HKKHN's extensive snow and ice cover, often referred to as the "Third Pole", feeds 10 major river systems to provide water for some 1.3 billion people (Molden et al., 2014). There, glaciers have had an overall negative mass balance historically and lost 150 ± 110 kg m^{-2} yr^{-1} on average from 2006 to 2015, though with balanced trends in the Karakoram (Bolch et al., 2019; Hock et al., 2019). Since the 1970s,

some Karakoram glaciers also accelerated in flow, whereas glaciers stalled elsewhere in the HKKHN (Dehecq et al., 2019). In the RCP8.5 scenario the HKKHN glaciers could lose 64 ± 5% of their total mass by 2100 compared to estimated glacier volumes for the interval 1995 to 2015 (Kraaijenbrink et al., 2017). How much of this melting of glaciers is due to EDW remains under debate (Palazzi et al., 2017; Rangwala and Miller, 2012; Tudoroiu et al., 2016). Snowfall at lower elevations is also likely to decrease (Hock et al., 2019; Terzago et al., 2014), judging from snowfall and glacier-mass balances of past decades (Kapnick et al., 2014; King et al., 2019). Monsoon precipitation is likely to become more episodic and intensive (Palazzi et al., 2013).

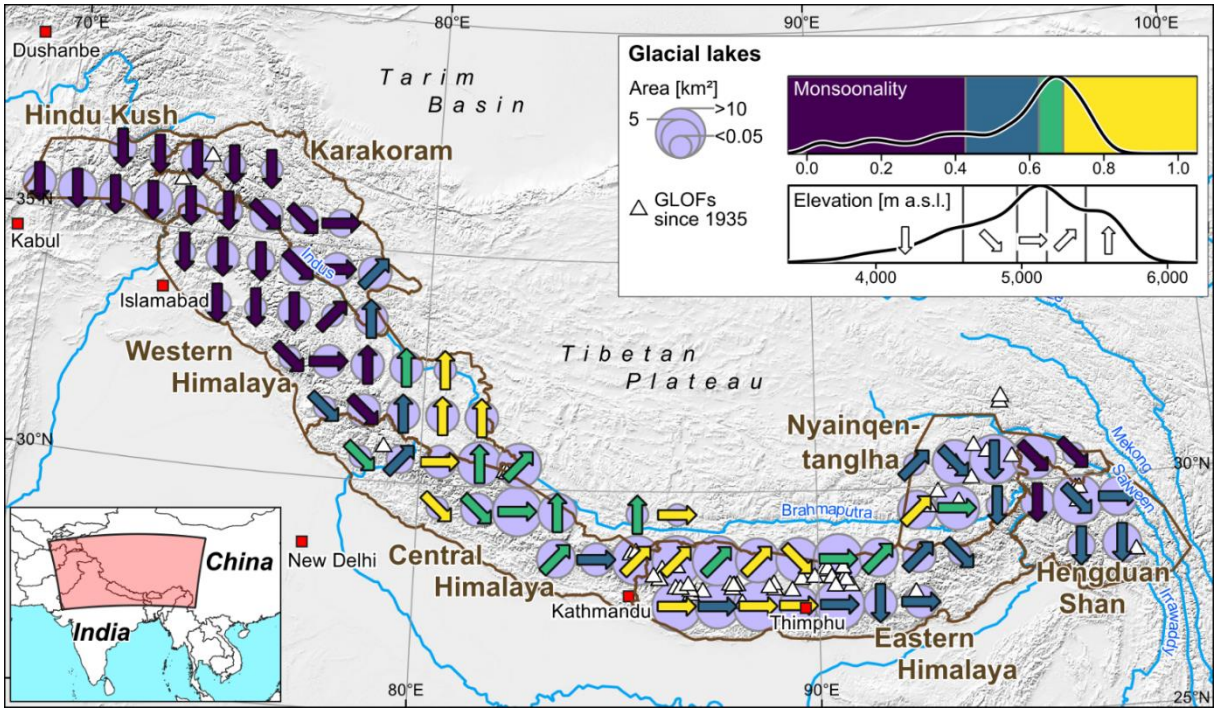

Figure 3.1: Overview map of the HKKHN showing the distribution of moraine-dammed lakes in 1° x 1° bins (blue bubbles scaled by area), their elevation (expressed as quantiles coded by arrows; see inset for elevation distribution), and average monsoonality (colour coded; see inset for monsoonality distribution), defined here as the fraction of total annual precipitation falling in the summer months. Orange and white triangles indicate reported moraine-dam failures before and after 2005, respectively (Veh et al., 2019). Background hillshade is from the GTOPO30 global 30 arcsec elevation dataset (https://doi.org/10.5066/F7DF6PQS).

Guided by these projections, we selected several widely used glacial lake susceptibility predictors (Table 3.2).

Table 3.2: Details on tested predictors and our reasoning for selection based on their commonly reported physical links to GLOF susceptibility.

GLOF susceptibility predictor	Symbol		Unit	Data source	Selection reasoning
Glacial lake elevation	z		m a.s.l.	SRTM DEM	- strong link between elevation and temperature in high altitudes (standard lapse rate of tropospheric air temperature) → elevation dependence of permafrost and precipitation patterns
Catchment area	C		m^2	SRTM DEM	- potential for surface runoff into lake from precipitation and snow melt
Glacial lake area	A		m^2	SRTM DEM	- proxy for lake volume and depth and, thus, hydrostatic pressure acting onto moraine dam
Lake-area change	ΔA	net change	-	Wang et al., 2020	- increasing lake area commonly reported as scaling with increasing lake depth → potentially increased hydrostatic pressure acting on the moraine dam - increased proximity to steep valley slopes → increased potential of mass movements entering the lake
	A^*	relative change (between) A^{*a} (1990-2005) A^{*b} (2005-2018) A^{*c} (1990-2018)	%		
Glacier-mass balance	r	glacier-mass balance region	-	Brun et al., 2017	- proxy for direct or surface runoff glacier meltwater input, calving potential of parent glacier front, and permafrost distribution in lake surroundings - link between regional glacier-mass balance and synoptic regime (winter westerlies versus monsoon dominated)
	Δm_r	average glacier-mass balance	m w.e. (water equivalent) yr^{-1}		
Monsoonality (annual proportion of summer precipitation)	M		% (mm)	CHELSA (Karger et al., 2017)	- high intensity precipitation events during monsoon season might lead to increased surface runoff into glacial lakes (cloudburst event) - seasonal increases in lake levels and, hence, lake depths increase hydrostatic pressure acting onto moraine dam - link between regional glacier-mass balance and synoptic regime (winter westerlies versus monsoon dominated)

We used **lake elevation** z (m a.s.l.) as a proxy for the standard lapse rate of tropospheric air temperature (Rolland, 2003; Yang and Smith, 1985). This elevation-dependent thermal gradient is also a major control on the distribution of alpine permafrost (Etzelmüller and Frauenfelder, 2009) and precipitation. Mean annual rainfall along the Himalayan front can exceed 4,000 mm at elevations some 4,000 m high, where ~25% of all glacial lakes occur (Fig. 3.1; Bookhagen and Burbank, 2010). Lake elevation should also represent first-order topographic effects of EDW. For

example, the stability of low-lying moraine dams may be compromised by the loss of permafrost and commensurate increases in permeability in the moraine barrier and adjacent valley slopes (Haeberli et al., 2017).

Glacial **lake area** A (m^2) and its rate of **change** ΔA (net change) and A^* (relative change, %) are other common predictors of susceptibility and hazard in GLOF studies (Allen et al., 2019; Bolch et al., 2011; Prakash and Nagarajan, 2017; see Table 3.1 for full list of references) that we considered here. Due to a general lack of available bathymetric data on a regional scale, a number of studies used the frequently observed phenomenon that lake area scales with lake volume and depth (Huggel et al., 2002; Iribarren Anacona et al., 2014). Growing lake depths increase the hydrostatic pressure acting on moraine dams, thus raising the potential of failure (Iribarren Anacona et al., 2014; Rounce et al., 2016). In the past decades, lake areas have grown largest in the Central Himalayas (+23% in 1990-2015; Nie et al., 2017) and Nyainqentanglha Mountains but lowest in the northwestern Himalayas (Chen et al., 2021a; Nie et al., 2017), and many studies have emphasised the role of growing lakes on GLOF susceptibility (e.g. GAPHAZ, 2017; Prakash and Nagarajan, 2017; Rounce et al., 2016). Many previous GLOF assessment schemes included lake area or lake-area growth as a proxy for the volume of water that could be potentially released by an outburst and thus the resulting downstream hazard (e.g. Allen et al., 2019; Bolch et al., 2011). However, a number of studies also stress that lake area and its growth define the exposure to external and internal triggers of moraine dam breach: larger and growing lakes offer more area for impacts from mass flows such as avalanches, rockfalls, and landslides originating from adjacent valley slopes (GAPHAZ, 2017; Haeberli et al., 2017; Prakash and Nagarajan, 2017; Rounce et al., 2016). Some authors also link growing lake areas to an increase in hydrostatic pressure acting on its moraine dam, thus making the latter more susceptible to sudden failure (Iribarren Anacona et al., 2014; Mergili and Schneider, 2011).

We also tested the impact of upstream **catchment area** C (m^2) on GLOF susceptibility. A larger upstream catchment area has been associated with an increased susceptibility to GLOFs as runoff from intense precipitation, as well as glacier and snow melt, can lead to sudden increases in lake volume (Allen et al., 2019; GAPHAZ, 2017). We find that catchment area C correlates with lake area A (Pearson's $\rho = 0.45$). We thus preferred C over A in two of our models as C is invariant at the timescale of our study; and we use these two models to explicitly test whether runoff by glacier melt or monsoonal precipitation had an effect on GLOFs in our study area.

Similar to changes in lake area, glacier dynamics are frequently mentioned though rarely incorporated quantitatively in susceptibility appraisals (Bolch et al., 2011; Ives et al., 2010). This motivated us to consider the average changes in **regional glacier-mass balances** between 2000 and 2016 Δm (m water equivalent yr^{-1}) from Brun et al. (2017). These readily available data on

regional glacier-mass balances are proxies for other, less accessible physical controls on GLOF susceptibility such as glacial meltwater input, either directly from the parent glacier or from glaciers upstream, as well as permafrost decay in slopes fringing the lake (see Table 3.2 for full list).

Meteorological drivers entered previous qualitative GLOF hazard appraisals mostly as (the probability of) extreme monsoonal precipitation events: the Kedarnath GLOF disaster, for example, was triggered by intense surface runoff (Huggel et al., 2004; Prakash and Nagarajan, 2017). Heavy rainfall may also trigger landslides or debris flows from adjacent hillslopes followed by displacement waves that overtop moraine dams (Huggel et al., 2004; Prakash and Nagarajan, 2017). Elevated lake levels during the monsoon season also raise the hydrostatic pressure acting on moraine dams (Richardson and Reynolds, 2000). Furthermore, different precipitation regimes and climatic preconditions may also influence moraine-dam failure mechanics (Wang et al., 2012b). Intense precipitation occurs in our study region largely during the summer monsoon, so we derived a synoptic measure of **monsoonality** *M* (%). We define monsoonality *M* in terms of the annual proportion of summer, i.e. the warmest quarter, precipitation, which is highest in the southeast HKKHN, where it is linked to monsoonal low-pressure systems (Krishnan et al., 2019).

We extracted information on these characteristics for glacial lakes recorded in two inventories. First, we used the ICIMOD database of 25,614 lakes manually mapped from Landsat imagery acquired in 2005 ± two years (Maharjan et al., 2018), from which we extracted 7,284 lakes dammed by moraines (classes m(l), m(e), and m(o) in Maharjan et al., 2018). Second, we identified from an independent regional GLOF inventory (Veh et al. 2019) 31 lakes that had at least one outburst between 1981 and 2017 and that are listed in the ICIMOD inventory. The triggering mechanism of these studied GLOFs is reported in only seven cases, four of which are attributed to ice avalanches entering the lake (e.g. Tam Pokhari, Nepal, and Kongyangmi La Tsho, India; Ives et al., 2010; Nie et al., 2018). Other triggers of the GLOFs studied here include piping (Yindapu Co, China; Nie et al., 2018) and the collapse of an ice-cored moraine (Luggye Tsho, Bhutan; Fujita et al., 2008). We focused on lakes >10,000 m^2 to ensure comparability between the two inventories, thus acquiring a final sample size of 3,390 lakes. Given the sparse network of weather stations in the HKKHN, we computed the monsoonality averaged for each lake from the 1-km resolution CHELSA bioclimatic variables (Karger et al., 2017). These variables are correlated with elevation because of the same underlying interpolation technique, so we limited our models to those with poorly correlated predictors. This meant omitting other predictors such as mean annual temperature, annual precipitation totals, and annual temperature and precipitation variability. We extracted topographic data from the void-free 30 m resolution SRTM (Shuttle Radar Topographic Mission of 2000) digital elevation model (DEM), and use approximate lake-area changes for two intervals (1990 to 2005 and 2005 to 2018) by Wang et al.

(2020). We discarded newer, higher-resolved DEMs to minimise data gaps and artefacts. Overall, we considered six topographic, synoptic, and glaciological predictors (Fig. 3.2, Table 3.2).

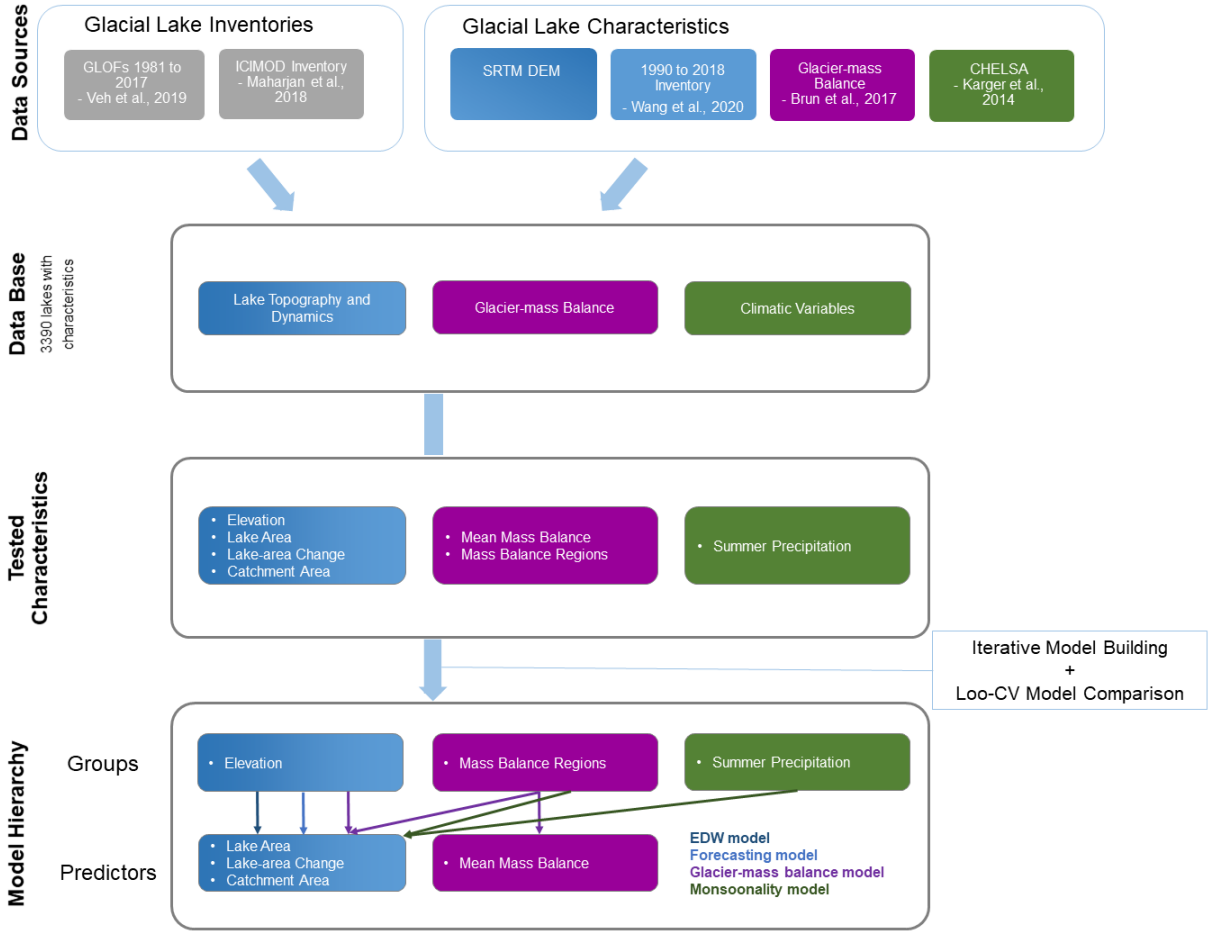

Figure 3.2: Data sources and workflow; EDW = elevation-dependent warming.

3.2.2 Bayesian Multi-level Logistic Regression

We used logistic regression to learn the probability of whether a given lake in the HKKHN had a reported GLOF in the past four decades. This method was pioneered for moraine-dammed lakes in British Columbia, Canada (McKillop and Clague, 2007b). Logistic regression estimates a binary outcome y from the optimal linear combination of p weighted predictors $x = \{x_1, \ldots, x_p\}$. The probability $y = P_{GLOF}$ that lake i had released a GLOF is expressed as follows:

$$y_i \sim \text{Bernoulli}(\mu_i) \tag{3.1}$$

$$\mu_i = \text{S}(\alpha_0 + \beta_1 x_{i,1} + \beta_2 x_{i,2} + \cdots + \beta_p x_{i,p}) \tag{3.2}$$

where

$$S(x) = \frac{1}{1+\exp(-x)} \tag{3.3}$$

Here α_0 is the intercept, and $\beta = \{\beta_1, \ldots, \beta_p\}^T$ are the p predictor weights (Gelman and Hill, 2007). The logit function $S^{-1}(x)$ describes the odds on a logarithmic scale (the log-odds ratio) such that a unit increase in predictor x_m raises the log-odds ratio by an amount of β_m, with all other predictors fixed. We used standardised data to ensure that the weights measure the relative contributions of their predictors to the classification, whereas the intercept expresses the base case for average predictor values.

Our strategy was to explore commonly reported predictors of GLOF susceptibility and dam stability as candidate predictors (Fig. 3.2, Table 3.1, Table 3.2). We further acknowledged that data on moraine-dammed lakes in the HKKHN are structured, reflecting, for example, the variance in topography and synoptic regime such as the summer monsoon in the eastern HKKHN and westerlies in the western HKKHN. Different data sources, collection methods, and resolutions also add structure. This structure is routinely acknowledged, often raised as a caveat, but rarely treated in GLOF studies. Ignoring such structure can lead to incorrect inference by bloating the statistical significance of irrelevant or inappropriate model parameter estimates (Austin et al., 2003). To explicitly address this issue, we chose a multi-level logistic regression as a compromise between a single pooled model and individual models for each group in the data (Fig. 3.3; Gelman and Hill, 2007; Shor et al., 2007).

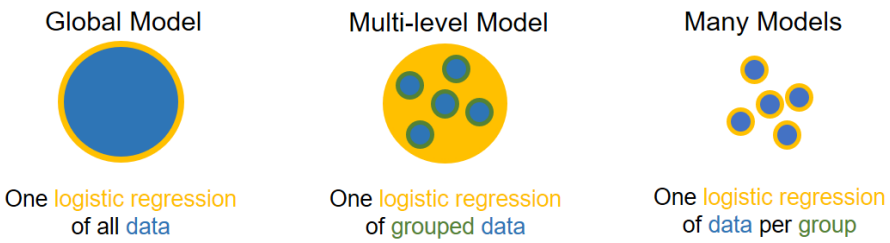

Figure 3.3: Schematic comparison of global vs. multi-level logistic regression models.

We recast Eq. (3.2) using a group index *j*:

$$\mu_i = S(\alpha_j + \beta_1 x_{i,1} + \beta_2 x_{i,2} + \cdots + \beta_p x_{i,p}) \tag{3.4}$$

$$\alpha_j \sim N(\mu_\alpha, \sigma_\alpha), \tag{3.5}$$

where μ_α is the mean, and σ_α is the standard deviation of the group-level intercepts α_j that are learned from all data and inform each other via the model hierarchy. We used a Bayesian framework (Kruschke and Liddell, 2018) by combining the likelihood of observing the data with prior knowledge from previous GLOF studies (Fischer et al., 2020). The small number of reported GLOFs introduces strong imbalance to our data given that some regions, and hence levels, had few or no reported GLOFs. Although this would be problematic in most other modelling approaches, Bayesian multi-level models are well suited for this kind of imbalanced training data (Gelman and Hill, 2007; Shor et al., 2007; Stegmueller, 2013).

We used the statistical programming language **R** with the package brms, which estimates joint posterior distributions using a Hamiltonian Monte Carlo algorithm and a No-U-Turn Sampler (NUTS; Bürkner, 2017). We ran four chains of 1500 samples after 500 warm-up runs each and checked for numerical divergences or other pathological issues. We only considered models with all values of $\hat{R}$ <1.01 - a measure of numerical convergence of sampling chains - to avoid unbiased posterior distributions (Nalborczyk et al., 2019).

Unless stated otherwise, we used a weakly informative half Student's *t* distribution with three degrees of freedom and a scale parameter of 10 for the standard deviations of group-level effects (Table 3.3; Bürkner, 2017; Gelman, 2006). At the population level, we chose weakly informative priors for the intercept and coefficients for which we had no other prior knowledge. We encoded this lack of knowledge with a prior Cauchy distribution centred at zero and with a scale of 2.5, following the recommendation of Gelman et al. (2008). Rapidly growing moraine-dammed lakes are a widely used predictor of high GLOF susceptibility (e.g. GAPHAZ, 2017; Prakash and Nagarajan, 2017; Rounce et al., 2016). We encoded this notion in a prior Gaussian distribution with 1 unit mean and standard deviation, hence shifting more probability mass towards positive regression weights without excluding the possibility of negative weight estimates (Table 3.3).

Table 3.3: Prior distributions for group- and population-level effects.

Level	Model coefficient	Probability density function
Group-level effects	Standard deviation σ of group model variables	$\sigma_\alpha \sim HalfStudentT(3,10)$
Population-level effects	Intercept	$\alpha_j \sim Cauchy(0,2.5)$
	Weight of predictors with weak prior knowledge	$\beta_p \sim Cauchy(0,2.5)$
	Weight of predictor lake area β_A	$\beta_A \sim Normal(1,2)$

We estimated the predictive performance of all models with leave-one-out (LOO) cross-validation as part of the brms package (Bürkner, 2017). LOO values like the expected log predictive density (ELPD) summarise the predictive error of Bayesian models similar to the Akaike information criterion or related metrics of model selection (Vehtari et al., 2017). They are based on the log-likelihood of the posterior simulations of parameter values (Vehtari et al., 2017).

3.3 Results

Elevation-dependent warming model

Our first model addresses the notion of elevation-dependent warming (EDW) by considering lake elevation as a grouping structure in the data. The model further assumes that the GLOF history of a given lake is a function of its area *A* and net change *ΔA*. This dependence differs by up to a constant, i.e. the varying model intercept, across elevation bands z that we define here in five quantile grouping levels (Fig. 3.1). The model intercept may vary across these elevation bands, whereas lake area (in 2005) and its net change remain fixed predictors. In essence, this varying-intercept model acknowledges that glacial lakes in the same elevation band may have had a common baseline susceptibility to GLOFs in the past four decades. The indicator variable *ΔA* records whether a given lake had a net growth or shrinkage between 1990 and 2018:

$$\mu_i = \mathrm{S}(\alpha_z + \beta_A A_i + \beta_{\Delta A} \Delta A_i) \tag{3.6}$$

$$\alpha_z \sim \mathrm{N}(\mu_z, \sigma_z), \tag{3.7}$$

where index *z* identifies the elevation band.

We obtain posterior estimates of $\beta_A = 0.79^{+0.27}/_{-0.27}$ and $\beta_{\Delta A} = 0.48^{+0.73}/_{-0.72}$ (95% highest density interval, HDI) which indicate that larger lakes are more likely classified as having had a GLOF, whereas net growth or shrinkage has ambivalent weight as its HDI includes zero (Fig. 3.4, Fig. 3.5, Table 3.4). On the population level, the low spread of intercepts ($\sigma_z = 0.29^{+0.68}/_{-0.28}$) estimated for each of the five elevation bands shows that elevation effects modulate the pooled model only minutely. These posterior effects are positive for the lower elevation bands but negative for the higher elevation bands. Thus, the mean posterior probability of a GLOF history, P_{GLOF}, under this model increases slightly for lakes in lower elevations and with a larger surface area in 2005. We also observe that P_{GLOF} is less than 0.5 regardless of reported lake elevation and that the associated uncertainties are higher for larger lakes.

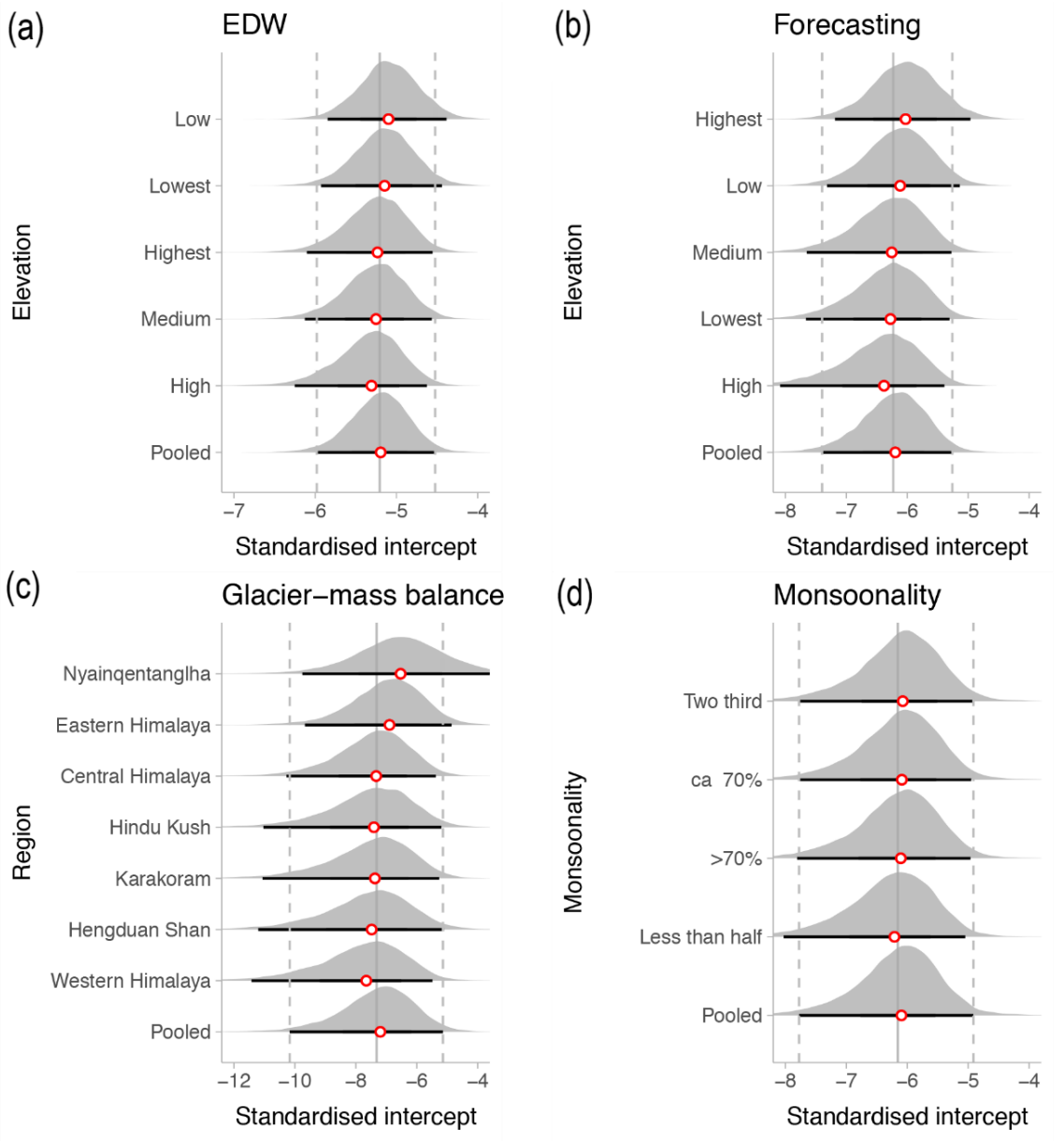

Figure 3.4: Posterior pooled and group-level intercepts for the four models considered. EDW = elevation-dependent warming. See Fig. 3.1 for a summary of the quantiles of elevation and monsoonality. Horizontal black lines delimit 95% HDI, and red circles indicate posterior medians. Vertical continuous (dashed) grey lines are posterior means (95% HDI) of the pooled intercept of each model. Intercepts are standardised and thus refer to lakes with average predictor values.

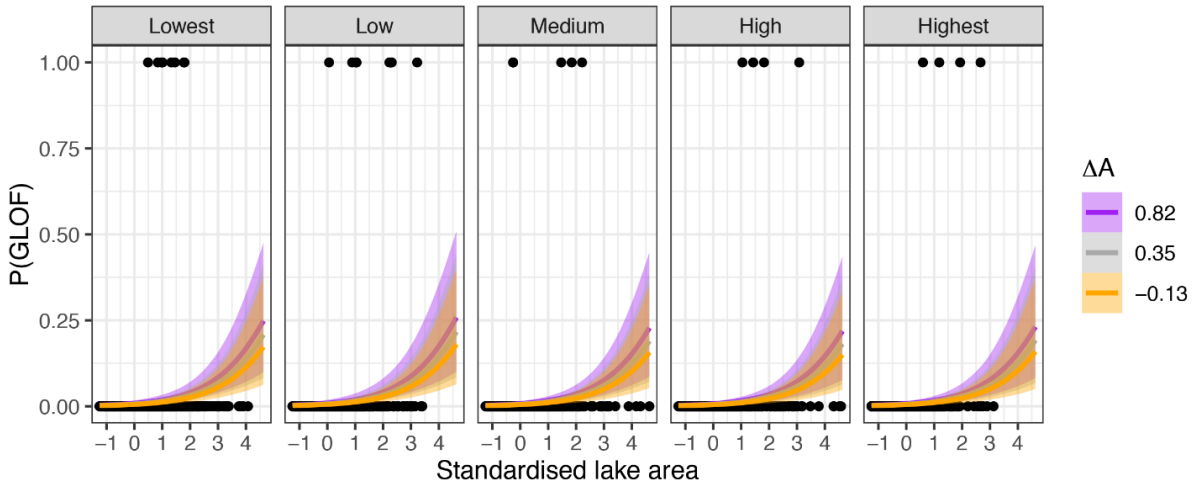

Figure 3.5: Elevation-dependent warming model: posterior probabilities P_{GLOF} as a function of standardised lake area A (in 2005) and the sign of standardised lake-area change ΔA (i.e. net growth or shrinkage), grouped by quantiles of elevation (defined in Fig. 3.1; lowest: 2470-4600 m a.s.l.; low: 4600-4970 m a.s.l.; medium: 4970-5180 m a.s.l.; high: 5180-5440 m a.s.l.; highest: 5440-6030 m a.s.l.). Black dots are lake data with (P_{GLOF} = 1) or without (P_{GLOF} = 0) reported GLOF records. Thick coloured lines are mean fits, and colour shades encompass the associated 95% HDIs.

Table 3.4: Summary of the results of our four models. CI = credible interval.

Model	Model parameter	Estimate	Estimation error	Lower 95% CI boundary	Upper 95% CI boundary
Elevation-dependent warming model	α_z	-5.22	0.36	-5.96	-4.56
	β_A	0.79	0.14	0.52	1.06
	$\beta_{\Delta A\ (1990\ to\ 2018)}$	0.49	0.38	-0.28	1.24
	σ_z	0.28	0.27	0.01	0.99
Forecasting model	α_z	-6.23	0.54	-7.39	-5.26
	β_A	0.87	0.22	0.44	1.31
	$\beta_{A^{*a}\ (1990\ to\ 2005)}$	-0.04	0.38	-0.71	0.73
	$\beta_{A\times A^{*a}}$	-0.16	0.24	-0.67	0.26
	σ_z	0.43	0.41	0.01	1.49
Glacier-mass balance model	$\alpha_{z,r}$	-7.31	1.26	-10.15	-5.19
	$\beta_{A^{*b}\ (2005\ to\ 2018)}$	-0.69	0.32	-1.31	-0.06
	β_C	0.85	0.26	0.35	1.36
	γ_r	-2.90	2.80	-9.27	1.80
	σ_z	0.47	0.44	0.01	1.61
	σ_r	0.83	0.66	0.03	2.47
Monsoonality model	$\alpha_{M,r}$	-6.14	0.70	-7.70	-4.91
	$\beta_{A^{*c}\ (1990\ to\ 2018)}$	-0.63	0.31	-1.23	-0.02
	β_C	0.82	0.24	0.34	1.28
	σ_M	0.40	0.42	0.01	1.49
	σ_r	0.78	0.62	0.03	2.31

Forecasting model

Our second model refines our approach by including only relative changes in lake area before the reported GLOFs happened. We can use this model to fore- or hindcast historic GLOFs in our inventory. Here we use lake area A (in 2005) and its relative change A^{*a} from 1990 to 2005 as predictors of 11 GLOFs that occurred between 2005 and 2018 across the five elevation bands. We assume that larger and deeper lakes are more robust to relative size changes and thus also include a multiplicative interaction term between lake area and its change:

$$\mu_i = \mathrm{S}(\alpha_z + \beta_A A_i + \beta_{A^{*a}} A_i^{*a} + \beta_{A\times A^{*a}} A_i \times A_i^{*a}) \tag{3.8}$$

We find that lake area has a credible positive posterior weight of $\beta_A = 0.86^{+0.44}/_{-0.43}$; hence greater lakes are more likely to have had a GLOF between 2005 and 2018. The weight of relative lake-area change in the 15 years before is ambiguous ($\beta_{A^{*a}} = -0.04^{+0.76}/_{-0.67}$) and so is the interaction ($\beta_{A\times A^{*a}} = -0.16^{+0.41}/_{-0.51}$). On average, however, relative increases in lake area between 1990 and 2005 slightly decrease P_{GLOF}. Unlike in the elevation-dependent warming model, the effects of elevation bands are less clear, while the uncertainties are more pronounced and highest for larger and shrinking lakes (Fig. 3.4, Fig. 3.6).

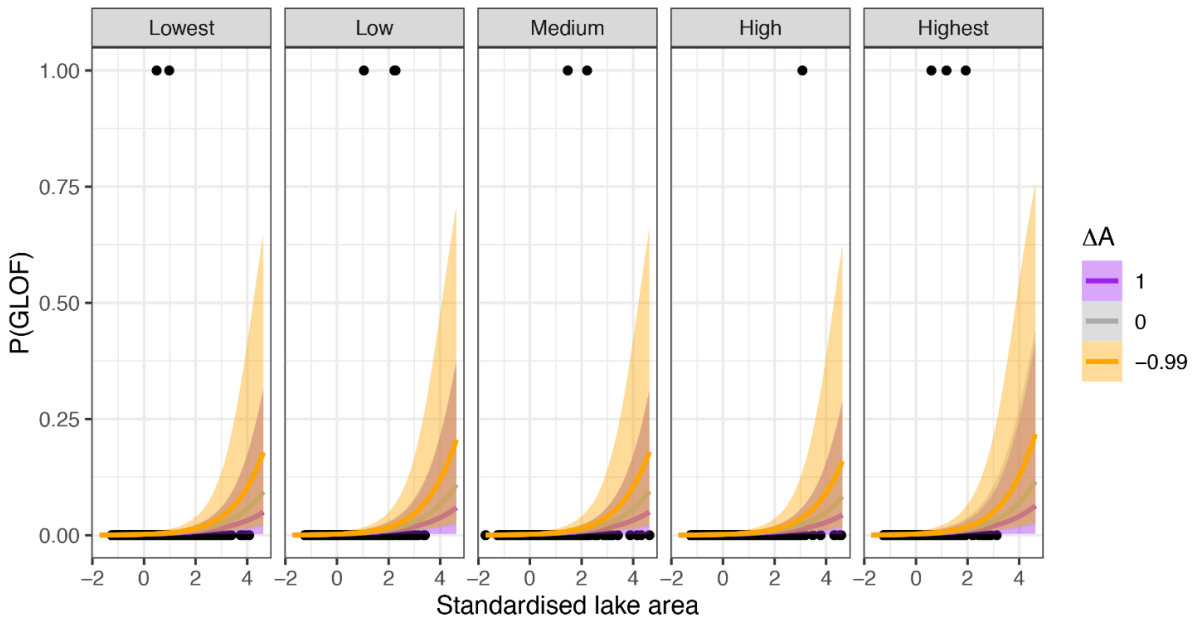

Figure 3.6: Forecasting model: posterior probabilities P_{GLOF} as a function of standardised lake area A (in 2005) and standardised lake-area change A^{*a} between 1990 and 2005, grouped by quantiles of elevation (defined in Fig. 3.1; lowest: 2470-4600 m a.s.l., low: 4600-4970 m a.s.l., medium: 4970-5180 m a.s.l., high: 5180-5440 m a.s.l., highest: 5440-6030 m a.s.l.). Black dots are lake data with (P_{GLOF} = 1) or without (P_{GLOF} = 0) reported GLOF records for the interval 2005 to 2018. Thick coloured lines are mean fits, and colour shades encompass the associated 95% HDIs.

Glacier-mass balance model

Besides elevation, our third model considers the average historic glacier-mass balances across the HKKHN. The model assumes that mean ice losses Δm add a distinctly regional structure to the susceptibility to GLOFs in the past four decades, given that accelerated glacier melt may raise GLOF potential (Emmer, 2017; Richardson and Reynolds, 2000). We use our seven study area regions as group levels *r* and their average glacier-mass balance, derived from Brun et al. (2017), as a group-level predictor Δm_r. Our pooled predictors are the relative change in lake area A^{*b} from 2005 to 2018 (to ensure a comparable time interval) and the catchment area *C* upstream of each lake. We replace lake area by its upstream catchment area, which is less prone to change but well correlated to lake area.

$$\mu_i = \mathrm{S}\left(\alpha_z + \alpha_r + \beta_{A^{*b}} A_i^{*b} + \beta_C C_i\right), \tag{3.8}$$

$$\alpha_r \sim \mathrm{N}(\mu_r + \gamma_r \Delta m_r, \sigma_r). \tag{3.9}$$

This model returns a positive weight for catchment area ($\beta_C = 0.85^{+0.50}/_{-0.50}$) and a negative weight for relative lake-area changes ($\beta_{A^{*b}} = -0.69^{+0.64}/_{-0.61}$), whereas the effect of the mean glacier-mass balance remains inconclusive ($\gamma_r = -2.98^{+4.87}/_{-6.70}$). On the basis of higher standard deviations, we learn that effects of glaciological regions vary more than those of elevation bands ($\sigma_r = 0.81^{+1.60}/_{-0.78}$ and $\sigma_z = 0.48^{+1.19}/_{-0.47}$). When training this model on a subset of glacial lakes with documented GLOFs that happened after 2000 (i.e. including only those in the interval covered by glacier-mass balance data), posterior estimates of σ_r increase to $1.11^{+1.77}/_{-1.03}$, further underlining our result that glacier-mass balance credibly affects P_{GLOF}. This is also reflected in the posterior distributions across the glacier-mass balance regions (Fig. 3.4), as well as the calculated group-level effects. This model has the highest values of P_{GLOF} for average lakes (i.e. all average predictor values combined) in the Nyainqentanglha Mountains and the Eastern Himalaya (Fig. 3.4). In contrast to the forecasting model, we observe that increases in lake area now credibly depress P_{GLOF} (Fig. 3.7).

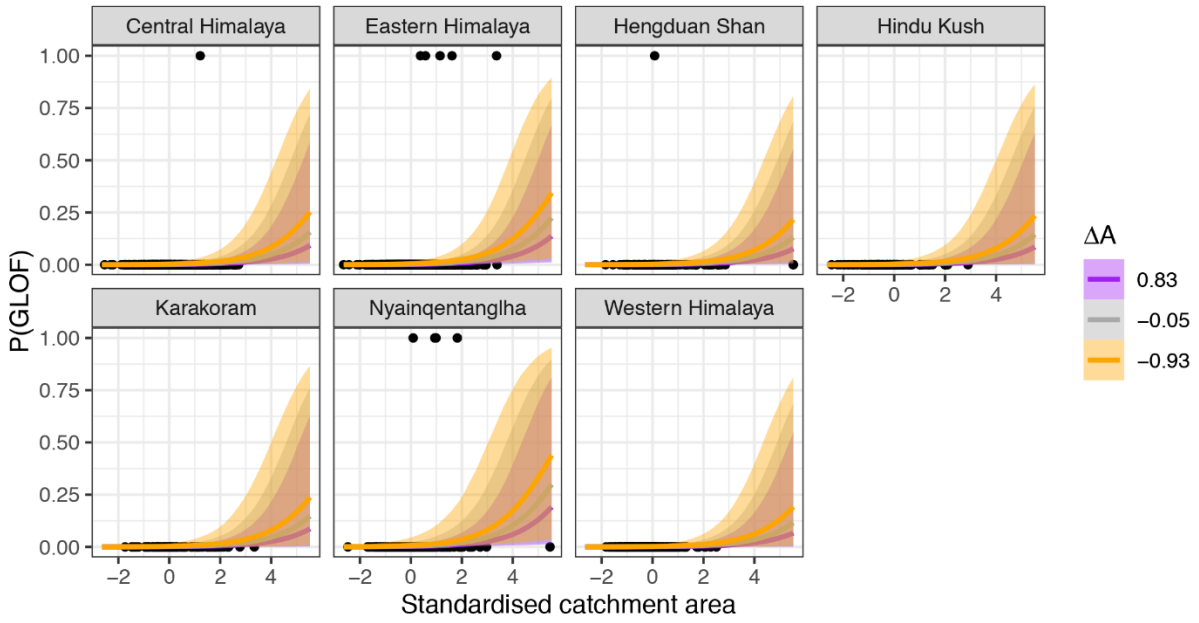

Figure 3.7: Glacier-mass balance model: posterior probabilities P_{GLOF} as a function of standardised catchment area C and standardised lake-area change A^{*b} between 2005 and 2018, grouped by regions of average glacier-mass balance (see Fig. 3.1). Black dots are lake data with (P_{GLOF} = 1) or without (P_{GLOF} = 0) reported GLOF records for the interval 2005 to 2018. Thick coloured lines are mean fits, and colour shades encompass the associated 95% HDIs.

Monsoonality model

Our last model explores a synoptic influence on GLOF susceptibility by grouping the data by the summer proportion of mean annual precipitation and thus by approximate monsoonal contribution. We defined five monsoonality levels based on quantiles of the annual proportions of summer precipitation (Fig. 3.1). We use relative lake-area change A^{*c} between 1990 and 2018, and catchment area C as population-level predictors, as well as the additional grouping by regional glacier-mass balance:

$$\mu_i = \mathrm{S}(\alpha_M + \alpha_r + \beta_{A^{*c}} A_i^{*c} + \beta_C C_i), \tag{3.10}$$

$$\alpha_M \sim \mathrm{N}(\mu_M, \sigma_M), \tag{3.11}$$

where index M identifies the monsoonality group. We find that larger catchment areas (β_C = $0.82^{+0.46}/_{-0.48}$) and lakes with relative shrinkage ($\beta_{A^{*c}} = -0.63^{+0.59}/_{-0.59}$) credibly raise P_{GLOF} (Fig. 3.4, Fig. 3.8). Higher standard deviations show that regional effects vary more for the mean glacial-mass balance than for monsoonality ($\sigma_r = 0.79^{+1.59}/_{-0.76}$ and $\sigma_M = 0.40^{+1.04}/_{-0.39}$), although both hardly change the pooled model trend.

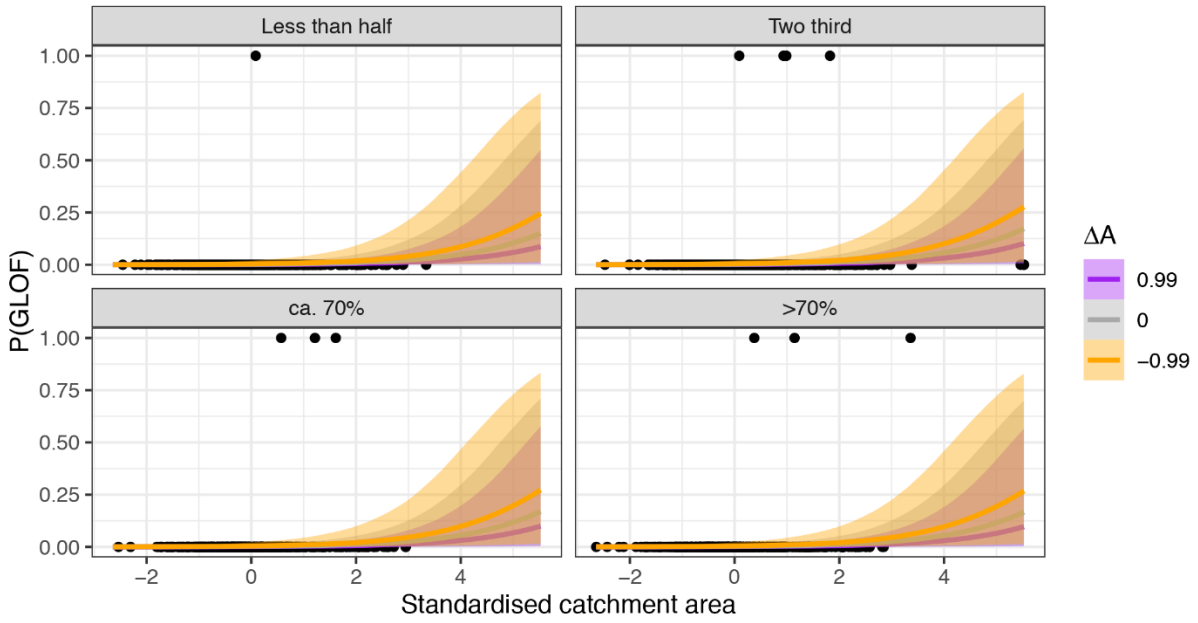

Figure 3.8: Monsoonality model: posterior probabilities P_{GLOF} as a function of standardised catchment area C and standardised lake-area change A^{*c} between 1990 and 2018, grouped by quantiles of the annual proportion of precipitation falling during summer (defined in Fig. 3.1). Black dots are lake data with (P_{GLOF} = 1) or without (P_{GLOF} = 0) reported GLOF records for the interval 1990 to 2018. Thick coloured lines are mean fits, and colour shades encompass the associated 95% HDIs.

Model performance and validation

We estimate the performance of our models in terms of the posterior improvement of our prior chance of finding a lake with known outburst in the past four decades in our inventory by pure chance. We compare the posterior predictive mean P_{GLOF} with a mean prior probability that we estimate from the ~1% proportion of lakes with known GLOFs in our training data. We measure what we have learned from each model in terms of the log-odds ratio that readily translates into probabilities using Eq. (3). A positive log-odds ratio means that we obtain a higher posterior probability of attributing a historic GLOF to a given lake compared to a random draw. Negative log-odd ratios indicate lakes for which the posterior probability of a reported GLOF is lower than the prior probability. Based on this metric, all models have higher true positive rates than true negative rates. For a prior probability informed by the historic frequency of GLOFs, the models have at least about 80% true positives and at least 70% true negatives on average (Fig. 3.9, Table 3.5).

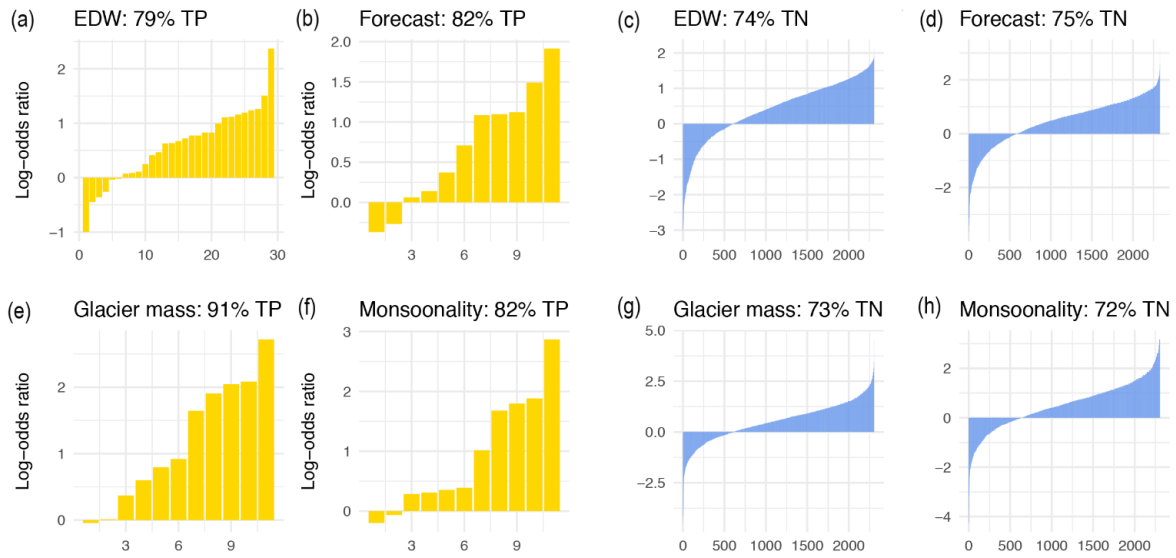

Figure 3.9: Average posterior log-odds ratios for true positives (TP) (true negatives, TN), i.e. lakes with (without) a GLOF in the period 1981 – 2018 (a and e) and 2005 – 2018 (b-d and f-h) on the x axis for the four different models. The log-odds ratios describe here the ratio of the mean posterior over the mean prior probability of classifying a given lake as having had a GLOF. We estimate the mean prior probability from the relative frequency of GLOFs in the datasets. EDW = elevation-dependent warming model.

The values of the LOO cross-validation of the predictive capabilities show that the EDW model formally has the least favourable, i.e. higher, values for both LOO metrics (Table 3.5). This is potentially due to the different true positive counts in the training datasets. However, the range of estimated ELPD values between the remaining three models is small (ΔELPD = 1.9).

Table 3.5: Overview of model validation measures for the predictive capabilities of our models. LOOIC = leave-one-out cross-validation information criterion.

Model	**Prior vs. posterior knowledge**		**LOO cross-validation metrics**	
	% true positives / % true negatives correctly identified	% false positives / % false negatives incorrectly identified	ELPD	LOOIC
Elevation-dependent warming model	79% / 74%	21% / 26%	-144.2	288.3
Forecasting model	82% / 75%	18% / 25%	-66.5	132.9
Glacier-mass balance model	91% / 73%	9% / 27%	-64.6	129.1
Monsoonality model	82% / 72%	18% / 28%	-65.6	131.2

3.4 Discussion

3.4.1 Topographic and Climatic Predictors of GLOFs

We used Bayesian multi-level logistic regression to test whether several widely advocated predictors of GLOF susceptibility and glacial lake stability are credible predictors of at least one outburst in the past four decades. All four models that we considered identify **lake area** and **catchment area** as predictors with weights that credibly differ from zero with 95% probability. Our model results quantitatively support qualitative notions of several basin-wide studies in the HKKHN (Ives et al., 2010; Khadka et al., 2021; Prakash and Nagarajan, 2017) and elsewhere (Iribarren Anacona et al., 2014; McKillop and Clague, 2007b), which proposed that larger moraine-dammed lakes have a higher potential for releasing GLOFs.

We also found that **changes in lake area** have partly inconclusive influences in the models. Two exceptions are the negative weight of lake-area changes $\beta_{A^{*}b}$ and $\beta_{A^{*}c}$ in the glacier-mass balance model and in the monsoonality model, regardless of the differing intervals that these changes were determined for (Table 3.4). While this result formally indicates that shrinking lakes are more likely to be classified as having had a historic GLOF, the period over which these lake-area changes are valid (2005 to 2018) overlaps with the timing of 11 recorded GLOFs (Eq. 9). In other words, the lake shrinkage could be a direct consequence of these GLOFs instead of vice versa. Nonetheless, our results indicate that lake-area changes, either absolute or directional, are somewhat inconclusive in informing us whether a given lake has a recent GLOF history. One advantage of our Bayesian approach is that we can express the role of lake-area changes in GLOF susceptibility by choosing different highest density intervals. For example, if we adopted a narrower, say 80% HDI for ΔA, we could be 80% certain that net lake-area growth increased P_{GLOF} under the elevation-dependent warming model (Eq. 6). However, in the forecasting model, in which we tested whether differing data observation periods have any credible effects, the influence of lake-area change remains negligible even for <50% HDIs. We thus conclude that relative lake-area change before outburst is an inconclusive predictor. This result contradicts the assumptions made in many previous studies that argued that rapidly growing lakes are the most prone to sudden outburst (GAPHAZ, 2017; Iribarren Anacona et al., 2014; Ives et al., 2010; Mergili and Schneider, 2011; Prakash and Nagarajan, 2017; Rounce et al., 2016).

The role of **elevation** in GLOF predictions is also less pronounced than that of lake or catchment area, at least at a group level. The weights of the elevation-dependent warming model indicate that lower (higher) lakes are slightly more (less) likely to have had a historic GLOF (Fig. 3.4) but hardly warrant any better model performance compared to the pooled (or elevation-independent) model. In the forecasting model, however, the contributions of lake elevation to P_{GLOF} are devoid of any

systematic pattern and likely reflect several, potentially combined drivers (Fig. 3.4). This model was trained on fewer GLOFs, and the imbalance in the data introduces more uncertainties in terms of broad 95% HDIs. Clearly, the role of elevation may need more future investigation. In terms of elevation bands, it hardly seems to aid GLOF detection with the models used here. Similarly, Emmer et al. (2016) reported that lake elevation was hardly affecting GLOF hazard in the Cordillera Blanca, Peru.

Judging from the regionally averaged **glacier-mass balances**, our models predict the highest GLOF probabilities in the Nyainqentanglha Mountains and the Eastern Himalaya, which have had the highest historic GLOF counts (Fig. 3.1). The timing and seasonality of snowfall affect how glaciers respond to rising air temperatures. Observed frequencies and predicted probabilities of historic GLOFs are lowest for several glaciers with positive mass balance in the Karakoram and Western Himalaya (Fig. 3.1, Fig. 3.10). Most moraine-dammed lakes in the HKKHN, however, are fed by glaciers with negative mass balances that likely help to elevate GLOF potential through increased meltwater input and glacier-tongue calving rates (Emmer, 2017; Richardson and Reynolds, 2000). This is also supported by the findings of King et al. (2019), which imply that higher rates of mass loss of lake-terminating glaciers since the 1970s might have also led to increased meltwater input into lakes adjacent to their termini. More than 70% of all lakes that burst out in the past four decades were in contact with their parent glaciers (Veh et al., 2019). However, systematically recorded time series of glacier fronts are even harder to come by when compared to systematic measurements of changes in glacial-lake areas. Given that the regional glacier-mass balance is linked to synoptic precipitation patterns (Kapnick et al., 2014; King et al., 2019; Krishnan et al., 2019), our glacier-mass balance model highlights that the regional ice loss outweighs the role of monsoonality in terms of higher changes to the group-level intercepts for comparable mean P_{GLOF} and associated uncertainties (Fig. 3.4, Fig. 3.7, Fig. 3.8).

Our results offer insights into the links between historic GLOFs and the **synoptic precipitation patterns**. Richardson and Reynolds (2000) presumed that seasonal floods and GLOFs are both caused by high monsoonal precipitation and summer ablation. In contrast, our results indicate that the fraction of summer precipitation changes the predictive probabilities of historic GLOFs only marginally, at least at the group level, so that deviations from a pooled model for the HKKHN are minute when compared to the spread of posterior group-level intercepts in the other models (Fig. 3.4). In essence, our results underline the need for exploring more the interactions of both precipitation and temperature as potential GLOF triggers. It may well be that seasonal timing of heavy precipitation events and type (rain or snow) at a given lake may be more meaningful to GLOF susceptibility than annual totals or averages. Whether our finding that glacier-mass balances driven

by superimposed synoptic regimes credibly influence regional GLOF susceptibility in the HKKHN is applicable to other regions, for example the Cordillera Blanca in the South American Andes (Emmer et al., 2016; Emmer and Vilímek, 2014; Iturrizaga, 2011), also needs further investigation.

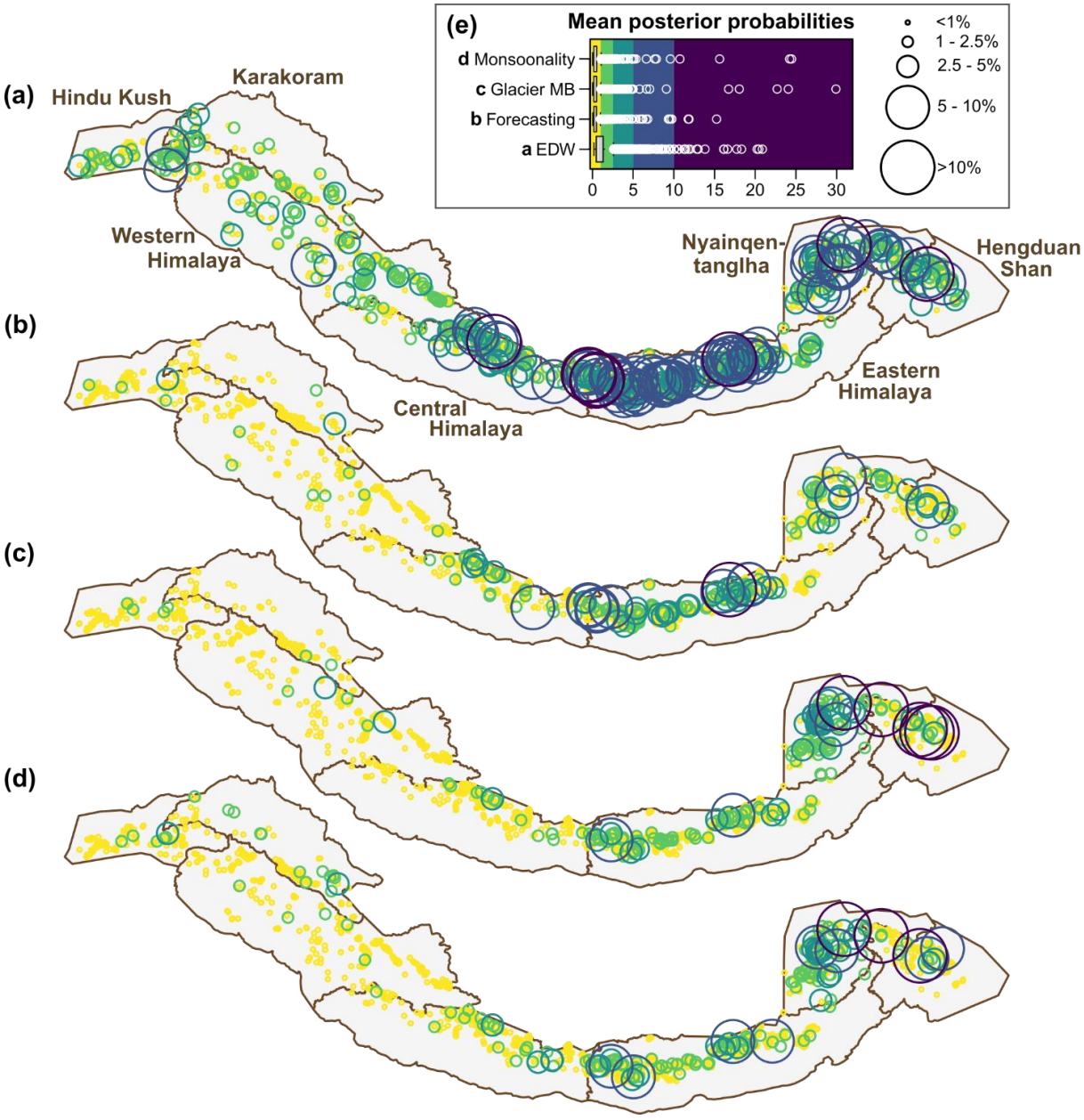

Figure 3.10: Mean posterior probabilities of HKKHN glacial lakes for having had a GLOF history (P_{GLOF}) in the past four decades as estimated in the (a) elevation-dependent warming model, (b) forecasting model, (c) glacier-mass balance model, and (d) monsoonality model. Size and colours of bubbles are scaled by posterior probabilities.

3.4.2 Model Assessment

We consider our quantitative and data-driven approach as complementary to existing qualitative and basin-wide GLOF hazard appraisals. Our models cannot replace field observations that deliver local details on GLOF-disposing factors such as moraine or adjacent rock-slope stability, presence of ice cores, glacier calving rates, or surges. Our selection of predictors is a compromise between widely used predictors of GLOF susceptibility and hazard and their availability as data covering the entire HKKHN. To this end, we used lake (or catchment) area and lake-area changes as predictors, as well as elevation, regional glacier-mass balance, and monsoonality as group levels of past GLOF activity of several thousand moraine-dammed lakes in the HKKHN. Among the many possible combinations of predictors and group levels we focused on those few combinations with minimal correlation among the input variables. We minimised the potential for misclassification by using a purely remote-sensing-based inventory of GLOFs, which reduces reporting bias for GLOFs too small to be noticed or happening in unpopulated areas: more destructive GLOFs are recorded more often than smaller GLOFs in remote areas (Veh et al., 2018, 2019). We are thus confident that we trained our models on lakes with a confirmed GLOF history at the expense of discarding known outbursts predating the onset of Landsat satellite coverage in 1981. We acknowledge that climate products such as precipitation can have large biases because of orographic effects or climate circulation patterns and interpolation using topography (Karger et al., 2017; Mukul et al., 2017). Cross-validation of CHELSA precipitation estimates with station data has a global mean coefficient of determination R^2 of 0.77, with regional variations between 0.53 and 0.90 (Karger et al., 2017). By accounting for orographic wind effects, CHELSA products outperform previous global datasets such as the WorldClim (Hijmans et al., 2005), especially in the rugged HKKHN topography. We stress that we therefore used all climatic data as aggregated group-level variables to avoid spurious model results. At the level of individual lakes, we thus resorted only to size, elevation, and upstream catchment area as more robust predictors.

Due to strong imbalance in our training data, we opted for a prior vs. posterior log-odd comparison instead of commonly applied receiver operating characteristics (ROCs) in estimating the predictive capabilities of our models (Saito and Rehmsmeier, 2015). In our models, only a few posterior estimates of P_{GLOF} are >0.5 and they thus offer very conservative estimates of a GLOF history (Fig. 3.10). All models have wide 95% HDIs that attest to a high level of uncertainty. This observation may be sobering but nevertheless documents objectively the minimum amount of accuracy that these simple models afford for objectively detecting historic outbursts.

The low fraction of lakes with a GLOF history (~1%) curtails a traditional logistic regression model and favours instead a Bayesian multi-level approach that can handle imbalanced training data and

collinear predictors (Gelman and Hill, 2007; Hille Ris Lambers et al., 2006; Shor et al., 2007). We prefer the straight-forward interpretation of posterior regression weights to random forest classifiers, neural networks, or support vector machines (Caniani et al., 2008; Falah et al., 2019; Kalantar et al., 2018; Taalab et al., 2018). While these methods may perform better, they disclose little about the relationship between model inputs and outputs (Blöthe et al., 2019; Dinov, 2018); much of their higher accuracy is also linked to the overwhelming number of true negatives. Yet so far, multi-criteria decision analysis or decision-making trees have been the method of choice in GLOF hazard assessments, both in High Mountain Asia (Bolch et al., 2011; Prakash and Nagarajan, 2017; Rounce et al., 2016; Wang et al., 2012b) and elsewhere (Emmer et al., 2016; Emmer and Vilímek, 2014; Huggel et al., 2002; Kougkoulos et al., 2018). While these methods strongly rely on expert judgement (Allen et al., 2019), a Bayesian logistic regression encodes any prior knowledge or constraints explicitly and reproducibly as probability distributions. Still, inconsiderate or inappropriate prior choices can introduce bias (van Dongen, 2006; Kruschke and Liddell, 2018). Therefore, we carefully considered our choice of weakly informative priors for predictors with limited prior knowledge, following the guidelines concerning regression models by Gelman (2006) and Gelman et al. (2008). We also cross-checked our results when applying varying prior choices and found negligible differences in the resulting posterior distributions.

To summarise, our simple classification models hardly support the notion that elevation or changes in lake area are straightforward predictors of a GLOF history, at least for the moraine-dammed lakes that we studied in the HKKHN. Lake size and regional differences in glacier-mass balance are items that future studies of GLOF susceptibility may wish to consider further. The performance of these models is moderate to good if compared to a random classification, yet it is associated with high uncertainties in terms of wide highest density intervals. We underline that these uncertainties have rarely been addressed, let alone quantified, in previous work. One way forward may be to create ensembles of such models to improve their predictive capability instead of relying on any single model.

3.5 Conclusions

We quantitatively investigated the susceptibility of moraine-dammed lakes to GLOFs in major mountain regions of High Asia. We used a systematically compiled and comprehensive inventory of moraine-dammed lakes with documented GLOFs in the past four decades to test how elevation, lake area and its rate of change, glacier-mass balance, and monsoonality perform as predictors and group levels in a Bayesian multi-level logistic regression. Our results show that larger lakes in larger catchments have been more prone to sudden outburst floods, as have those lakes in regions with

pronounced negative glacier-mass balance. While elevation-dependent warming (EDW) may control a number of processes conducive to GLOFs, grouping our classification by elevation bands adds little to a pooled model for the entire HKKHN. Historic changes in lake area, both in absolute and relative values, have an ambiguous role in these models. We observed that shrinking lakes favour the classification as GLOF-prone, although this may arise from overlapping measurement intervals such that the reduction in lake size arises from outburst rather than vice versa. In any case, the widely adapted notion that (rapid) lake growth may be a predictor of impending outburst remains poorly supported by our model results. Our Bayesian approach allows explicit probabilistic prognoses of the role of these widely cited controls on GLOF susceptibility but also attests to previously hardly quantified uncertainties, especially for the larger lakes in our study area. While individual models offer some improvement with respect to a random classification based on average GLOF frequency, we recommend considering ensemble models for obtaining more accurate and flexible predictions of outbursts from moraine-dammed lakes.

4 Himalayan Hazard Cascades – Modern and Ancient Outburst Floods in Pokhara, Nepal

Under review as:

Fischer, M., Lehnigk, K., Lützow, N., Brettin, J., Veh, G., Larsen, I., Korup, O., and Walz, A. (2022): Himalayan Hazard Cascades - Modern and Ancient Outburst Floods in Pokhara, Nepal, Earth Surface Processes and Landforms, submitted December 2021.

Abstract

In May 2012, a sediment-laden flood along the Seti Khola (= river) caused 72 fatalities and widespread devastation for more than 40 km downstream in Pokhara, Nepal's second largest city. The flood was the terminal phase of a hazard cascade that likely began with a major rock-slope collapse in the Annapurna massif upstream, followed by intermittent ponding of meltwater and subsequent outburst flooding. Similar hazard cascades have been reported in other mountain belts, but peak discharges for these events have rarely been quantified. We use two hydrodynamic models to simulate the extent and geomorphic impacts of the 2012 flood and attempt to reconstruct the water discharge linked to even larger Mediaeval sediment pulses. The latter are reported to have deposited several cubic kilometres of debris into the Pokhara valley; however, the process behind these sediment pulses is debated. We traced evidence of aggradation along the Seti Khola during field surveys and from RapidEye satellite images. We use two steady-state flood models, HEC-RAS and ANUGA, and high-resolution topographic data, to constrain the initial flood discharge with the lowest mismatch between observed and predicted flood extents downstream. We explore the physically plausible range of flood scenarios, from meteorological (1,000 m^3 s^{-1}) to cataclysmic outburst floods (600,000 m^3 s^{-1}). We find that the 2012 flood most likely had a peak discharge of 3,700 m^3 s^{-1} in the upper Seti Khola and attenuated to 500 m^3 s^{-1} when arriving in Pokhara city. Simulations of larger flood magnitudes show extensive backwater effects in tributary valleys that match with the locations of upstream-dipping Mediaeval slackwater sediments in several tributaries of the Seti Khola. This finding is consistent with the notion that the associated Mediaeval sediment pulses were linked to outburst floods with peak discharges of >50,000 m^3 s^{-1}, though more likely an order of magnitude higher.

4.1. Introduction

Unprecedented rates of atmospheric warming in past years have spurred research on geomorphic responses of high-mountain areas (Haeberli and Whiteman, 2021; Hock et al., 2019). The recent surge in interest in cryospheric mass flows, and especially landslides, as parts of entire process cascade has offered a number of detailed case studies that reconstruct how rapid slope failures of rock and ice impact naturally dammed lakes, cause outburst waves, and transform into long-runout debris flows (Shugar et al., 2021). These cascades may have destructive consequences for settlements and infrastructure on valley floors tens of kilometres beyond the original source. Recent destructive landslides have received extensive attention: the 2017 Xinmo rock avalanche, China, for example has been the focus of nearly 80 scientific papers (e.g. Fan et al., 2017; Huang et al., 2019). Other examples include the 2000 Yigong rock avalanche, southeastern Tibetan Plateau (Shang et al., 2003); the 1987 Parraguirre rock avalanche, Chile (Hauser, 2002); and 1970 Nevados Huascaran rock avalanche, Peru (Evans et al., 2009). Sedimentary evidence is often used to reconstruct the magnitude and behaviour of palaeo-hazards (Ely and Baker, 1985; Toonen et al., 2020; Wilhelm et al., 2018). However, mass flow deposits are subsequently modified by geomorphic activity and stratigraphic exposures are often limited, which makes it challenging to reconstruct palaeo-flow. Here we utilize fresh sedimentary deposits and hydrodynamic modelling to place constraints on the terminal flow phase of a recent hazard cascade in the Annapurna massif in Nepal. We then reconstruct the discharge associated with older and larger floods, using sedimentary evidence preserved in stratigraphic sections.

On May 5, 2012 a hyperconcentrated flood impacted the Seti Khola (= river) in the Pokhara Basin, Nepal's second most densely populated area. The flood claimed at least 72 lives and incurred a loss of some 50 million NPR (370,000 €) (Gurung et al., 2015, see Gurung et al., 2021 for a list of impacts). International media initially attributed the flood to a glacial lake outburst, whereas subsequent field and satellite studies identified a series of rock-slope failures in the Annapurna massif >20 km upstream as the cause (Kargel et al., 2013). Immediate investigations included field reconnaissance reports (e.g. Gurung et al., 2015; Kargel et al., 2013; Oi et al., 2012; SANDRP, 2014) and studies (e.g. Dwivedi and Neupane, 2013; Hanisch et al., 2013) to infer the mechanism(s) that triggered the sediment-laden flood. Debris generated by the landslides blocked the narrow and steep headwater gorge of the Seti Khola, impounding meltwaters from the partly glacier-covered Sabche Cirque (Gurung et al., 2015; Kargel et al., 2013). A subsequent rock- and ice-avalanche of 33 million m^3 (Oi et al., 2014) fell from the southwestern ridgeline of Annapurna IV (7,525 m a.s.l.), and caused the rockslide dam to burst, although the sequence of events remains debated. The sediment-laden flood released by the dam burst rushed through a steep bedrock gorge, and destroyed Kharapani

village (1,100 m a.s.l.) some 18 km downstream during more than 20 surges involving some 7.5 million m^3 of water and sediment with a peak discharge Q_p of 8,400 $m^3 s^{-1}$ (Gurung et al., 2015; Kargel et al., 2013). As Seti Khola was ungauged at the time of the May 2012 flood, previous studies estimated Q_p from video footage and empirical flow equations (Table 4.1).

Table 4.1: Flood estimates of the May 2012 flood along the Seti Khola proposed in the literature (for a comparison with this study's results also see Fig. 4.10).

Location (see Fig. 4.1)	Flood estimates		Reference
	Peak discharge Q_p	Flood volume V	
Kharapani village	8,400 $m^3 s^{-1}$	7.48×10^6 m^3	Gurung et al., 2015
	8,400 $m^3 s^{-1}$	8.32×10^6 m^3	Oi et al., 2012
Seti dam	>1,000 $m^3 s^{-1}$	2×10^6 to 10^7 m^3	Kargel et al., 2013
	935 $m^3 s^{-1}$ (2.15 m water level)	-	SANDRP, 2014
Karuwa village	12,300 $m^3 s^{-1}$	8.32×10^6 m^3	Oi et al., 2012
Ghachok	3,300 $m^3 s^{-1}$	8.32×10^6 m^3	Oi et al., 2012

The extent and size of the 2012 hazard cascade are much smaller than those of at least three Mediaeval (12th to 14th century) catastrophic aggradation events originating in the Annapurna massif and recorded in the valley fill of the Pokhara Basin (Fort, 2010; Schwanghart et al., 2016a). These sediment pulses were likely derived from a combination of earthquake-triggered rock-ice avalanches, dam-break floods, debris flows, and intermittent fluvial reworking (Schwanghart et al., 2016a; Stolle et al., 2017). Although a number of large prehistoric outburst events or hazard cascades are known from the Himalayas (Coxon et al., 1996; Srivastava et al., 2017; Turzewski et al., 2019), flow characteristics of these events are harder to estimate. Late Pleistocene (26.9 to 43.4 ka BP) outburst of former glacial lake Batal in the Lahul Himalaya, India, impacted the Chandra Valley with an estimated Q_p of 27,000 $m^3 s^{-1}$ and a total flood volume of 1.5 km^3 (Coxon et al., 1996; Richardson and Reynolds, 2000). Even larger Quaternary glacier- and landslide-dammed outburst floods ($Q_p > 10^5$ $m^3 s^{-1}$) occured along the Yigong River, China (Korup and Montgomery, 2008; Turzewski et al., 2019).

Here we use numerical hydrodynamic models to estimate the peak discharges during both the 2012 and Mediaeval hazard cascades in the Pokhara Basin. We thus focus on the downstream flow phases

of these event chains. We pursue two objectives. First, we use HEC-RAS modelling calibrated using mapped sedimentary evidence of the 2012 hazard cascade to assess whether and how well our simulations match estimates of peak discharge largely derived from eyewitness accounts and amateur video footage. Second, we use ANUGA to simulate a much higher range of peak discharges for the proposed Mediaeval outburst floods, and check which of these is most consistent with reported sedimentary evidence.

4.2 Study Area

The Pokhara Basin is one of several Himalayan intramontane basins that formed during the Paleogene collision of the Eurasian and Indo-Australian plates between 50 to 45 Ma. The basin is in the Pahar zone between the Higher Himalaya and the Lesser Himalaya (Mahabharat Range) (Fort, 2010). Tectonic uplift rate near the Annapurna massif is 7 mm yr^{-1}, partly caused by reactivation of faults running along the Main Central Thrust, which separates the Higher and Lesser Himalayan units (Burbank et al., 2003; Grandin et al., 2012). This fault zone juxtaposes the >8-km high Annapurna massif from the <1-km high Pokhara Basin along of the steepest topographic gradients in the Central Himalayas. The pre-Cenozoic bedrock is mainly sedimentary and metamorphic rocks of the Tethyan sedimentary series (TSS), the Higher-Himalaya crystalline (HHC), and the Lower Himalayan Sequence (LHS). The Seti Khola is the main river draining the Annapura massif to the south, where it has built a 140-km^2 fan in the Pokhara Basin. The river originates at 3,700 m a.s.l. in the Sabche cirque, fed by meltwaters from the Annapurna massif, and reaches Pokhara city at 850 m a.s.l. some 35 km downstream (Fig. 4.1). The basin's most recent sediment fill is a large alluvial fan with an estimated volume of >1 km^3 (Blöthe and Korup, 2013) and at least three depositional units, the Tallakot, Ghachok, and Pokhara Formation (Fort, 2010; Schwanghart et al., 2016a). The conglomeratic deposits of the stratigraphically oldest Tallakot and the overlying Ghachok Formation were presumably Pleistocene to post-glacial mass flows from the Sabche cirque (Fort, 2010). The stratigraphically youngest Pokhara Formation is 60-100 m thick (Fort, 2010), with decimetre- to metre-thick cobble to boulder beds of HHC provenance (Fort, 2010; Schwanghart et al., 2016a). Radiocarbon dates have Mediaeval ages consistently, and coincide with the timing of at least three recorded M>8 earthquakes (1100, 1255, 1344 C.E.), such that the deposits may have arisen from seismically triggered long-runout mass flows (Schwanghart et al., 2016a). The processes responsible for these sediment pulses along the Seti Khola remain unclear, both glacial lake outburst floods and ice-rock avalanches are likely candidates (Schwanghart et al., 2016a; Stolle et al., 2017). The Seti Khola cuts through the Pokhara basin fill for 70 km, having formed broad, unpaired cut-and-fill terraces up to >100 m high in the Pokhara urban area (Fort, 2010; Hormann, 1974; Stolle et al., 2019).

Several gorges less than 1 km long but up to 90 m deep occur in the indurated, calcareous Ghachok Formation and the LHS bedrock (Fort, 2010; Stolle et al., 2019). Several lakes (Phewa, Rupa, and Begnas) formed when the Mediaeval and older mass-flow deposits of the Seti Khola dammed several tributary mouths (Fort, 2010; Stolle et al., 2019).

The climate is seasonal with heavy summer monsoon rainfall on the southern flank of the Annapurna from May to October, when >80% of the mean annual precipitation of 4,000 mm occurs (Ross and Gilbert, 1999). The central Pokhara Basin has a humid sub-tropical to humid temperate climate with mean monthly temperatures of 12.8 to 25.8°C (Ross and Gilbert, 1999), whereas the Annapurna massif has temperate to alpine climate.

Pokhara is Nepal's second largest city with an estimated population of 523,000 in 2020 that tripled since the 1990s (Rimal et al., 2015). In past decades, the city and the surrounding basin have seen rapid growth in population and tourism. Urban areas increased by 30 km^2 between 1990 and 2013; migration caused a 45% increase of urban areas from 1977 to 2010 (Rimal, 2012; Rimal et al., 2015). Urbanisation also led to an increase in informal settlements, also, along the active channel of the Seti Khola (Rimal et al., 2015, 2018).

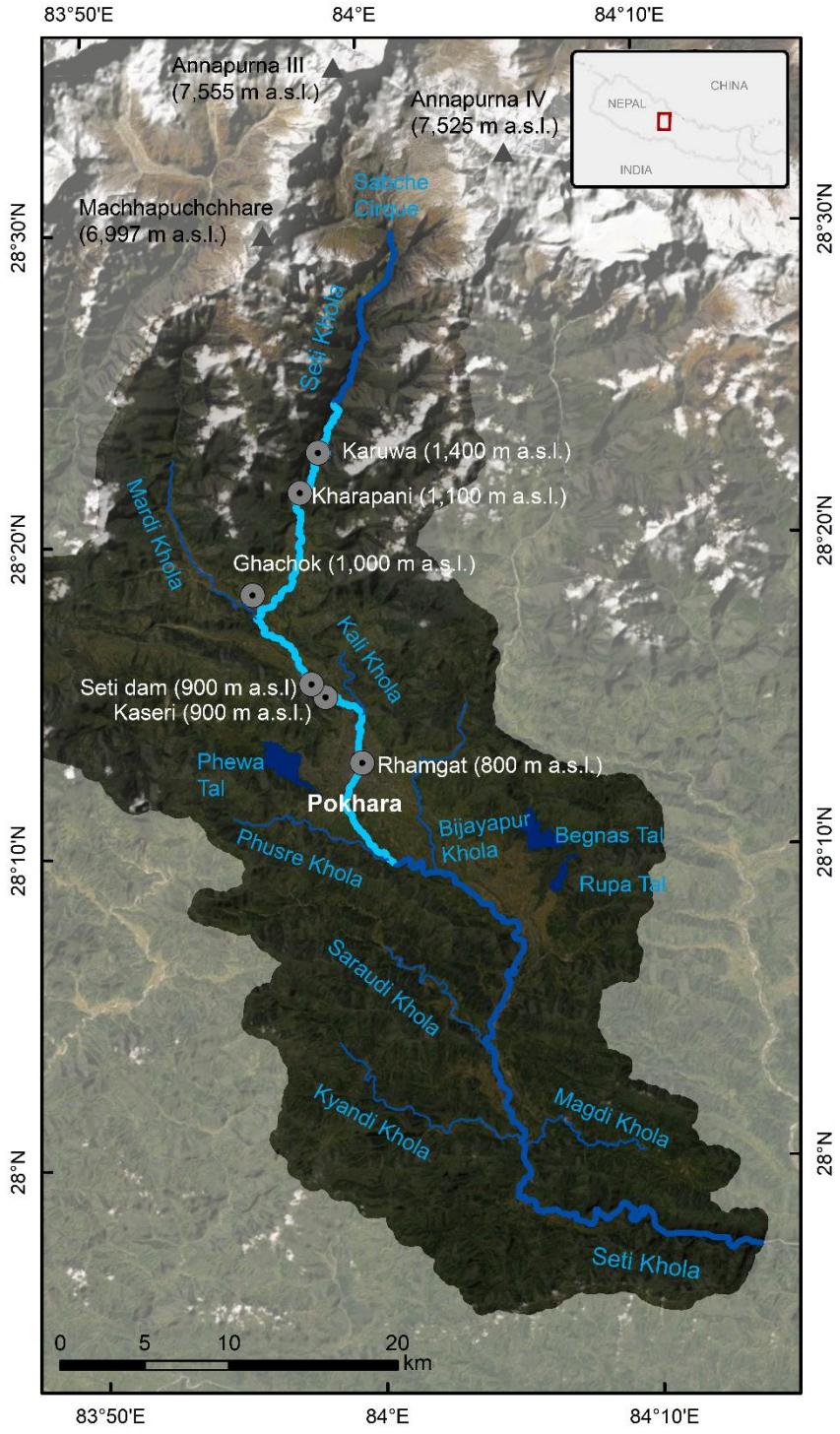

Figure 4.1: The Pokhara valley and its main drainage system, the Seti Khola and its tributaries. We studied the light blue river reach during our field seasons in October of 2016 and 2019. Displayed on ESRI basemap Maxar satellite imagery acquired in 2020 (ESRI and Maxar Technologies, 2022).

4.3 Methodology and Methods

4.3.1 Data and Data Acquisition

For the hydrodynamic simulations we used a 5-m ALOS digital elevation model (DEM) of the Seti Khola catchment, referenced to the EGM96 geoid and projected to UTM Zone 44N. In the field we surveyed 93 cross-sections along a 30-km long stretch of the Seti Khola and its terraces from near Karuwa village (1,550 m a.s.l.) to the Phusre Khola confluence in the southern outskirts of Pokhara (646 m a.s.l.) with a TruPulse 360 laser range finder and a Garmin eTrex handheld GPS in October 2016 and 2019. We used our field data to manually correct the DEM-derived cross-sections along the Seti Khola's deep and narrow gorges.

We estimated Manning's *n*, i.e. a hydraulic loss coefficient, for the channel at 61 field sites following the method of Arcement Jr and Schneider (1984) and Chow (1959). For the extensive floodplains, we linked Manning's *n* to land-cover types that we manually mapped from a 2020 Maxar satellite image available as ESRI basemap in 1-m resolution (ESRI and Maxar Technologies, 2022). We converted land-cover classes by the USGS National Land Cover Database into Manning's *n* values following recommendations by Brunner (2020b) (Fig. 4.2). Manning's *n* is a major source of uncertainty in numerical hydraulic models (Brunner, 2020a; Klimeš et al., 2014) and we conducted a sensitivity analysis to estimate this uncertainty.

We mapped flood deposits and inundation limits of the 2012 outburst from orthorectified 5-m resolution RapidEye images acquired on October 18, 2012, which was the first cloud-free image following the flood (Planet Team, 2017). Flood sediments stood out as bright pixels on otherwise dark green, vegetated terraces. Mapped extents of upstream-dipping slackwater deposits located up to several kilometres upstream of tributary junctions served as approximate markers of Mediaeval sediment pulses (Fort, 2010; Stolle et al., 2019). These markers may have been subject to subsequent erosion, and hence delineate the minimum extent of Mediaeval sediment pulses.

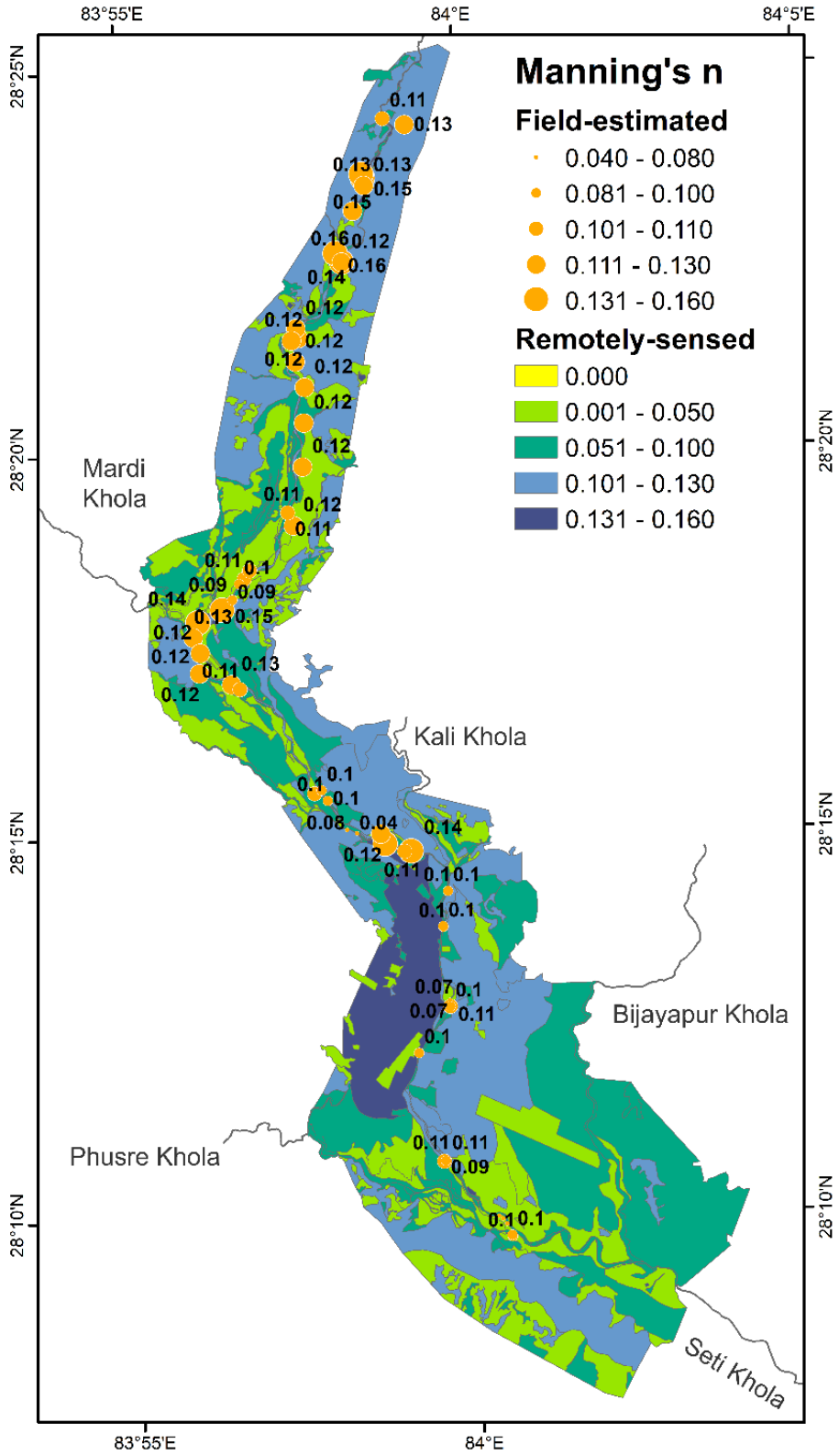

Figure 4.2: Manning's n values estimated in the field (or from field-photos) with the Arcement Jr and Schneider (1984) method (beige circles) and as remotely-sensed land-cover class mapping (coloured polygons) from ESRI basemap Maxar satellite imagery acquired in 2020 (ESRI and Maxar Technologies, 2022).

4.3.2 Numerical Flood Routing with HEC-RAS

Studies of Himalayan outburst floods increasingly use numerical hydrodynamic models to simulate downstream flood routing (Westoby et al., 2014; Worni et al., 2014; Zhang and Liu, 2015). These models are based on the conservation of mass and momentum and solved for channels and floodplains with known geometry and surface roughness (Westoby et al., 2014; Worni et al., 2014; Zhang and Liu, 2015). Among the many models to choose from (e.g. BASEMENT by Faeh et al., 2011; Flo-2D by O'Brien et al., 1993; and DAMBRK by Fread, 1988), we opted for the widely used HEC-RAS to simulate the 2012 hazard cascade (Cenderelli and Wohl, 2003; Klimeš et al., 2014; Wang et al., 2018).

Numerical hydrodynamic modelling of water flows in open channels is based on the hydraulic principles described by the shallow water equations (SWE) or, for 1D flow, by the Saint-Venant equation (Westoby et al., 2014; Worni et al., 2014; Zhang and Liu, 2015). We used HEC-RAS version 5.0.7 (https://www.hec.usace.army.mil/software/hec-ras/), which applies a step method for simulating one-dimensional steady, i.e. gradually varied but constant, channel flow (Brunner, 2020a; Klimeš et al., 2014). Water surface profiles are computed by iteratively solving the energy equation (Eq. 4.1) in which flow energy losses are included as friction, contraction, and expansion in the natural channel geometry (Brunner, 2020a).

$$Z_2 + Y_2 + \frac{a_2 V_2^2}{2g} = Z_1 + Y_1 + \frac{a_1 V_1^2}{2g} + h_e, \tag{4.1}$$

where Z_1 and Z_2 are the elevations of the main channel bed at cross-sections 1 and 2, Y_1 and Y_2 are the corresponding flow depths, V_1 and V_2 are the mean flow velocities, and a_1 and a_2 are weighting coefficients; g is the gravitational acceleration and h_e is the energy head loss (Eq. 4.2):

$$h_e = L\overline{S}_f + C\left|\frac{a_2 V_2^2}{2g} - \frac{a_1 V_1^2}{2g}\right|, \tag{4.2}$$

where L is the distance weighted reach length, $\overline{S}_f$ is the energy gradient, and C is the expansion (or contraction) loss coefficient. The discharge Q for each cross-section is calculated using Manning's equation (Eq. 4.3):

$$Q = \frac{1}{n} A R^{2/3} S_f^{1/2}, \quad (4.3)$$

where A is the cross-sectional area of the flow and R is the hydraulic radius.

HEC-RAS allows for modelling steady flow in subcritical, supercritical, or mixed flow regimes (Brunner, 2020a). For modelling supercritical flow in HEC-RAS, the necessary critical depth for each cross-section is iteratively solved via the total energy head H (Eq. 4.4):

$$H = WS + \frac{aV^2}{2g}, \quad (4.4)$$

where WS is the water surface elevation and $\frac{aV^2}{2g}$ is the velocity head.

We computed water-surface-profiles in HEC-RAS for a total of 572 cross-sections at roughly 90-m spacing for the main reach of the Seti Khola and three major tributaries (Mardi, Kali, and Phusre Khola) (Fig. 4.3). We also assigned our land-cover- and field-based estimates of Manning's *n* values to the channel and overbank portions of each cross-section.

We used several model scenarios of initial Q_p between 1,000 and 10,000 $m^3 s^{-1}$ and iteratively approximated local Q_p during the May 2012 flood by comparing model results with the mapped flood inundation and high-water evidence. We distinguished between areas where simulations under- or overestimated the observed sedimentation. We assumed a mixed flow regime with critical flow depth as an upper boundary condition and normal depth with an approximated energy slope of 0.0065 as a lower boundary condition, given the high channel gradient and frequent alterations in channel geometry (Klimeš et al., 2014). We also specified a steady base flow of 100 $m^3 s^{-1}$ (i.e. <10% of our Q_p scenarios) in the tributaries for all scenarios.

4.3.3 Numerical Flood Routing with ANUGA

For simulating the larger floods of the Mediaeval hazard cascade we used ANUGA, a model successfully used for outburst floods from breaches of man-made (Mungkasi et al., 2013) and natural dams (Guerra et al., 2014; Larsen and Lamb, 2016) and meteorological floods (Chen et al., 2021b). We chose ANUGA over HEC-RAS to optimise computational loads when simulating scenarios with larger Q_p. The purpose of these simulations is to determine the smallest discharge to inundate locations of slackwater deposits that we use as planform flood markers rather than to simulate a

flood hydrograph. ANUGA is a two-dimensional, finite-volume hydrodynamic modelling software that solves the depth-averaged shallow water equations (Roberts et al., 2015). ANUGA uses a triangular mesh for computation, constructed from 5-m ALOS DEM data, with a default maximum triangle area of 2,500 m^2 throughout the domain (Fig. 4.3). A smaller maximum triangle area of 50 m^2 was specified surrounding six features of interest, including a relict landslide dam and the Karuwa and Kharapani villages in the upper reach, Seti dam, Ramghat, and the Phusre confluence. The node locations in the computational mesh were automatically generated by ANUGA, with higher node density in areas with higher relief. All boundary segments were modelled as Dirichlet boundaries at which flow was permitted to exit the domain except for the inlet, which was assigned a reflective boundary condition. Grids of flow depth and stage were interpolated from the computational mesh at 5-m cell resolution for model timesteps of interest. All simulations used a spatially-uniform Manning's roughness coefficient of 0.091, based on our Manning's *n* estimates. Schwanghart et al. (2016) estimated a maximum discharge of 600,000 $m^3 s^{-1}$ for the Mediaeval mass flows based on the geometry of Sabche Cirque and three relict landslide dams in the upper Seti Khola gorge; discrete discharges up to this maximum were simulated in increments of up to 100,000 $m^3 s^{-1}$ using a stair-step hydrograph (Table 4.2). Each discharge was maintained for a model run time of 150,000 s (41.67 h), which was sufficient time for flow to reach steady state as indicated by constant stage at multiple gage points throughout the domain; results were saved every 10,000 s (2.78 h).

Table 4.2: Simulated Q_p scenarios [$m^3 s^{-1}$] for HEC-RAS and ANUGA and documented case studies.

Q_p scenario	HEC-RAS	ANUGA	Estimated Q_p ranges for analogues or other scenario selection reasoning			
1,000	✓		1.6×10^3 1985 Dig Tsho GLOF (Vuichard and Zimmermann, 1987)	1 – 12.3 $\times 10^3$ 2012 Seti Khola (Gurung et al., 2015; Kargel et al., 2013; Oi et al., 2012; SANDRP, 2014)		
2,000	✓					
3,000	✓					
4,000	✓					
5,000	✓	✓				
6,000	✓					
7,000	✓					
8,000	✓				8 - 14 $\times 10^3$ 2021 Chamoli (Shugar et al., 2021)	
9,000	✓					
10,000	✓	✓				

Q_p scenario	HEC-RAS	ANUGA	Estimated Q_p ranges for analogues or other scenario selection reasoning	
50,000		✓	$61 - 173 \times 10^3$ 2000 Yigong outburst flood (Turzewski et al., 2019)	$50 - 600 \times 10^3$ Mediaeval Pokhara sediment pulses Schwanghart et al. (2016)
100,000		✓		
200,000		✓		
300,000		✓		
400,000		✓		
500,000		✓		
600,000		✓		

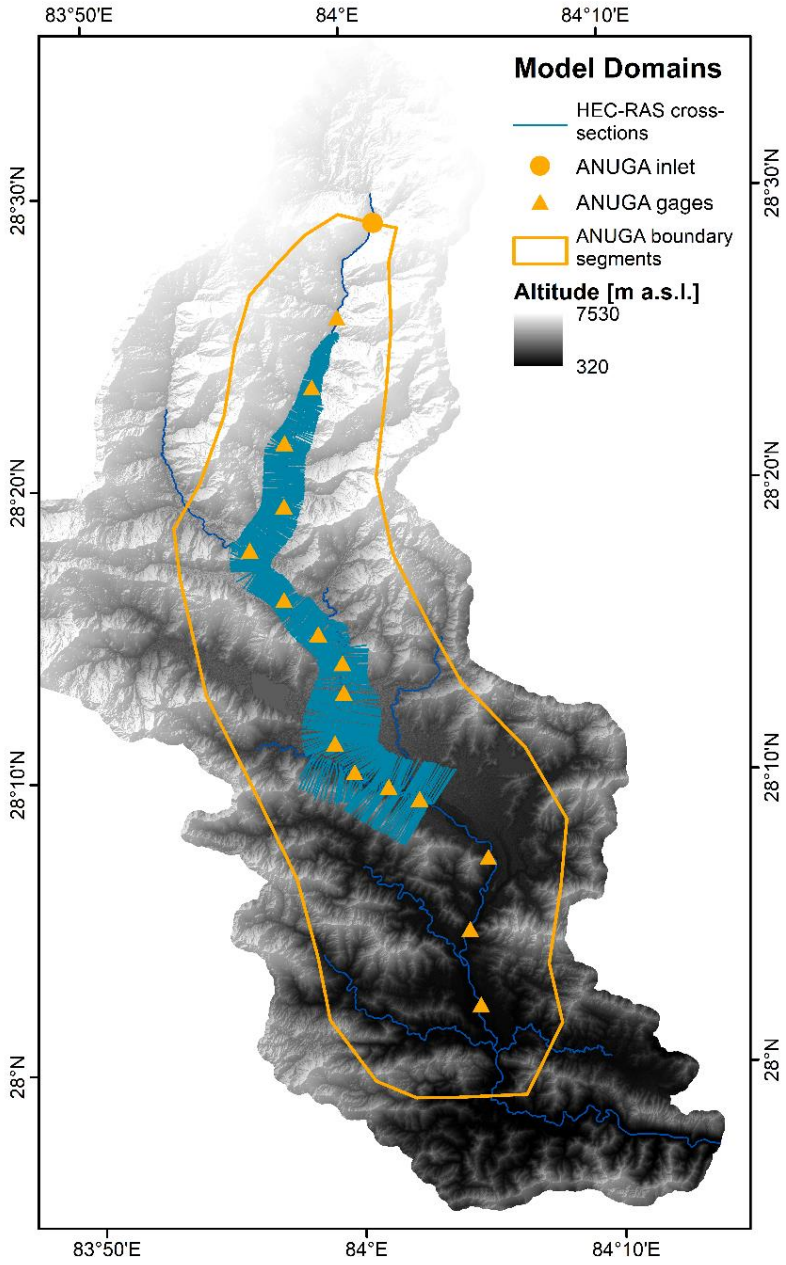

Figure 4.3: The HEC-RAS and ANUGA model domains and the topography as derived from the 5-m ALOS DEM (©NTT DATA, RESTEC/ Included©JAXA). Note that although depicted as point, the ANUGA inlet is defined as reflective boundary segment.

4.3.4 Discharge Constraints from Modelling and Field Evidence

A further constraint for both models is their sensitivity to the choice of Manning's *n* (Westoby et al., 2014; Wohl, 1998). To assess the weight of Manning's *n* on our HEC-RAS simulations, we compared inundation areas and depths between models with both spatially varying and uniform Manning's *n* = 0.1 for a mixed flow for the scenario with the highest Q_p = 10,000 $m^3 s^{-1}$. This roughness has been used in steep gravel-bed rivers (Cenderelli and Wohl, 2001). We also estimated the sensitivity of one-dimensional flow simulations in HEC-RAS with respect to contributions from tributaries (Mardi, Kali, and Phusre Khola) compared to a model run for the Seti Khola without any tributaries.

To estimate the most likely Q_p of the potential Mediaeval outburst floods, we used independent field evidence found in the Pokhara Formation. In addition to slackwater deposits mapped by Stolle et al. (2017), we studied the sedimentary structures of the Pokhara Formation's mainly breccious conglomerates at two outcrops near the Mardi and Phusre confluences. We computed the horizontal distance between mapped slackwater deposits in the tributary valleys and our simulated inundation limits for scenarios involving Q_p >50,000 $m^3 s^{-1}$ to find a 'best fit' (i.e. minimum mean horizontal distance). This analysis provides conservative estimates of flood size, as the elevation slackwater deposits in the tributary valleys may mismatch simulated inundation levels – reflecting some reworking of the fan materials since the Pokhara Formation was emplaced.

4.4 Results

4.4.1 Reconstruction of the May 2012 Outburst Flood

We find that the 2012 outburst flow formed 1.41 km^2 of fresh sediment deposits outside the active channel area (Fig. 4.4, 4.5). Most aggradation, lateral channel migration of up to 100 m and meander cutoffs occurred upstream of the Mardi Khola. Only at Ramghat in Pokhara city did the channel migrate laterally by some 145 m. The average lateral channel shift before and after the 2012 flood is 14 m, compared to an average channel width of 63 m before the flood. The active channel of the Seti Khola had an area of 3.98 km^2 in March and 5.08 km^2 in October 2012, with a net gain of 1.1 km^2 or +28% over a 55-km long reach. Compared to seasonal channel changes in response to monsoonal floods of the previous year (RapidEye images from February 2, 2011 to March 22, 2012; Planet Team, 2017), the net loss is 0.15 km^2 (4%) and likely below annual variations caused by monsoon floods.

Gurung et al. (2015) estimated a peak discharge of 8,400 $m^3 s^{-1}$ at Kharapani. Our simulation for this discharge at this location had a maximum inundation depth of 22 m and flow velocities of 3 m s^{-1} to 14 m s^{-1} (Fig. 4.4). Compared to local flood sediments mapped along this reach, this simulation overestimates the inundation area by 16%. SANDRP (2014) estimated a Q_p of 935 $m^3 s^{-1}$ for a

measured flow depth of 2.15 m at Seti dam. We used this information as steady flow input with the water level as an upper boundary condition in a mixed and a supercritical flow simulation (Fig. 4.5). Under mixed flow conditions, the overestimate between local simulated inundation and mapped flood-sediment extent is 257%. When assuming supercritical flow at Seti dam, however, modelled flood areas overestimate inferred flood areas by 36%. Our simulation of mixed flow with 935 m^3 s^{-1} at the Seti dam has a maximum flow depth of 39 m and flow velocity of 3.7 m s^{-1}. For supercritical conditions maximum inundation depth is 28 m and flow velocity range between 0.3 m s^{-1} and 8.5 m s^{-1}. Both scenarios apply to a reach directly upstream of where the river enters a narrow gorge and, hence, a reach of abrupt confinement.

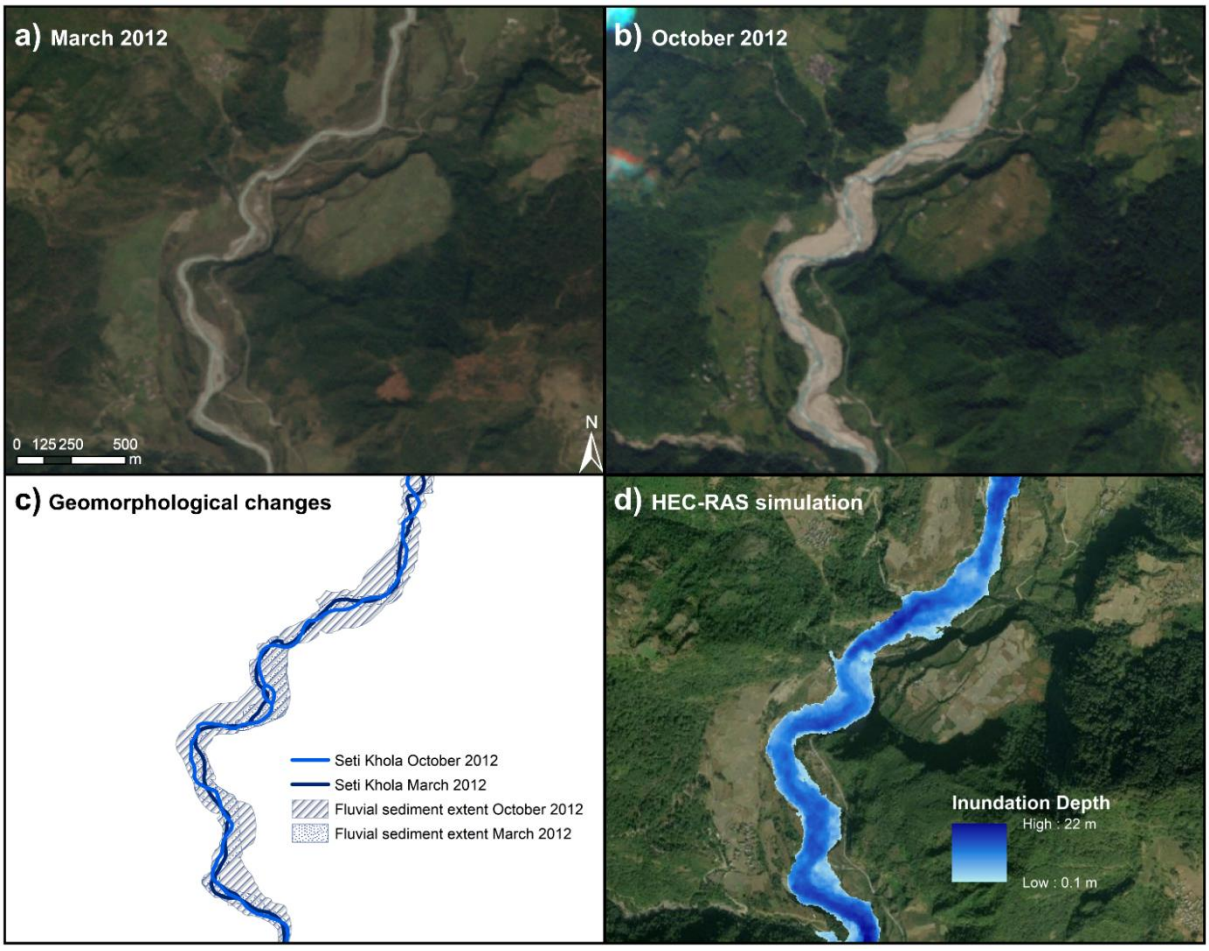

Figure 4.4: Geomorphic flood impacts at Kharapani (see Fig. 4.1 for location). Comparison of RapidEye scenes acquired before (22/03/2012, a) and after (18/10/2012, b) the May 2012 flood (Planet Team, 2017). Panel c shows inundation extents and pre- and post-event course of the Seti Khola mapped from satellite imagery in a and b. Modelled inundation depths when simulating Q_p = 8,400 m^3 s^{-1} in steady state (d), displayed on ESRI basemap Maxar satellite imagery acquired in 2020 (ESRI and Maxar Technologies, 2022).

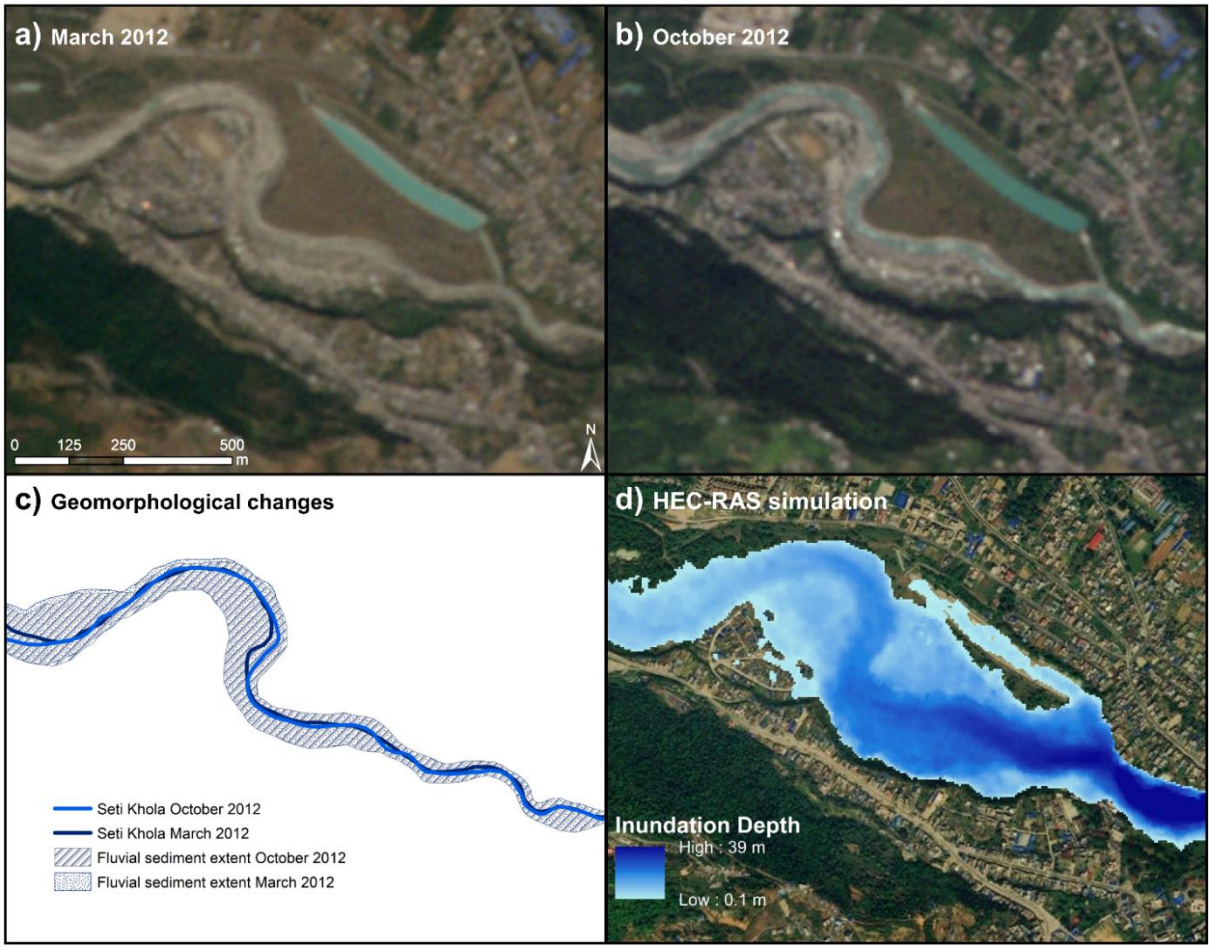

Figure 4.5: Geomorphic flood impacts at Seti dam (see Fig. 4.1 for location). Comparison of RapidEye scenes acquired before (22/03/2012, a) and after (18/10/2012, b) the May 2012 flood (Planet Team, 2017). Panel c shows inundation extents and pre- and post-event course of the Seti Khola mapped from satellite imagery in a and b. Modelled inundation depths when simulating Q_p = 935 m^3 s^{-1} in steady state (d), displayed on ESRI basemap Maxar satellite imagery acquired in 2020 (ESRI and Maxar Technologies, 2022).

We iteratively assessed the most likely initial Q_p upstream of the Mardi Khola confluence using 29 mixed steady-flow scenarios with discharges ranging from 1,000 m^3 s^{-1} to 10,000 m^3 s^{-1}. We find the smallest mismatch between mapped and simulated flood extents for Q_p = 3,700 m^3 s^{-1} (Fig. 4.6). In this scenario, inundation depths attain 45 m and the simulated steady-flow velocity is 28 m s^{-1}. We obtained flow depths >22 m just upstream from a relict, breached landslide dam 2.7 km north of Karuwa village. At Kharapani, we model a maximum flow depth of 15 m and speeds from 3 m s^{-1} to 10 m s^{-1}.

We also iteratively assessed the characteristics of the May 2012 flood at Seti dam. We set up a more detailed model of this area for steady-flow in both mixed and supercritical regimes, using our flood extent mapping and the recorded water level of 2.15 m (SANDRP 2014) as an upper boundary condition. Our model predicts supercritical flow of 500 m^3 s^{-1} and flow velocities of 0.2-6.7 m s^{-1} at Seti dam (Fig. 4.6).

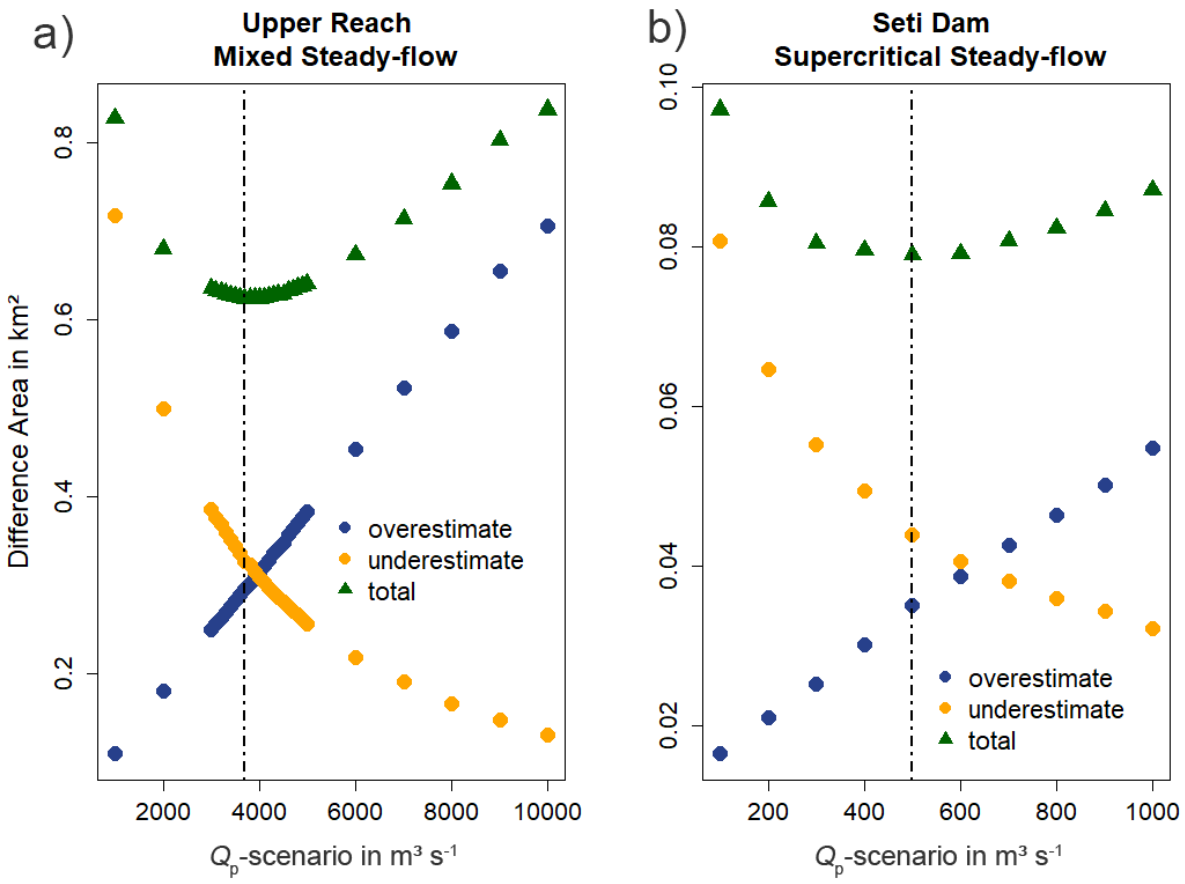

Figure 4.6: Areas of difference (green) between the simulated inundation boundaries and the mapped flood sediment extents from RapidEye imagery in the upper reach (a) and at Seti dam (b). These are further differentiated in overestimates (blue) and underestimates (orange). In the upper reach, minimum total difference area (622,800 m^2) is achieved when simulating a Q_p of 3,700 $m^3 s^{-1}$ as upper steady flow condition. At the Seti dam, minimum total difference area (78,960 m^2) is achieved when simulating a Q_p of 500 $m^3 s^{-1}$ and a water level of 2.5 m. as the upper flow condition.

4.4.2 Simulation of Mediaeval Outburst Flood Scenarios

Flow depths and inundation limits of smaller Q_p scenarios (5,000 and 10,000 $m^3 s^{-1}$) modelled with ANUGA are largely consistent with those modelled by HEC-RAS. All ANUGA flood scenarios consistently simulate highest flow depths in the proximal and distal parts of the Pokhara Basin modelled flow is less confined in the central parts of the basin (Fig. 4.7). The fan surface is inundated for simulated floods with Q_p >200,000 $m^3 s^{-1}$. Between the Q_p scenarios, flood limits in up- and downstream reaches vary where tributaries enter the Seti Khola. There, the ANUGA simulations show several-kilometre-scale backwater flooding of main tributaries such as the Mardi and Phusre Khola for Q_p >50,000 $m^3 s^{-1}$ (Fig. 4.7, 4.8). Tributary backwater flooding of >8 km could occur about 65 km downstream from the flood source below the Sabche Cirque for Q_p >200,000 $m^3 s^{-1}$ in the Kyandi and Magdi Khola tributaries. In the Q_p = 600,000 $m^3 s^{-1}$ scenario, backwater effects could involve mean flow depths of 10 to 20 m on average at the Mardi, Kali, and Phusre Khola tributaries,

while predicted mean depths of 44 m in the southern part of our study area at the Kyandi and Magdi Khola confluence. The maximum simulated flow depths for this Q_p = 600,000 m^3 s^{-1} scenario are up to 200 m in the reaches upstream of the Mardi Khola. When comparing our simulated flood extents along tributary valleys with the location of slackwater deposit outcrops described by Stolle et al. (2017), we find that they fit best with inundation limits linked to a Q_p of 500,000 m^3 s^{-1} (Fig. 4.8).

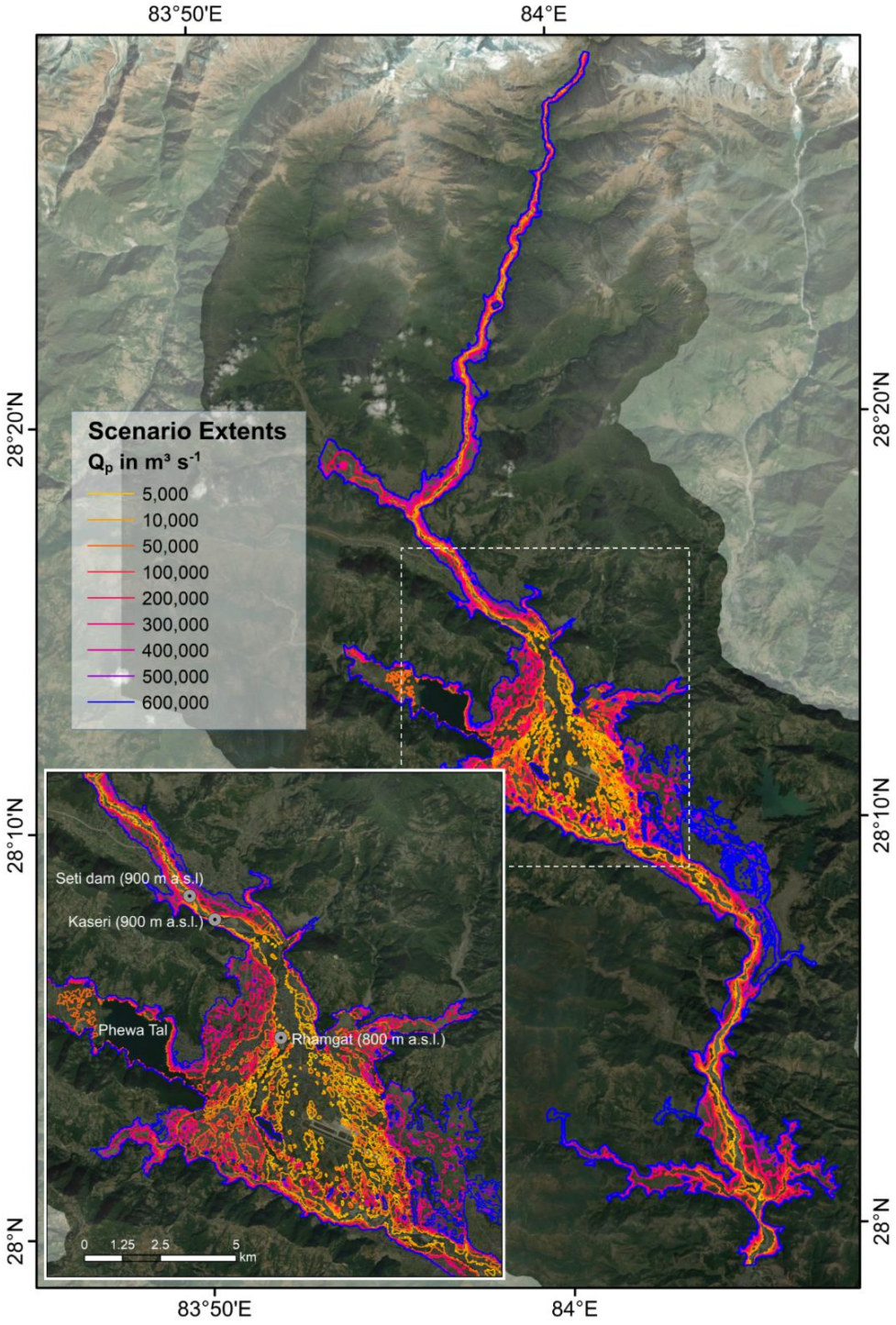

Figure 4.7: Maximum inundation limits when modelling Q_p ranging from 5,000 m^3 s^{-1} to 600,000 m^3 s^{-1} in ANUGA. Note extensive simulated backwater effects in tributary valleys for discharges >100,000 m^3 s^{-1}. Displayed on ESRI basemap Maxar satellite imagery acquired in 2020 (ESRI and Maxar Technologies, 2022).

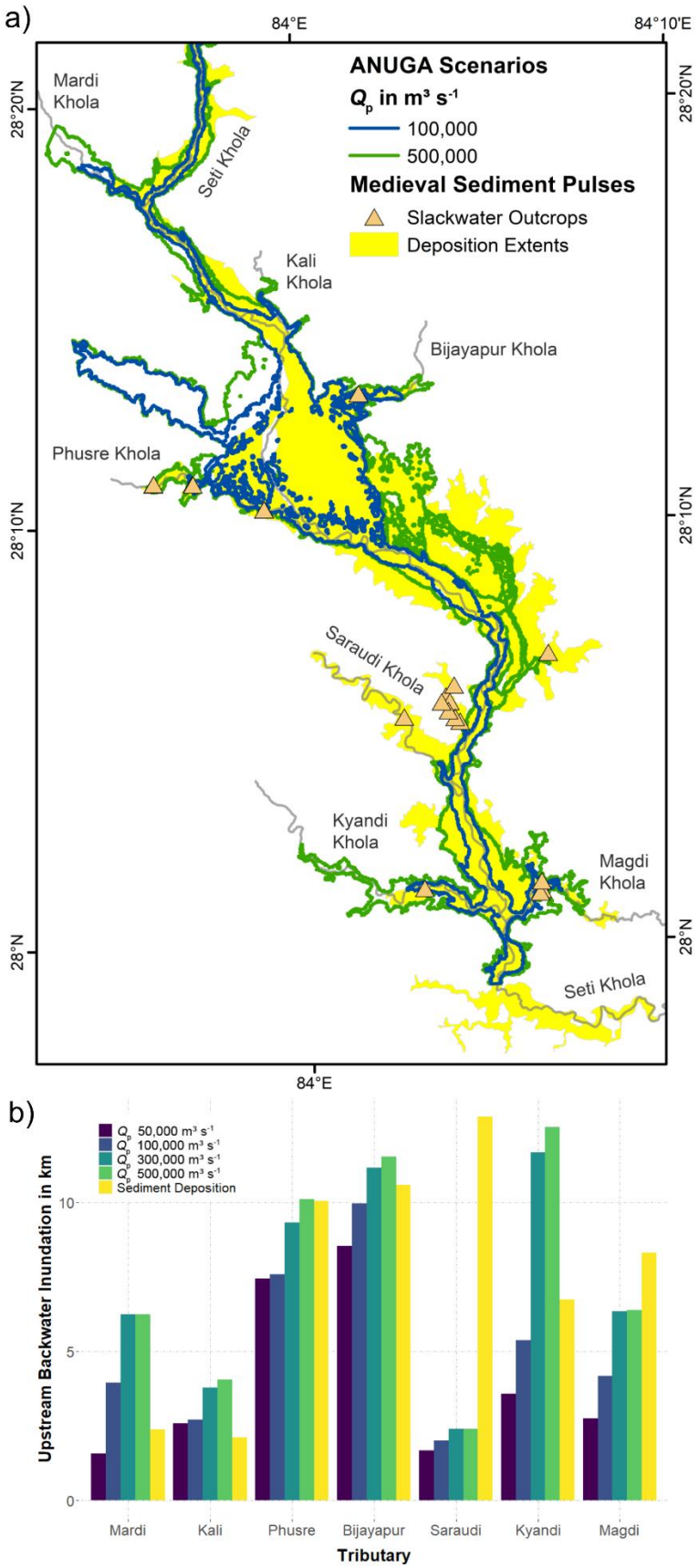

Figure 4.8: Comparison of selected maximum inundation limits of ANUGA flood scenarios with sedimentary evidence of the catastrophic Mediaeval events' extents (1100 to 1344 C.E.; Schwanghart et al., 2016; Stolle et al., 2017; data provided by A. Stolle).

4.5 Discussion

4.5.1 Model Applicability

The resolution and quality of our topographic data constrain to first order the accuracy of our hydraulic models. The 5-m ALOS DEM appears suitable for HEC-RAS modelling of outburst floods (Westoby et al., 2014; Zhang and Liu, 2015), but only partly resolves the steep gorges along the Seti Khola fan. Hence, we manually edited the DEM data using our field-measured cross sections. Field surveys with terrestrial laser scanning were hampered by haze and water vapour, while airborne mapping using UAVs are legally restricted in Nepal. Hence, we found that a handheld laser rangefinder proved most useful and economic during field work. While our topographic data are more detailed than in most previous lake-outburst studies (e.g. Mergili et al., 2011; Somos-Valenzuela et al., 2014; Wang et al., 2018), the DEM postdates the Mediaeval events. Earlier topographic data are unavailable and limit volumetric estimates, which is a common issue in reconstructing past outburst floods (Westoby et al., 2014). Reported flood stages for the 2012 flood are limited to the Seti dam (SANDRP, 2014). Hence, we mapped flood deposits as indicators for peak flow stage, following the methods that Wohl (1995) used to reconstruct GLOFs in eastern Nepal.

Both HEC-RAS and ANUGA draw on several simplified hydrodynamic flow properties. They simulate clear-water flow and, hence, ignore potential geomorphic effects during large floods such as changing topography by scouring and deposition or a lowering of fluid viscosity due to entrainment of sediments (Mungkasi et al., 2013). The latter might also alter flow mobility and runout (Westoby et al., 2014). Models such as Flo-2D simulate non-Newtonian flows but require rheological input parameters (Cesca and D'Agostino, 2008; Zhang and Liu, 2015) that remain unknown at the scale of our study. Due to a similar lack of information regarding initial outburst flood generation, we considered only steady flow. The Seti Khola was ungauged during the May 2012 flood, so that assuming a simple triangular hydrograph as the necessary upper boundary condition for unsteady flow models would only add more uncertainty. Moreover, empirical equations for input hydrographs are mostly site-specific (Dussaillant et al., 2010; Walder and Costa, 1996) and need additional estimates such as breach rate and depths or potential water volumes impounded by dams in the headwaters of the Seti Khola, which is unconstraint for the 2012 flood.

Our Manning's n sensitivity analysis showed, that the model with uniform roughness had a slightly larger flood extent on average (~4%). These differences are more pronounced in areas with for our study area low surface roughness (Manning's n <0.08) such as grassland, bare floodplains or gravel mining sites, consistent with findings from previous work (e.g. Jha and Khare, 2016; Wang et al., 2018; Wohl, 1998). Although these differences seem minute and a varying Manning's n might be less important for larger Q_p scenarios, we argue that roughness may capture important local effects

of smaller floods. HEC-RAS is sensitive with to flow contributions from tributaries with mismatches of up to 1.2 km^2 (13%) compared to a simple trunk-channel model with a steady mixed flood of Q_p = 10,000 $m^3 s^{-1}$. Highest mismatches are at the Kali and Phusre Khola confluences. We infer that including tributaries into our geometric model setup provides more realistic flood scenarios.

Our two-dimensional steady state simulations with ANUGA focused on scenarios with Q_p >10,000 $m^3 s^{-1}$ are a compromise between high computational loads and spatial resolution. We, thus, had to use a spatially uniform surface roughness and a lower spatial resolution of the triangulated mesh when compared to the original DEM. Modelled flood inundation for Q_p = 5,000 and Q_p = 10,000 $m^3 s^{-1}$ agree well with those modelled for 1-D flow by HEC-RAS except for mid-reaches containing several gorges, where mean inundation areas differ by a factor of two.

4.5.2 The May 2012 and Mediaeval Outburst Floods in Context

Our modelling predicts a lower peak discharge of the 2012 flood than prior findings at Kharapani and Seti dam (Dwivedi and Neupane, 2013; Kargel et al., 2013; SANDRP, 2014) (Table 4.1; Fig. 4.10). Published values were derived from hydraulic flow calculations at single river cross sections, informed by maximum water stages estimated from video footage or local high-water marks. These divergent Q_p estimates might reflect the different methods and spatial scales of assessment. Our mapping of geomorphic impacts by the May 2012 flood agrees well with reported changes in four channel cross sections (Gurung et al., 2021), but covers longer reaches of the Seti Khola.

Our estimate of the 2012 peak discharge (Q_p of 3,700 $m^3 s^{-1}$ attenuating to 500 $m^3 s^{-1}$) is in range of the 100-year flood derived from meteorological flood frequency estimates: Gurung et al. (2021) used HEC-RAS to model local flood stages at two bridges in the upper Seti Khola, and empirically estimated a 100-year flood Q_p of 2,420 $m^3 s^{-1}$ based on local rainfall station data. Basnet et al. (2019) and Basnet and Acharya (2019) estimated peak discharges with HEC-RAS for 10-, 50-, and 100-year floods downstream of the Mardi confluence and Ramghat. Basnet and Acharya (2019)'s 100-year flood estimate of 1,270 $m^3 s^{-1}$ just downstream of the Mardi confluence and Basnet et al.'s (2019) estimate of 2,340 $m^3 s^{-1}$ at Ramghat is based on gauge data from several kilometres downstream of our study area. At Ramghat and Seti Dam, our scenarios of Q_p = 1,000 $m^3 s^{-1}$ and Q_p = 2,000 $m^3 s^{-1}$ also yielded comparable results to those by Basnet et al. (2019) and Basnet and Acharya (2019), who used ensembles of HEC-RAS runs, each covering a discrete reach of the Seti Khola exclusive of any gorges.

Our simulations expand on Basnet et al.'s (2019) and Basnet and Acharya's (2019), and Gurung et al.'s (2021) findings by highlighting the importance of hydraulic ponding and tributary backwater effects, especially during larger floods (Q_p >10,000 $m^3 s^{-1}$). Extensive flooding in all major tributary

valleys that extend several kilometres upstream commences for scenarios with Q_p >100,000 m^3 s^{-1} (Fig. 4.7, 4.8). Backwater flooding and the associated sedimentation of characteristic slackwater deposits is consistent with independently reported outcrops of slackwater deposits in several tributaries laid down during Mediaeval aggradation events (Schwanghart et al., 2016a; Stolle et al., 2017) (Fig. 4.8, 4.10). Similar slackwater deposits elsewhere have been interpreted as evidence of phases of backwater effects during floods (Baker et al., 1983; Carrivick and Rushmer, 2006), for example, for the late Pleistocene Missoula floods (Smith, 1993; Waitt, 1985) as well as Holocene and historic GLOFs in Patagonia (Benito and Thorndycraft, 2020). Based on sedimentary evidence, Stolle et al. (2017) proposed catastrophic failure of one or several natural dams potentially linked to rock-slope failures in the Seti Khola's headwaters as mechanism behind the Mediaeval sedimentation pulses that deposited the Pokhara Formation. Our modelling results, which indicate that a large discharge is required to form these deposits, are consistent with this hypothesis, given the generally good match between predicted inundation limits and mapped slackwater deposits. Nonetheless, the spatial coincidence of modelled backwater effects in tributary valleys with the location of Mediaeval slackwater deposits supports the notion that outburst floods as part of larger hazard cascade may have shaped the sedimentary record of the Pokhara valley (Fig. 4.8). Our ANUGA results slightly overpredict flood limits in the upper tributaries, but underpredict in the lower tributaries. This pattern might hint at multiple Mediaeval flood pulses, during which sediments were deposited first in the upper, and then in the lower, tributary valleys (Schwanghart et al., 2016a; Stolle et al., 2017). One exception is Saraudi Khola, where the modelled inundation does not reach the locations of slackwater sediments because of a prominent bedrock knickpoint 2.5 km upstream of the confluence with the Seti Khola (Stolle et al., 2019) (Fig. 4.10). The most probable explanation for this mismatch is that we ran our hydraulic models on the current topography, which may have differed during the Mediaeval sediment pulses. Depositional features of the Pokhara Formation show evidence of rapid sedimentation from bedload-rich, turbulent flow such as stratification and imbrication of clasts, partial clast-support, and normal grading (Fig. 4.9). Stolle et al. (2017) attributed these structures to deposition from highly energetic non-cohesive flows. The necessary amounts of water for such flow conditions could have been provided by the sudden rupture of natural dam(s) forming lake(s) in the Sabche Cirque.

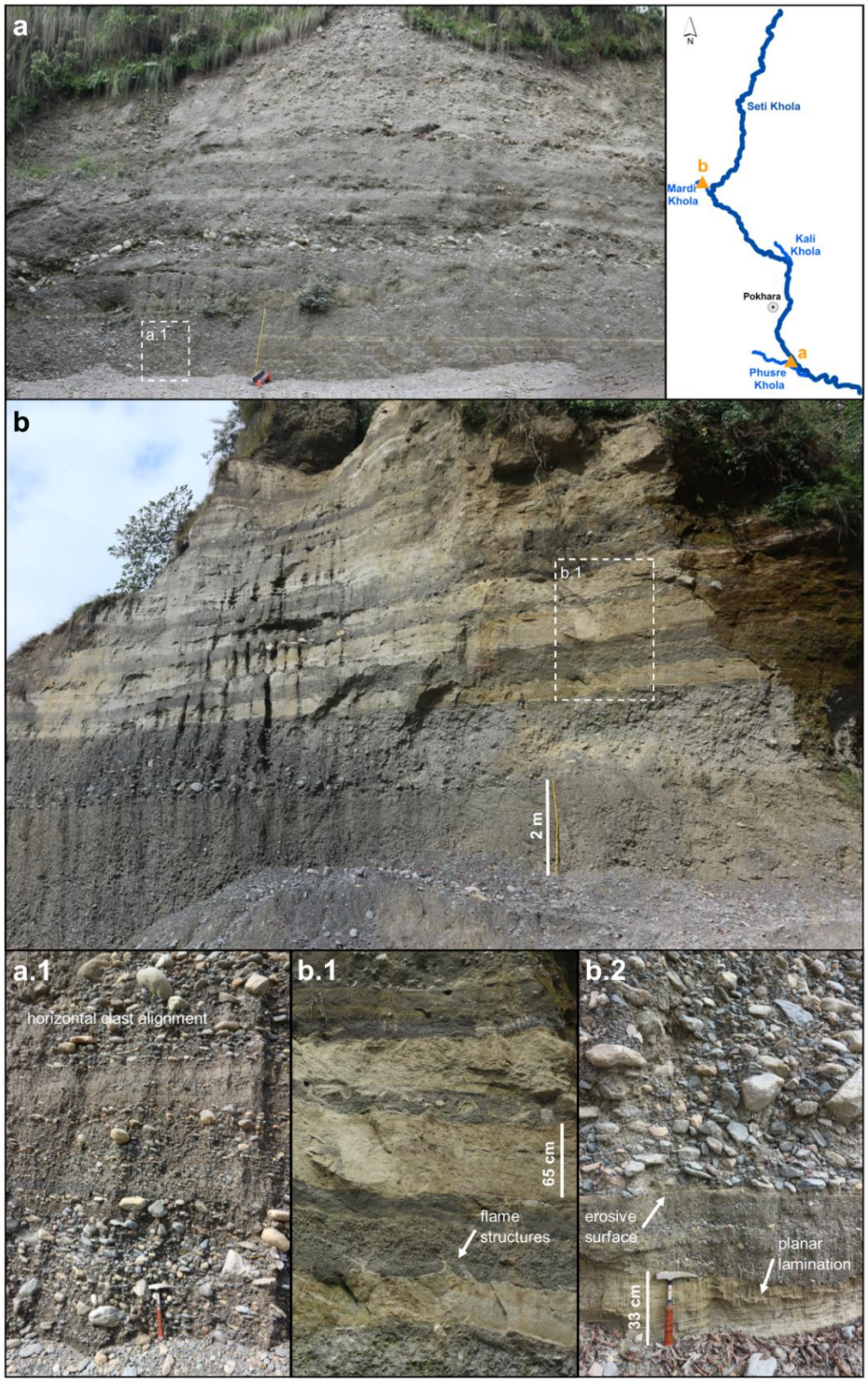

Figure 4.9: Outcrops of the Pokhara Formation indicating turbulent-flow conditions during deposition. a) SWS-NEN-orientated road-cut outcrop of Pokhara Formation close to the Phusre confluence. Beds consisting of polymictic, poorly-sorted, matrix-supported breccious conglomerates intercalated with sandier, normal graded beds. Detail a.1): distinct horizontal stratification (incl. horizontal clast alignment), b) ESE-WNW-orientated road-cut outcrop of Pokhara Formation in the Mardi tributary valley. Two massive beds of polymictic, poorly-sorted, matrix-supported breccious conglomerates showing distinct normal grading in the lower part of the outcrop. Upper part consists of layers of light clay to silts alternating with dark grey coarse sand to granule layers. The latter also contain few lenses of larger cobbles (potential gravel lag). Detail b.1): soft-sediment deformation structures (flame structures, load casts) evidencing rapid deposition of coarser dark material on top of the unconsolidated, water-saturated finer light material. Detail b.2) (smaller outcrop in c. 5 m distance from b): planar lamination in predominantly medium sandy material is erosively overlain by a massive bed of breccious conglomerate with partial clast-support and imbrication of longitudinal clasts.

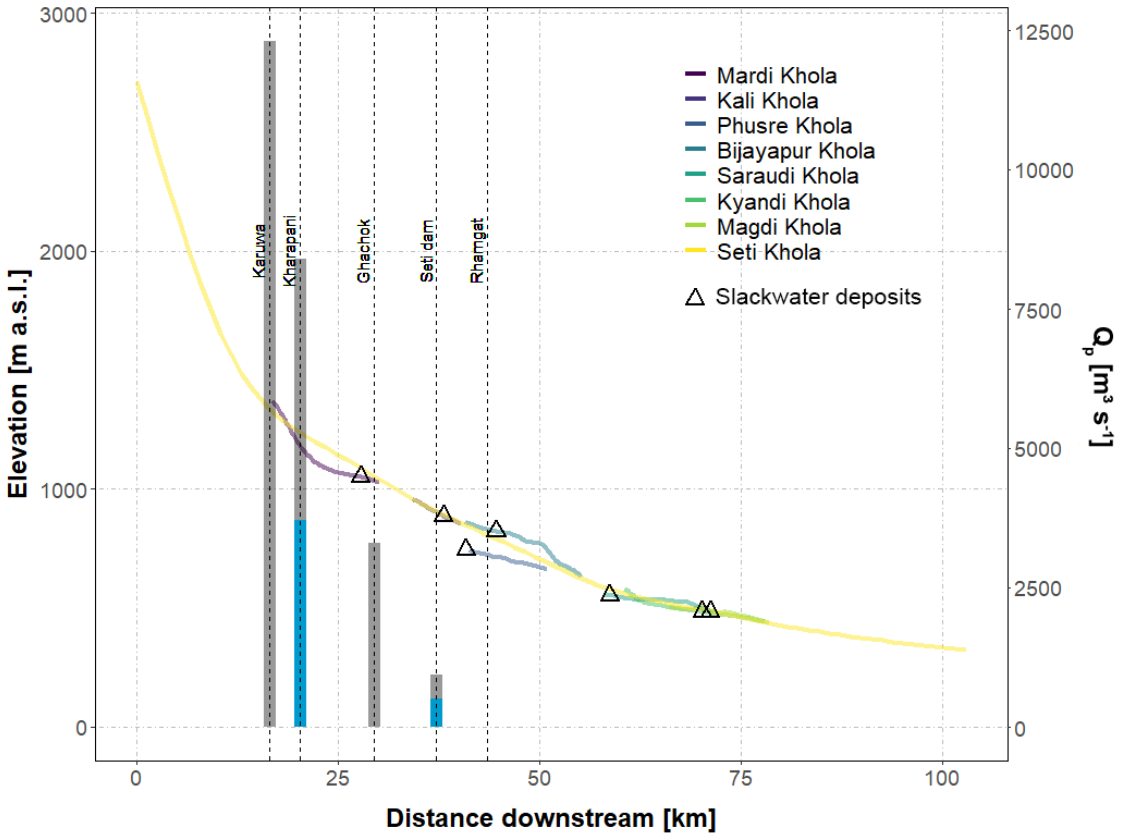

Figure 4.10: Smoothed longitudinal profile of the Seti Khola and its main tributaries. Locations of slackwater deposits in the tributaries are marked by triangles. Bars illustrate peak discharge estimates at certain locations – literature estimates in grey (Oi et al., 2012; SANDRP, 2014) and our HEC-RAS-based estimates in blue.

Overall, our flood scenarios in ANUGA cover a wide range of flood peaks informed by estimates of Mediaeval sediment pulses and their legacy in the Pokhara valley (Fort, 2010; Schwanghart et al., 2016a), but are also comparable to other observed and reconstructed outbursts in High Mountain Asia, such as in the Tsangpo gorge, southeastern Tibetan Plateau. There, large Q_p were attained not only during the Yigong outburst flood of 2000 (1.73×10^5 m^3 s^{-1} Q_p) but also during Quaternary megafloods caused by the outburst of ice-dammed lakes which had estimated Q_p of 5×10^6 m^3 s^{-1} (Turzewski et al., 2019). Our first-order estimate of Q_p of up to 5×10^5 m^3 s^{-1} for the Mediaeval fluvial sediment pulses in Pokhara indicate that floods of this size may have occurred as dam-break hazard cascades at several locations in the Himalayas. The reconstructed discharge of the 2012 outburst flood is of similar magnitude to reported historic flood discharges, including the Nepalese Dig Tsho GLOF of 1985 (1.6×10^3 m^3 s^{-1} Q_p; Vuichard and Zimmermann, 1987) and Tam Phokari GLOF of 1998 (1×10^4 m^3 s^{-1} Q_p; Osti and Egashira, 2009) or the flood triggered by the recent 2021 Chamoli rock and ice avalanche, Uttarakhand, India (8 - 14 $\times 10^3$ m^3 s^{-1}; Shugar et al., 2021) (Fig. 4.11). This latter event was similar to the May 2012 outburst in the Seti Khola's catchment as it also had a cascading character while propagating along a comparably steep topographic gradient (Gurung et al., 2021; Petley, 2021b).

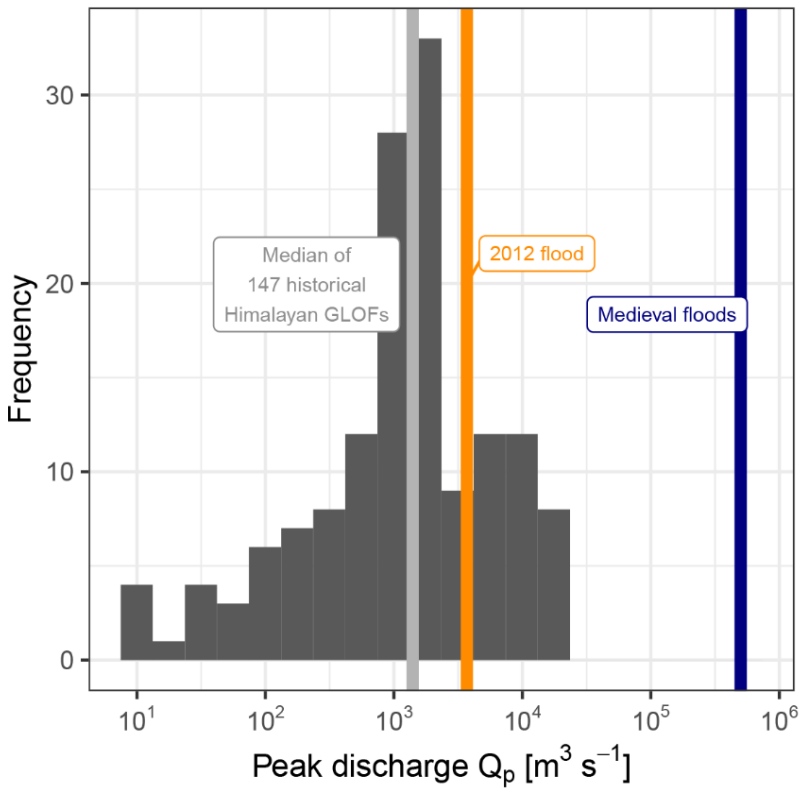

Figure 4.11: Estimated peak discharges of outburst floods in the Pokhara valley compared to known or reconstructed discharges of glacial lake outburst floods (GLOFs) in the greater Himalayan region derived from Veh and Lützow (2021).

4.6 Conclusions

We provide new quantitative insights into the catastrophic flood along the Seti Khola in May 2012 and much larger Mediaeval predecessors. We document channel widening and meander cutting, most pronounced in upper river reaches (above Mardi Khola confluence). The May 2012 flood increased the active channel area by nearly 30% along a 55-km reach. Using these sediments as flood markers, we reconstruct a most likely peak discharge of 3,700 m^3 s^{-1} in the upper Seti Khola, where most of the fatalities and damage occurred. Some 15 km below, at Seti dam in Pokhara city, the estimated, strongly attenuated, discharge is 500 m^3 s^{-1}. Our findings suggest lower peak discharges than several (empirical) flood estimates reports (Gurung et al., 2015; Oi et al., 2012; SANDRP, 2014) who proposed a roughly doubled Q_p at Kharapani (227%) and Seti dam (187%).

ANUGA simulations show that extensive backwater effects in the Seti Khola's mid reach tributaries like Mardi and Phusre Khola but also in the Kyandi and Magdi Khola further downstream are likely during outburst floods with Q_p >10,000 m^3 s^{-1}. Modelled backwater effects match best with the location of sedimentary evidence, i.e. slackwater deposits, at a simulated outburst flood with a Q_p >500,000 m^3 s^{-1}. Our findings are consistent with the hypothesis that several Mediaeval sediment

pulses were largely fluvial in character – potentially caused by outbursts of meltwater lakes as part of a hazard cascade originating in the Annapurna massif (Stolle et al., 2017). Our ANUGA results of large-scale outburst floods in the estimated range of Mediaeval predecessors also indicate flow dispersion and possible channel avulsions in the central Pokhara valley as the alluvial fan's surface could be completely inundated in scenarios with Q_p >300,000 $m^3 s^{-1}$.

Reoccurrences of cascading hazards similar to the studied recent and historical events are plausible in the Seti Khola catchment's future, as unique glaciological and geomorphological conditions in its headwaters might promote surge-related or landslide-dam and glacial lake outburst floods. Therefore, planning of regional development in the Pokhara valley may wish to consider this hazard from outburst floods, given their repeated historic and potential future, impacts and the rising number of people living in close proximity to the Seti Khola.

5 Outburst Flood Scenarios and Risks for a Rapidly Growing High-mountain City: Pokhara, Nepal

Under review as:

Fischer, M., Brettin, J., Roessner, S., Walz, A., Fort, M., and Korup, O. (2022): Outburst flood scenarios and risks for a rapidly growing high-mountain city: Pokhara, Nepal, Natural Hazards and Earth System Sciences, https://doi.org/10.5194/nhess-2022-64, submitted February 2022.

Abstract

Pokhara (c. 850 m a.s.l.), Nepal's second largest city, lies at the foot of the Higher Himalayas and has more than tripled its population in the past three decades. Rapidly expanding built-up areas are high in demand for construction materials and several informal settlements cater to unregulated sand and gravel mining in the Pokhara valley's main river, the Seti Khola. This river is fed by the Sabche glacier below Annapurna III (7,555 m a.s.l.), some 35 km upstream of the city, and traverses one of the steepest topographic gradients in the Himalayas. In May 2012 an outburst flood caused >70 fatalities and intense damage along this river and rekindled concerns about flood-risk management. We estimate the flow dynamics and inundation depths of outburst flood scenarios using the hydrodynamic model HEC-RAS. We simulate the potential impacts of peak discharges from 1,000 to 10,000 $m^3 s^{-1}$ on land cover based on high-resolution Maxar satellite imagery and OpenStreetMap data (buildings and road network). We also trace the dynamics of two informal settlements near Kaseri and Yamdi with high potential flood impact from RapidEye, PlanetScope, and Google Earth imagery of the past two decades. Our hydrodynamic simulations highlight several sites of potential hydraulic ponding that would largely affect these informal settlements and sites of sand and gravel mining. These built-up areas grew between three and twentyfold, thus likely raising local flood risk well beyond changes in outburst hazard. Besides these drastic local changes, about 1% of Pokhara's urban built-up area and essential rural road network is in the highest hazard zones highlighted by our outburst simulations. Our results stress the need to adapt early-warning strategies for locally differing hydrological and geomorphic conditions in this rapidly growing urban watershed.

5.1 Introduction

Many mountain communities and their infrastructure have become exposed and vulnerable to natural hazards (Fort, 2015; Hock et al., 2019). The Hindu-Kush Himalayas, home to some 200 million people and "water tower" to 1.3 billion people living downstream (Immerzeel et al., 2010; Schild, 2008), have seen rapid population growth, expanding road networks, shifts from agriculture to tourism as the main economic revenue, and the rise of hydropower projects (Hock et al., 2019; Schwanghart et al., 2018; Sidle and Ziegler, 2012). The Pokhara valley in Nepal, home to the nation's second largest city, is a prime example of such rapid socio-economic development: emerging job opportunities in the tourism sector triggered the steep rise of Pokhara's population since the 1970s, fuelled by unabated migration from rural to urban areas (Rimal et al., 2015, 2018). Urbanisation pressure has also forced informal settlements of marginalised communities on the lowermost river terraces and floodplains of the valley's main river, the Seti Khola (Fort et al., 2018; Thapa et al., 2022).

Apart from annual monsoonal floods, this river has a history of rare outburst floods. On May 5, 2012, a hyperconcentrated flood killed 72 persons and destroyed roads, bridges, and drinking water pipelines in the northern Pokhara valley (Gurung et al., 2015; Gurung et al., 2021). The exact sequence of events remains debated, but is likely to have been initiated by rock-slope failures on the western flank of the Annapurna IV massif at 7,525m a. s. l., observed by chance by a pilot (Hanisch et al., 2013; Kargel et al., 2013). Half an hour later, a sudden flood wave reached Kharapani village (1,100 m a.s.l.), some 23 km downstream, causing most of the damage and fatalities at an estimated peak discharge of 8,400 $m^3 s^{-1}$ (Hanisch et al., 2013; Oi et al., 2014; SANDRP, 2014). Thanks to the pilot, a radio warning was issued, most likely preventing a higher death toll further downstream (Kargel et al., 2013).

Even larger outburst floods may have occurred in the Seti Khola in Mediaeval times (Fort, 1987; Schwanghart et al., 2016a). Yet appraisals of flood hazard have so far largely focused on the 100-year meteorological flood as estimated from rainfall data (Basnet and Acharya, 2019; Gurung et al., 2021). The associated risk estimates rely on land-use and land-cover (LULC) mapping and projections from Landsat data (Gurung et al., 2021; Rimal et al., 2015, 2018), floodplain mapping (Rimal et al., 2015, 2018), and hydrodynamic modelling for selected reaches (Basnet and Acharya, 2019; Gurung et al., 2021).

We aim to expand on these studies by providing a comprehensive, semi-quantitative estimation of potential outburst flood impacts for the city of Pokhara and surrounding regions. In our approach we recognise possibly inundated areas for different outburst flood scenarios, the types of land cover and infrastructure most likely affected and the role of rapid urban expansion. We intersect the results of hydrodynamic modelling with land-cover data on buildings and the road network, and highlight

the rapid recent growth of two informal settlements. Our appraisal forms a building block for a more formal risk assessment that is currently curtailed by a lack of data on outburst flood probabilities as well as exposed values. Nonetheless, our study is one of the few to combine outburst flood scenarios with land-cover and land-use changes and might aid both urban planning and anticipatory risk management in the Pokhara valley (Nussbaumer et al., 2014).

5.2 Study Area

Pokhara is the second largest city of Nepal, capital of the Kaski District and the Gandaki Province, and lies at the southern foot of the 8-km high, seismically active Annapurna massif of the Higher Himalaya (Fort, 2010; Grandin et al., 2012). The Seti Khola is Pokhara's main river and traverses one of the steepest topographic gradients in the Himalayas, originating at 3,700 m a.s.l. in the Sabche Cirque of the Annapurna massif and entering the city 850 m a.s.l. some 35 km downstream (Fig. 5.1). The headwaters are mainly fed by Sabche glacier, the only glacier with observed surges in the central Himalayas (Lovell et al., 2018). The Seti Khola is also fed by the Mardi Khola, entering the valley in the north-west, and the Phusre Khola, to the south-east of Pokhara.

Pokhara is built on a large (>120 km^2) intramontane alluvial fan of the Seti Khola. The youngest of three depositional units of this fan is the 60-100 m thick Pokhara Formation that was formed by (post-)seismic sediment pulses in the 12th to 14th century CE (Fort, 2010; Schwanghart et al., 2016a). These mostly unconsolidated gravel beds cap the more indurated, but undated, Ghachok Formation (Fort, 2010). Over a course of 70 km, the Seti Khola cuts through its own sediments, forming broad, unpaired, and 100-m high terraces (Fort, 2010; Stolle et al., 2017). These cut-and-fill terraces alternate with several short (<1 km), narrow (<10 m) but up to 90-m deep gorges, in resistant calcareous rocks of the Ghachok Formation and the bedrock of the Lower Himalayan Sequence (Stolle et al., 2019). Some of these gorges are connected to karst features like potholes, tunnels, and caves (Fort, 2010).

Climate in the Seti Khola catchment is distinctly seasonal. The summer monsoon (May to October) brings >80% of the annual precipitation of about 4000 mm per year (Gabet et al., 2004). Climate also strongly varies with topographic relief (Rimal et al., 2018): the central Pokhara valley has a humid sub-tropical to humid temperate climate with mean monthly temperatures of 13°C to 26°C (Ross and Gilbert, 1999), whereas temperate to alpine climate characterises the Annapurna massif to the north (Rimal et al., 2015, 2018).

With a population of 518,452 in 2021 (Central Bureau of Statistics, 2022) the city and its surrounding valley have seen rapid socio-economical changes following the construction of major transportation

infrastructure since the 1970s, driven by better access to higher standards of living, and inbound migration attracted by the growing tourism sector and new employment opportunities (Fort et al., 2018).

Between 1990 and 2013, the urban area increased by 30 km^2, or 2.6% of the total watershed, whereas cultivated land decreased by 2.5% (Rimal et al., 2015). Population migration dynamics are also reflected by an increase of 45% in areas classified as urban in 2010 when compared to Pokhara's municipal area in 1977 (Rimal, 2012; Rimal et al., 2015). The urban population more than tripled since the 1990s (Rimal et al., 2015; United Nations Department of Economic and Social Affairs, 2019). Many informal settlements formed on the lowermost river terraces or the floodplain of the Seti Khola (Fig. 5.1), where squatters largely rely on gravel and sand mining as an income source (Fort et al., 2018; Stolle, 2018).

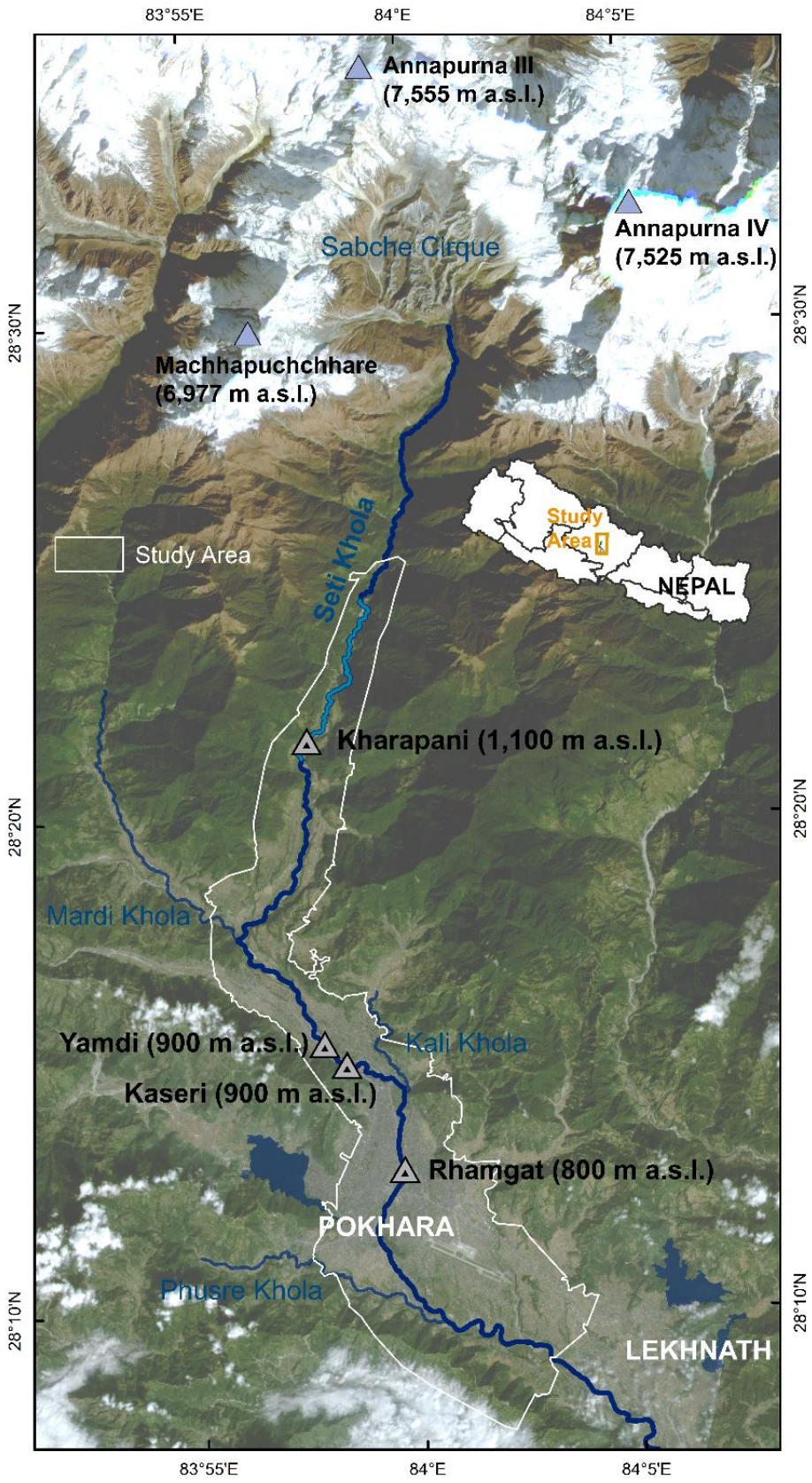

Figure 5.1: The Pokhara valley and the Seti Khola river in November 2021. Our HEC-RAS model domain and manual land-cover mapping covers the study area (white polygon). Most intense damages during the May 2012 outburst flood occurred along the uppermost inhabited reach of the Seti Khola (light blue). Image: PlanetScope (13/11/2021) (Planet Team, 2017); Nepal administrative boundaries are from UN Office for the Coordination of Humanitarian Affairs - Field Information Services Section (OCHA FISS, 2020).

5.3 Data and Methods

5.3.1 Overall Approach

We analyse potential flood impacts from physically plausible magnitudes of outburst floods along a 40-km long reach of the Seti Khola. Our assessment is built on combining scenario-based inundation modelling with current land use and land cover (LULC) and data of buildings and the road network to identify areas of potential flood impact (Fig. 5.2). We also selected two informal settlements close to the river and estimate how the growth of their built-up area between 2008 and 2021 affected their exposure to outburst floods. Stream-gauge data is unavailable for the Seti Khola, hence we validated our model with mapped damage and sediment traces caused by the May 2012 flood.

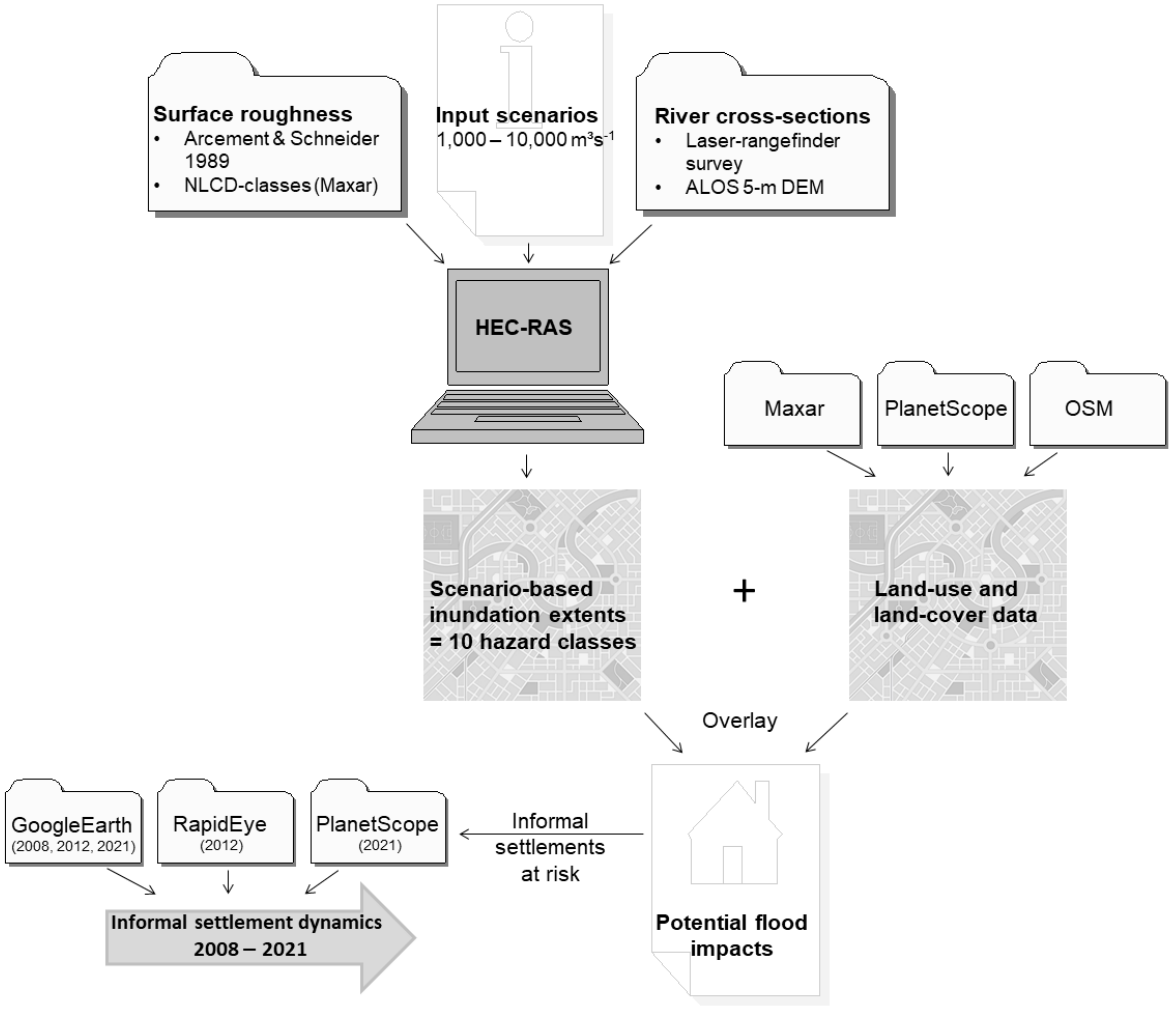

Figure 5.2: Data sources and workflow of our semi-quantitative assessment of outburst flood impacts in the Pokhara valley.

5.3.2 Scenarios for Numerical Flood Routing

We simulated ten flood scenarios with the Hydrologic Engineering Center's River Analysis System, HEC-RAS (version 5.0.7; https://www.hec.usace.army.mil/software/hec-ras/). HEC-RAS uses a step method for simulating steady, i.e. constant but gradually varied, open-channel flow in one dimension – based on the Saint-Venant equations (Brunner, 2020a; Westoby et al., 2014). The standard step method computes water-level profiles between two river cross-sections that describe the geometry of the channel and the adjacent overbank areas by iteratively solving the Energy equation (Eq. 5.1):

$$Z_2 + Y_2 + \frac{a_2 V_2^2}{2g} = Z_1 + Y_1 + \frac{a_1 V_1^2}{2g} + h_e \quad (5.1)$$

For cross-sections 1 and 2, Z_1 and Z_2 describe their main channel bed elevations, Y_1 and Y_2 the corresponding flow depths, V_1 and V_2 the mean flow velocities, and a_1 and a_2 the weighting coefficients; g is the gravitational acceleration. The energy head loss h_e specifies the effects of friction, as well as expansion and contraction caused by the channel geometry. At each cross-section, Manning's equation is used to compute discharge *Q* (Eq. 5.2):

$$Q = \frac{1}{n} A R^{2/3} S_f^{1/2}, \quad (5.2)$$

where *A* is cross-section area, R is the hydraulic radius, S_f is the energy gradient, and *n* is a hydraulic loss (or roughness) coefficient (Brunner, 2020a).

Geometric data for our HEC-RAS runs came from the 5-m resolution ALOS digital elevation model, projected to UTM Zone 44N (Fig. 5.2). We also acquired field data with a TruPulse 360 laser range finder and a Garmin eTrex handheld GPS during two campaigns in October of 2016 and 2019. We used these field data to derive 572 channel cross-sections of the Seti Khola and its major tributaries from the DEM, especially in the narrow gorges (Fig. 5.1). The average spacing between cross-sections was 90 m. We estimated Manning's *n* from manual mapping of land-cover classes based on 1-m resolution Maxar satellite data (ESRI and Maxar Technologies, 2022) following guidelines by Brunner (2020b). We also estimated Manning's *n* at 61 field locations following methods by Arcement Jr and Schneider (1984) and Chow (1959). We defined ten outburst discharge scenarios with peak discharge 1,000 ≤ Q_p ≤ 10,000 $m^3 s^{-1}$ in the main channel. This range covers monsoonal floods (1,500 to 2,300 $m^3 s^{-1}$; Basnet and Acharya, 2019) and also larger but rarer outbursts like the one in May 2012 (8,400 $m^3 s^{-1}$; Oi et al., 2014). The steepness of the Seti Khola's upper reach led us to

specify mixed flow conditions with the critical flow depth as the upper boundary condition, while we set a normal depth of 0.0065 as the lower boundary condition. We assumed a constant base flow of 100 m^3 s^{-1} (i.e. 10% of our lowest outburst scenario) in the Seti Khola's three likewise ungauged tributaries (Mardi Khola, Kali Khola, Phusre Khola).

5.3.3 Land-use and Land-cover Data

Using 1-m Maxar satellite imagery acquired in 2020 (ESRI and Maxar Technologies, 2022), we manually mapped ten land-cover (LC) classes in our model domain with an area of 136 km^2 (Fig. 5.1). Following the USGS National Land Cover Database classification, we assigned the LC classes "developed, open", "developed - low (intensity)", "developed - medium (intensity)", "developed – high (intensity)", "(open) water", "barren (land)", "grassland(/herbaceous)" (might include grazing of livestock), "(cultivated) crops", "shrub (scrubs)", and "(mixed) forest". The different levels of "developed" LC classes are based on the percentage of area covered by impervious materials (built-up areas), i.e. <20% in "developed, open" and highest (>80%) in "developed – high (intensity)" areas (Multi-Resolution Land Characteristics Consortium, 2019). We also mapped "revegetated floodplain", delineating the May 2012 flood's deposits and included in the "grassland(/herbaceous)" LC class, as well as the two land-use (LU) classes "airport" and "sand and gravel mining". The latter is assigned to the "barren (land)" LC class.

We derived object-scale data on Pokhara city's buildings, as well as roads and footpaths from the OpenStreetMap (OSM) collaborative project (https://www.openstreetmap.org/) via the Overpass Turbo tool (https://overpass-turbo.eu/) to capture the situation in September 2021.

We mapped built-up areas in two informal settlements from medium- to high-resolution satellite imagery of April 2008 (Google Earth), November 2012 (Google Earth and RapidEye), and November 2021 (Google Earth and PlanetScope). In these images, we also identified sand and gravel mining activities based on the presence of artificial groynes and gravel heaps at the active channel margins.

5.3.4 Potential Flood Impact Analysis

We used a geospatial overlay of our modelled flood inundation boundaries with the LULC data to assess on a semi-quantitative basis the likely impacts of ten peak discharge scenarios. We defined ten flood hazard classes by assigning areas and objects of the lowest scenario (Q_p = 1,000 m^3 s^{-1}) to the highest hazard class (HC) 10. Conversely, the lowest hazard class 1 is attributed to areas and objects that would be inundated in the highest magnitude scenario (Q_p = 10,000 m^3 s^{-1}).

To check the plausibility of our modelling results, we mapped the uppermost reach of the Seti Khola between Karuwa and Kharapani (Fig. 5.1), where the 2012 flood caused most damage. We used high-resolution Google Earth satellite imagery from December 2011 (pre-flood) and June 2012 (post-flood) to map man-made structures, including houses, huts, and temples. We also recorded the extent of sediment deposited during the May 2012 flood along this 8.4-km long reach from orthorectified 5-m resolution RapidEye imagery of October 18, 2012.

5.4 Results

5.4.1 Impacts of the 2012 Flood and Outburst Flood Scenarios

Our mapping of the impacts of the May 2012 outburst flood along the Seti Khola show that nearly 30% of the 145 man-made structures visible in satellite images before the flood were undetectable after. We estimate a loss in built-up area of 945 m^2 or 14%. In the most heavily affected reach near Kharapani, only five of the 29 buildings remained, while 60% of built-up area was lost (Fig. 5.3). The best agreement between modelled inundation extent and observed flood sediment in this reach is for a simulated Q_p of 3,700 $m^3 s^{-1}$, which underestimates inundated areas by 13.5%.

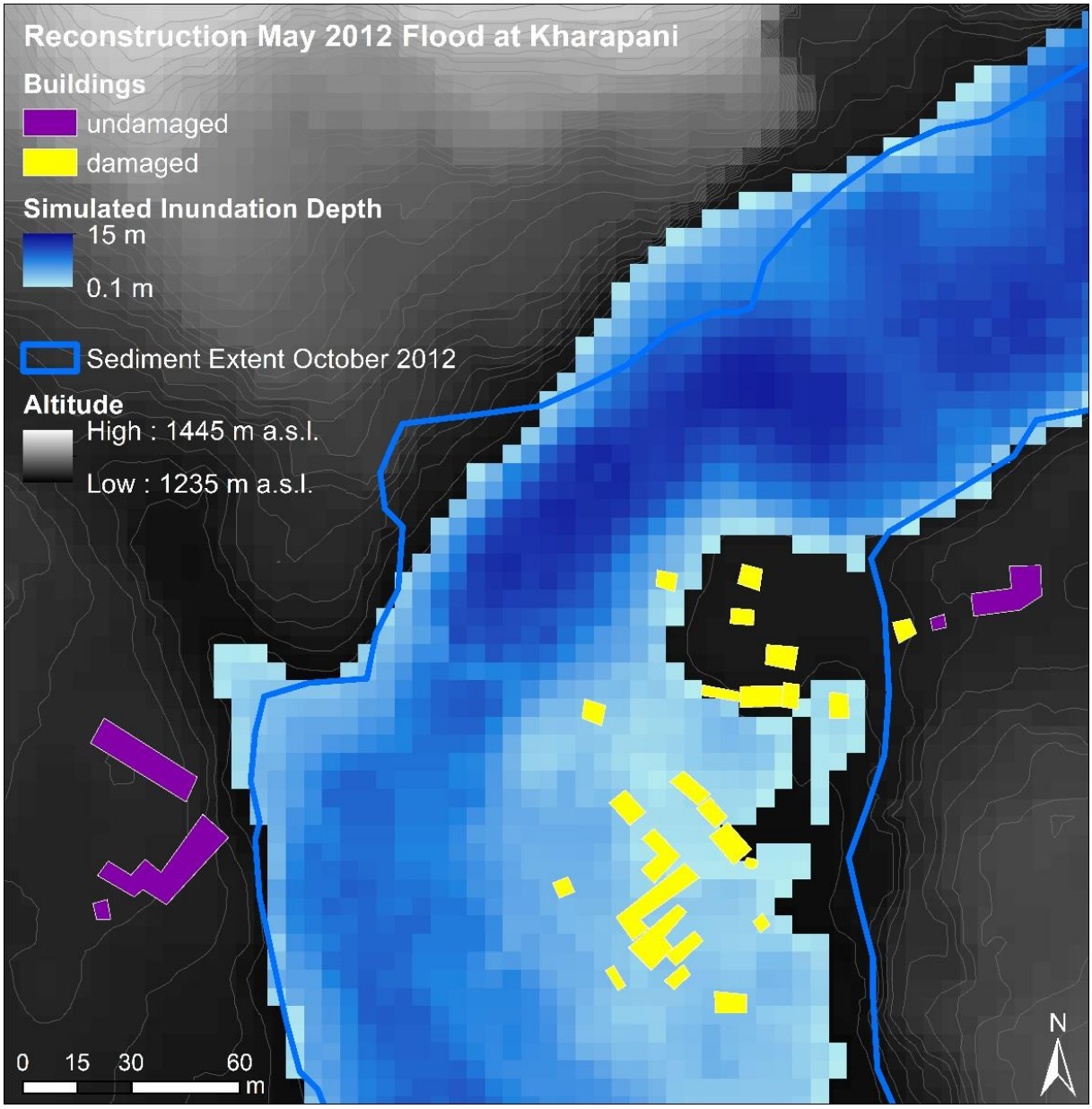

Figure 5.3: Simulated flow depths of the May 2012 flood at Kharapani village, assuming a flood peak of 3,700 $m^3 s^{-1}$. Blue lines delimit patches of flood-derived sediment mapped from RapidEye imagery (October 2012). Building damage is based on comparing Google Earth imagery of December 2011 and June 2012.

Our scenario-based simulations reveal a spatially variable downstream pattern of areas potentially inundated by outbursts along the Seti Khola (Fig. 5.4). In the uppermost reach north of the Mardi Khola confluence, simulated flood extents are very similar for all scenarios but funnel out further downstream where the May 2012 flood deposited gravel sheets. Gravel bars near or below Kharapani are currently exploited for gravel mining and likely to be flooded in all scenarios; local flow depth be as much as 14 m for peak discharge Q_p of 10,000 $m^3 s^{-1}$ (Fig. 5.4).

Between the Mardi Khola and Kali Khola confluences, inundation would largely affect a number of informal settlements and infrastructure as well as the Seti dam, given that the lowermost river

terrace would be extensively flooded for Q_p >3,000 m^3 s^{-1}. One of these informal settlements at Yamdi would be inundated in all scenarios (Fig. 5.5), together with a major road connecting Pokhara with north-eastern Nepal. For another informal settlement at Kaseri, all flood scenarios indicate extensive flooding with a mean flow depth of 23 m and a mean flow velocity of 1.3 m s^{-1} for Q_p = 10,000 m^3 s^{-1} (Fig. 5.6).

Further downstream, Ramghat is another informal settlement and also a site of religious importance that could be affected by up to 32-m deep flows in the Q_p = 10,000 m^3 s^{-1} scenario. Flood-water levels could reach the edge of the uppermost terrace if Q_p >7,000 m^3 s^{-1} and thus affect the surrounding dense urban areas (Fig. 5.4).

The less confined, meandering channel downstream of the Phusre Khola confluence has the largest variations in inundation areas in the Pokhara valley, and point bars mined for gravel or used for crop production are likely to be flooded at Q_p >6,000 m^3 s^{-1}. We observe pronounced backwater flooding in at least three tributaries of the Seti Khola in all Q_p scenarios, likely inundating the lowest reaches of these tributaries for several hundred metres for Q_p >6,000 m^3 s^{-1} (Fig. 5.4). Our results also indicate an isolated inundation in central Pokhara, some 1.5 km away from the Seti Khola and close to the Phirke Khola tributary (Fig. 5.4).

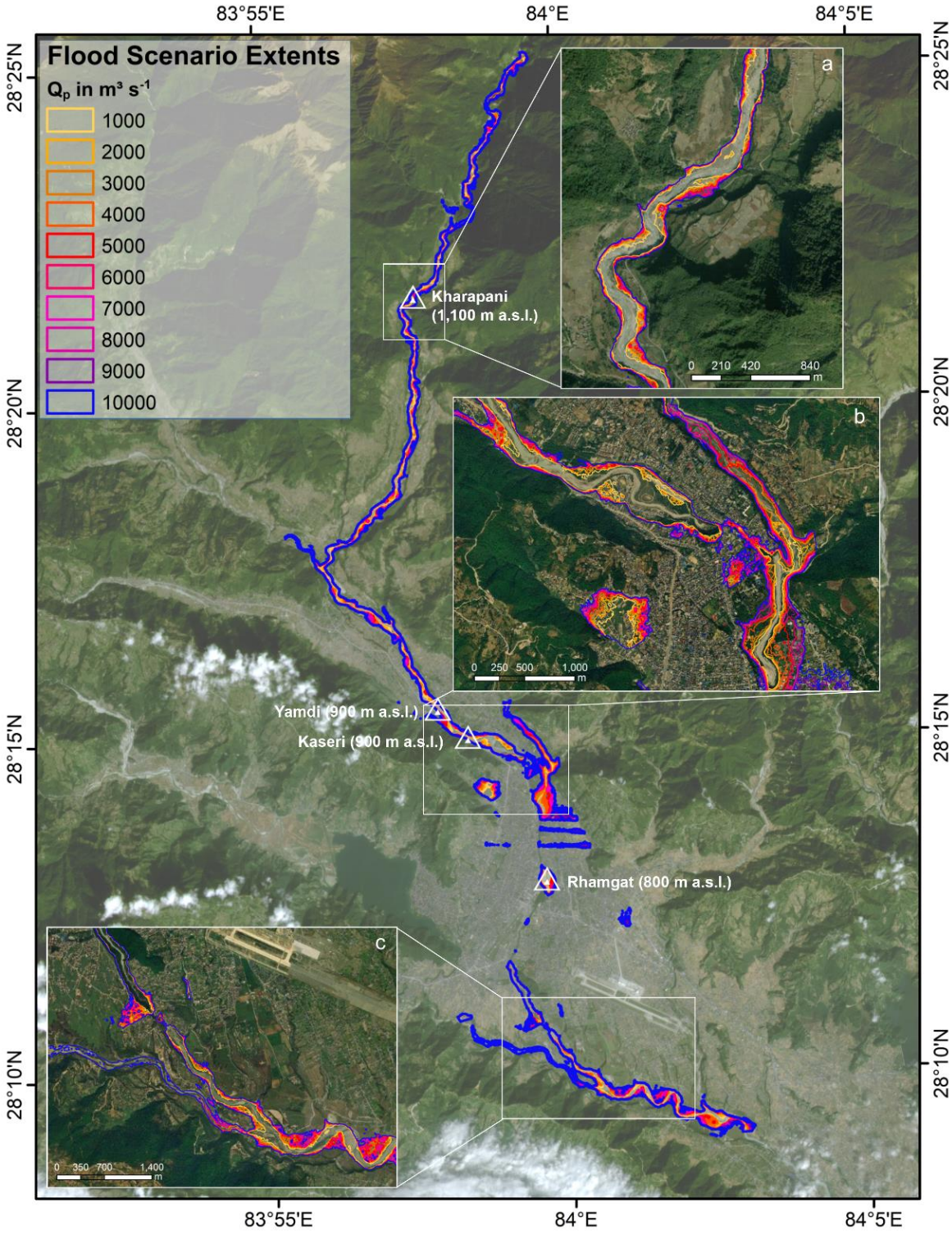

Figure 5.4: Flood extents for HEC-RAS modelling of steady flow with Q_p ranging from 1,000 $m^3 s^{-1}$ to 10,000 $m^3 s^{-1}$. Insets highlight results at Kharapani (a), Seti dam (b), and Phusre Khola confluence (c). Image: PlanetScope (13/11/2021) (Planet Team, 2017), inserts ESRI basemap Maxar imagery of 2020 (ESRI and Maxar Technologies, 2022).

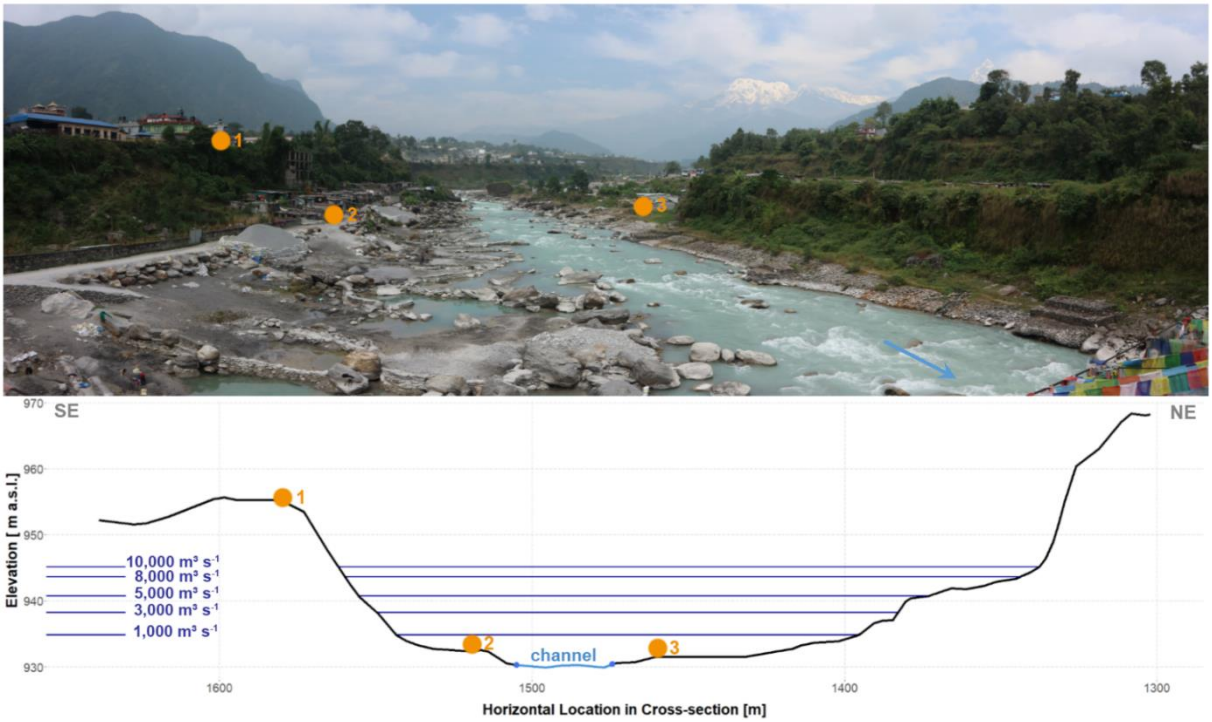

Figure 5.5: Simulated water-levels at an informal settlement and gravel mining site at Yamdi (Fig. 5.4) for five selected Q_p scenarios. Buildings on overbank areas would be inundated in all modelled scenarios. Groynes and gravel heaps (in foreground) aid the detection of gravel mining activities from optical satellite images.

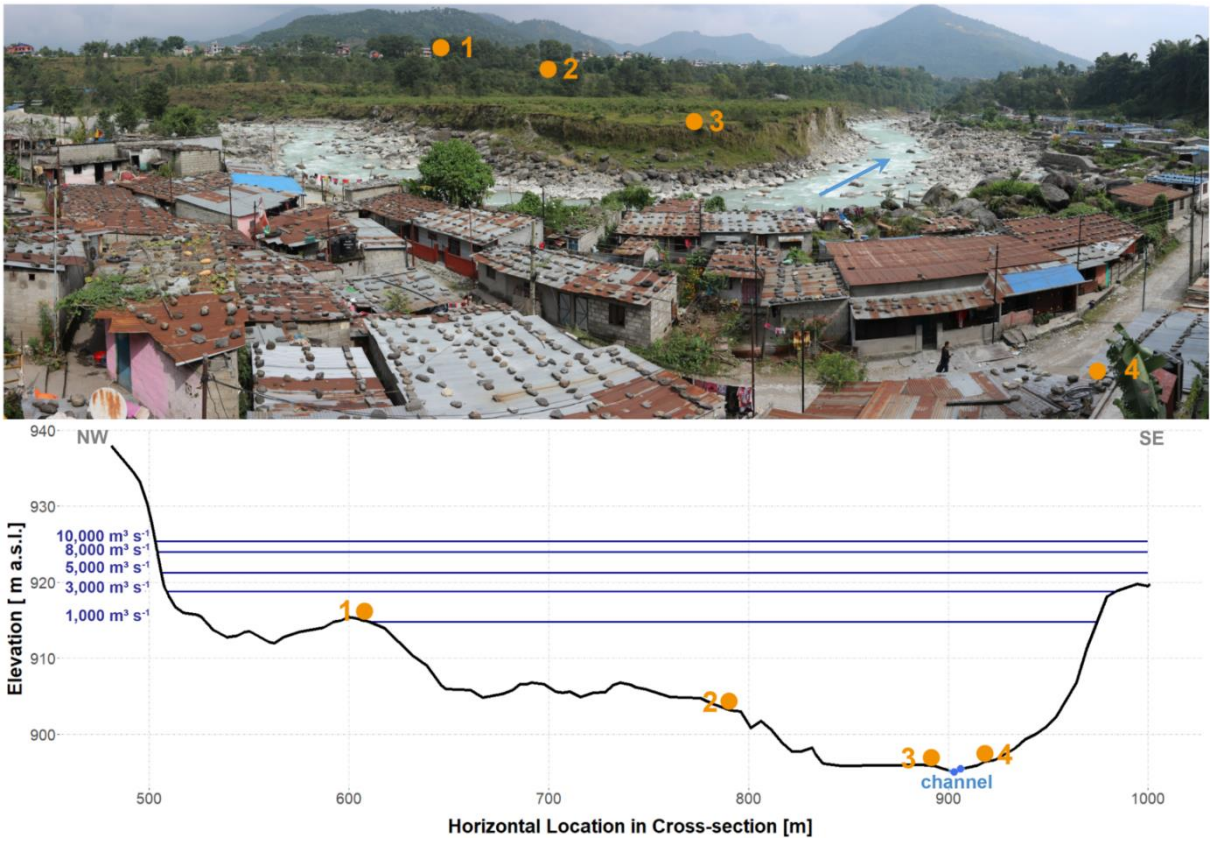

Figure 5.6: Simulated water-levels at the Kaseri informal settlement (Fig. 5.4) for five Q_p scenarios. View from the edge of the settlement's core, which formed in the 1980s on a low terrace (Gurung et al., 2021), onto newer houses built close to the active channel bed of the Seti Khola.

5.4.2 Potential Future Flood Impacts

In 2020, 41% of the study area was covered by developed land, while mixed forest covered 27% mostly in the northern and southern parts (Fig. 5.7). Our simulations indicate that grassland, forests and barren classes (including heavily mined gravel bars) would be flooded widely in all Q_p scenarios (Table 5.1, Fig. 5.8). Some 0.5 km^2 or 2.3% of the total crop area could be submerged for Q_p = 10,000 m^3 s^{-1}. Of all developed LC classes, 0.3 km^2 or 0.6% would be affected by a peak discharge Q_p of 1,000 m^3 s^{-1}, compared to 2.8% (1.5 km^2) for a peak discharge ten times higher. Low developed areas appear to be affected most extensively in all scenarios (Fig. 5.9). For the worst Q_p scenario, some 0.6 km^2 of both low (2%) and medium developed (4.1%) area would be flooded, as opposed to 0.09 km^2 (1%) and 0.25 km^2 (2.8%) for the densest urban areas. Thus, most of the affected areas of the "developed – high" and "developed – open" classes are rated as hazard class 10 (Table 5.1, Fig. 5.9). Only airport areas seem completely devoid of flooding under the scenarios considered here.

Table 5.1: Hazard matrix listing the area (in m^2) of each LULC class located within the respective hazard class (HC). Dev = developed.

Hazard class	Dev - high	Dev - medium	Dev – low	Dev - open	Airport	Barren	Grass-land	Crops	Shrub	Forest
HC 10 (Q_p=1,000 m^3 s^{-1})	88,404	49,981	146,863	47,781	0	785,620	890,852	49,427	261,705	592,295
HC 9 (Q_p=2,000 m^3 s^{-1})	39,769	26,588	67,375	21,663	0	87,289	276,359	29,972	75,234	116,667
HC 8 (Q_p=3,000 m^3 s^{-1})	24,472	18,408	63,907	3,297	0	49,084	203,291	33,648	64,760	88,116
HC 7 (Q_p=4,000 m^3 s^{-1})	14,426	42,852	62,663	3,841	0	21,335	205,548	33,764	78,507	76,140
HC 6 (Q_p=5,000 m^3 s^{-1})	11,086	50,432	44,528	2,766	0	15,639	183,582	45,584	52,529	86,229
HC 5 (Q_p=6,000 m^3 s^{-1})	10,524	30,214	32,089	896	0	17,966	163,655	45,691	49,145	83,334
HC 4 (Q_p=7,000 m^3 s^{-1})	10,997	46,156	33,134	90	0	11,522	158,692	51,518	45,704	64,897
HC 3 (Q_p=8,000 m^3 s^{-1})	12,226	41,392	37,610	93	0	10,218	138,063	49,926	50,186	53,428
HC 2 (Q_p=9,000 m^3 s^{-1})	16,247	129,499	46,675	85	0	6,737	111,848	66,802	42,282	49,208

Hazard class	Dev - high	Dev - medium	Dev – low	Dev - open	Airport	Barren	Grass-land	Crops	Shrub	Forest
HC 1 (Q_p=10,000 $m^3 s^{-1}$)	21,157	153,446	82,444	90	0	4,258	100,775	83,456	33,911	45,499
No hazard	8,610,038	13,799,295	30,803,189	619,173	2,056,873	192,916	6,057,324	20,772,845	7,037,390	35,073,597

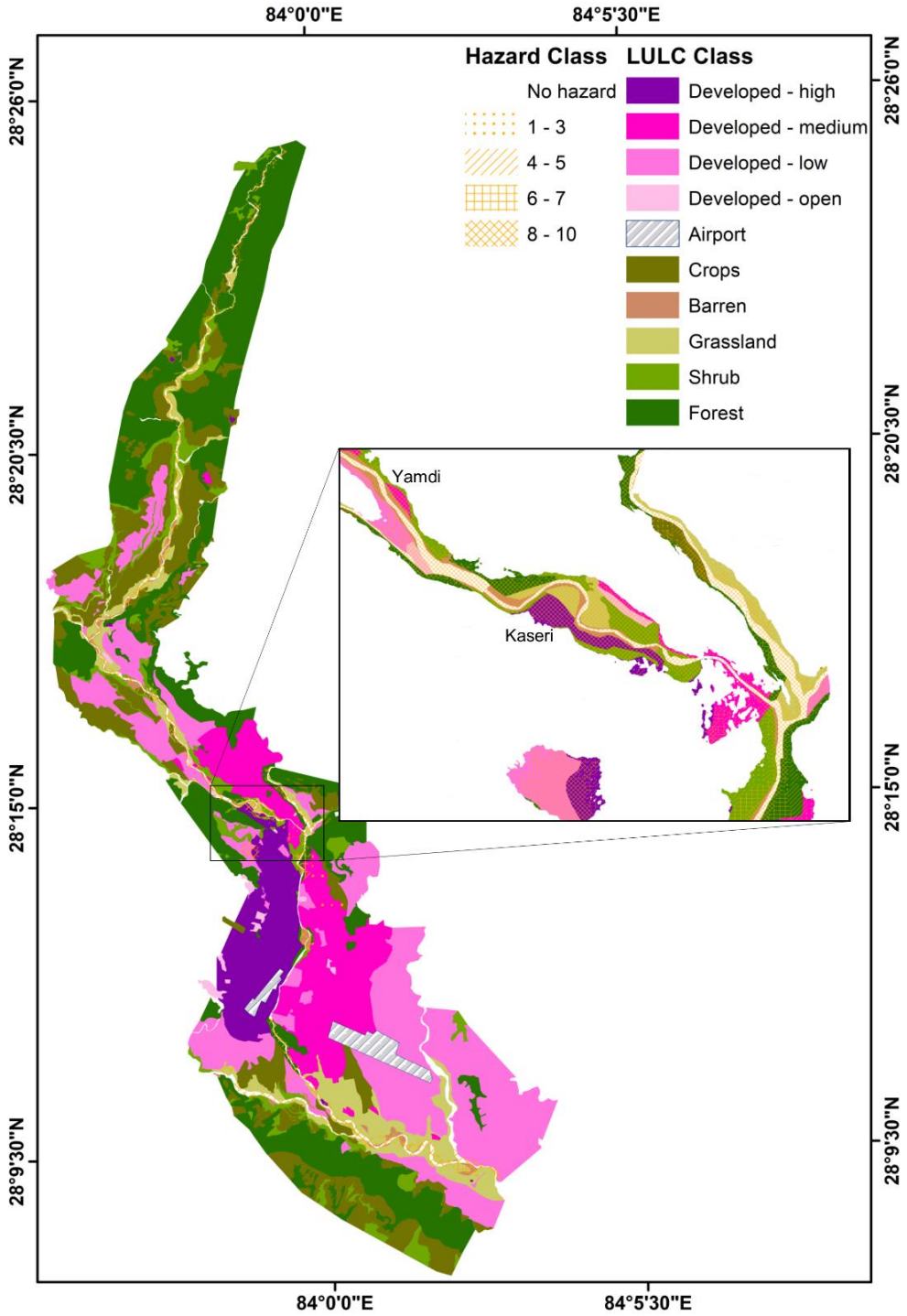

Figure 5.7: Land-use and land-cover (LULC) map with outburst flood hazard classes. Inset shows overlap of high hazard classes (HC 8 – 10) and densely populated areas (developed high to medium) at Yamdi and Kaseri informal settlements. LULC classes mapped from 2020 ESRI basemap Maxar imagery (ESRI and Maxar Technologies, 2022).

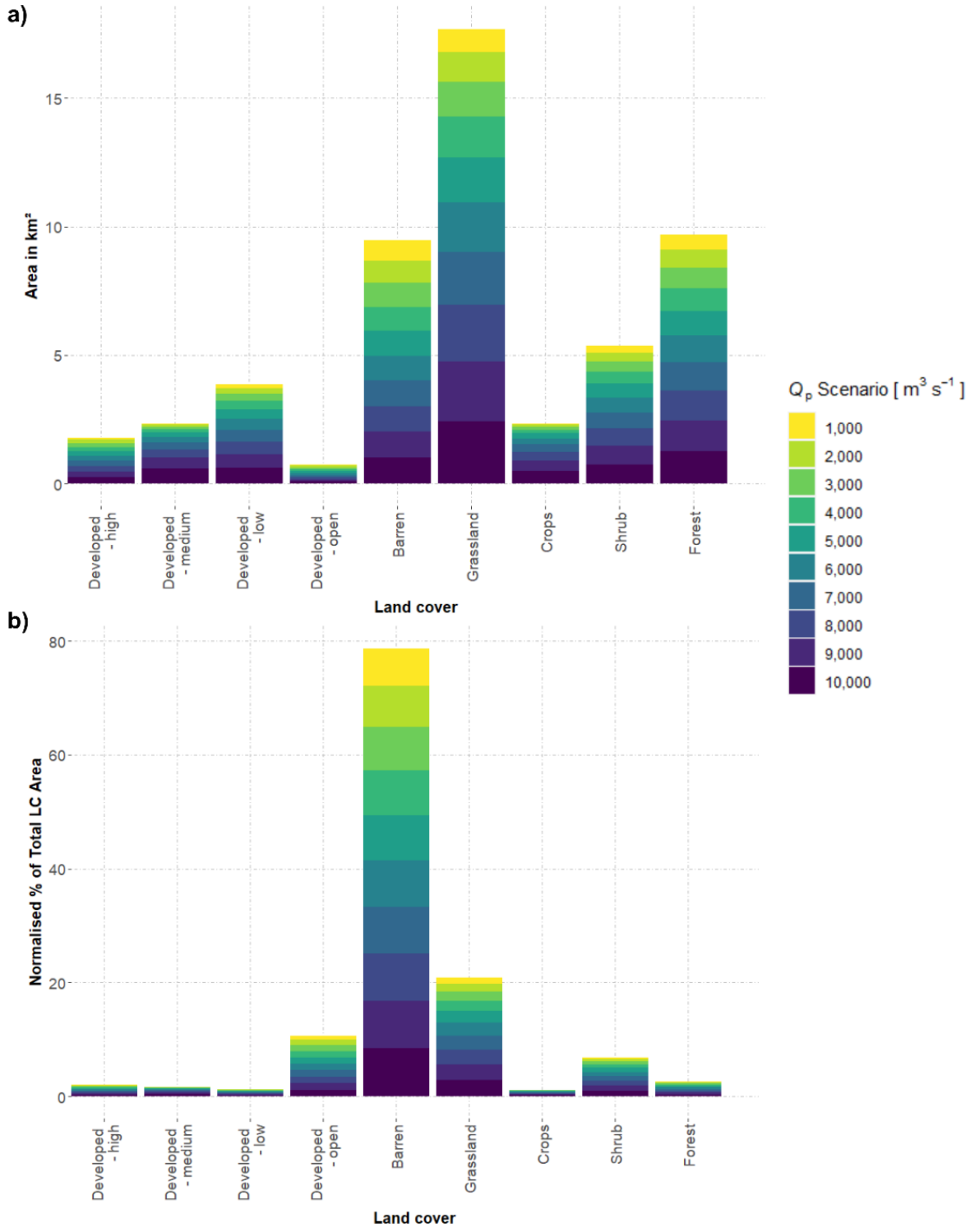

Figure 5.8: Results of the overlay of manually mapped land-cover (LC) classes and Q_p scenario inundation boundaries. a) Area of LC class affected; b) affected normalised percentage of total mapped LC class areas in our study area.

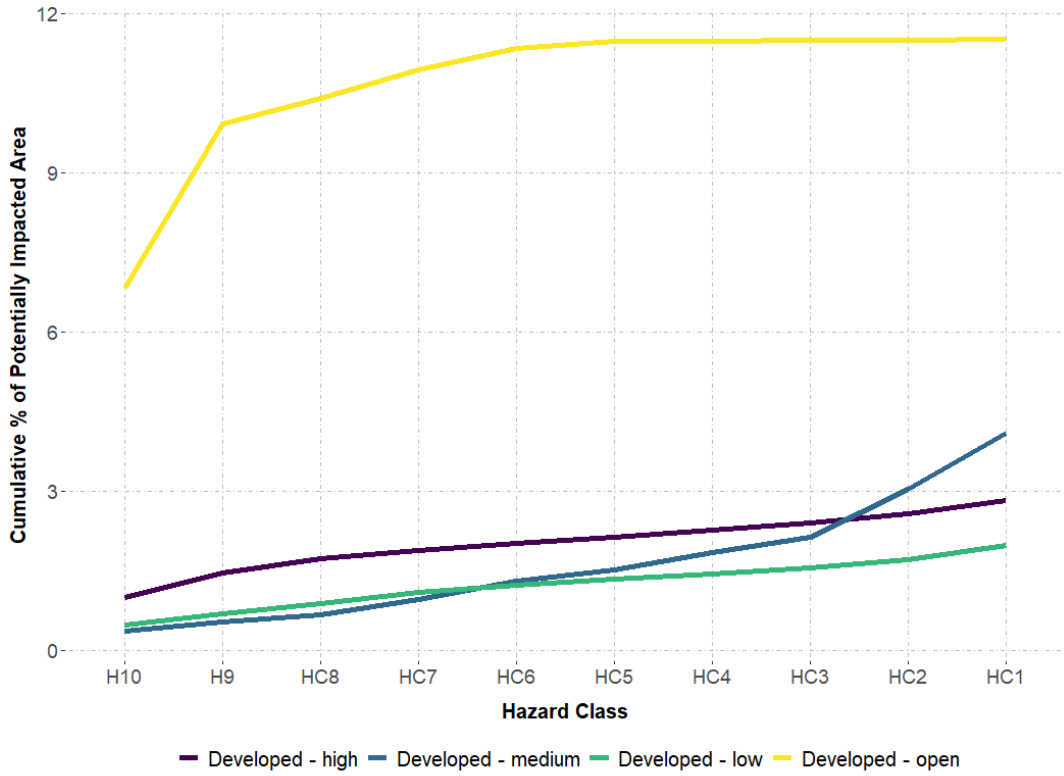

Figure 5.9: Each hazard class' cumulative percentage of areas at potential flood impact for each of the four developed LC classes.

Our analysis of the 2021 OSM route network shows that 4% of its length is prone to flooding, with 0.7% being in the highest hazard class 10 (Table 5.2, Fig. 5.10). Most roads and paths with HC >7 run along the upper Seti Khola upper reach, upstream of Kaseri.

Table 5.2: Relative hazard classification of the Pokhara route network and buildings. Data from OpenStreetMap (September 2021).

Hazard class	Route network		Buildings		
	Length [km]	% of total	No. buildings	Built-up area [m^2]	% of total
10	32.0	0.74	282	21118	0.34
9	19.3	0.45	145	12116	0.19
8	15.1	0.35	81	6956	0.11
7	13.5	0.31	118	10111	0.16
6	15.2	0.35	105	8476	0.14
5	15.2	0.35	63	6763	0.11
4	13.4	0.31	73	8376	0.13
3	13.0	0.30	88	8957	0.14
2	16.8	0.39	250	28627	0.46
1	19.0	0.44	409	42312	0.68
No hazard	4160.5	96.02	61316	6074320	97.53

As of September 2021, OSM users have mapped a total of 62930 buildings in Pokhara and 2.6% of these buildings and 2.5% of the total built-up area are prone to flooding scenarios (Table 5.2, Fig. 5.11). A peak discharge of 10,000 m^3 s^{-1} could affect 282 buildings (0.5%), which translates to 0.3% (0.02 km^2) of the total built-up area falling into hazard class 10. Many of the buildings categorized into the higher hazard classes (HC >7) are in Pokhara's north-western urban areas, especially in the Yamdi and Kaseri settlements.

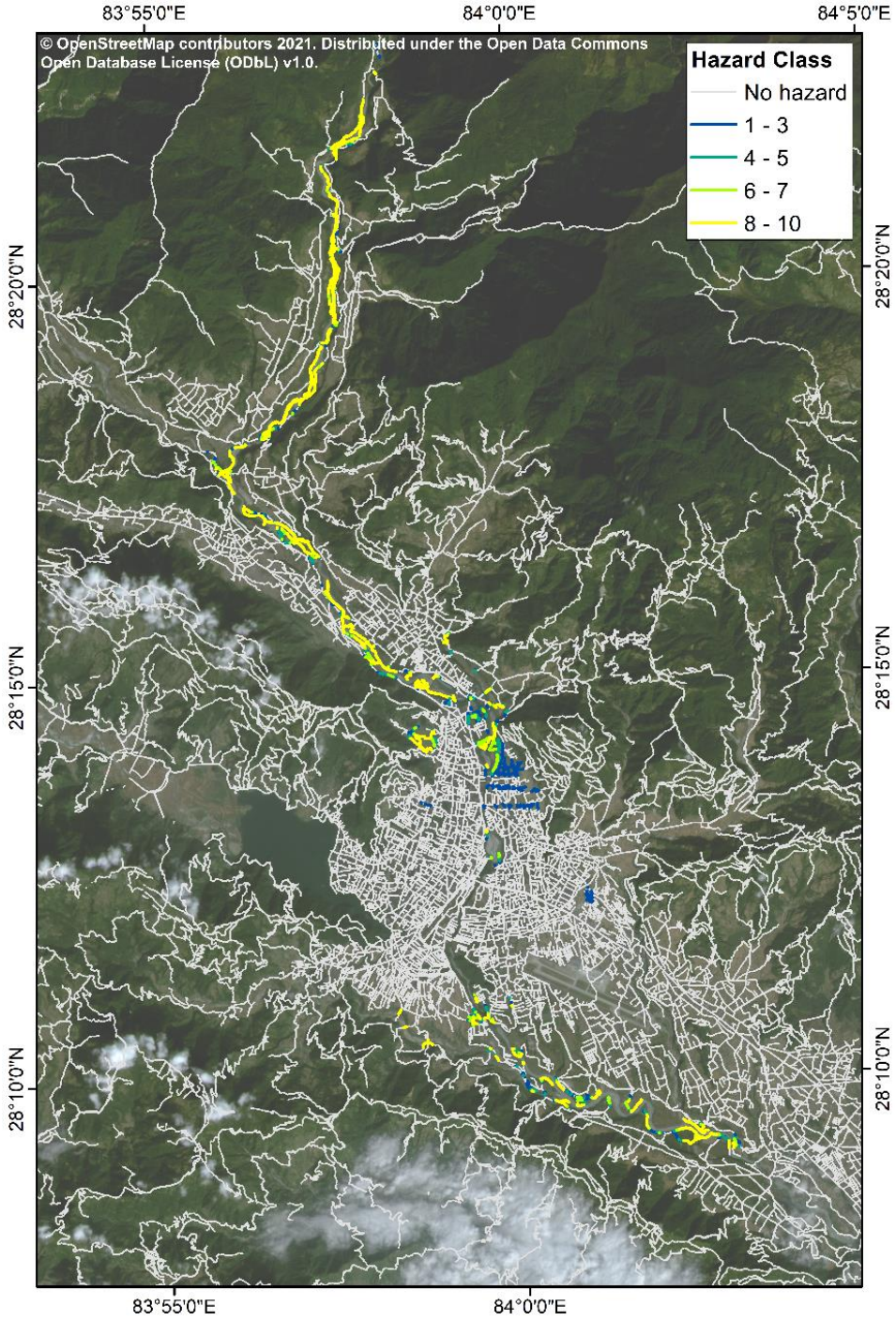

Figure 5.10: Relative hazard classification of the Pokhara route network. Data from OpenStreetMap in September 2021 and draped on PlanetScope imagery (13/11/2021) (Planet Team, 2017).

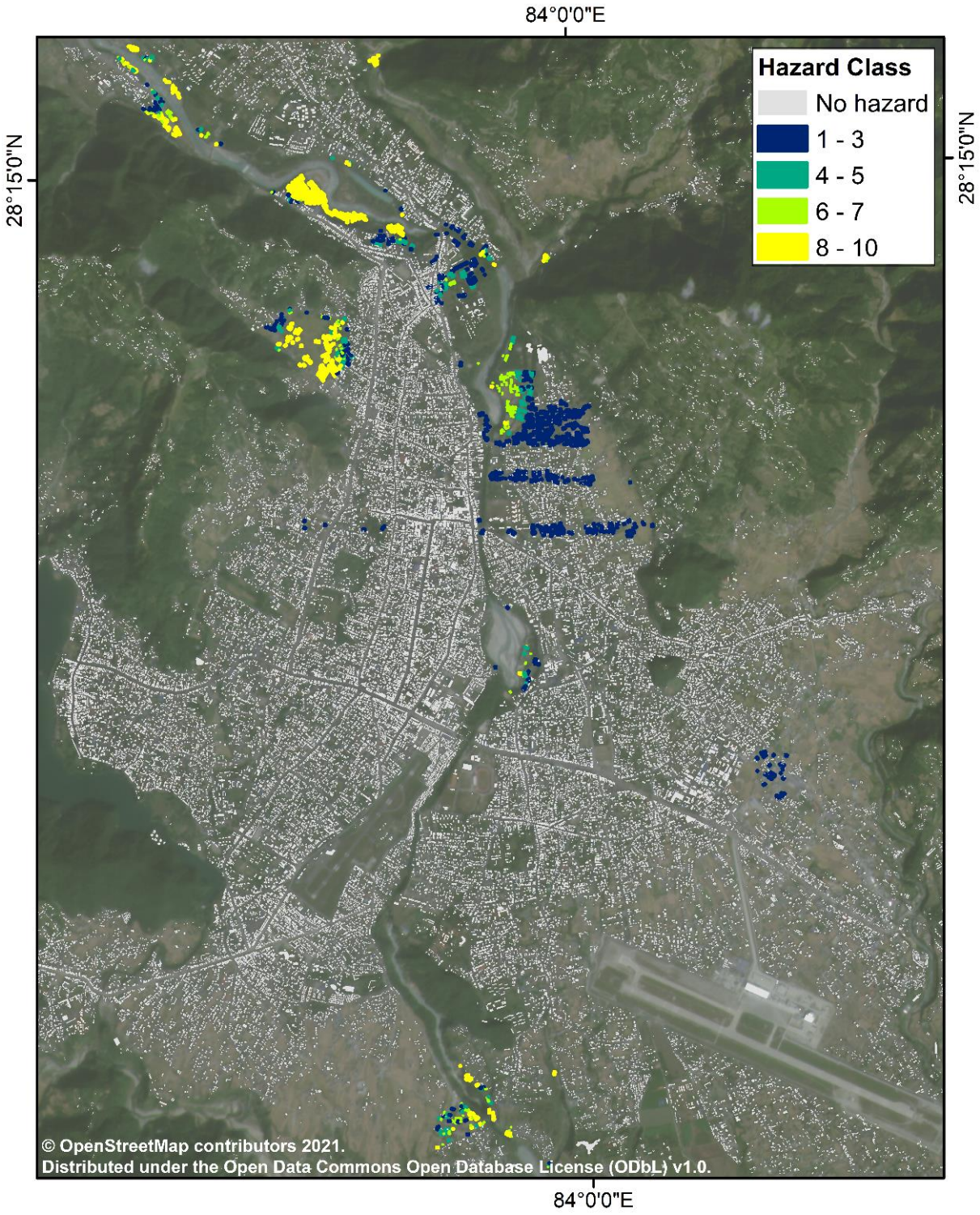

Figure 5.11: Relative hazard classification of Pokhara's mapped buildings. Data from OpenStreetMap (September 2021) draped on PlanetScope imagery (13/11/2021) (Planet Team, 2017).

5.4.3 Informal Settlement Dynamics

The two informal settlements at Kaseri and Yamdi developed rapidly since 2008 (Table 5.3, Fig. 5.12). We find that Kaseri had expanded rapidly from a low terrace in 2008 towards the floodplain by 2012, thus more than doubling its built-up area. This growth continued until at least 2021, covering more than a fifth of the overbank area. The built-up area at Yamdi covered a much lower proportion of overbank area in 2008 (0.4%). Yet, growth was more rapid since, and the built- up area more than tripled between 2008 and 2012 and increased by a factor of six from 2012 to 2021. Comparing November 2012 and November 2021, we also observed a significant expansion of sand- and gravel mining in this particular reach.

Table 5.3: Growth of built-up areas of informal settlements at Kaseri and Yamdi, Pokhara, 2008 - 2021.

	Kaseri		**Yamdi**	
	Built-up area [m^2]	% of overbank area	Built-up area [m^2]	% of overbank area
Apr-2008	12092	7.3	726	0.4
Nov-2012	24886	15.1	2351	1.4
Nov-2021	36703	22.3	14848	9.1

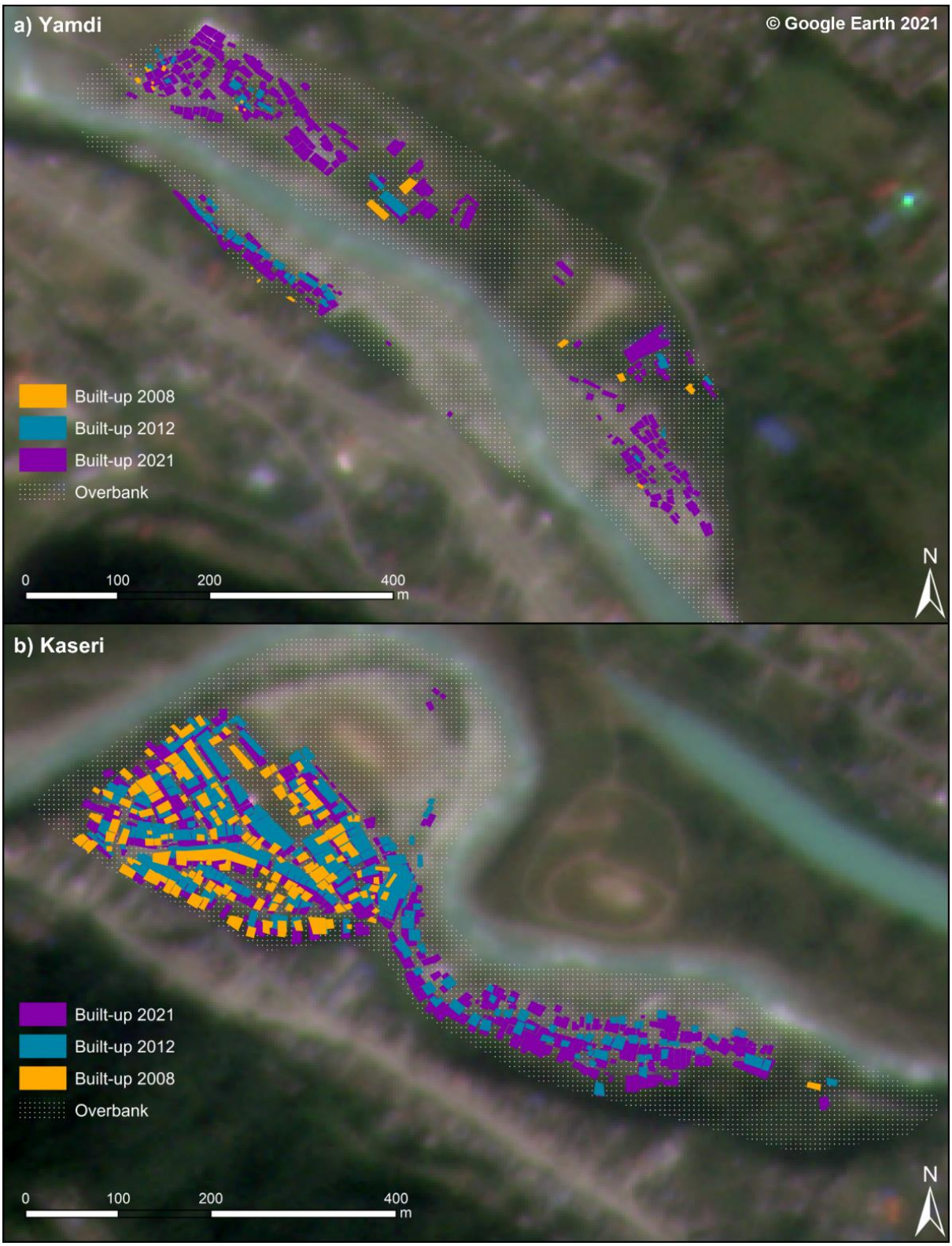

Figure 5.12: Changes in built-up area between April 2008 and November 2021 at Yamdi (a) and Kaseri (b) informal settlements. Built-up area mapped from Google Earth and draped on Planet Scope imagery (13/11/2021) (Planet Team, 2017).

5.5 Discussion

5.5.1 Inundation Modelling

Our scenario-based models of potential outburst flood impacts in Pokhara highlight that especially recent and rapidly growing informal settlements close to the active channel have a high likelihood of being inundated. Before we discuss the implications, we comment on the applicability of our methods. HEC-RAS has been widely applied to model outburst floods (Cenderelli and Wohl, 2003; Klimeš et al., 2014; Wang et al., 2018), albeit at the cost of simplifying outburst flood dynamics in terms of sediment content and channel-bed stability, as entrainment of sediments by bed erosion may alter flow rheology and runout (Westoby et al., 2014). Exact channel geometries are inaccessible in the high-alpine headwaters of the Seti Khola, thus curtailing the use of physically more advanced flow models. Although these could handle erosion and sedimentation dynamics in the propagation of sediment-laden flows, many of the required input parameters remain unconstrained (Cesca and D'Agostino, 2008; Westoby et al., 2014; Zhang and Liu, 2015). Hence, we restricted our scenario simulations to one-dimensional steady flow.

The accuracy of our results hinges on the accuracy of river cross-sections and the estimates of channel and overbank roughness (Manning's *n*; Westoby et al., 2014; Wohl, 1998). Previous studies of HEC-RAS for outburst floods have used mostly coarser digital elevation data than the 5-m ALOS DEM we used here (Mergili et al., 2011; Somos-Valenzuela et al., 2014; Wang et al., 2018; Zhang and Liu, 2015). The stereo satellite imagery forming the basis for this DEM was acquired between 2006 and 2011 and excludes channel changes by the May 2012 flood (Gurung et al., 2021). We minimised potential resulting effects on our models by manually adjusting cross-sections with our additional field-surveyed elevation data. We tested the sensitivity of our HEC-RAS simulations related to the choice of Manning's *n* by comparing the results of two Q_p = 10,000 $m^3 s^{-1}$ scenario models, one with spatially varying and one with a constant Manning's *n*. Variations between these two models are minimal such that a spatially varied Manning's *n* slightly improves the local accuracy of simulations. Yet these local improvements might be crucial in assessing flood hazard for the informal settlements near the Seti Khola. If the accuracy of our simulations of the May 2012 outburst is anything to go by, we surmise that our inundation scenarios are potential underestimates.

Our HEC-RAS simulations also show apparent flooding in places that are likely artefacts of the poorly resolved geometry of several narrow gorges and some subsurface drainage (Fig. 5.4). Sinkholes and caves in the Ghachok Formation may route some of the discharge of the Seti Khola below the surface, especially in urban areas (Fort, 2010; Rimal et al., 2015; Stolle et al., 2019). Modelling the groundwater flow in these potential karst structures is beyond the scope of this study and would require hydrological details that remain largely unresolved. We thus modelled flood flows for an

idealized gorge geometry informed by DEM and field data. Hence, interpretation of these model artefacts has to be handled with care.

5.5.2 Flood Scenarios and their Potential Impact

Our results offer a first comprehensive set of outburst flood scenarios along the Seti Khola, and thus expand on previous studies of a more qualitative (Rimal et al., 2015, 2018) or local focus (Gurung et al., 2021; Thapa et al., 2022). By intersecting modelled inundation extents with spatial data on individual buildings and the route network, we are able to outline relative hazard zones on the assumption that smaller outburst flood magnitudes are more frequent than larger ones. We show that zones with higher relative flood hazard (HC >7) are mostly along the Seti Khola's upper reach. Despite the May 2012 flood's intense damage to infrastructure in this area, a number of infrastructure projects have been developed close to the Seti Khola, including several road bridges and a run-of-the-river hydroelectric station (Gurung et al., 2021).

Further downstream, our mapping of the recent spread of informal settlements along the Seti Khola at Kaseri and Yamdi between 2008 and 2021 substantiates residence interviews about this rapid growth (Gurung et al., 2021). We found that unregulated sand and gravel extraction at Yamdi has, like in many other Nepalese rivers, increased in past decades, but has especially accelerated after large amount of sediments were deposited by the May 2012 flood (Dahal et al., 2012; Fort et al., 2018). Our results illustrate the coupling of intense outburst flood sediment deposition and built-up area expansion along the Seti Khola's mid reaches, where more people were and still are attracted by this emerging opportunity of income. Although interviews with gravel and sand miners have shown that they are aware of this risk (Henzmann, 2020), they successively move into these flood-prone locations and raise their vulnerability to outburst floods. Gravel mining of this scale is likely to further modulate the roughness of the active channel, while enhancing bank erosion and cliff collapse, thus propagating the flood hazards also to the densely populated river terraces further up (Fort et al., 2018; Kondolf, 1994).

One key finding of our simulations is that hydraulic ponding upstream of gorges and backwater flooding at tributaries occurs in all scenarios, leading to high local flow depth and reduced flow velocities. The Seti dam and Kaseri informal settlement appear to be particularly prone to hydraulic ponding, which might cause severe flooding there. Locally sustained flood peaks might cause spatially much more diverse outburst flood hazard along this reach. While our models simulate clear-water flow, hydraulic ponding is likely exacerbated by entrained sediment and debris that may further clog or block the gorges (Thapa et al., 2022). Hydraulic ponding is a common process during

outburst floods in bedrock or resistant-boundary channels and reported for Holocene jökulhlaups in Iceland (Carrivick, 2006, 2007) and historic outbursts of moraine-dammed lakes in British Columbia (Kershaw et al., 2005). This importance of hydraulic ponding complements the findings of previous studies concerned with estimating flood frequency at several sites (Basnet and Acharya, 2019; Gurung et al., 2021). Estimates of the 100-year flood based on rainfall data are $Q_p = 2{,}336$ m^3 s^{-1} (Basnet and Acharya, 2019) and $Q_p = 2{,}423$ m^3 s^{-1} (Gurung et al., 2021). These are consistent with the lower range of outburst flood scenarios and offer comparable flood limits in the Ramghat (Basnet and Acharya, 2019) and Kharapani areas (Gurung et al., 2021).

Overall, several studies have emphasised the potential for future outburst floods along the Seti Khola (Fort, 2010; Gurung et al., 2021; Kargel et al., 2013; Lovell et al., 2018). Especially the steep-walled and sediment-filled Sabche Cirque, above the narrow Seti Khola gorge, is geomorphically active and subject to rare, but strong earthquakes (Grandin et al., 2012). The upper Seti Khola gorge is a bottleneck prone to blockage by landslides detaching from the cirque walls (Kargel et al., 2013). Further downstream, landslides triggered by monsoonal storms (Talchabhadel et al., 2018) could also form temporary dams that might fail catastrophically like in the Melamchi outburst flood in June 2021 (Petley, 2021a). Fort (1987) and Kargel et al. (2013) reported that the Sabche Cirque hosts large amounts of unconsolidated material to nourish floods and debris flows. New meltwater lakes in the Sabche Cirque may form outburst flood sources in the near future (Kargel et al., 2013). The Sabche glacier could also contribute to generating outburst floods during of following one of its surges (Lovell et al., 2018). One surge phase began in 2012, with the glacier having advanced by 2.2 km at up to 1.6 ± 0.1 m per day (Lovell et al., 2018). Future research may want to explore possible links between surges and outburst flood potential along the Seti Khola.

5.5.3 Recommendations

No early-warning strategy was in place during the May 2012 outburst flood and several authors suggested that a chance warning presumably prevented a higher death toll in the north-western outskirts of Pokhara (Gurung et al., 2015; Kargel et al., 2013). In the flood's immediate aftermath, public flood risk awareness and preparation trainings as well as an early-warning system were implemented – including a water-level sensor in the Seti Khola just above the furthest upstream settlement (Gurung et al., 2015). However, recent interviews with local residents showed that a lack of maintenance has rendered the early-warning system inoperable in the past years (Henzmann, 2020). Thapa et al. (2022) pointed out, that existing evacuation routes from Yamdi and Kaseri settlements towards higher ground are inadequate. A regularly maintained warning system might want to provide full coverage of settlements along the Seti Khola's course through the Pokhara

valley and include the four major components of risk knowledge, monitoring and warning, dissemination and communication, and response capability (Huggel et al., 2020). The May 2012 flood also demonstrated that outburst floods can travel fast in the steep headwaters of the Seti Khola (Kargel et al., 2013; Oi et al., 2014). Stream gauges and comparable monitoring stations may need to be located further upstream than presently implemented, ideally close to the outlet of Sabche Cirque to maximise warning times for downstream communities. Continued monitoring of the Sabche Cirque using optical and SAR satellite data acquired at short repeat rates afforded via the Sentinel and Planet platforms might further assist early warning, while ground movement and deformations of the cirques walls, surge-phases of the Sabche glacier, and lake formation might be tell-tale warning signs (Grebby et al., 2021; Hermle et al., 2021; Kirschbaum et al., 2019; Quincey et al., 2005).

5.6 Conclusions

The Seti Khola is the lifeline of Nepal's second largest city, but also a river prone to outburst floods, given that it traverses one of the steepest topographic gradients in the Higher Himalayas. We provide the first comprehensive assessment of potential outburst discharge scenarios and intersect hydrodynamically modelled inundation extents with land-cover data. Our simulations demonstrate the high spatial variability of potential outburst flood impacts in the Pokhara valley. All model runs point to potential hydraulic ponding with high flow depths and low flow velocities above deeply incised gorges in urban areas.

We find that even a moderate outburst flood scenario with peak discharge well within the ranges of monsoonal floods (Q_p = 1,000 $m^3 s^{-1}$), could inundate some 0.6% (0.3 km^2) of the developed area and 3.2% of cropland and grassland. A larger outburst flood involving a peak discharge ten times higher would flood 2.8% (1.5 km^2) of the Pokhara valley's developed areas and 9.8% of its agricultural areas. OSM data of built-up area in Pokhara's urban areas show, that relative inundation hazard is highest in the city's north-western outskirts, where a rapidly growing number of informal buildings linked to gravel mining is has moved close to the Seti Khola. These sites of extensive unregulated sand and gravel mining would be extensively inundated in all our discharge scenarios – putting workers and informal settlement dwellers at risk. Built-up area in both Kaseri and Yamdi has grown intensively in the past decade: While built-up area in Kaseri, Pokhara's oldest established informal settlement, tripled between 2008 and 2021, built-up area rapidly increased by a factor of 20 in the recently forming settlements at Yamdi. Since 2012, a sixfold increase in built-up area at the latter is accompanied by an intense expansion of gravel and sand mining activities. Several roads that are

crucial for the supply reliability of rural communities are also prone to more frequent flooding by outbursts as these roads run parallel to the Seti Khola on its lower alluvial terraces.

We conclude that urban planning and risk mitigation strategies in the Pokhara valley might wish to consider the hazard posed by outburst floods in more detail, given the accumulating evidence of repeated historic and prehistoric events. Potential risk reduction measures may include in-field and remote monitoring of the Seti Khola's headwaters as well as early-warning strategies, including a statutorily determined chain of warning as well as public awareness training. Such training could be aided by considering scenario-based limits of inundation for different flood sources.

6 Discussion

The studies presented in Chapters 3, 4, and 5 individually addressed the regional ***susceptibility*** and the local ***flow characteristics*** as well as ***hazards*** posed by outburst floods in the Greater Himalayan region. After summarising the main findings and answering the three research questions formulated in Chapter 1.6, I will discuss the overarching implications and future research challenges in the following subchapters. In the latter, I will discuss my findings within the greater context of regional and local modelling of outburst floods in a changing world – transforming both the cryosphere and the anthroposphere.

I *What can the few data on past glacial lake outburst floods in the Greater Himalayan region tell us about a glacial lake's **susceptibility** to this hazard?*

> To address this question, I quantitatively investigated the credibility of the predictors elevation, catchment and lake area, lake area change, glacier-mass balance, and monsoonality, in terms of estimating the susceptibility of observed outburst from moraine-dammed lakes in the past four decades. Although expert knowledge on GLOF processes highlights the importance of all of these commonly applied predictors of outburst potential, several of the data-driven models that I explored only partly supported this notion. While larger lakes situated in larger catchments and within regions of strong negative glacier-mass balances seem more prone to sudden outburst floods, the effects of monsoonality, elevation, and change in lake area were more ambiguous. This major finding contradicts the common notion, that (rapidly) growing glacial lakes are a sufficiently reliable indicator of a pending outburst.

II *What can we learn from sedimentary evidence and numerical modelling about **flow characteristics** of moderate modern to cataclysmic historic floods in the Pokhara valley?*

> To test the plausibility of large outburst floods in the Pokhara valley of Nepal, I used mapped flood sediments to validate numerically simulated flood extent and to reconstruct the flow behaviour of two events of widely varying peak discharge scales (1,000s vs. 100,000s $m^3 s^{-1}$). This study is the first to comprehensively simulate flow velocities and flow depths during the Seti Khola flood in May 2012 and results consistently indicate considerably lower peak discharges than several previous (empirical) estimates. I also provide first-order estimates of the peak discharge of the much larger Mediaeval events and provide first quantitative proof that they were of fluvial origin – probably caused by the outbursts of large former lakes in the headwaters of the Seti Khola. This main finding is supported by the good match of

modelled extensive backwater effects and slackwater deposition limits found in exposed fill deposits of tributary valleys.

III *What **hazards** could potential future outburst flood scenarios pose to a rapidly growing high-mountain city like Pokhara?*

My comprehensive assessment of physically plausible peak discharge scenarios demonstrates the localised variability of outburst flood hazards in terms of flow depth and velocity along the Seti Khola, the lifeline of the rapidly expanding city of Pokhara. The relative inundation hazard, which is locally aggravated by the potential effects of hydraulic ponding above deeply cut and narrow gorges, is highest in the city's north-western periphery, where gravel mining activities and associated informal settlements close to the active river channel have emerged or increasingly expanded in the past decade.

6.1 Challenges of Regional and Local Outburst Flood Assessments

6.1.1 What Makes a Glacial Lake Susceptible to Sudden Outburst?

Glacial lake outburst floods are rare events and their full dynamics, from triggering to overtopping or breaching mechanisms are, apart from few exceptions like the Tam Pokhari GLOF of 1998 (Osti and Egashira, 2009), mostly unobserved phenomena (Wang et al., 2022). Thus, our understanding of the geomorphic processes at play before and during a GLOF are mainly based on the retrospective reconstruction of single events from their sedimentary and geomorphic legacy (Richardson and Reynolds, 2000) – informed by post-event reconnaissance visits and the analysis of satellite images (e.g. Lemthang Tsho 2015: Gurung et al., 2017; Dig Tsho 1985: Vuichard and Zimmermann, 1987). Similarly, preconditioning factors that might make a given lake more susceptible to sudden outburst were defined by experts based on few case studies and theoretical considerations of physically plausible processes (Clague and Evans, 2000; Costa and Schuster, 1988). While learned from a given set of lakes in a specific mountain region, these case-specific observations are often transferred to assess glacial lakes in other regions with differing environmental settings and constraints. For example, the approach by Huggel et al. (2002, 2004) included decision criteria and empirical relations describing lake volume and travel distances specific for outbursts from glacial lakes in the Swiss Alps. Although the authors state that "Open questions and limitations of the approach might be related to the applicability outside the European Alps" (Huggel et al., 2004), subsequent studies have transferred it to glacial lakes in other mountain ranges (Andes: Drenkhan et al., 2018; British Columbia: McKillop and Clague, 2007; Greater Himalayas: Jain et al., 2012; Zheng et al., 2021). However, a direct transfer of GLOF observations from

one high-mountain region to another might neglect local characteristics of GLOF causes and mechanisms – as discussed by Emmer and Vilímek (2014) in regard to their GLOF susceptibility assessment, which they specifically adapted to conditions in the Cordillera Blanca, Peru. This underlines the need to recognise and address regionally specific controls of GLOF susceptibility based on available data on past GLOFs in this region. This also holds true for the Greater Himalayan region, where previous assessments have mostly relied on predictors learned from other mountain regions around the globe.

In the Greater Himalayas, the summer monsoon might be one of these potentially region-specific controls. Although Richardson and Reynolds (2000) proposed a causal link between GLOF occurrence and heavy monsoonal precipitation, summer precipitation has so far been considered only in few assessments utilising sparse meteorological station data (Wang et al., 2008, 2012b). The potential influence of "monsoonality" on past GLOFs in the Greater Himalayan region has been explicitly acknowledged and probabilistically tested for the first time in Chapter 3. However, the applied definition of monsoonality, i.e. summer proportion of annual precipitation as derived from interpolated meteorological data at a 30 arc sec resolution, is unable to resolve sudden, highly localised cloudburst events (Liu et al., 2014). As a majority of heavy rainstorms occurring in the study area are tied to the summer monsoon, seen in the Chorabari GLOF of 2013 (Allen et al., 2016b), this approach at monsoonality remains relevant – at least until time series of precipitation measurements are available on a lake level across the whole Greater Himalayan region.

Considering the topographic and climatic heterogeneity along the extensive Greater Himalayan mountain arc (Bolch et al., 2019), internal grouping within the data for the >3,000 considered moraine-dammed lakes is likely. By applying Bayesian logistic regression on two levels, this potential intra-regional variability in the influences of tested GLOF susceptibility predictors is explicitly acknowledged and probabilistically explored for the first time.

It has to be stressed that this probabilistic exploration of past controls on GLOFs in the Greater Himalayas cannot replace local (geo-) technical dam-stability assessments (Costa and Schuster, 1988; Worni et al., 2012). However, my findings could inform ensemble models of GLOF prediction, allowing for remote lake assessments which are more adapted to local circumstances.

6.1.2 Integrating Remote and In-field Data

Regional-scale outburst flood assessments are to first order limited by the availability of spatially consistent information and, hence, predominantly rely on remotely sensed data (McKillop and Clague, 2007b). As a result, a number of empirical relations between parameters which are only

measurable in the field and those which are readily remotely derivable have been described and widely applied in regional studies of lake stability or hazard (Huggel et al., 2002). One prominent example is the estimation of a moraine-dam's stability based on the height-to-width ratio of the dam, derived from digital terrain data, instead of information on its composition and internal structure from field measurements. Another example is the use of lake surface area to approximate lake volume in the absence of bathymetric measurements (Clague and Evans, 2000; Huggel et al., 2002). When assessing the climatic variability of lake catchments in remote, high-altitude areas, meteorological station data is sparse, especially in the Greater Himalayan region (Liu et al., 2014). Hence, modelled climatologic data based on topographic parameters provides the areal coverage needed for regional assessments - although it comes with the drawback of potential multi-collinearity of parameters.

The problem of correlation, which is minimised in my regional GLOF susceptibility study (Chapter 3) by applying advanced Bayesian multi-level regression to few selected parameters, was rarely addressed in other studies. Figure 6.1 shows the linear correlation of several candidate predictors widely thought to promote GLOF susceptibility. I further tested, which of the >100 highly correlated potential GLOF predictors are considered to be statistically significant when using automated predictor selection algorithms (step-wise predictor selection and the variance inflation factor) within a simple regression model. In some cases, automated predictor selection identified commonly described lake stability predictors, such as the valley slope steepness or the distance of the lake to the parent-glacier snout, as not statistically relevant. Apart from the problem of multi-collinearity, using this many potential predictors introduces high dimensionality of the predictor space, which cannot be sufficiently sampled with available data points and is, hence, also problematic. Further, seemingly statistically relevant parameters could be proxies for other, unknown parameters and are, hence, not reflecting true natural drivers of GLOF generation. Thus, I opted to apply a more advanced statistical machine learning algorithm – Bayesian multi-level logistic regression – to learn more about what available data is actually telling us about the regional controls on past GLOFs in the Greater Himalayan region.

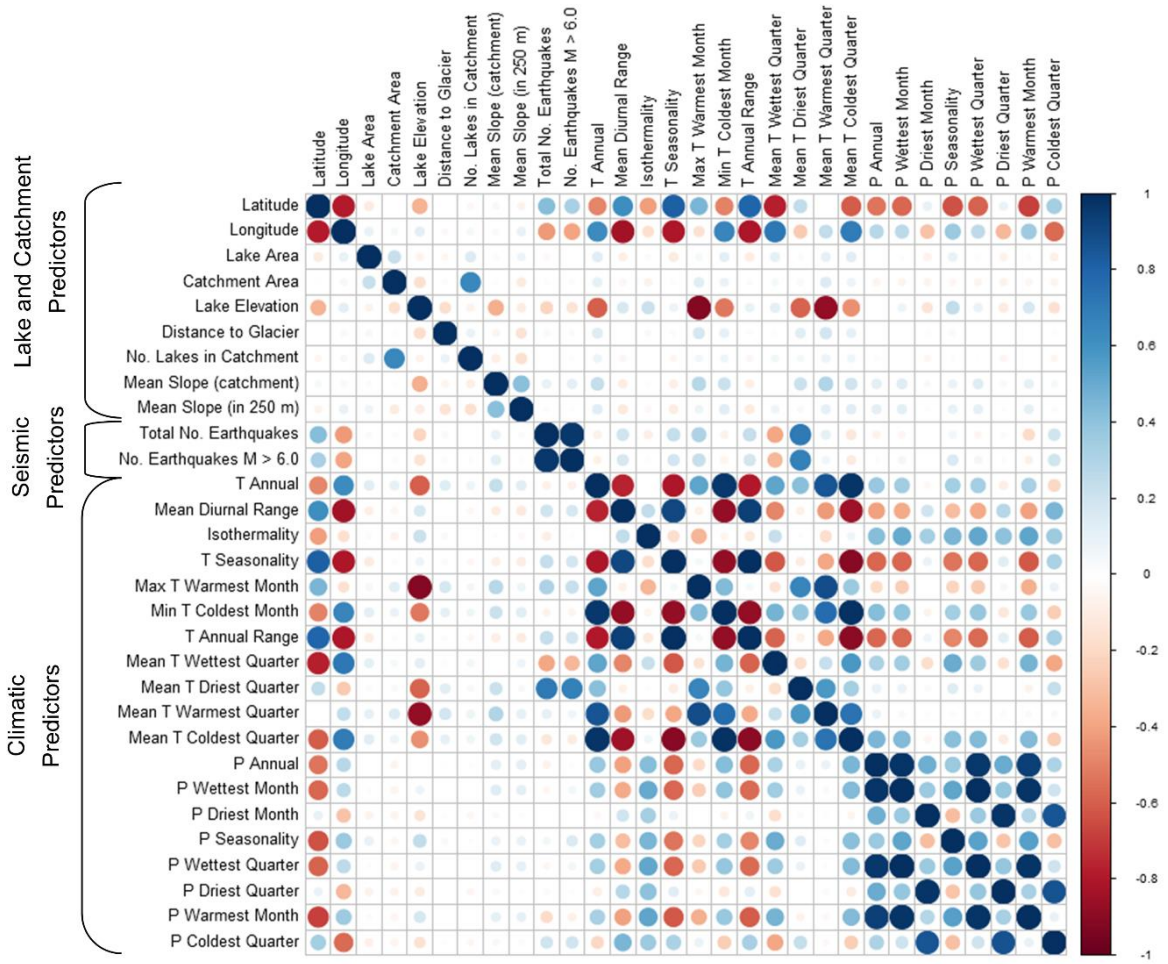

Figure 6.1: Correlation plot showing linear correlation of several candidate predictors of a lake's susceptibility to GLOFs using Pearson's correlation coefficient. Colour intensity of the bubbles is proportional to the correlation coefficient while their size shows the absolute value. Data derived from the SRTM DEM, the Randolph Glacier Inventory 6.0 (RGI Consortium, 2017), the USGS Earthquake catalogue (USGS, 2019), and CHELSA (Karger et al., 2017). T = temperature, P = precipitation.

Generally, field-data collection is more applicable in local outburst flood assessments and might, for example, include lake bathymetric surveys (Rafiq et al., 2019; Wang et al., 2018) or studies of internal (moraine) dam structures (Mool et al., 2011; Worni et al., 2012). However, these field studies are costly and limited by the inaccessibility of lakes or other potential source areas due to their remoteness and hazardous high-mountain conditions. This also applies to the geomorphically active Sabche Cirque (>3,500 m a.s.l.), the source area of past and potential future outburst floods along the Seti Khola discussed in Chapters 4 and 5. Although potentially less hazardous, downstream field-data acquisition like the mapping of flood sediment extents (Mergili et al., 2011) might also be not feasible due to local restrictions: for example, during my field work in the Pokhara valley in 2019, UAV usage was not permitted. Thus, I opted to combine other available remote-sensing data with ground truthing. For example, I jointly derived Manning's *n* values from field observations and land cover mapped from high-resolution satellite imagery. I also integrated field-

surveyed with DEM-derived channel cross-sections. Thus, the numerical simulations of outburst flood scenarios in Chapters 4 and 5 are a compromise between highly-resolved but spatially more restricted (i.e. fully field-data-based; Klimeš et al., 2014) and low-resolved but spatially more extensive (i.e. fully remote-sensing-based; Jha and Khare, 2016) assessments.

6.1.3 Transient Assessment Scales

So far, most studies assessing lake stability or outburst flood hazard at a regional scale aimed at detecting "potentially hazardous" lakes, which are often ranked on an ordinal scale and recommended for further, more detailed local assessments, such as fieldwork or flood propagation modelling (Emmer and Vilímek, 2014; Khadka et al., 2021). Worni et al. (2013) combine both scales into one study by classifying glacial lakes in the Indian Himalayas as "critical", "potentially critical", and "not critical" and subsequently offering a detailed risk assessment for three selected "critical" lakes. Although easier to communicate to the non-scientific public, including local authorities and stakeholders, the uncertainties of these regional classification schemes remain unspecified. Thus, the reasons behind often inconsistent classifications of a given lake are not always reproducible or fully traceable - further complicating the decision at which lakes more costly local hazard assessments should be performed (Mal et al., 2021; Rounce et al., 2016). Allen et al. (2021) also comment on this issue of inconsistent classification of lakes as "potentially dangerous" between a growing number of large-scale assessments in the Greater Himalayan region; they "[…] recommend a consensus approach, drawing across multiple studies, and including the knowledge of local authorities to arrive at a final listing of high priority lakes which may be subject to further monitoring, Early Warning Systems and other response strategies.". Thus, data-derived modelling of a posterior GLOF probability of a given lake in the Greater Himalayas, or its GLOF susceptibility as discussed in Chapter 3, provides a more objective approach to prior ordinal classifications, while propagating all underlying uncertainties. However, the aim of my study was not to provide stability assessments at the lake scale but to learn more about the overarching controls on GLOF susceptibility and whether it is possible to identify past events from multi-variate data on a regional scale. The divergences in posterior probability estimates between the glacier-mass balance model and the elevation-dependent warming model underline the varying effects of predictor choice at the lake scale, which Rounce et al. (2016) described as main reason for discrepancies between previous ordinal assessments (Table 6.1).

Table 6.1: Comparison of mean posterior probability of a GLOF history (P_{GLOF}, Chapter 3) with ordinal lake classifications as presented by Bajracharya et al. (2020) and Rounce et al. (2016) for five selected glacial lakes. Rounce et al. (2016) also applied the methods by Bolch et al. (2011) and Wang et al. (2011) to the selected lakes. Bajracharya et al. (2020) identified all five example lakes as "potentially dangerous" and further ranked their "danger level" (rank I = highest, rank III = lowest). GMB = glacier-mass balance model; EDW = elevation-dependent warming model.

Lake	Location	Bolch et al. (2011)	Wang et al. (2011)	Rounce et al. (2016)	Bajracharya et al. (2020)	P_{GLOF} (0 to 1)	
						GMB estimate (est. error)	EDW estimate (est. error)
Chamlang South Tsho	27◦45.3′ N 86◦57.5′ E	medium	very high	very high	II	0.0107 (0.1027)	0.0172 (0.1298)
Imja Tsho	27◦53.9′ N 86◦55.5′ E	high	low	low	I	0.0077 (0.0874)	0.0225 (0.1483)
Lower Barun Tsho	27◦47.9′ N 87◦05.7′ E	high	medium	very high	I	0.0082 (0.0899)	0.015 (0.1216)
Lumding Tsho	27◦46.8′ N 86◦36.8′ E	high	medium	very high	I	0.0046 (0.06730)	0.0177 (0.1319)
Thulagi Tsho	28◦29.3′ N 84◦29.1′ E	high	medium	high	I	0.022 (0.1467)	0.0216 (0.1454)

Few large-scale studies in the Greater Himalayan region add the component of risk to their lake stability assessments (Dubey and Goyal, 2020; Rounce et al., 2016). In these studies, GLOF risk is based on a classification of downstream impacts to buildings and infrastructure, especially hydropower schemes, derived from inundation modelling. However, in contrast to the advanced, physically-based numerical models used at the local scale, computationally less expensive GIS-based GLOF routing across a DEM-surface can be useful (Dubey and Goyal, 2020; Rounce et al., 2016). Thus, one of the major challenges for future outburst flood research in the Greater Himalayas, but also in other high-mountain belts of the world, is the integration of local methodologies into regional-scale hazard assessments. Although regional-scale approaches have been transferred to global studies (Kougkoulos et al., 2018), there is a distinct gap between data and methodologies used on the local and regional scales, which is, hitherto, to a first order limited by data availability and computational costs.

6.2 Reconstructions of Past and Simulations of Future Outburst Floods

6.2.1 The Data Scarcity Issue

Outburst floods are highly infrequent and often occur in remote areas (Korup and Clague, 2009; Veh et al., 2019). Inventories of outburst floods are crucial for traditional time-series-based hazard estimations, but also suffer from reporting and detecting biases (Veh et al., 2019). An unknown, but likely substantial, number of cases could have happened without notice in the decades prior to a pronounced scientific interest since the 1970s (Veh et al., 2022). Hence, directly measured data on

outburst floods are rare, while approximate and model-based data of past outbursts prevail (Westoby et al., 2014). Uncertainties are inevitable and may affect several aspects of the outburst flood process chain. For example, the initial breach conditions, that largely control flood generation, are commonly unknown and have to be approximated for physical-based and numerical models (Zhang and Liu, 2015). However, where dam and potential outburst flood sources have yet to form – as is the case in the Seti Khola's headwaters – dam-breach modelling becomes even more uncertain. Another common issue concerns the volumetric estimates of net erosion and deposition during outburst floods, because information on the channel topography before an event, often in the form of DEMs, is rarely available for comparison (Westoby et al., 2014). Direct measurements of the hydraulic properties of an outburst flood are rarely captured by stream gauges, as these instruments are sparse in mountainous headwaters or simply destroyed by these highly energetic water and sediment flows (Westoby et al., 2014). Thus, few directly measured and complete hydrographs are available for research. For example, data on the propagating flood wave generated by the sudden drainage of the Luggye Tsho (Nepal) in 1994 comes from a gauge some 100 km downstream of the lake (Richardson and Reynolds, 2000).

6.2.2 Retrospective Learning from Sediment Archives

Quantitative hazard estimates of low frequency, high magnitude events are commonly limited by short and incomplete time series – a problem of many hazard appraisals in general and outburst flood assessments in particular (Korup and Clague, 2009). Although extreme-value statistics, based on heavy-tailed extreme-value distributions, have been applied to Himalayan outburst flood hazard assessments at a regional scale (Veh et al., 2020), they are less applicable in local studies due to a lack of data. There, Quaternary sediment records can provide valuable insights into frequency-magnitude relationships if facies can be correctly attributed to a given hazard and dated sediment layers can be directly attributed to one or several events (Korup and Clague, 2009). This combined approach of sedimentary facies interpretation and geochronology has been successfully applied to extent palaeo-flood records in the Indus, Ganges, and Brahmaputra rivers (Srivastava et al., 2017).

Sedimentological evidence can also be used to inform palaeo-hydraulic reconstructions and the geomorphic signature that outburst floods leave behind in mountain stream channels can be used to estimate flood magnitudes of unobserved or unmeasured events (Kershaw et al., 2005; Wohl, 1995). Several authors utilised these palaeo-stage indicators or flood markers, which include both erosional markers such as scour lines and depositional features such as fine-grained overbank deposition features, for retrospective step-backwater hydraulic modelling of GLOFs, for example in the Andes (Klimeš et al., 2014) or in the Himalayas (Cenderelli and Wohl, 2001). The reconstructions

of recent and ancient outburst floods in the Pokhara valley of Nepal (Chapter 4) also relied on sedimentary evidence such as slackwater deposits in tributary mouths or the remotely-sensed extents of overbank deposition. However, both markers provide only conservative estimates of the flood hydraulics: potential erosion during and after an event, particularly of the thick slackwater deposits of the Pokhara formation, can limit the reconstruction of high flood stages. Similarly, channel incisions during outburst floods might lead to overestimated flow depths when measuring high-stage indicators (Costa, 1983; Lehnigk and Larsen, 2022).

6.2.3 Scenario-based Hazard and Anticipatory Risk Assessments

In the absence of long-term time series of water level stages in many rivers of the Greater Himalayan region, a number of flood hazard assessments have relied on the statistical interpolation of local hydrologic data across larger regions (Delalay et al., 2020; Wohl, 1995). Empirical estimates of the flood magnitude's return-period based on local precipitation data, which is more readily available in most populated valleys, have also been used (Sharma and Adhikari, 2004). In Pokhara, both approaches have been applied to assess flood hazard and risk in several recent studies (Basnet et al., 2019; Basnet and Acharya, 2019; Gurung et al., 2021). However, these methodologies mainly take into account the hydraulic conditions prevalent during meteorological floods, whereas the rare, potentially more destructive, impacts of outburst-flood generated peak discharges are neglected (Wohl, 1995). For example, Cenderelli and Wohl (2001) reconstructed, that the discharge of two historic GLOFs in the Mount Everest region exceeded those of seasonal meteorological floods by factors of seven to 60. Hence, local flood risk management plans, which are solely informed by return periods of meteorological floods such as the 100-year event, may seriously underestimate the effect of outburst flood peaks. In Pokhara, this practise has been in place (Basnet et al., 2019; Basnet and Acharya, 2019; Gurung et al., 2021; Rimal et al., 2015), except for the study of Thapa et al. (2022), who considered the estimated peak discharge of the May 2012 flood in their local assessment of flood hazard to informal settlements. However, larger outburst flood magnitudes along the Seti Khola, which are so far unobserved but evidenced in the sediment record, are hitherto not reflected in the valley's hazard assessments.

Given the notion that global climate warming likely causes the high-altitude cryosphere and associated hazards from cascading events to transform beyond historic comparisons (Watson and Haeberli, 2004), Allen et al. (2021) suggest that scenario-based outburst flood modelling might significantly improve risk awareness and preparedness. Anticipatory modelling of outburst flood scenarios applied to existing lakes may consider the effect of different proportions of lake volume being potentially drained (Zhang et al., 2021), while scenarios considering potential future lakes may

focus on worst-case simulations representing the complete filling and drainage of glacier-bed overdeepenings by meltwaters under ice-free scenarios (Allen et al., 2021; Zheng et al., 2021a). Chapter 5 explores the potential impacts of such a wide range of flood scenarios, which are informed by estimates of the precipitation-driven *100 year flood* (Gurung et al., 2021) and peak discharge magnitudes observed in Himalayan valleys with comparable geomorphic conditions, for example in the 2021 Chamoli event (Shugar et al., 2021). Although the higher end of the simulated magnitude scenarios is arguably poorly supported by data in the Pokhara valley, its recent geologic past provides evidence of sediment aggradation events with peak discharges well beyond those recorded in history (Chapter 1.4). However, the results of such an exploration of flood magnitudes with high return periods or "worst-case scenarios" should be communicated with care.

In a next step, anticipatory assessments of risk from outburst floods could be supplemented by scenarios of future land-use change, as demonstrated by Nussbaumer et al. (2014).

6.3 Transient High-mountain Hazards Meet Growing Cities

6.3.1 Changes in Hazard, Exposure, and Vulnerability

Watson and Haeberli (2004) underlined the sensitivity of high-mountain systems to changes in energy fluxes between lithosphere, cryosphere, and atmosphere. The IPCC's observations and projections of the impacts of global warming hold that natural hazards in mountains will occur at different locations and times in the year than previously observed and that their frequencies and magnitudes have increased and will continue to do so (Hock et al., 2019). Although an increased frequency of outburst floods in the past decades is still under debate (Veh et al., 2019, 2022), their potential triggers are generally projected to occur more frequently, including geomorphic processes like ice and rock falls from retreating glaciers and valley slopes destabilised by permafrost degradation or meteorological triggers like rain-on-snow floods at higher elevations (Bolch et al., 2019; GAPHAZ, 2017; Hock et al., 2019). However, Allen et al. (2021) argue that the latter, which has so far only been observed in the devastating Kedarnath GLOF disaster of 2013 (Allen et al., 2016b), may replace mass-flow impacts as the dominant trigger of lake outburst in the future. This replacement might have implications regarding the finding of a statistically significant link between larger catchment areas and GLOF susceptibility (Chapter 3), where catchment area is a proxy for the potential for surface runoff that a lake receives from precipitation and snow melt (Allen et al., 2019).

A projected population increase by 3 billion by 2050 globally (Watson and Haeberli, 2004) and by 66 million by 2030 in the Greater Himalayan region alone (Sharma et al., 2019) will also alter the exposure of human settlements and infrastructure to high-mountain hazards (Hock et al., 2019).

Regarding outburst floods, Allen et al. (2021) state that, instead of cryospheric change, "[…] socio-economic developments and related changes in exposure and vulnerability, [..] could, in some regions, be the most significant drivers of future GLOF risk". Nonetheless, the impacts of this cryospheric change will potentially also negatively affect mountain-ecosystem services like water, food, and energy (i.e. hydropower plants) production (Rasul and Molden, 2019). A prominent example of the complex relationship between cryospheric change adaptation and high-mountain hazards is the Melamchi Khola outburst flood of July 2021, in which the 800 million USD Melamchi Water Supply Project was heavily damaged (Pokhrel, 2021). Nepal's hitherto largest and most expensive infrastructure scheme was completed just three months prior to the outburst flood and designed to provide 170 million litres of potable water per day for Kathmandu valley residents (Phuyal, 2020; Rasul and Molden, 2019).

Wang et al. (2019) propose, that local conflicts, which will likely result from compromises in supply reliability and impacts of natural hazards, will increase and drive future refugee dynamics in the Greater Himalayan region. Upon arrival, these migrants commonly reside in informal settlements, which are rapidly emerging in the suburban areas of expanding Himalayan cities (Wang et al., 2019), for example in locations close to active river channels such as Ramghat, Kaseri, or Yamdi in Pokhara city (Chapter 5). Structurally, informal settlements are more vulnerable to hazards like flooding due to generally low quality construction of houses and disregards of local building regulations (Abunyewah et al., 2018). Limited access to basic urban infrastructures also makes informal settlements less resilient, for example because poor wastewater management makes the potable water sources of these marginalised communities more vulnerable to contamination during floods (Williams et al., 2019). Thus, future resilience of urban populations, which are projected to make up 66% of the world's total population by 2050, are heavily dependent on the conditions in informal settlements, whose numbers of residents are projected to increase by 10% each year worldwide (Abunyewah et al., 2018; Williams et al., 2019). This calls for increased research efforts in hazard and risk assessments with special focus on these highly vulnerable local communities.

6.3.2 Adaptation to Mountain Cryosphere Change

Watson and Haeberli (2004) underlined, that societies living in mountain areas need a decision basis for planning, mitigation, and adaptation with regard to potential impacts by cryospheric change, and that this decision basis should be based on statistically calibrated models. Thus, robust modelling is crucial for the anticipation of consequences and plausible future scenarios of hazards (Watson and Haeberli, 2004). To better understand which sustainable adaptation measures these communities could aim for in the near future, Rasul and Molden (2019) call for more interdisciplinary

studies by retracing the cascade of effects that high-mountain cryosphere change might pose on the regionally increasingly exposed and vulnerable anthroposphere (Fig. 6.2). Throughout this thesis, I followed these calls for statistically-based and interdisciplinary approaches by exploring advanced statistical modelling and scenario simulations of outburst floods, and mapping of basin-wide land-use-and land-cover status to local informal settlement dynamics.

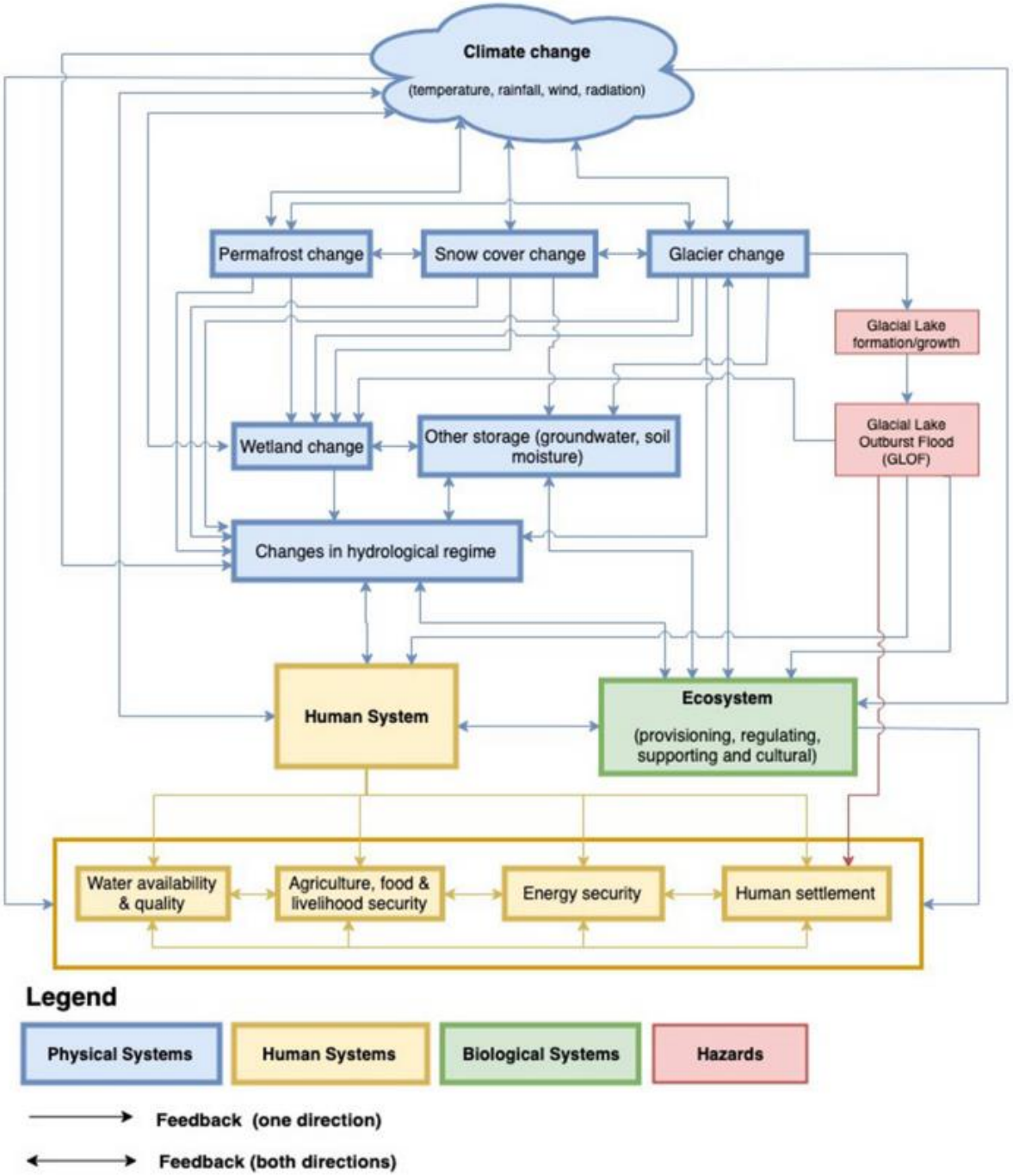

Figure 6.2: Conceptual linkages of cryospheric change in mountain regions (Rasul and Molden, 2019).

With regard to outburst flood mitigation works in the Greater Himalayan region, a number of controlled lake drainages, performed in immediate response to the formation of landslide dams in river valleys, are described in the literature (e.g. 2014 Sunkoshi LLOF, Nepal; Shrestha and Nakagawa, 2016). However, there are fewer examples of anticipatory structural remedy work performed at Himalayan glacial lakes – also when compared to the number of engineered GLOF mitigation measures in the Peruvian Andes (Wang et al., 2022) or the Swiss Alps (Harrison et al., 2018). This relative shortage might be linked to the affordability constraints of such costly measures for state economies like Nepal. There, artificial lake lowerings at Tsho Rolpa and Imja Tsho remain the sole examples of engineered GLOF mitigation measures (Bajracharya, 2010; Sherry and Curtis, 2017). Under the current projections of increases in magnitude and frequency of natural hazards related to cryospheric change, the costs of implementations and maintenance of risk reduction measures are believed to also increase in the future (Rasul and Molden, 2019). So far, apart from installing a few early-warning systems (EWS; Zhang and Wang, 2022), the relocation of settlements in many Himalayan valleys has been regarded as a much less expensive non-structural risk reduction strategy for outburst floods (Rasul et al., 2020). Thorough prior assessments of the suitability of a place for relocation are crucial: in the Pokhara valley, a relocation project of nine households was conducted in immediate response to the May 2012 flood (Henzmann, 2020). Unfortunately, multiple socio-economical and environmental aspects were not considered when locating the resettlement destination within the protected Annapurna Conservation Area (Project; ACAP). Interviews with locals suggest that the determining factors for the failure of this immediate response measure were the resident's loss of livelihood (i.e. loss of farmland) and social status (i.e. loss of landownership) when being resettled into the densely forested, public land (Henzmann, 2020). Thus, future resettlement projects within the study area should apply more holistic approaches by also considering cultural, social, and economic implications.

Apart from gabion flood walls and the now inoperative EWS installed in the upper Seti Khola's reach after the 2012 event (Gurung et al., 2015; Henzmann, 2020), flood risk mitigation strategies in Pokhara city have recently seen the release of a planning act that prohibits the construction of new buildings within a horizontal 10 m buffer zone around the Seti Khola (Thapa et al., 2022). However, it remains unclear whether this regulation also affects already existing houses and infrastructure. Based on OSM and manually mapped data (Chapter 5), 4 km of paths and more than 40 existing buildings lie within this restriction zone. Most of theses buildings are in the city centre where they are perched on top of the gorge sections. Yet, the inundation simulations indicate, that lateral spread of floodwaters during potential future scenarios could greatly exceed 10 m – especially at locations affected by hydraulic ponding.

6.3.3 The Impacts of Gravel Mining

A striking observation I made when visiting the Seti Khola in October 2019 and when looking at recent high-resolution satellite imagery is the intensity of sand and gravel mining operations undertaken along this river (Chapter 5). Material is extracted from quarries within the Pokhara Formation's deposits as well as from active point bars or the main channel (Fig. 6.3). This observation is exemplary for many Nepalese rivers, which have been increasingly exploited for raw sands and gravels since the late 1990s (Dahal et al., 2012), both on a small-scale, using mainly manual extraction methods, but also on a larger, more industrialised scale. Like in the Kathmandu valley, mining efforts are driven by rapid urbanisation and its need of construction materials. Dahal et al. (2012) state that "[…] in 2009/10, the revenue collected (for the whole of Nepal) by the local bodies […] was 1 billion [NPR; c. 14 million USD]". However, in contrast to terrace quarrying, most extraction of material from river beds is illegal (Sayami and Kazi Tamrakar, 2007). The potential effects of this unregulated mining on flow dynamics and associated hazards to settlements and infrastructures in close proximity to the Seti Khola remain unstudied. In the early 1990s haphazard extraction activities led to the destruction of two bridges and exposed the fundaments of several other in the Kathmandu valley (Sayami and Kazi Tamrakar, 2007). This clearly warrants further studies in the Pokhara valley. These physical impacts, caused by the up- and downstream propagation of channel incision, arise from the imbalance between sediment supply and stream power that artificial material extraction introduces to the fluvial system (Kondolf, 1994). Other geomorphic impacts on the Seti Khola could include channel changes and a greater erosion potential during phases of elevated discharge such as during monsoonal floods. In turn, toe cutting of the locally densely populated river terraces makes them unstable and susceptible to landslides.

From a risk perspective, increasing gravel mining along the Seti Khola is likely to raise both exposure and vulnerability. A growing number of labourers are working within the active river bed during the day and reside with their families in informal settlements on the nearby floodplain during night – exposing them to outburst flood hazards essentially 24 hours a day. As a growing number of people base their livelihood on the income from illegal river material extraction (Thapa et al., 2022), they also become more vulnerable economically. Risk awareness regarding outburst floods within these communities also requires further studies (Henzmann, 2020), especially motivated by the developments following the May 2012 flood. In Chapter 5 I noted the sharp increase in mining activities and informal built-up area in the years following the flood. At a first glance, this seems counterintuitive. But instead of discouraging exploitation and settling of floodplains and river banks, the large amounts of sediments deposited during the event actually seem to have attracted more people (Fort et al., 2018).

Figure 6.3: Different scales of gravel mining along the Seti Khola. a) Quarrying of gravel beds of the Pokhara Formation near Hemja. b) Groynes built to trap sand carried as suspended sediment load in the upper Seti Khola near Chaura. c) Gravel mining on a point bar near Ghachok. d) Heaps of material extracted from the Seti Khola's bed at Yamdi.

6.3.4 Pokhara: Multi-hazards and Infrastructure Expansion

Apart from sudden floods, Pokhara's geomorphology and geophysical setting (Chapter 1.4) make it susceptible to a number of other natural hazards that should ideally be addressed in a multi-hazard assessment. For example, Rimal et al. (2018) and Stolle (2018) discuss the hazard posed by poorly mapped or undetected subsurface karst structures, which form in the calcareous valley fill. The resulting hazard from land collapse, land subsidence, and sinkholes is most prominent within Pokhara's urban areas (Rimal et al., 2018). Hence, Stolle (2018) proposes cavity detection in order to mitigate the high hazard from gradual land subsidence or sudden sinkhole opening. The Pokhara valley's karst-system, which is predominantly associated with the occurrence of materials of the

Ghachok Formation in the central valley, could rely on electric (e.g. electrical resistivity tomography, ERT) or electromagnetic (e.g. ground-penetrating radar, GPR) geophysical methods (Chalikakis et al., 2011).

The Pokhara valley is also situated in a seismically active area and a report by the "Earthquake Risk Reduction and Recovery Preparedness Programme for Nepal" found that Pokhara "can be considered as moderately vulnerable to earthquake hazard with probability of intensity of VIII MMI [Modified Mercalli Intensity] earthquake in the region"(GENESIS Consultancy (P) Ltd., 2009). Many overbank areas of the Seti Khola, which are increasingly densely populated and potentially inundated by outburst floods, may also be highly susceptible to liquefaction during such a strong earthquake (GENESIS Consultancy (P) Ltd., 2009). Moreover, high seismic activity and orographic rainfall during the summer monsoon make the Pokhara valley susceptible to landslides from numerous steep slopes (Rimal et al., 2015).

Landslide susceptibility is also raised by the construction of earthen roads in rural valley parts (Leibundgut et al., 2016). The network of such roads expanded exponentially in the Phewa watershed in the past three decades, causing numerous shallow landslides (Leibundgut et al., 2016). When visiting the northernmost part of the Pokhara valley in 2019, I made similar observations while travelling along recently constructed roads there, which are prone to outburst floods (Chapter 5; Fig. 6.4). Pokhara's almost completed 216-million USD international airport is another major infrastructure project (Baral, 2021). Unlike the bridges and rural roads north of Pokhara, this significant investment would likely remain unaffected by outburst floods with peak discharges <10,000 $m^3 s^{-1}$ (Chapter 5). However, the ANUGA simulations of floods with higher peak discharges considered in Chapter 4 indicate that both the existing domestic and the new international airport are located in areas prone to flow expansion and possible channel avulsion, at least for extremely large magnitudes such as those assumed for the Mediaeval megafloods. Along the upper Seti Khola, which was heavily impacted by the May 2012 flood, two new run-of-the-river hydropower plants are planned: the Karuwa Seti Hydropower Project (planned capacity: 35 MW) is already under construction and the Upper Seti Hydropower Project (planned capacity: 20 MW) has recently received a construction licence (United Idi Mardi and RB Hydropower Ltd., 2022). Newly built facilities, detected in high-resolution Google Earth satellite imagery (October 2020), lie within the inundation limits of outburst flood scenarios >4,000 $m^3 s^{-1}$, which quantifies concerns of Gurung et al. (2021) regarding possible impacts on these projects by future outburst floods (Fig. 6.4). Thus, this added exposure of cost-intensive infrastructure projects will further increase the existing outburst flood risk along the Seti Khola.

Figure 6.4: Infrastructure in the upper reach of the Seti Khola. a) Flood limits of three scenarios displayed on Google Earth imagery from October 2020 (© Google Earth 2020) also showing locations of facilities of the Karuwa Seti Hydropower plant. b) Dirt road obstructed by a landslide north of Karuwa, visited in October 2019. c) Motor bridge on the level of the May 2012 floodplain near Kharapani, visited in October 2019. d) Motor and suspension bridges crossing the Seti Khola near Ghachok, visited in October 2019.

6.4 Outlook on Future Outburst-Flood Research in the Pokhara Valley

6.4.1 Risk Management and Early-Warning Strategies

Lessons learned from the May 2012 flood as well as the simulated scenarios in Chapter 5 underline the need for more comprehensive disaster risk management along the Seti Khola than is currently in place. This could bring together data from monitoring not only flow stages but also of climatological, glaciological, and geomorphic processes in the Sabche Cirque. Future research might therefore focus on the appropriate mitigation strategies, which should be developed by an interdisciplinary team of experts in close coordination with the local authorities and stake holders. The importance of such a strengthening of the preparedness of communities in the Pokhara valley to risks is underlined by the statement of Gaire et al. (2015) that "The Government of Nepal focuses more on the response phase than on the preparedness phase of disasters.".

The May 2012 flood highlighted the rapidity of flood wave propagation in the Seti Khola and the need for coordinated monitoring and warning procedures to minimise warning lag-times. Currently, larger water bodies do not exist in the Seti Khola's headwaters and standard engineered mitigation measures targeting the sources of potential future outburst floods are, hence, not applicable at this

point. However, Kargel et al. (2013) point out that lakes in the Sabche Cirque can form and grow unnoticed in short amounts of time. Therefore, I would recommend water-level monitoring in the Seti Khola in combination with real-time, *in situ* and remote monitoring of the Sabche Cirque (Fig. 6.5) as key components of future risk management efforts. Zhang and Wang (2022) recently proposed an advanced monitoring and early-warning system for Lake Cirenmaco, China. They state, that their four-part management plan (monitoring, data processing, early-warning system, and local response capacity development) is largely applicable to similar future projects aimed at of GLOF prevention and mitigation from existing lakes in the Himalayas (Wang et al., 2022). Although some aspects of their approach are not directly transferable to the situation in the Seti Khola's headwaters, including observations of moraine-dam dynamics and bathymetric surveys, other components seem promising. Particularly the real-time transmission of optical and thermal data, captured by 360° cameras, via satellite or mobile signal to a round-the-clock-operating data processing centre could track potentially hazardous developments in the Sabche Cirque. Figure 6.5 shows a potential adaptation of Zhang and Wang's (2022) system to the Pokhara valley, which constitutes a preliminary attempt at answering the research question: *How could an outburst flood early-warning system along the Seti Khola look like, which includes customisations to address the unique conditions in this river's headwaters?*

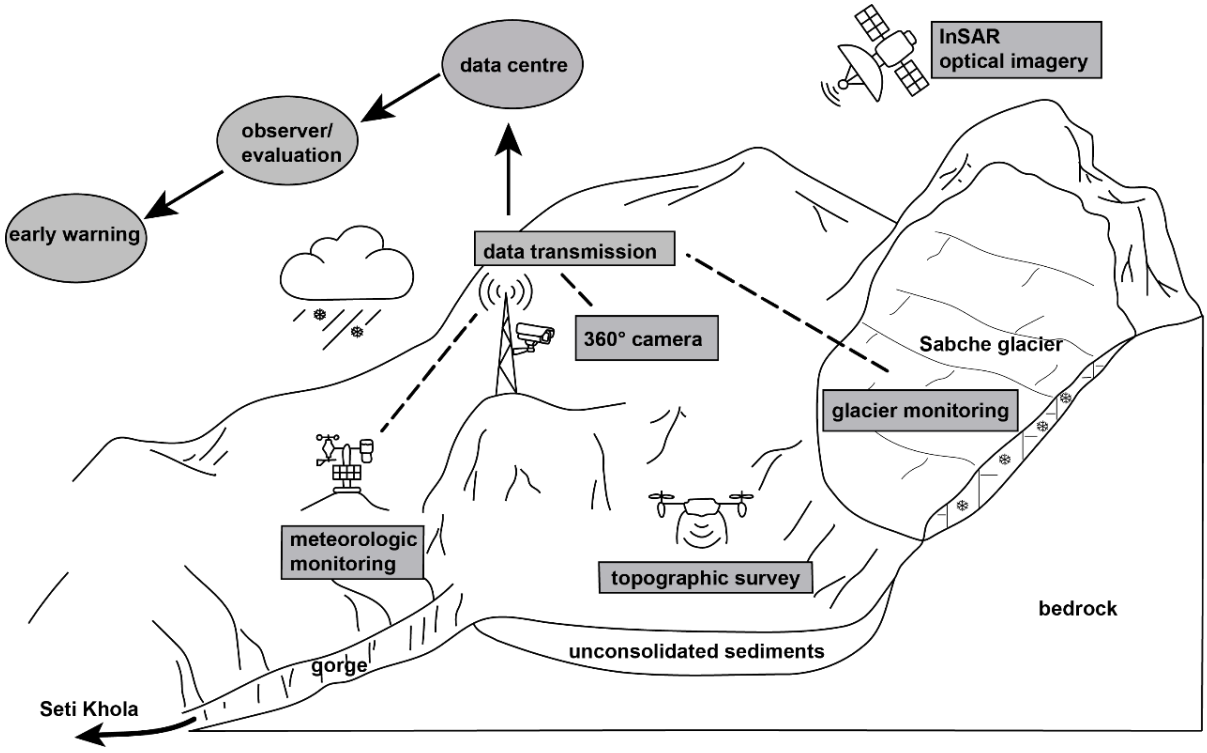

Figure 6.5: Potential components of an early-warning system in the Sabche Cirque adapted from Zhang and Wang (2022). System could be complemented by water-level monitoring at the exit of the Seti Khola gorge not shown here. Not to scale. InSAR = interferometric synthetic-aperture radar.

6.4.2 Informal Settlement Monitoring and Modelling Future Urban Expansion

Thapa et al. (2022) conducted a socioeconomic survey in some of the settlements studied in Chapter 5. According to their study, most inhabitants are living in poverty (i.e. living on an annual income of ≤1025 USD), earning their livelihoods from manual labour, and have only recently migrated into Pokhara (Thapa et al., 2022). Thapa et al. (2022) also describe an anti-correlation between the poverty level of a given household within these informal settlements and its distance from the Seti Khola. Hence, a better monitoring and modelling of the present and future dynamics of informal settlements, especially at Yamdi and Kaseri but also Ramghat, is needed to more accurately estimate the future exposure and, hence, risk from outburst floods. Future research focused on Pokhara's informal settlements might want to answer the following questions: *What were and are the dynamics of specific informal settlements located in the Seti Khola's floodplain on a single-structure-level? Where will the rapid expansion of built-up area in Pokhara continue and what are the future urban areas at risk to outburst flooding?*

To answer these questions, automated object-based classification of informal settlement structures from high-resolution satellite imagery could help, judging from studies around the world (Fallatah et al., 2020; Hofmann et al., 2015; Taubenböck and Kraff, 2014). Regarding landscape analysis, Aplin and Smith (2011) state that "Object-based approaches, which operate at the scale of real-world objects rather than pixels, offer a means of analysing EO [earth observation] data in a realistic context and integrating associated ancillary information to support real-world applications." In the case of Pokhara's informal settlements, application of this remote-sensing technique would allow for cost-efficient and regular monitoring of built-up area on the scale of individual buildings instead of image pixels of undifferentiated roof areas (Hofmann et al., 2015). Plausible future scenarios of urban area expansion could be simulated using an agent-based housing model, as proposed by Augustijn-Beckers et al. (2011) for informal settlements in Tanzania.

6.4.3 Relating Pokhara's Mediaeval Floods to Future Outburst Flood Hazard in the Greater Himalayas

One main result of Chapter 4 is that hydrodynamic modelling quantitatively supports the notion of Schwanghart et al. (2016) and Stolle et al. (2017) that several Mediaeval earthquake-triggered sediment pulses in the Pokhara valley were generated by the sudden failure of glacial lakes in the Sabche Cirque. My finding of a best match between sedimentary evidence and a flood scenario of 500,000 $m^3 s^{-1}$ peak discharge provides a first-order assessment, which could be substantiated by a more in-depth reconstruction of the rheology and flow dynamics of these palaeo-GLOFs. We could use this information on the Mediaeval outburst processes itself but also the necessary preconditions,

i.e., the local topographic, glaciologic, climatologic, and seismic setting in the Sabche Cirque at the time of triggering, to better constrain the potential for a future reoccurrence of such cataclysmic floods. The hazard that outburst floods of such landscape-changing-scales might pose on the rapidly growing population of the Pokhara valley has been pointed out before (Fort, 1987; Hanisch et al., 2013). However, an improved understanding of palaeo-GLOF susceptibility and mechanisms in the Pokhara valley could be used to identify other catchments within the Annapurna massif or the Greater Himalayas hosting similar conditions today.

Thus, future research might aim at answering the following questions: *Were the Pokhara Formation sediments deposited by few (at least three) cataclysmic events or by several smaller more frequent events? What were the rheological characteristics of these palaeo-GLOFs? What can we learn from the Mediaeval events about the potential for future outburst floods of comparable scale in the Pokhara valley, the Annapurna massif, and the Greater Himalayas in general?*

These questions could be approached by performing a reconstruction of the valley's palaeo-topography (i.e. pre-deposition of the Pokhara Formation's thick gravel beds) by interpolating field information on the distribution of Ghachok Formation material across the Pokhara valley. Simulated clear-water flow could then be routed across this palaeo-surface in two dimensions to further improve the initial peak discharge estimate in Chapter 4. Eventually, state-of-the-art morphometric modelling of sediment entrainment and deposition on this palaeo-surface by the highly-energetic flood waters (Carrivick, 2007; Xia et al., 2010) is suggested. Yet, Westoby et al. (2014) identified the application of such models to palaeo-GLOF reconstructions as one of the major challenges in current GLOF research and a reconstruction of palaeo-topography likely comes with high uncertainties.

In conclusion, the combination of several features makes the Pokhara valley a prime object of study: both its geologic history and its unique geomorphic conditions foster – additional to the outburst flood scenarios presented in this thesis – other natural hazards, including earthquakes, landslides, and sinkholes as well as land subsidence. In the future, it is plausible that these hazards will have far-reaching impacts on the community, which continues to undergo rapid socio-economic transformations. The many facets of this change, such as rapid population growth, urbanisation, expansion of informal settlements and gravel mining, tourism-sector rise, investments in major transportation (roads, motor bridges, international airport) and energy infrastructure (hydropower plants), are exemplary for other valleys not only in Nepal or the Greater Himalayas but also, in some aspects, for high-mountain belts worldwide.

7 Conclusions

Sudden outbursts of lakes have affected and will continue to impact rapidly growing populations and economies in the Greater Himalayan region. Projected changes to the cryosphere of this mountain belt likely involve changes to the occurrence frequency of outburst floods and their triggers. We therefore need a better understanding of this rare but destructive cascading hazard. Within this thesis, I have analysed past outburst floods to learn more about the susceptibility of moraine-dammed lakes to sudden failure across the Greater Himalayan region, while investigating in detail the potential flow characteristics of Mediaeval and recent outburst floods in the Pokhara valley of Nepal. There, I quantified exposure dynamics and used these new insights to estimate the associated and physically plausible future hazard of sudden inundation.

My first study in this context is based on a systematic compilation of a comprehensive inventory of >3,000 moraine-dammed lakes across the Greater Himalayan region. Little more than 1% of these lakes had released a documented GLOF in the past four decades. Using this data, the statistical relevance of candidate predictors of lake stability such as elevation, catchment and lake area, lake-area dynamics, glacier-mass balance, and monsoonality, is tested in the probabilistic framework of Bayesian multi-level modelling. This approach not only explicitly acknowledges uncertainties but also spatial variability in GLOF susceptibility across the mountain belt. This variability is likely linked to differences in topography, glacier-mass balance (for example the "Karakoram Anomaly"), or seasonally differing precipitation patterns caused by the monsoon and winter westerlies. Both uncertainties and intra-regional variability have not been addressed in previous GLOF assessments covering the whole Greater Himalayas. The Bayesian multi-level models attest that, from a purely data-driven point of view, larger lakes in larger catchments have been more prone to release sudden outburst floods in the past. Additionally, moraine-dammed lakes in regions with strong negative glacier-mass balances, like the Nyainqentanglha and Eastern Himalayas, have been on average less stable than those in the Western Himalaya in the past four decades. A direct influence of monsoonality and lake elevation, however, is statistically ambiguous. Crucially, the model results are inconsistent with the widely held notion that a rapidly increasing surface area makes a given moraine-dammed lake more susceptible to GLOF.

Within the Greater Himalayan region, many Nepalese valleys have been affected by hazard cascades involving outburst floods, both from glacial and landslide-dammed lakes, in the past. The Pokhara valley, home to Nepal's second largest and most rapidly growing city, is no exception. In my second

study, I used sedimentary evidence to provide new quantitative insights into, and constraints about, the catastrophic May 2012 flood along the Seti Khola, and likely several magnitudes larger historic predecessors. The May 2012 event altered the river's morphology and deposited large amounts of sediments, increasing the area of the active channel by about 30% along a 55 km long reach. Using this as a proxy of maximum inundation limits, the clear-water flow reconstructed from step-backwater modelling is only half of the flood peak discharge reported by previous studies relying on empirical flood magnitude estimates. The reconstructions also show a strong attenuation of flood dynamics between the heavily affected Kharapani village in the upper reach (Q_p = 3,700 m^3 s^{-1}) and Pokhara's north-western suburbs 15 km downstream (Q_p = 500 m^3 s^{-1}). Two-dimensional simulations of outburst flood scenarios in the magnitude range hypothesised for the Mediaeval events (50,000 to 600,000 m^3 s^{-1} Q_p), show backwater effects, which reach several kilometres upstream into the Seti Khola's mid-reach tributary streams. Sediment evidence of such hydraulic conditions comes in the form of thick beds of slackwater deposits, and their location matches modelled inundation levels for simulated clear-water floods with >500,000 m^3 s^{-1} peak discharges. Thus, these simulations provide first-order support for the hypothesis that the Mediaeval sediment pulses in the Pokhara valley's fill were caused by glacial lake outbursts in the Annapurna massif's front, possibly in the wake of major earthquakes.

A future reoccurrence of hazard cascades resulting in outburst floods along the Seti Khola is plausible, although most likely not of the scale of these cataclysmic Mediaeval events. This outburst plausibility is based on a combination of geomorphic and glaciologic conditions in the river's high-alpine headwaters, which include the observed surging behaviour of the Sabche glacier as well as the susceptibility of the steep Sabche Cirque walls to landslides, which could potentially (temporarily) block the narrow upper Seti Khola gorge. These conditions could give rise to surge-related or landslide-dam and glacial lake outburst floods in the future.

My third study offers the first comprehensive assessment of physically plausible outburst flood scenarios, ranging from 1,000 to 10,000 m^3 s^{-1} of clear-water peak discharge routed through the Seti Khola. All simulations reveal localised variability of flow depths and velocities along the course of the river. Some of this variability is caused by abrupt restrictions in cross-sectional areas where the Seti Khola enters numerous gorges in Pokhara city. Hydraulic ponding appears to occur at peak discharges >1,000 m^3 s^{-1}, meaning that floods might inundate larger areas upstream of these gorges. Flow depths and exposure of built-up area are highest in the north-western urban periphery, where the Seti Khola has become a popular source for gravel mining, while overbank areas have begun to sustain informal settlement ground. In just over a decade (2008 to 2021), the built-up area in two informal settlements increased between three- to twentyfold. This rapid growth reflects the socio-

economic changes Pokhara and its surrounding valley are undergoing, which is also reflected in the construction of new, cost-intensive infrastructure, including roads and run-of-the-river hydropower projects. These investments in the upper Seti Khola reach are exposed to outburst floods and, hence, add to the overall risk. Thus, the potential impacts by this infrequent type of floods should be considered on top of the monsoonal floods along the Seti Khola. Potential risk reduction, not only from outburst floods but also from other hazard cascades, like highly mobile rock avalanches, could benefit from constant monitoring – in-field and remotely – of meteorologic, geomorphic, and glaciologic conditions in the Sabche Cirque.

A joint element of these three studies is the use of a wide array of remote-sensing and field data to improve modelling of outburst floods at the interface of geomorphological research with hazard and exposure assessments. In this thesis, I have presented the first statistically rigorous analysis of a comprehensive inventory of past GLOFs across the vast Greater Himalayan region. With a purely probabilistic point of view, I was able to show which predictors most likely controlled GLOF susceptibility across the different subregions of this mountain arc in the past four decades. In the future, these results might be useful in ensemble-modelling of regional GLOF hazards. Considering outburst flood hazards at a local scale, hydrodynamic modelling provided new insights into the flow characteristics of unrecorded floods in the past. In lieu of time-series of event frequencies and magnitudes, these new insights informed the assessment of the potential impacts of a wide range of outburst flood scenarios – a novel approach in the Pokhara valley.

Bibliography

Abunyewah, M., Gajendran, T. and Maund, K.: Profiling Informal Settlements for Disaster Risks, Procedia Eng., 212(2017), 238–245, doi:10.1016/j.proeng.2018.01.031, 2018.

Aggarwal, A., Jain, S. K., Lohani, A. K. and Jain, N.: Glacial lake outburst flood risk assessment using combined approaches of remote sensing, GIS and dam break modelling, Geomatics, Nat. Hazards Risk, 7(1), 18–36, doi:10.1080/19475705.2013.862573, 2016.

Allen, S. K., Linsbauer, A., Randhawa, S. S., Huggel, C., Rana, P. and Kumari, A.: Glacial lake outburst flood risk in Himachal Pradesh, India: an integrative and anticipatory approach considering current and future threats, Nat. Hazards, 84(3), 1741–1763, doi:10.1007/s11069-016-2511-x, 2016a.

Allen, S. K., Rastner, P., Arora, M., Huggel, C. and Stoffel, M.: Lake outburst and debris flow disaster at Kedarnath, June 2013: hydrometeorological triggering and topographic predisposition, Landslides, 13(6), 1479–1491, doi:10.1007/s10346-015-0584-3, 2016b.

Allen, S. K., Zhang, G., Wang, W., Yao, T. and Bolch, T.: Potentially dangerous glacial lakes across the Tibetan Plateau revealed using a large-scale automated assessment approach, Sci. Bull., 64(7), 435–445, doi:10.1016/j.scib.2019.03.011, 2019.

Allen, S. K., Bolch, T., Frey, H., Zhang, G., Zheng, G., Mal, S., Chen, N., Sattar, A. and Stoffel, M.: Glacial lake outburst floods in High Mountain Asia : From large scale assessment to local disaster risk management, in EGU General Assembly, p. 2., 2021.

Anup, K. C., Rijal, K. and Sapkota, R. P.: Role of ecotourism in environmental conservation and socioeconomic development in Annapurna conservation area, Nepal, Int. J. Sustain. Dev. World Ecol., 22(3), 251–258, doi:10.1080/13504509.2015.1005721, 2015.

Aplin, P. and Smith, G. M.: Introduction to object-based landscape analysis, Int. J. Geogr. Inf. Sci., 25(6), 869–875, doi:10.1080/13658816.2011.566570, 2011.

Arcement Jr, G. J. and Schneider, V. R.: Guide for selecting Manning's roughness coefficients for natural channels and flood plains: U.S. Geological Survey Water Supply Paper 2339, US Department of Transportation, Federal Highway Administration., 1984.

Augustijn-Beckers, E.-W., Flacke, J. and Retsios, B.: Simulating informal settlement growth in Dar es Salaam, Tanzania: An agent-based housing model, Comput. Environ. Urban Syst., 35(2), 93–103, doi:10.1016/j.compenvurbsys.2011.01.001, 2011.

Austin, P. C., Tu, J. V. and Alter, D. A.: Comparing hierarchical modeling with traditional logistic regression analysis among patients hospitalized with acute myocardial infarction: Should we be analyzing cardiovascular outcomes data differently?, Am. Heart J., 145(1), 27–35, doi:10.1067/mhj.2003.23, 2003.

Bajracharya, B., Shrestha, A. B. and Rajbhandari, L.: Glacial lake outburst floods in the Sagarmatha region: Hazard assessment using GIS and hydrodynamic modelling, Mt. Res. Dev., 27(4), 336–344, doi:10.1659/mrd.0783, 2007.

Bajracharya, S. R.: Glacial Lake Outburst Flood Disaster Risk Reduction Activities in Nepal, Int. J. Eros. Control Eng., 3(1), 92–101, doi:10.13101/ijece.3.92, 2010.

Bajracharya, S. R. and Shrestha, B.: The Status of Glaciers in the Hindu Kush–Himalayan Region, International Centre for Integrated Mountain Development (ICIMOD), Kathmandu., 2011.

Bajracharya, S. R., Maharjan, S. B., Shrestha, F., Sherpa, T. C., Wagle, N. and Shrestha, A. B.: Inventory of glacial lakes and identification of potentially dangerous glacial lakes in the Koshi, Gandaki, and Karnali river basins of Nepal, the Tibet Autonomous Region of China, and India, International Centre for Integrated Mountain Development (ICIMOD), Kathmandu., 2020.

Baker, V. R.: High-energy megafloods: planetary settings and sedimentary dynamics, in Flood and megaflood processes and deposits: recent and ancient examples, edited by I. P. Martini, V. R. Baker, and G. Garzón, pp. 3–15, Blackwell Science Ltd, Oxford., 2002.

Baker, V. R., Kochel, R. C., Patton, P. C. and Pickup, G.: Palaeohydrologic Analysis of Holocene Flood Slack-Water Sediments, in Modern and Ancient Fluvial Systems, edited by D. Collinson and J. Lewin, pp. 229–239, Blackwell Science Ltd, Oxford., 1983.

Baral, K.: Cabinet indecision delays Pokhara Airport, Nepali Times [online] Available from: https://www.nepalitimes.com/banner/cabinet-indecision-delays-pokhara-airport/ (Accessed 17 June 2022), 2021.

Basnet, K. and Acharya, D.: Flood Analysis at Ramghat, Pokhara, Nepal Using HEC-RAS, Tech. J., 1(1), 41–53, doi:10.3126/tj.v1i1.27591, 2019.

Basnet, K., Acharya, D., Bhandari, K. P. and Sadadev, B. B.: Floodplain Mapping using HEC-RAS (A Case Study of Seti River, Pokhara), Pokhara., 2019.

Benito, G. and Thorndycraft, V. R.: Catastrophic glacial-lake outburst flooding of the Patagonian Ice Sheet, Earth-Science Rev., 200(102996), 1–22, doi:10.1016/j.earscirev.2019.102996, 2020.

Bhambri, R., Mehta, M., Dobhal, D. P., Gupta, A. K., Pratap, B., Kesarwani, K. and Verma, A.: Devastation in the Kedarnath (Mandakini) Valley, Garhwal Himalaya, during 16–17 June 2013: a remote sensing and ground-based assessment, Nat. Hazards, 80(3), 1801–1822, doi:10.1007/s11069-015-2033-y, 2016.

Bhandary, N. P., Dahal, R. K. and Okamura, M.: Preliminary Understanding of the Seti River Debris-Flood in Pokhara, Nepal, on May 5th, 2012 - A Report based on a Quick Field Visit Program, ISSMGE Bull., 6(4), 8–18, 2012.

Björnsson, H. and Pálsson, F.: Icelandic glaciers, Jökull, 58, 365–386, 2008.

Blöthe, J. H. and Korup, O.: Millennial lag times in the Himalayan sediment routing system, Earth Planet. Sci. Lett., 382, 38–46, doi:10.1016/j.epsl.2013.08.044, 2013.

Blöthe, J. H., Rosenwinkel, S., Höser, T. and Korup, O.: Rock-glacier dams in High Asia, Earth Surf. Process. Landforms, 44(3), 808–824, doi:10.1002/esp.4532, 2019.

Bolch, T., Peters, J., Yegorov, A., Pradhan, B., Buchroithner, M. and Blagoveshchensky, V.: Identification of potentially dangerous glacial lakes in the northern Tien Shan, Nat. Hazards, 59(3), 1691–1714, doi:10.1007/s11069-011-9860-2, 2011.

Bolch, T., Kulkarni, A., Kääb, A., Huggel, C., Paul, F., Cogley, J. G., Frey, H., Kargel, J. S., Fujita, K., Scheel, M., Bajracharya, S. and Stoffel, M.: The State and Fate of Himalayan Glaciers, Science, 336(6079), 310–314, doi:10.1126/science.1215828, 2012.

Bolch, T., Shea, J. M., Liu, S., Azam, F. M., Gao, Y., Gruber, S., Immerzeel, W. W., Kulkarni, A., Li, H., Tahir, A. A., Zhang, G. and Zhang, Y.: Status and Change of the Cryosphere in the Extended Hindu Kush Himalaya Region, in The Hindu Kush Himalaya Assessment: Mountains, Climate Change, Sustainability and People, edited by P. Wester, A. Mishra, A. Mukherji, and A. B. Shrestha, pp. 209–255, Springer International Publishing, Cham., 2019.

Bookhagen, B. and Burbank, D. W.: Topography, relief, and TRMM-derived rainfall variations along the Himalaya, Geophys. Res. Lett., 33(8), 1–5, doi:10.1029/2006GL026037, 2006.

Bookhagen, B. and Burbank, D. W.: Toward a complete Himalayan hydrological budget: Spatiotemporal distribution of snowmelt and rainfall and their impact on river discharge, J. Geophys. Res. Earth Surf., 115(3), 1–25, doi:10.1029/2009JF001426, 2010.

Brun, F., Berthier, E., Wagnon, P., Kääb, A. and Treichler, D.: A spatially resolved estimate of High Mountain Asia glacier mass balances from 2000 to 2016, Nat. Geosci., 10(9), 668–673, doi:10.1038/ngeo2999, 2017.

Brunner, G. W.: HEC-RAS, River Analysis System - Hydraulic Reference Manual, , 520, 2020a.

Brunner, G. W.: HEC-RAS River Analysis System - 2D Modeling User's Manual, , 283, 2020b.

Burbank, D. W., Blythe, A. E., Putkonen, J., Pratt-Sitaula, B. A., Gabet, E., Oskin, M., Barros, A. and Ojha, T. P.: Decoupling of erosion and precipitation in the Himalayas, Nature, 426(6967), 652–655, doi:10.1038/nature02187, 2003.

Bürkner, P.-C.: brms: An R package for Bayesian multilevel models using Stan, J. Stat. Softw., 80(1), 1–28, doi:10.18637/jss.v080.i01, 2017.

Byers, A. C., Shugar, D. H., Chand, M. B., Portocarrero, C., Shrestha, M., Rounce, D. R. and Watanabe, T.: Three Recent and Lesser-Known Glacier-Related Flood Mechanisms in High Mountain Environments, Mt. Res. Dev., 42(2), 12–22, doi:10.1659/MRD-JOURNAL-D-21-00045.1, 2022.

Caniani, D., Pascale, S., Sdao, F. and Sole, A.: Neural networks and landslide susceptibility: A case study of the urban area of Potenza, Nat. Hazards, 45(1), 55–72, doi:10.1007/s11069-007-9169-3, 2008.

Carey, M.: Living and dying with glaciers: People's historical vulnerability to avalanches and outburst floods in Peru, Glob. Planet. Change, 47(2-4 SPEC. ISS.), 122–134, doi:10.1016/j.gloplacha.2004.10.007, 2005.

Carey, M., Huggel, C., Bury, J., Portocarrero, C. and Haeberli, W.: An integrated socio-environmental framework for glacier hazard management and climate change adaptation: Lessons from Lake 513, Cordillera Blanca, Peru, Clim. Change, 112(3–4), 733–767, doi:10.1007/s10584-011-0249-8, 2012.

Carrivick, J. L.: Application of 2D hydrodynamic modelling to high-magnitude outburst floods: An example from Kverkfjöll, Iceland, J. Hydrol., 321(1–4), 187–199, doi:10.1016/j.jhydrol.2005.07.042, 2006.

Carrivick, J. L.: Modelling coupled hydraulics and sediment transport of a high-magnitude flood and associated landscape change, Ann. Glaciol., 45, 143–154, doi:10.3189/172756407782282480, 2007.

Carrivick, J. L. and Rushmer, E. L.: Understanding high-magnitude outburst floods, Geol. Today, 22(2), 60–65, doi:10.1111/j.1365-2451.2006.00554.x, 2006.

Carrivick, J. L. and Tweed, F. S.: A global assessment of the societal impacts of glacier outburst floods, Glob. Planet. Change, 144, 1–16, doi:10.1016/j.gloplacha.2016.07.001, 2016.

Cenderelli, D. A. and Wohl, E. E.: Peak discharge estimates of glacial-lake outburst floods and "normal" climatic floods in the Mount Everest region, Nepal, Geomorphology, 40(1–2), 57–90, doi:10.1016/S0169-555X(01)00037-X, 2001.

Cenderelli, D. A. and Wohl, E. E.: Flow hydraulics and geomorphic effects of glacial-lake outburst floods in the Mount Everest region, Nepal, Earth Surf. Process. Landforms, 28(4), 385–407, doi:10.1002/esp.448, 2003.

Central Bureau of Statistics: National Population and Housing Census 2021, Natl. Popul. Hous. Census 2021 [online] Available from: https://cbs.gov.np/ (Accessed 21 February 2022), 2022.

Cesca, M. and D'Agostino, V.: Comparison between FLO-2D and RAMMS in debris-flow modelling: A case study in the Dolomites, WIT Trans. Eng. Sci., 60, 197–206, doi:10.2495/DEB080201, 2008.

Chalikakis, K., Plagnes, V., Guerin, R., Valois, R. and Bosch, F. P.: Contribution of geophysical methods to karst-system exploration: An overview, Hydrogeol. J., 19(6), 1169–1180, doi:10.1007/s10040-011-0746-x, 2011.

Chen, F., Zhang, M., Guo, H., Allen, S. K., Kargel, J. S., Haritashya, U. K. and Watson, C. S.: Annual 30 m dataset for glacial lakes in high mountain asia from 2008 to 2017, Earth Syst. Sci. Data, 13(2), 741–766, doi:10.5194/essd-13-741-2021, 2021a.

Chen, M., Li, Z., Gao, S., Luo, X., Wing, O. E. J., Shen, X., Gourley, J. J., Kolar, R. L. and Hong, Y.: A comprehensive flood inundation mapping for Hurricane Harvey using an integrated hydrological and hydraulic model, J. Hydrometeorol., 1713–1726, doi:10.1175/jhm-d-20-0218.1, 2021b.

Chow, V. T.: Open-channel hydraulics, McGraw-Hill Civ. Eng. Ser., 1959.

Clague, J. J. and Evans, S. G.: A review of catastrophic drainage of moraine-dammed lakes in British Columbia, Quat. Sci. Rev., 19, 1763–1783, 2000.

Cole, S. and Guiltenane, E.: Global survey using NASA data shows dramatic growth of glacial lakes, Third Pole, 1 [online] Available from: https://www.thethirdpole.net/en/climate/global-survey-using-nasa-data-shows-dramatic-growth-of-glacial-lakes/ (Accessed 11 May 2022), 2020.

Cook, K. L., Andermann, C., Gimbert, F., Adhikari, B. R. and Hovius, N.: Glacial lake outburst floods as drivers of fluvial erosion in the Himalaya, Science, 362(6410), 53–57, doi:10.1126/science.aat4981, 2018.

Costa, J. E.: Paleohydraulic reconstruction of flash- flood peaks from boulder deposits in the Colorado Front Range., Geol. Soc. Am. Bull., 94(8), 986–1004, doi:10.1130/0016-7606(1983)94<986:PROFPF>2.0.CO;2, 1983.

Costa, J. E. and Schuster, R. L.: The Formation and Failure of Natural Dams, Bull. Geol. Soc. Am., 100(7), 1054–1068, doi:10.1130/0016-7606(1988)100<1054:TFAFON>2.3.CO;2, 1988.

Coxon, P., Owen, L. A. and Mitchell, W. A.: A Late Quaternary catastrophic flood in the Lahul Himalayas, J. Quat. Sci., 11(6), 495–510, 1996.

Dahal, K. R., Sharma, S. and Sharma, C. M.: A Review of Riverbed Extraction and its Effects on Aquatic Environment with Special Reference to Tinau River, Nepal, Hydro Nepal J. Water, Energy Environ., 11, 49–56, doi:10.3126/hn.v11i0.7163, 2012.

Dai, F. C., Lee, C. F., Deng, J. H. and Tham, L. G.: The 1786 earthquake-triggered landslide dam and subsequent dam-break flood on the Dadu River, southwestern China, Geomorphology, 65(3–4), 205–221, doi:10.1016/j.geomorph.2004.08.011, 2005.

Dangol, G. M. S.: Geology of the Kathmandu fluviatile lacustrine sediments in the light of new vertebrate fossil occurrences, J. Nepal Geol. Soc., 3, 43–57, 1985.

Decelles, P. G., Robinson, D. M., Quade, J., Ojha, T. P., Garzione, C. N., Copeland, P. and Upreti, B. N.: Stratigraphy, structure, and tectonic evolution of the Himalayan fold-thrust belt in Western Nepal, Tectonics, 20(4), 487–509, doi:10.1029/2000TC001226, 2001.

Dehecq, A., Gourmelen, N., Gardner, A. S., Brun, F., Goldberg, D., Nienow, P. W., Berthier, E., Vincent, C., Wagnon, P. and Trouvé, E.: Twenty-first century glacier slowdown driven by mass loss in High Mountain Asia, Nat. Geosci., 12(1), 22–27, doi:10.1038/s41561-018-0271-9, 2019.

Delalay, M., Ziegler, A. D., Shrestha, M. S. and Gopal, V.: Methodology for future flood assessment in terms of economic damage: Development and application for a case study in Nepal, J. Flood Risk Manag., 13(3), 1–14, doi:10.1111/jfr3.12623, 2020.

Delaney, K. B. and Evans, S. G.: The 2000 Yigong landslide (Tibetan Plateau), rockslide-dammed lake and outburst flood: Review, remote sensing analysis, and process modelling, Geomorphology, 246, 377–393, doi:10.1016/j.geomorph.2015.06.020, 2015.

Dhital, M. R.: Geology of the Nepal Himalaya, Springer International Publishing, Cham., 2015.

Dinov, I. D.: Data science and predictive analytics: Biomedical and health applications using R, Springer International Publishing, Cham., 2018.

van Dongen, S.: Prior specification in Bayesian statistics: Three cautionary tales, J. Theor. Biol., 242(1), 90–100, doi:10.1016/j.jtbi.2006.02.002, 2006.

Drenkhan, F., Guardamino, L., Huggel, C. and Frey, H.: Current and future glacier and lake assessment in the deglaciating Vilcanota-Urubamba basin, Peruvian Andes, Glob. Planet. Change, 169, 105–118, doi:10.1016/j.gloplacha.2018.07.005, 2018.

Dubey, S. and Goyal, M. K.: Glacial Lake Outburst Flood Hazard, Downstream Impact, and Risk Over the Indian Himalayas, Water Resour. Res., 56(4), 1–21, doi:10.1029/2019WR026533, 2020.

Dunning, S. A., Rosser, N. J., Petley, D. N. and Massey, C. R.: Formation and failure of the Tsatichhu landslide dam, Bhutan, Landslides, 3(2), 107–113, doi:10.1007/s10346-005-0032-x, 2006.

Dussaillant, A., Benito, G., Buytaert, W., Carling, P., Meier, C. and Espinoza, F.: Repeated glacial-lake outburst floods in Patagonia: An increasing hazard?, Nat. Hazards, 54(2), 469–481, doi:10.1007/s11069-009-9479-8, 2010.

Dwivedi, S. and Neupane, Y.: Cause and mechanism of the Seti River flood, 5th May 2012, western Nepal, J. Nepal Geol. Soc., 46, 11–18, 2013.

Ely, L. L. and Baker, V. R.: Reconstructing Paleoflood Hydrology with Slackwater Deposits: Verde River, Arizona, Phys. Geogr., 6(2), 103–126, doi:10.1080/02723646.1985.10642266, 1985.

Emmer, A.: Glacier Retreat and Glacial Lake Outburst Floods (GLOFs), Oxford Res. Encycl. Nat. Hazard Sci., 1–37, doi:10.1093/acrefore/9780199389407.013.275, 2017.

Emmer, A.: GLOFs in the WOS: Bibliometrics, geographies and global trends of research on glacial lake outburst floods (Web of Science, 1979-2016), Nat. Hazards Earth Syst. Sci., 18(3), 813–827, doi:10.5194/nhess-18-813-2018, 2018.

Emmer, A. and Cuřín, V.: Can a dam type of an alpine lake be derived from lake geometry? A negative result, J. Mt. Sci., 18(3), 614–621, doi:10.1007/s11629-020-6003-9, 2021.

Emmer, A. and Vilímek, V.: Review article: Lake and breach hazard assessment for moraine-dammed lakes: An example from the Cordillera Blanca, Nat. Hazards Earth Syst. Sci., 13(6), 1551–1565, doi:10.5194/nhess-13-1551-2013, 2013.

Emmer, A. and Vilímek, V.: New method for assessing the susceptibility of glacial lakes to outburst floods in the Cordillera Blanca, Peru, Hydrol. Earth Syst. Sci., 18(9), 3461–3479, doi:10.5194/hess-18-3461-2014, 2014.

Emmer, A., Klimeš, J., Mergili, M., Vilímek, V. and Cochachin, A.: 882 lakes of the Cordillera Blanca: An inventory, classification, evolution and assessment of susceptibility to outburst floods, Catena, 147, 269–279, doi:10.1016/j.catena.2016.07.032, 2016.

Emmer, A., Vilímek, V. and Zapata, M. L.: Hazard mitigation of glacial lake outburst floods in the Cordillera Blanca (Peru): the effectiveness of remedial works, J. Flood Risk Manag., 11, 489–501, doi:10.1111/jfr3.12241, 2018.

ESRI and Maxar Technologies: World Imagery, [online] Available from: https://services.arcgisonline.com/ArcGIS/rest/services/World_Imagery/MapServer (Accessed 17 May 2022), 2022.

Etzelmüller, B. and Frauenfelder, R.: Factors controlling the distribution of mountain permafrost in the northern hemisphere and their influence on sediment transfer, Arctic, Antarct. Alp. Res., 41(1), 48–58, doi:10.1657/1523-0430-41.1.48, 2009.

Evans, S. G.: The formation and failure of landslide dams: an approach to risk assessment, Ital. J. Eng. Geol. Environ., 1(1), 15–19, doi:10.4408/IJEGE.2006-01.S-02, 2006.

Evans, S. G. and Clague, J. J.: Recent climatic change and catastrophic geomorphic processes in mountain environments, Geomorphology, 10(1–4), 107–128, doi:10.1016/0169-555X(94)90011-6, 1994.

Evans, S. G., Bishop, N. F., Smoll, L. F., Murillo, P. V., Delaney, K. B. and Oliver-Smith, A.: A re-examination of the mechanism and human impact of catastrophic mass flows originating on Nevado Huascarán, Cordillera Blanca, Peru in 1962 and 1970, Eng. Geol., 108(1–2), 96–118, 2009.

Faeh, R., Mueller, R., Rousselot, P., Veprek, R., Vetsch, D., Volz, C., Vonwiller, L. and Farshi, D.: BASEMENT–Basic Simulation Environment for Computation of Environmental Flow and Natural Hazard Simulation, VAW, ETH Zurich, 2011.

Falah, F., Rahmati, O., Rostami, M., Ahmadisharaf, E., Daliakopoulos, I. N. and Pourghasemi, H. R.: Artificial Neural Networks for Flood Susceptibility Mapping in Data-Scarce Urban Areas, in Spatial Modeling in GIS and R for Earth and Environmental Sciences, edited by H. R. Pourghasemi and C. B. T.-S. M. in G. I. S. and R. for E. and E. S. Gokceoglu, pp. 323–336, Elsevier, Amsterdam, Oxford, Cambridge., 2019.

Fallatah, A., Jones, S. and Mitchell, D.: Object-based random forest classification for informal settlements identification in the Middle East: Jeddah a case study, Int. J. Remote Sens., 41(11), 4421–4445, doi:10.1080/01431161.2020.1718237, 2020.

Fan, X., Xu, Q., Scaringi, G., Dai, L., Li, W., Dong, X., Zhu, X., Pei, X., Dai, K. and Havenith, H. B.: Failure mechanism and kinematics of the deadly June 24th 2017 Xinmo landslide, Maoxian, Sichuan, China, Landslides, 14(6), 2129–2146, doi:10.1007/s10346-017-0907-7, 2017.

Fischer, M., Korup, O., Veh, G. and Walz, A.: GLOFsusceptibility: First release of the GLOF susceptibility model (Version v.1.0), doi:10.5281/ZENODO.4161577, 2020.

Fisher, T. G.: River Warren boulders, Minnesota, USA: Catastrophic paleoflow indicators in the southern spillway of glacial Lake Agassiz, Boreas, doi:10.1080/0300948041001938, 2004.

Fort, M.: Sporadic morphogenesis in a continental subduction setting: an example from the Annapurna Range, Nepal Himalaya., Zeitschrift für Geomorphol. Suppl., 63, 9–36, 1987.

Fort, M.: The Pokhara Valley: A product of a natural catastrophe, in Geomorphological Landscapes of the World, edited by P. Migon, pp. 265–274, Springer Science+Business Media B. V., 2010.

Fort, M.: Impact of climate change on mountain environment dynamics, Rev. géographie Alp., 103(2), 1–7, doi:10.4000/rga.2877, 2015.

Fort, M., Adhikari, B. R. and Rimal, B.: Chapter 12 - Pokhara (Central Nepal): A Dramatic Yet Geomorphologically Active Environment Versus a Dynamic, Rapidly Developing City, in Urban Geomorphology, edited by M. J. Thornbush and C. D. Allen, pp. 231–258, Elsevier, Amsterdam, Oxford, Cambridge., 2018.

Fread, D. L.: The NWS DAMBRK Model: Quick Users Guide, National Weather Service (NWS), NOAA, Silver Spring., 1988.

Fujita, K., Suzuki, R., Nuimura, T. and Sakai, A.: Performance of ASTER and SRTM DEMs, and their potential for assessing glacial lakes in the Lunana region, Bhutan Himalaya, J. Glaciol., 54(185), 220–228, doi:10.3189/002214308784886162, 2008.

Gabet, E. J., Burbank, D. W., Putkonen, J. K., Pratt-Sitaula, B. A. and Ojha, T.: Rainfall thresholds for landsliding in the Himalayas of Nepal, Geomorphology, 63(3–4), 131–143, doi:10.1016/j.geomorph.2004.03.011, 2004.

Gaire, S., Delgado, R. C. and González, P. A.: Disaster risk profile and existing legal framework of Nepal: Floods and landslides, Risk Manag. Healthc. Policy, 8, 139–149, doi:10.2147/RMHP.S90238, 2015.

GAPHAZ: Assessment of Glacier and Permafrost Hazards in Mountain Regions: Technical Guidance Document., Standing Group on Glacier and Permafrost Hazards in Mountains (GAPHAZ) of the International Association of Cryospheric Sciences (IACS) and the International Permafrost Association (IPA), Zürich, Lima., 2017.

Gelman, A.: Prior distributions for variance parameters in hierarchical models, Bayesian Anal., 1(3), 515–533, doi:10.1002/cjs.5550340302, 2006.

Gelman, A. and Hill, J.: Data Analysis using Regression and Multilevel/Hierarchical Models, Cambridge University Press, New York., 2007.

Gelman, A., Jakulin, A., Pittau, M. G. and Su, Y. S.: A weakly informative default prior distribution for logistic and other regression models, Ann. Appl. Stat., 2(4), 1360–1383, doi:10.1214/08-AOAS191, 2008.

GENESIS Consultancy (P) Ltd.: Report on Impact of Settlement Pattern, Land-Use Practice and Options in High Risk Areas, Pokhara Sub-Metropolitan City, Kathmandu., 2009.

Grandin, R., Doin, M. P., Bollinger, L., Pinel-Puysségur, B., Ducret, G., Jolivet, R. and Sapkota, S. N.: Long-term growth of the Himalaya inferred from interseismic InSAR measurement, Geology, 40(12), 1059–1062, doi:10.1130/G33154.1, 2012.

Grebby, S., Sowter, A., Gee, D., Athab, A., De la Barreda-Bautista, B., Girindran, R. and Marsh, S.: Remote monitoring of ground motion hazards in high mountain terrain using InSAR: A case study of the Lake Sarez area, Tajikistan, Appl. Sci., 11(18), doi:10.3390/app11188738, 2021.

Grinsted, A., Hvidberg, C. S., Campos, N. and Dahl-Jensen, D.: Periodic outburst floods from an ice-dammed lake in East Greenland, Sci. Rep., 7(1), 7–12, doi:10.1038/s41598-017-07960-9, 2017.

Guerra, M., Cienfuegos, R., Escauriaza, C., Marche, F. and Galaz, J.: Modeling Rapid Flood Propagation Over Natural Terrains Using a Well-Balanced Scheme, J. Hydraul. Eng., 140(7), 04014026, doi:10.1061/(asce)hy.1943-7900.0000881, 2014.

Gurung, D. R., Maharjan, S. B., Khanal, N. R., Joshi, G. and Murthy, M. S. R.: Nepal disaster report 2015, Kathmandu., 2015.

Gurung, D. R., Khanal, N. R., Bajracharya, S. R., Tsering, K., Joshi, S., Tshering, P., Chhetri, L. K., Lotay, Y. and Penjor, T.: Lemthang Tsho glacial Lake outburst flood (GLOF) in Bhutan: cause and impact, Geoenvironmental Disasters, 4(1), doi:10.1186/s40677-017-0080-2, 2017.

Gurung, N.: Causes and Effects of Seti River Flash Flood 2012, Int. J. Landslide Environ., 1(1), 21–22, 2013.

Gurung, N., Fort, M., Bell, R., Arnaud-Fassetta, G. and Maharjan, N. R.: Hydro-torrential hazard vs. anthropogenic activities along the Seti valley, Kaski, Nepal: Assessment and recommendations from a risk perspective, J. Nepal Geol. Soc., 62, 58–87, doi:10.3126/jngs.v62i0.38695, 2021.

Haeberli, W. and Whiteman, C.: Snow and ice-related hazards, risks, and disasters: Facing challenges of rapid change and long-term commitments, in Snow and Ice-Related Hazards, Risks, and Disasters, pp. 1–33, Elsevier, Amsterdam, Oxford, Cambridge., 2021.

Haeberli, W., Kääb, A., Mühll, D. V. and Teysseire, P.: Prevention of outburst floods from periglacial lakes at Grubengletscher, Valais, Swiss Alps, J. Glaciol., 47(156), 111–122, doi:10.3189/172756501781832575, 2001.

Haeberli, W., Schaub, Y. and Huggel, C.: Increasing risks related to landslides from degrading permafrost into new lakes in de-glaciating mountain ranges, Geomorphology, 293, 405–417, doi:10.1016/j.geomorph.2016.02.009, 2017.

Hagen, T.: Report on the Geological survey of Nepal, Vol. 1: preliminary reconnaissance, Schweizerische Naturforschende Gesellschaft, Zürich., 1969.

Hanisch, J., Koirala, A. and Bhandary, N. P.: The Pokhara May 5th flood disaster: a last warning sign sent by nature?, J. Nepal Geol. Soc., 46, 1–10, 2013.

Harrison, S., Kargel, J. S., Huggel, C., Reynolds, J. M., Shugar, D. H., Betts, R. A., Emmer, A., Glasser, N., Haritashya, U. K., Klimeš, J., Reinhardt, L., Schaub, Y., Wiltshire, A., Regmi, D. and Vilímek, V.: Climate change and the global pattern of moraine-dammed glacial lake outburst floods, Cryosphere, 12(4), 1195–1209, doi:10.5194/tc-12-1195-2018, 2018.

Hauser, A.: Rock avalanche and resulting debris flow in Estero Parraguirre and Rio Colorado, Region Metropolitana, Chile, in Catastrophic landslides: effects, occurrence and mechanisms, vol. 15, edited by S. G. Evans and J. V. DeGraff, pp. 135–148, Geological Society of America Reviews in Engineering Geology, Boulder., 2002.

Henzmann, I.: Local Peoples Risk Perception of Natural Hazards in the Seti River Valley, Nepal, University of Zurich., 2020.

Hermle, D., Keuschnig, M., Hartmeyer, I., Delleske, R. and Krautblatter, M.: Timely prediction potential of landslide early warning systems with multispectral remote sensing: A conceptual approach tested in the Sattelkar, Austria, Nat. Hazards Earth Syst. Sci., 21(9), 2753–2772, doi:10.5194/nhess-21-2753-2021, 2021.

Hewitt, K.: Catastrophic landslides and their effects on the Upper Indus streams, Karakoram Himalaya, northern Pakistan, Geomorphology, 26(1–3), 47–80, doi:10.1016/S0169-555X(98)00051-8, 1998.

Hewitt, K.: The Karakoram anomaly? Glacier expantion and the "Elevation effect," Karakoram Himalaya, Mt. Res. Dev., 25(4), 332–340, doi:10.1659/0276-4741(2005)025[0332:TKAGEA]2.0.CO;2, 2005.

Hewitt, K.: Glaciers of the Karakoram Himalaya, Springer Netherlands, Dordrecht., 2014.

Hewitt, K. and Liu, J.: Ice-Dammed lakes and outburst floods, Karakoram Himalaya: Historical perspectives on emerging threats, Phys. Geogr., 31(6), 528–551, doi:10.2747/0272-3646.31.6.528, 2010.

Hijmans, R. J., Cameron, S. E., Parra, J. L., Jones, P. G. and Jarvis, A.: Very high resolution interpolated climate surfaces for global land areas, Int. J. Climatol., 25(15), 1965–1978, doi:10.1002/joc.1276, 2005.

Hille Ris Lambers, J., Aukema, B., Diez, J., Evans, M. and Latimer, A.: Effects of global change on inflorescence production : a Bayesian hierarchical analysis, in Hierarchical Modelling for the Environmental Sciences - Statistical Methods and Applications, edited by J. S. Clark and A. E. Gelfand, pp. 59–76, Oxford University Press North Carolina, Cary., 2006.

Hock, R., Rasul, G., Adler, C., Cáceres, B., Gruber, S., Hirabayashi, Y., Jackson, M., Kääb, A., Kang, S., Kutuzov, S., Milner, A., Molau, U., Morin, S., Orlove, B. and Steltzer, H. I.: High Mountain Areas, in IPCC Special Report on the Ocean and Cryosphere in a Changing Climate, edited by H.-O. Pörtner, D. C. Roberts, V. Masson-Delmotte, P. Zhai, M. Tignor, E. Poloczanska, K. Mintenbeck, A. Alegría, M. Nicolai, A. Okem, J. Petzold, B. Rama, and N. M. Weyer, pp. 131–202, Genf., 2019.

Hofmann, P., Taubenböck, H. and Werthmann, C.: Monitoring and modelling of informal settlements - A review on recent developments and challenges, in 2015 Joint Urban Remote Sensing Event (JURSE), pp. 1–6, Lausanne., 2015.

Hormann, K.: Die Terrassen an der Seti Khola - Ein Beitrag zur quartären Morphogenese in Zentralnepal, Erdkunde, 28(3), 161–176, 1974.

Huang, D., Li, Y. Q., Song, Y. X., Xu, Q. and Pei, X. J.: Insights into the catastrophic Xinmo rock avalanche in Maoxian county, China: Combined effects of historical earthquakes and landslide amplification, Eng. Geol., 258, 105–158, doi:10.1016/j.enggeo.2019.105158, 2019.

Hubbard, B., Heald, A., Reynolds, J. M., Quincey, D. J., Richardson, S. D., Luyo, M. Z., Portilla, N. S. and Hambrey, M. J.: Impact of a rock avalanche on a moraine-dammed proglacial lake: Laguna Safuna Alta, Cordillera Blanca, Peru, Earth Surf. Process. Landforms, 30(10), 1251–1264, doi:10.1002/esp.1198, 2005.

Huggel, C., Kääb, A., Haeberli, W., Teysseire, P. and Paul, F.: Remote sensing based assessment of hazards from glacier lake outbursts: a case study in the Swiss Alps, Can. Geotech. J., 39(2), 316–330, doi:10.1139/t01-099, 2002.

Huggel, C., Haeberli, W., Kääb, A., Bieri, D. and Richardson, S.: An assessment procedure for glacial hazards in the Swiss Alps, Can. Geotech. J., 41(6), 1068–1083, doi:10.1139/T04-053, 2004.

Huggel, C., Cochachin, A., Drenkhan, F., Fluixá-Sanmartín, J., Frey, H., García Hernández, J., Jurt, C., Muñoz, R., Price, K. and Vicuña, L.: Glacier Lake 513, Peru: Lessons for early warning service development, WMO Bull., 69(1), 45–52 [online] Available from: https://public.wmo.int/en/resources/bulletin/glacier-lake-513-peru-lessons-early-warning-service-development (Accessed 17 May 2022), 2020.

Immerzeel, W. W., van Beek, L. P. H. and Bierkens, M. F. P.: Climate change will affect the Asian water towers, Science, 328(5984), 1382–1385, doi:10.1126/science.1183188, 2010.

Iribarren Anacona, P., Norton, K. P. and Mackintosh, A.: Moraine-dammed lake failures in Patagonia and assessment of outburst susceptibility in the Baker Basin, Nat. Hazards Earth Syst. Sci., 14(12), 3243–3259, doi:10.5194/nhess-14-3243-2014, 2014.

Iturrizaga, L.: Glacier Lake Outburst Floods, in Encyclopedia of Snow, Ice and Glaciers, edited by V. P. Singh, P. Singh, and U. K. Haritashya, pp. 381–399, Springer Netherlands, Dodrecht., 2011.

Ives, J. D., Shrestha, R. B. and Mool, P. K.: Formation of Glacial Lakes in the Hindu Kush-Himalayas and GLOF Risk Assessment, International Centre for Integrated Mountain Development (ICIMOD), Kathmandu., 2010.

Jain, S. K., Lohani, A. K., Singh, R. D., Chaudhary, A. and Thakural, L. N.: Glacial lakes and glacial lake outburst flood in a Himalayan basin using remote sensing and GIS, Nat. Hazards, 62(3), 887–899, doi:10.1007/s11069-012-0120-x, 2012.

Jha, L. K. and Khare, D.: Glacial lake outburst flood (GLOF) study of Dhauliganga basin in the Himalaya, Cogent Environ. Sci., 2(1), 1–13, doi:10.1080/23311843.2016.1249107, 2016.

Kalantar, B., Pradhan, B., Naghibi, S. A., Motevalli, A. and Mansor, S.: Assessment of the effects of training data selection on the landslide susceptibility mapping : a comparison between support vector machine (SVM), logistic regression (LR) and artificial neural networks (ANN), Geomatics, Nat. Hazards Risk, 9(1), 49–69, doi:10.1080/19475705.2017.1407368, 2018.

Kapnick, S. B., Delworth, T. L., Ashfaq, M., Malyshev, S. and Milly, P. C. D.: Snowfall less sensitive to warming in Karakoram than in Himalayas due to a unique seasonal cycle, Nat. Geosci., 7(11), 834–840, doi:10.1038/ngeo2269, 2014.

Kargel, J. S.: One Scientist's Search for the Causes of the Deadly Seti River Flash Flood, NASA Earth Obs. [online] Available from: https://earthobservatory.nasa.gov/blogs/fromthefield/2014/01/24/setiriverclues/ (Accessed 21 March 2022), 2014.

Kargel, J. S., Paudel, L., Leonard, G., Regmi, D., Joshi, S., Poudel, K., Thapa, B., Watanabe, T. and Fort, M.: Causes and human impacts of the Seti River (Nepal) disaster of 2012, in Glacial Flooding & Disaster Risk Management Knowledge Exchange and Field Training; High Mountains Adaptation Partnership: Huaraz, Peru, pp. 1–11, Huaraz., 2013.

Kargel, J. S., Leonard, G. J., Shugar, D. H., Haritashya, U. K., Bevington, A. and Fielding, E. J.: Geomorphic and geologic controls of geohazards induced by Nepal's 2015 Gorkha earthquake., Science, 3(1), 1–10, doi:10.1126/science.aac8353, 2015.

Karger, D. N., Conrad, O., Böhner, J., Kawohl, T., Kreft, H., Soria-Auza, R. W., Zimmermann, N. E., Linder, H. P. and Kessler, M.: Climatologies at high resolution for the earth's land surface areas, Sci. Data, 4, 1–20, doi:10.1038/sdata.2017.122, 2017.

Kershaw, J. A., Clague, J. J. and Evans, S. G.: Geomorphic and sedimentological signature of a two-phase outburst flood from moraine-dammed Queen Bess Lake, British Columbia, Canada, Earth Surf. Process. Landforms, 30(1), 1–25, doi:10.1002/esp.1122, 2005.

Khadka, N., Chen, X., Nie, Y., Thakuri, S., Zheng, G. and Zhang, G.: Evaluation of Glacial Lake Outburst Flood Susceptibility Using Multi-Criteria Assessment Framework in Mahalangur Himalaya, Front. Earth Sci., 8, 1–16, doi:10.3389/feart.2020.601288, 2021.

King, O., Bhattacharya, A., Bhambri, R. and Bolch, T.: Glacial lakes exacerbate Himalayan glacier mass loss, Sci. Rep., 9(1), 1–9, doi:10.1038/s41598-019-53733-x, 2019.

Kirschbaum, D., Watson, C. S., Rounce, D. R., Shugar, D. H., Kargel, J. S., Haritashya, U. K., Amatya, P., Shean, D., Anderson, E. R. and Jo, M.: The State of Remote Sensing Capabilities of Cascading Hazards Over High Mountain Asia, Front. Earth Sci., 7, 1–25, doi:10.3389/feart.2019.00197, 2019.

Klimeš, J., Benešová, M., Vilímek, V., Bouška, P. and Cochachin Rapre, A.: The reconstruction of a glacial lake outburst flood using HEC-RAS and its significance for future hazard assessments: An example from Lake 513 in the Cordillera Blanca, Peru, Nat. Hazards, 71(3), 1617–1638, doi:10.1007/s11069-013-0968-4, 2014.

Koike, T. and Takenaka, S.: Scenario Analysis on Risks of Glacial Lake Outburst Floods on the Mangde Chhu River, Bhutan, Glob. Environ. Res., 16, 41–49, 2012.

Kondolf, G. M.: Geomorphic and environmental effects of instream gravel mining, Landsc. Urban Plan., 28(2–3), 225–243, doi:10.1016/0169-2046(94)90010-8, 1994.

Korup, O. and Clague, J. J.: Natural hazards, extreme events, and mountain topography, Quat. Sci. Rev., 28(11–12), 977–990, doi:10.1016/j.quascirev.2009.02.021, 2009.

Korup, O. and Montgomery, D. R.: Tibetan plateau river incision inhibited by glacial stabilization of the Tsangpo gorge, Nature, 455(7214), 786–789, doi:10.1038/nature07322, 2008.

Korup, O. and Tweed, F. S.: Ice, moraine, and landslide dams in mountainous terrain, Quat. Sci. Rev., 26(25), 3406–3422, doi:https://doi.org/10.1016/j.quascirev.2007.10.012, 2007.

Kougkoulos, I., Cook, S. J., Jomelli, V., Clarke, L., Symeonakis, E., Dortch, J. M., Edwards, L. A. and Merad, M.: Use of multi-criteria decision analysis to identify potentially dangerous glacial lakes, Sci. Total Environ., 621, 1453–1466, doi:10.1016/j.scitotenv.2017.10.083, 2018.

Kraaijenbrink, P. D. A., Bierkens, M. F. P., Lutz, A. F. and Immerzeel, W. W.: Impact of a global temperature rise of 1.5 degrees Celsius on Asia's glaciers, Nature, 549(7671), 257–260, doi:10.1038/nature23878, 2017.

Krishnan, R., Shrestha, A. B., Ren, G., Rajbhandari, R., Saeed, S., Sanjay, J., Syed, M. A., Vellore, R., Xu, Y., You, Q. and Ren, Y.: Unravelling Climate Change in the Hindu Kush Himalaya: Rapid Warming in the Mountains and Increasing Extremes, in The Hindu Kush Himalaya Assessment: Mountains, Climate Change, Sustainability and People, edited by P. Wester, A. Mishra, A. Mukherji, and A. B. Shrestha, pp. 57–97, Springer International Publishing, Cham., 2019.

Kruschke, J. K. and Liddell, T. M.: Bayesian data analysis for newcomers, Psychon. Bull. Rev., 25(1), 155–177, doi:10.3758/s13423-017-1272-1, 2018.

Lala, J. M., Rounce, D. R. and McKinney, D. C.: Modeling the glacial lake outburst flood process chain in the Nepal Himalaya: Reassessing Imja Tsho's hazard, Hydrol. Earth Syst. Sci., 22(7), 3721–3737, doi:10.5194/hess-22-3721-2018, 2018.

Larsen, I. J. and Lamb, M. P.: Progressive incision of the Channeled Scablands by outburst floods, Nature, 538(7624), 229–232, doi:10.1038/nature19817, 2016.

Lehnigk, K. E. and Larsen, I. J.: Pleistocene Megaflood Discharge in Grand Coulee, Channeled Scabland, USA, J. Geophys. Res. Earth Surf., 127(1), 1–25, doi:10.1029/2021JF006135, 2022.

Leibundgut, G., Sudmeier-Rieux, K., Devkota, S., Jaboyedoff, M., Derron, M. H., Penna, I. and Nguyen, L.: Rural earthen roads impact assessment in Phewa watershed, Western region, Nepal, Geoenvironmental Disasters, 3(1), 1–21, doi:10.1186/s40677-016-0047-8, 2016.

Liu, J. J., Cheng, Z. L. and Su, P. C.: The relationship between air temperature fluctuation and Glacial Lake Outburst Floods in Tibet, China, Quat. Int., 321, 78–87, doi:10.1016/j.quaint.2013.11.023, 2014.

Lliboutry, L., Arnao, B. M., Pautre, A. and Schneider, B.: Glaciological Problems Set by the Control of Dangerous Lakes in Cordillera Blanca, Peru, J. Glaciol., 19(81), 673–674, doi:10.3189/s0022143000029610, 1977.

Lovell, A. M., Carr, J. R. and Stokes, C. R.: Topographic controls on the surging behaviour of Sabche Glacier, Nepal (1967 to 2017), Remote Sens. Environ., 210, 434–443, doi:10.1016/j.rse.2018.03.036, 2018.

Maharjan, S. B., Mool, P. K., Lizong, W., Xiao, G., Shrestha, F., Shrestha, R. B., Khanal, N. R., Bajracharya, S. R., Joshi, S., Shai, S. and Baral, P.: The Status of Glacial Lakes in the Hindu Kush Himalaya, International Centre for Integrated Mountain Development (ICIMOD), Kathmandu., 2018.

Maharjan, S. B., Steiner, J. F., Shrestha, A. B., Maharjan, A., Nepal, S., Shrestha, M. S., Bajracharya, B., Rasul, G., Shrestha, M., Jackson, M. and Gupta, N.: The Melamchi flood disaster: Cascading hazard and the need for multihazard risk management, onal Centre for Integrated Mountain Development (ICIMOD), Kathmandu., 2021.

Mal, S., Allen, S. K., Frey, H., Huggel, C. and DImri, A. P.: Sectorwise Assessment of Glacial Lake Outburst Flood Danger in the Indian Himalayan Region, Mt. Res. Dev., 41(1), 1–12, doi:10.1659/MRD-JOURNAL-D-20-00043.1, 2021.

Maurer, J. M., Schaefer, J. M., Rupper, S. and Corley, A.: Acceleration of ice loss across the Himalayas over the past 40 years, Sci. Adv., 5(6), 1–12, doi:10.1126/sciadv.aav7266, 2019.

McKillop, R. J. and Clague, J. J.: A procedure for making objective preliminary assessments of outburst flood hazard from moraine-dammed lakes in southwestern British Columbia, Nat. Hazards, 41(1), 131–157, doi:10.1007/s11069-006-9028-7, 2007a.

McKillop, R. J. and Clague, J. J.: Statistical, remote sensing-based approach for estimating the probability of catastrophic drainage from moraine-dammed lakes in southwestern British Columbia, Glob. Planet. Change, 56(1–2), 153–171, doi:10.1016/j.gloplacha.2006.07.004, 2007b.

MCTCA: Nepal Tourism Statistics 2019, Ministry of Culture, Tourism & Civil Aviation, Kathmandu., 2020.

Meon, G. and Schwarz, W.: Estimation of glacier lake outburst flood and its impact on a hydro project in Nepal, Snow glacier Hydrol. Proc. Int. Symp. Kathmandu, 1992, (218), 331–339, 1993.

Mergili, M. and Schneider, J. F.: Regional-scale analysis of lake outburst hazards in the southwestern Pamir, Tajikistan, based on remote sensing and GIS, Nat. Hazards Earth Syst. Sci., 11(5), 1447–1462, doi:10.5194/nhess-11-1447-2011, 2011.

Mergili, M., Schneider, D., Worni, R. and Schneider, J. F.: Glacial lake outburst floods in the Pamir of Tajikistan: Challenges in prediction and modelling, Int. Conf. Debris-Flow Hazards Mitig. Mech. Predict. Assessment, Proc., 973–982, doi:10.4408/IJEGE.2011-03.B-106, 2011.

Mergili, M., Emmer, A., Juřicová, A., Cochachin, A., Fischer, J. T., Huggel, C. and Pudasaini, S. P.: How well can we simulate complex hydro-geomorphic process chains? The 2012 multi-lake outburst flood in the Santa Cruz Valley (Cordillera Blanca, Perú), Earth Surf. Process. Landforms, 43(7), 1373–1389, doi:10.1002/esp.4318, 2018.

Mergili, M., Pudasaini, S. P., Emmer, A., Fischer, J. T., Cochachin, A. and Frey, H.: Reconstruction of the 1941 GLOF process chain at Lake Palcacocha (Cordillera Blanca, Peru), Hydrol. Earth Syst. Sci., 24(1), 93–114, doi:10.5194/hess-24-93-2020, 2020.

Ministry of Forest and Environment: Vulnerability and Risk Assessment and Identifying Adaptation Options, Sectoral Report Tourism, Natural and Cultural Heritage, Ministry of Forests and Environment, Kathmandu., 2021.

Mohanty, L. and Maiti, S.: Probability of glacial lake outburst flooding in the Himalaya, Resour. Environ. Sustain., 5(100031), 1–13, doi:10.1016/j.resenv.2021.100031, 2021.

Molden, D. J., Vaidya, R. A., Shrestha, A. B., Rasul, G. and Shrestha, M. S.: Water infrastructure for the Hindu Kush Himalayas, Int. J. Water Resour. Dev., 30(1), 60–77, doi:10.1080/07900627.2013.859044, 2014.

Montgomery, D. R., Hallet, B., Yuping, L., Finnegan, N., Anders, A., Gillespie, A. and Greenberg, H. M.: Evidence for Holocene megafloods down the Tsangpo River gorge, Southeastern Tibet, Quat. Res., 62(2), 201–207, doi:10.1016/j.yqres.2004.06.008, 2004.

Mool, P. K., Maskey, P. R., Koirala, A., Joshi, S. P., Wu, L., Shrestha, A. B., Eriksson, M., Gurung, B., Pokharel, B., Khanal, N. R., Panthi, S., Adhikari, T., Kayastha, R. B., Ghimire, P., Thapa, R., Shrestha, B., Shrestha, S. and Shrestha, R. B.: Glacial Lakes and Glacial Lake Outburst Floods in Nepal, International Centre for Integrated Mountain Development (ICIMOD), Kathmandu., 2011.

Mukul, M., Srivastava, V., Jade, S. and Mukul, M.: Uncertainties in the Shuttle Radar Topography Mission (SRTM) Heights: Insights from the Indian Himalaya and Peninsula, Sci. Rep., 7(1), 1–10, doi:10.1038/srep41672, 2017.

Multi-Resolution Land Characteristics (MRLC) Consortium: National Land Cover Database 2019 (NLCD2019) Legend, NLCD2019 [online] Available from: https://www.mrlc.gov/data/legends/national-land-cover-database-2019-nlcd2019-legend (Accessed 12 January 2022), 2019.

Mungkasi, S., van Drie, R. and Roberts, S. G.: Predictions on arrival times of water of the St. Francis dam break flood using ANUGA, in Proceedings - 20th International Congress on Modelling and Simulation (MODSIM 2013), pp. 304–309, Adelaide., 2013.

Nalborczyk, L., Batailler, C., Loevenbruck, H., Vilain, A. and Bürkner, P. C.: An introduction to bayesian multilevel models using brms: A case study of gender effects on vowel variability in standard Indonesian, J. Speech, Lang. Hear. Res., 62(5), 1225–1242, doi:10.1044/2018_JSLHR-S-18-0006, 2019.

Nautiyal, A.: Devastating floods in Uttarakhand were a disaster waiting to happen, Dly. Mail Online India, 1 [online] Available from: https://www.dailymail.co.uk/indiahome/indianews/article-2349048/Devastating-floods-Uttarakhand-disaster-waiting-happen.html (Accessed 10 May 2022), 2013.

Nie, Y., Sheng, Y., Liu, Q., Liu, L., Liu, S., Zhang, Y. and Song, C.: A regional-scale assessment of Himalayan glacial lake changes using satellite observations from 1990 to 2015, Remote Sens. Environ., 189, 1–13, doi:10.1016/j.rse.2016.11.008, 2017.

Nie, Y., Liu, Q., Wang, J., Zhang, Y., Sheng, Y. and Liu, S.: An inventory of historical glacial lake outburst floods in the Himalayas based on remote sensing observations and geomorphological analysis, Geomorphology, 308, 91–106, doi:10.1016/j.geomorph.2018.02.002, 2018.

Nussbaumer, S., Schaub, Y., Huggel, C. and Walz, A.: Risk estimation for future glacier lake outburst floods based on local land-use changes, Nat. Hazards Earth Syst. Sci., 14(6), 1611–1624, doi:10.5194/nhess-14-1611-2014, 2014.

O'Brien, J. S., Julien, P. Y. and Fullerton, W. T.: Two-dimensional water flood and mudflow simulation, J. Hydraul. Eng., 119(2), 244–261, 1993.

O'Connor, J. E. and Baker, V. R.: Magnitudes and implications of peak discharges from glacial Lake Missoula, Geol. Soc. Am. Bull., 104(3), 267–279, doi:10.1130/0016-7606(1992)104<0267:MAIOPD>2.3.CO;2, 1992.

Oi, H., Higaki, D., Yagi, H., Usuki, N. and Yoshino, K.: Survey Report on the Seti River Flood, Nepal (May 5, 2012), Sabo Frontier Foundation, Tokyo., 2012.

Oi, H., Higaki, D., Yagi, H., Usuki, N. and Yoshino, K.: Report of the investigation of the flood disaster that occurred on May 5, 2012 along the Seti River in Nepal, Int. J. Eros. Control Eng., 7(4), 111–117, doi:10.13101/ijece.7.111, 2014.

Osti, R. and Egashira, S.: Hydrodynamic characteristics of the Tam Pokhari glacial lake outburst flood in the Mt. Everest region, Nepal, Hydrol. Process., 23(20), 2943–2955, doi:10.1002/hyp.7405, 2009.

Palazzi, E., von Hardenberg, J. and Provenzale, A.: Precipitation in the Hindu-Kush Karakoram Himalaya: Observations and future scenarios, J. Geophys. Res. Atmos., 118(1), 85–100, doi:10.1029/2012JD018697, 2013.

Palazzi, E., Filippi, L. and von Hardenberg, J.: Insights into elevation-dependent warming in the Tibetan Plateau-Himalayas from CMIP5 model simulations, Clim. Dyn., 48(11–12), 3991–4008, doi:10.1007/s00382-016-3316-z, 2017.

Pepin, N., Bradley, R. S., Diaz, H. F., Baraer, M., Caceres, E. B., Forsythe, N., Fowler, H., Greenwood, G., Hashmi, M. Z., Liu, X. D., Miller, J. R., Ning, L., Ohmura, A., Palazzi, E., Rangwala, I., Schöner, W., Severskiy, I., Shahgedanova, M., Wang, M. B., Williamson, S. N. and Yang, D. Q.: Elevation-dependent warming in mountain regions of the world, Nat. Clim. Chang., 5(5), 424–430, doi:10.1038/nclimate2563, 2015.

Petley, D.: More information on the landslide that caused the Seti Flood in Nepal, Landslide Blog - AGU Blogosph. [online] Available from: https://blogs.agu.org/landslideblog/2012/05/12/more-information-on-the-landslide-that-caused-the-seti-flood-in-nepal/ (Accessed 15 June 2021a), 2012.

Petley, D.: Using seismic data to analyse the Seti River landslide in Nepal, Landslide Blog - AGU Blogosph. [online] Available from: https://blogs.agu.org/landslideblog/2012/05/09/using-seismic-data-to-analyse-the-seti-river-landslide-in-nepal/ (Accessed 15 June 2021b), 2012.

Petley, D.: Melamchi: a landslide dam break flood in Nepal last week, Landslide Blog - AGU Blogosph. [online] Available from: https://blogs.agu.org/landslideblog/2021/06/21/melamchi-a-landslide-dam-break-flood-in-nepal-last-week/ (Accessed 16 July 2021a), 2021.

Petley, D.: The catastrophic landslide and flood in Chamoli in Uttarakhand: the sequence of events, Landslide Blog - AGU Blogosph. [online] Available from: https://blogs.agu.org/landslideblog/2021/02/08/chamoli-2/ (Accessed 16 July 2021b), 2021.

Petley, D. and Stark, C.: Understanding the Seti River landslide in Nepal, Landslide Blog - AGU Blogosph. [online] Available from: https://blogs.agu.org/landslideblog/2012/05/23/understanding-the-seti-river-landslide-in-nepal/ (Accessed 15 June 2021), 2012.

Phuyal, S.: Light at the end of the Melamchi tunnel, Nepali Times, 1 [online] Available from: https://www.nepalitimes.com/here-now/light-at-the-end-of-the-melamchi-tunnel/ (Accessed 10 March 2022), 2020.

Planet Team: Planet Application Program Interface: In Space for Life on Earth, [online] Available from: https://www.planet.com/explorer (Accessed 17 May 2022), 2017.

Pokhrel, M.: Still chasing the Melamchi mirage, Nepali Times [online] Available from: https://www.nepalitimes.com/banner/still-chasing-the-melamchi-mirage/ (Accessed 10 March 2022), 2021.

Prakash, C. and Nagarajan, R.: Outburst susceptibility assessment of moraine-dammed lakes in Western Himalaya using an analytic hierarchy process, Earth Surf. Process. Landforms, 42(14), 2306–2321, doi:10.1002/esp.4185, 2017.

Quincey, D. J., Lucas, R. M., Richardson, S. D., Glasser, N. F., Hambrey, M. J. and Reynolds, J. M.: Optical remote sensing techniques in high-mountain environments: Application to glacial hazards, Prog. Phys. Geogr., 29(4), 475–505, doi:10.1191/0309133305pp456ra, 2005.

Rafiq, M., Romshoo, S. A., Mishra, A. K. and Jalal, F.: Modelling Chorabari Lake outburst flood, Kedarnath, India, J. Mt. Sci., 16(1), 64–76, doi:10.1007/s11629-018-4972-8, 2019.

Rangwala, I. and Miller, J. R.: Climate change in mountains: A review of elevation-dependent warming and its possible causes, Clim. Change, 114(3–4), 527–547, doi:10.1007/s10584-012-0419-3, 2012.

Rasul, G. and Molden, D.: The global social and economic consequences of mountain cryospheric change, Front. Environ. Sci., 7, 1–18, doi:10.3389/fenvs.2019.00091, 2019.

Rasul, G., Pasakhala, B., Mishra, A. and Pant, S.: Adaptation to mountain cryosphere change: issues and challenges, Clim. Dev., 12(4), 297–309, doi:10.1080/17565529.2019.1617099, 2020.

Reynolds, J. M.: High-altitude glacial lake hazard assessment and mitigation: a Himalayan perspective, in Geohazards in Engineering Geology, edited by J. G. Maund and M. Eddleston, pp. 25–34, Geological Society London, London., 1998.

RGI Consortium: Randolph Glacier Inventory – A Dataset of Global Glacier Outlines: Version 6.0: Technical Report, Global Land Ice Measurements from Space (GLIM), Boulder., 2017.

Richardson, S. D. and Reynolds, J. M.: An overview of glacial hazards in the Himalayas, Quat. Int., 65/66, 31–47, doi:10.1016/S1040-6182(99)00035-X, 2000.

Rimal, B.: Urbanization and the Decline of Agricultural Land in Pokhara Sub-metropolitan City, Nepal, J. Agric. Sci., 5(1), 54–65, doi:10.5539/jas.v5n1p54, 2012.

Rimal, B., Baral, H., Stork, N., Paudyal, K. and Rijal, S.: Growing City and Rapid Land Use Transition: Assessing Multiple Hazards and Risks in the Pokhara Valley, Nepal, Land, 4(4), 957–978, doi:10.3390/land4040957, 2015.

Rimal, B., Zhang, L., Keshtkar, H., Sun, X. and Rijal, S.: Quantifying the spatiotemporal pattern of urban expansion and hazard and risk area identification in the Kaski District of Nepal, Land, 7(37), 1–22, doi:10.3390/land7010037, 2018.

Roberts, S., Nielsen, O., Gray, D. and Sexton, J.: ANUGA User Manual, Release 2.0, Commonwealth of Australia (Geoscience Australia) and the Australian National University 2004-2010, Canberra., 2015.

Rolland, C.: Spatial and seasonal variations of air temperature lapse rates in alpine regions, J. Clim., 16(7), 1032–1046, doi:10.1175/1520-0442(2003)016<1032:SASVOA>2.0.CO;2, 2003.

Ross, J. and Gilbert, R.: Lacustrine sedimentation in a monsoon environment: The record from Phewa Tal, middle mountain region of Nepal, Geomorphology, 27(3–4), 307–323, doi:10.1016/S0169-555X(98)00079-8, 1999.

Rounce, D. R., McKinney, D. C., Lala, J. M., Byers, A. C. and Watson, C. S.: A new remote hazard and risk assessment framework for glacial lakes in the Nepal Himalaya, Hydrol. Earth Syst. Sci., 20(9), 3455–3475, doi:10.5194/hess-20-3455-2016, 2016.

Saito, T. and Rehmsmeier, M.: The Precision-Recall Plot Is More Informative than the ROC Plot When Evaluating Binary Classifiers on Imbalanced Datasets, PLoS One, 10(3), 1–25, doi:10.1371/journal.pone.0118432, 2015.

SANDRP: Explained: Seti River floods in May 2012, Nepal- A chain of events, starting at 25,000 feet!, [online] Available from: https://sandrp.in/2014/01/26/explained-seti-river-floods-in-may-2012-nepal-a-chain-of-events-starting-at-25000-feet/ (Accessed 18 March 2021), 2014.

Sayami, M. and Kazi Tamrakar, N.: Status of sand mining and quality in northern Kathmandu, Bull. Dep. Geol., 10, 89–98, 2007.

Schaub, Y., Haeberli, W., Huggel, C., Künzler, M. and Bründl, M.: Landslides and New Lakes in Deglaciating Areas: A Risk Management Framework, in Landslide Science and Practice, vol. 7, edited by C. Margottini, P. Canuti, and K. Sassa, pp. 31–38, Springer Berlin Heidelberg, Berlin, Heidelberg., 2013.

Schild, A.: ICIMOD's Position on Climate Change and Mountain Systems, Mt. Res. Dev., 28(3), 328–331, doi:10.1659/mrd.mp009, 2008.

Schwanghart, W., Bernhardt, A., Stolle, A., Hoelzmann, P., Adhikari, B. R., Andermann, C., Tofelde, S., Merchel, S., Rugel, G., Fort, M. and Korup, O.: Repeated catastrophic valley infill following medieval earthquakes in the Nepal Himalaya, Science, 351(6269), 147–150, doi:10.1126/science.aac9865, 2016a.

Schwanghart, W., Worni, R., Huggel, C., Stoffel, M. and Korup, O.: Uncertainty in the Himalayan energy-water nexus: Estimating regional exposure to glacial lake outburst floods, Environ. Res. Lett., 11(7), 1–10, doi:10.1088/1748-9326/11/7/074005, 2016b.

Schwanghart, W., Ryan, M. and Korup, O.: Topographic and Seismic Constraints on the Vulnerability of Himalayan Hydropower, Geophys. Res. Lett., 45(17), 8985–8992, doi:10.1029/2018GL079173, 2018.

Scott, C. A., Zhang, F., Mukherji, A., Immerzeel, W. W., Mustafa, D. and Bharati, L.: Water in the Hindu Kush Himalaya, in The Hindu Kush Himalaya Assessment: Mountains, Climate Change, Sustainability and People, edited by P. Wester, A. Mishra, A. Mukherji, and A. B. Shrestha, pp. 257–299, Springer International Publishing, Cham., 2019.

Shang, Y., Yang, Z., Li, L., Liu, D., Liao, Q. and Wang, Y.: A super-large landslide in Tibet in 2000: Background, occurrence, disaster, and origin, Geomorphology, 54(3–4), 225–243, doi:10.1016/S0169-555X(02)00358-6, 2003.

Sharma, E., Molden, D., Rahman, A., Khatiwada, Y. R., Zhang, L., Singh, S. P., Yao, T. and Wester, P.: Introduction to the Hindu Kush Himalaya Assessment, in The Hindu Kush Himalaya Assessment: Mountains, Climate Change, Sustainability and People, edited by P. Wester, A. Mishra, A. Mukherji, and A. B. Shrestha, pp. 1–16, Springer International Publishing, Cham., 2019.

Sharma, K. P. and Adhikari, N. R.: Hydrological estimations in Nepal, Department of Hydrology and Meteorology, Kathmandu., 2004.

Sherry, J. and Curtis, A.: At the intersection of disaster risk and religion: interpretations and responses to the threat of Tsho Rolpa glacial lake, Environ. Hazards, 16(4), 314–329, doi:10.1080/17477891.2017.1298983, 2017.

Shor, B., Bafumi, J., Keele, L. and Park, D.: A Bayesian multilevel modeling approach to time-series cross-sectional data, Polit. Anal., 15(2), 165–181, doi:10.1093/pan/mpm006, 2007.

Shrestha, A. B., Eriksson, M., Mool, P. K., Ghimire, P., Mishra, B. and Khanal, N. R.: Glacial lake outburst flood risk assessment of Sun Koshi basin, Nepal, Geomatics, Nat. Hazards Risk, 1(2), 157–169, doi:10.1080/19475701003668968, 2010.

Shrestha, B. B. and Nakagawa, H.: Hazard assessment of the formation and failure of the Sunkoshi landslide dam in Nepal, Nat. Hazards, 82(3), 2029–2049, doi:10.1007/s11069-016-2283-3, 2016.

Shugar, D. H., Jacquemart, M., Shean, D., Bhushan, S., Upadhyay, K., Sattar, A., Schwanghart, W., McBride, S., de Vries, M. V. W., Mergili, M., Emmer, A., Deschamps-Berger, C., McDonnell, M., Bhambri, R., Allen, S. K., Berthier, E., Carrivick, J. L., Clague, J. J., Dokukin, M., Dunning, S. A., Frey, H., Gascoin, S., Haritashya, U. K., Huggel, C., Kääb, A., Kargel, J. S., Kavanaugh, J. L., Lacroix, P., Petley, D., Rupper, S., Azam, M. F., Cook, S. J., Dimri, A. P., Eriksson, M., Farinotti, D., Fiddes, J., Gnyawali, K. R., Harrison, S., Jha, M., Koppes, M., Kumar, A., Leinss, S., Majeed, U., Mal, S., Muhuri, A., Noetzli, J., Paul, F., Rashid, I., Sain, K., Steiner, J., Ugalde, F., Watson, C. S. and Westoby, M. J.: A massive rock and ice avalanche caused the 2021 disaster at Chamoli, Indian Himalaya, Science, 373(6552), 300–306, doi:10.1126/science.abh4455, 2021.

Sidle, R. C. and Ziegler, A. D.: The dilemma of mountain roads, Nat. Geosci., 5(7), 437–438, doi:10.1038/ngeo1512, 2012.

Smith, G. A.: Missoula flood dynamics and magnitudes inferred from sedimentology of slack-water deposits on the Columbia Plateau, Washington, Geol. Soc. Am. Bull., 105(1), 77–100, doi:10.1130/0016-7606(1993)105<0077:MFDAMI>2.3.CO;2, 1993.

Somos-Valenzuela, M. A., McKinney, D. C., Byers, A. C., Voss, K., Moss, J. and McKinney, J. C.: Ground Penetrating Radar Survey for Risk Reduction at Imja Lake, Nepal, Center for Research in Water Resources, University of Texas at Austin, Austin., 2012.

Somos-Valenzuela, M. A., McKinney, D. C., Byers, A. C., Rounce, D. R., Portocarrero, C. and Lamsal, D.: Assessing downstream flood impacts due to a potential GLOF from Imja Lake in Nepal, Hydrol. Earth Syst. Sci. Discuss., 11(11), 13019–13053, doi:10.5194/hessd-11-13019-2014, 2014.

Somos-Valenzuela, M. A., Chisolm, R. E., Rivas, D. S., Portocarrero, C. and McKinney, D. C.: Modeling a glacial lake outburst flood process chain: The case of Lake Palcacocha and Huaraz, Peru, Hydrol. Earth Syst. Sci., 20(6), 2519–2543, doi:10.5194/hess-20-2519-2016, 2016.

Srivastava, P., Kumar, A., Chaudhary, S., Meena, N., Sundriyal, Y. P., Rawat, S., Rana, N., Perumal, R. J., Bisht, P., Sharma, D., Agnihotri, R., Bagri, D. S., Juyal, N., Wasson, R. J. and Ziegler, A. D.: Paleofloods records in Himalaya, Geomorphology, 284, 17–30, doi:10.1016/j.geomorph.2016.12.011, 2017.

Stegmueller, D.: How many countries for multilevel modeling? A comparison of frequentist and bayesian approaches, Am. J. Pol. Sci., 57(3), 748–761, doi:10.1111/ajps.12001, 2013.

Stolle, A.: Catastrophic Sediment Pulses in the Pokhara Valley, Nepal, University of Potsdam., 2018.

Stolle, A., Bernhardt, A., Schwanghart, W., Hoelzmann, P., Adhikari, B. R., Fort, M. and Korup, O.: Catastrophic valley fills record large Himalayan earthquakes, Pokhara, Nepal, Quat. Sci. Rev., 177, 88–103, doi:10.1016/j.quascirev.2017.10.015, 2017.

Stolle, A., Schwanghart, W., Andermann, C., Bernhardt, A., Fort, M., Jansen, J. D., Wittmann, H., Merchel, S., Rugel, G., Adhikari, B. R. and Korup, O.: Protracted river response to medieval earthquakes, Earth Surf. Process. Landforms, 44(1), 331–341, doi:10.1002/esp.4517, 2019.

Taalab, K., Cheng, T. and Zhang, Y.: Mapping landslide susceptibility and types using Random Forest, Big Earth Data, 2(2), 159–178, doi:10.1080/20964471.2018.1472392, 2018.

Talchabhadel, R., Karki, R., Thapa, B. R., Maharjan, M. and Parajuli, B.: Spatio-temporal variability of extreme precipitation in Nepal, Int. J. Climatol., 38(11), 4296–4313, doi:10.1002/joc.5669, 2018.

Taubenböck, H. and Kraff, N. J.: The physical face of slums: a structural comparison of slums in Mumbai, India, based on remotely sensed data, J. Hous. Built Environ., 29(1), 15–38, doi:10.1007/s10901-013-9333-x, 2014.

Teller, J. T., Leverington, D. W. and Mann, J. D.: Freshwater outbursts to the oceans from glacial Lake Agassiz and their role in climate change during the last deglaciation, Quat. Sci. Rev., 21(8–9), 879–887, doi:10.1016/S0277-3791(01)00145-7, 2002.

Terzago, S., von Hardenberg, J., Palazzi, E. and Provenzale, A.: Snowpack Changes in the Hindu Kush–Karakoram–Himalaya from CMIP5 Global Climate Models, J. Hydrometeorol., 15(6), 2293–2313, doi:10.1175/JHM-D-13-0196.1, 2014.

Thapa, B., Watanabe, T. and Regmi, D.: Flood Assessment and Identification of Emergency Evacuation Routes in Seti River Basin, Nepal, Land, 11(82), 1–33, doi:10.3390/land11010082, 2022.

The World Bank: Poverty and Inequality Platform, [online] Available from: https://pip.worldbank.org/country-profiles/NPL (Accessed 8 May 2022), 2022.

Toonen, W. H. J., Munoz, S. E., Cohen, K. M. and Macklin, M. G.: High-Resolution Sedimentary Paleoflood Records in Alluvial River Environments: A Review of Recent Methodological Advances and Application to Flood Hazard Assessment, in Palaeohydrology: Traces, Tracks and Trails of Extreme Events, edited by J. Herget and A. Fontana, pp. 213–228, Springer International Publishing, Cham., 2020.

Tudoroiu, M., Eccel, E., Gioli, B., Gianelle, D., Schume, H., Genesio, L. and Miglietta, F.: Negative elevation-dependent warming trend in the Eastern Alps, Environ. Res. Lett., 11(4), 1–13, doi:10.1088/1748-9326/11/4/044021, 2016.

Turzewski, M. D., Huntington, K. W. and LeVeque, R. J.: The Geomorphic Impact of Outburst Floods: Integrating Observations and Numerical Simulations of the 2000 Yigong Flood, Eastern Himalaya, J. Geophys. Res. Earth Surf., 124(5), 1056–1079, doi:10.1029/2018JF004778, 2019.

UN Office for the Coordination of Humanitarian Affairs - Field Information Services Section (OCHA FISS): Nepal - Subnational Administrative Boundaries, Humanit. Data Exch. [online] Available from: https://data.humdata.org/dataset/administrative-bounadries-of-nepal (Accessed 5 January 2022), 2020.

UNISDR: 2009 UNISDR Terminology on Disaster Risk Reduction, United Nations International Strategy on Disaster Risk Reduction (UNISDR), Geneva, Switzerland., 2009.

United Idi Mardi and RB Hydropower Ltd.: Ongoing Hydropower Projects, [online] Available from: https://idimardihydro.com.np (Accessed 9 April 2022), 2022.

United Nations Department of Economic and Social Affairs: Glossary of Environment Statistics, United Nations Publications, New York., 1997.

United Nations Department of Economic and Social Affairs: World Population Prospect 2019, World Popul. Prospect. [online] Available from: https://population.un.org/wpp/ (Accessed 13 January 2022), 2019.

Upreti, B. R., Upadhayaya, P. K. and Sapkota, T.: Tourism in Pokhara, Issues, Trends and Future Prospects for Peace and Prosperity, Pokhara Tourism Council (PTC), South Asia Regional Coordination Office of the Swiss National Centre of Competence in Research (NCCR NorthSouth) and Nepal Center for Contemporary Research (NCCR), Kathmandu., 2013.

USGS: Earthquake Catalogue, Earthq. Hazards Progr. [online] Available from: https://earthquake.usgs.gov/earthquakes/search/ (Accessed 9 September 2019), 2019.

Veh, G. and Lützow, N.: Glacial Lake Outburst Flood Database version 1.0, [online] Available from: http://glofs.geoecology.uni-potsdam.de/ (Accessed 30 November 2021), 2021.

Veh, G., Korup, O., Roessner, S. and Walz, A.: Detecting Himalayan glacial lake outburst floods from Landsat time series, Remote Sens. Environ., 207, 84–97, doi:10.1016/j.rse.2017.12.025, 2018.

Veh, G., Korup, O., Specht, S., Roessner, S. and Walz, A.: Unchanged frequency of moraine-dammed glacial lake outburst floods in the Himalaya, Nat. Clim. Chang., 2000, 1–5, doi:10.1038/s41558-019-0437-5, 2019.

Veh, G., Korup, O. and Walz, A.: Hazard from Himalayan glacier lake outburst floods, Proc. Natl. Acad. Sci. U. S. A., 117(2), 907–912, doi:10.1073/pnas.1914898117, 2020.

Veh, G., Lützow, N., Kharlamova, V., Petrakov, D., Hugonnet, R. and Korup, O.: Trends, Breaks, and Biases in the Frequency of Reported Glacier Lake Outburst Floods, Earth's Futur., 10(3), 1–14, doi:10.1029/2021EF002426, 2022.

Vehtari, A., Gelman, A. and Gabry, J.: Practical Bayesian model evaluation using leave-one-out cross-validation and WAIC, Stat. Comput., 27(5), 1413–1432, doi:10.1007/s11222-016-9696-4, 2017.

Vuichard, D. and Zimmermann, M.: The 1985 catastrophic drainage of a moraine-dammed lake, Khumbu Himal, Nepal: cause and consequences., Mt. Res. Dev., 7(2), 91–110, doi:10.2307/3673305, 1987.

Waitt, R. B.: Case for periodic, colossal jokulhlaups from Pleistocene glacial Lake Missoula., Geol. Soc. Am. Bull., 96(10), 1271–1286, doi:10.1130/0016-7606(1985)96<1271:CFPCJF>2.0.CO;2, 1985.

Walder, J. S. and Costa, J. E.: Outburst Floods From Glacier-Dammed Lakes: the Effect of Mode of Lake Drainage on Flood Magnitude, Earth Surf. Landforms, 21, 701–723, doi:10.1002/(SICI)1096-9837(199608)21:8<701::AID-ESP615>3.0.CO;2-2, 1996.

Walder, J. S. and O'Connor, J. E.: Methods for predicting peak discharge of floods caused by failure of natural and constructed earthen dams, Water Resour. Res., 33(10), 2337–2348, doi:10.1029/97WR01616, 1997.

Wang, W., Yao, T., Gao, Y., Yang, X. and Kattel, D. B.: A First-order Method to Identify Potentially Dangerous Glacial Lakes in a Region of the Southeastern Tibetan Plateau, Mt. Res. Dev., 31(2), 122–130, doi:10.1659/MRD-JOURNAL-D-10-00059.1, 2011.

Wang, W., Yang, X. and Yao, T.: Evaluation of ASTER GDEM and SRTM and their suitability in hydraulic modelling of a glacial lake outburst flood in southeast Tibet, Hydrol. Process., 26(2), 213–225, doi:10.1002/hyp.8127, 2012a.

Wang, W., Gao, Y., Iribarren Anacona, P., Lei, Y., Xiang, Y., Zhang, G., Li, S. and Lu, A.: Integrated hazard assessment of Cirenmaco glacial lake in Zhangzangbo valley, Central Himalayas, Geomorphology, 306, 292–305, doi:10.1016/j.geomorph.2015.08.013, 2018.

Wang, W., Zhang, T., Yao, T. and An, B.: Monitoring and early warning system of Cirenmaco glacial lake in the central Himalayas, Int. J. Disaster Risk Reduct., 73, 1–12, doi:10.1016/j.ijdrr.2022.102914, 2022.

Wang, X., Liu, S., Guo, W. and Xu, J.: Assessment and simulation of glacier lake outburst floods for Longbasaba and Pida lakes, China, Mt. Res. Dev., 28(3–4), 310–317, doi:10.1659/mrd.0894, 2008.

Wang, X., Liu, S., Ding, Y., Guo, W., Jiang, Z., Lin, J. and Han, Y.: An approach for estimating the breach probabilities of moraine-dammed lakes in the Chinese Himalayas using remote-sensing data, Nat. Hazards Earth Syst. Sci., 12(10), 3109–3122, doi:10.5194/nhess-12-3109-2012, 2012b.

Wang, X., Guo, X., Yang, C., Liu, Q., Wei, J., Zhang, Y., Liu, S., Zhang, Y., Jiang, Z. and Tang, Z.: Glacial lake inventory of high-mountain Asia in 1990 and 2018 derived from Landsat images, Earth Syst. Sci. Data, 12, 2169–2182, doi:10.5194/essd-12-2169-2020, 2020.

Wang, Y., Wu, N., Kunze, C., Long, R. and Perlik, M.: Drivers of Change to Mountain Sustainability in the Hindu Kush Himalaya, in The Hindu Kush Himalaya Assessment, edited by P. Wester, A. Mishra, A. Mukherji, and A. B. Shrestha, pp. 17–56, Springer International Publishing, Cham., 2019.

Watson, R. T. and Haeberli, W.: Environmental threats, mitigation strategies and high-mountain areas, Ambio, 33(13), 2–10, doi:10.1007/0044-7447-33.sp13.2, 2004.

Westoby, M. J., Glasser, N. F., Brasington, J., Hambrey, M. J., Quincey, D. J. and Reynolds, J. M.: Modelling outburst floods from moraine-dammed glacial lakes, Earth-Science Rev., 134, 137–159, doi:10.1016/j.earscirev.2014.03.009, 2014.

Wilhelm, B., Ballesteros Canovas, J. A., Corella Aznar, J. P., Kämpf, L., Swierczynski, T., Stoffel, M., Støren, E. and Toonen, W.: Recent advances in paleoflood hydrology: From new archives to data compilation and analysis, Water Secur., 3, 1–8, doi:10.1016/j.wasec.2018.07.001, 2018.

Williams, D. S., Costa, M. M., Sutherland, C., Celliers, L. and Scheffran, J.: Vulnerability of informal settlements in the context of rapid urbanization and climate change, Environ. Urban., 31(1), 157–176, doi:10.1177/0956247818819694, 2019.

Wohl, E. E.: Estimating flood magnitude in ungauged mountain channels, Nepal, Mt. Res. Dev., 15(1), 69–76, doi:10.2307/3673701, 1995.

Wohl, E. E.: Uncertainty in Flood Estimates Associated with Roughness Coefficient, J. Hydraul. Eng., 124(2), 219–223, doi:10.1061/(asce)0733-9429(1998)124:2(219), 1998.

Worni, R., Stoffel, M., Huggel, C., Volz, C., Casteller, A. and Luckman, B.: Analysis and dynamic modeling of a moraine failure and glacier lake outburst flood at Ventisquero Negro, Patagonian Andes (Argentina), J. Hydrol., 444–445, 134–145, doi:10.1016/j.jhydrol.2012.04.013, 2012.

Worni, R., Huggel, C. and Stoffel, M.: Glacial lakes in the Indian Himalayas - From an area-wide glacial lake inventory to on-site and modeling based risk assessment of critical glacial lakes, Sci. Total Environ., 468–469, 71–84, doi:10.1016/j.scitotenv.2012.11.043, 2013.

Worni, R., Huggel, C., Clague, J. J., Schaub, Y. and Stoffel, M.: Coupling glacial lake impact, dam breach, and flood processes: A modeling perspective, Geomorphology, 224, 161–176, doi:10.1016/j.geomorph.2014.06.031, 2014.

Wu, Q., Zhao, Z., Liu, L., Granger, D. E., Wang, H., Cohen, D. J., Wu, X., Ye, M., Bar-Yosef, O., Lu, B., Zhang, J., Zhang, P., Yuan, D., Qi, W., Cai, L. and Bai, S.: Outburst flood at 1920 BCE supports historicity of China's Great Flood and the Xia dynasty, Science, 353(6299), 579–582, doi:10.1126/science.aaf0842, 2016.

Xia, J., Lin, B., Falconer, R. A. and Wang, G.: Modelling dam-break flows over mobile beds using a 2D coupled approach, Adv. Water Resour., 33(2), 171–183, doi:10.1016/j.advwatres.2009.11.004, 2010.

Yamanaka, H.: Radiocarbon ages of upper Quaternary deposit in central Nepal and their geomorphological significance, Sci. Reports Tohoku Univ., 32(1), 46–60, 1982.

Yang, S.-K. and Smith, G. L.: Further study on atmospheric lapse rate regimes, J. Atmos. Sci., 42(9), 961–966, doi:0.1175/1520-0469(1985)042<0961:fsoalr>2.0.co;2, 1985.

Yin, A.: Cenozoic tectonic evolution of the Himalayan orogen as constrained by along-strike variation of structural geometry, exhumation history, and foreland sedimentation, Earth-Science Rev., 76(1–2), 1–131, doi:10.1016/j.earscirev.2005.05.004, 2006.

Yin, A. and Harrison, T. M.: Geologic Evolution of the Himalayan-Tibetan Orogen, Annu. Rev. Earth Planet. Sci., 28(1), 211–280, doi:10.1146/annurev.earth.28.1.211, 2000.

Zhang, T., Wang, W., Gao, T. and An, B.: Simulation and assessment of future glacial lake outburst floods in the Poiqu river basin, central Himalayas, Water, 13(1376), 1–18, doi:10.3390/w13101376, 2021.

Zhang, X. and Liu, S.: A framework of numerical simulation on moraine-dammed glacial lake outburst floods, J. Arid Land, 7(6), 728–740, doi:10.1007/s40333-015-0133-x, 2015.

Zheng, G., Allen, S. K., Bao, A., Ballesteros-Cánovas, J. A., Huss, M., Zhang, G., Li, J., Yuan, Y., Jiang, L., Yu, T., Chen, W. and Stoffel, M.: Increasing risk of glacial lake outburst floods from future Third Pole deglaciation, Nat. Clim. Chang., 11(5), 411–417, doi:10.1038/s41558-021-01028-3, 2021a.

Zheng, G., Bao, A., Allen, S., Antonio Ballesteros-Cánovas, J., Yuan, Y., Jiapaer, G. and Stoffel, M.: Numerous unreported glacial lake outburst floods in the Third Pole revealed by high-resolution satellite data and geomorphological evidence, Sci. Bull., 66(13), 1270–1273, doi:10.1016/j.scib.2021.01.014, 2021b.